Application of Effective Field Theories to Problems in Nuclear and Hadronic Physics

by
Emanuele Mereghetti

A Dissertation Submitted to the Faculty of the
Graduate Program in Physics
In Partial Fulfillment of the Requirements
For the Degree of
Doctor of Philosophy
In the Graduate College
The University of Arizona

2 0 1 1

THE UNIVERSITY OF ARIZONA
GRADUATE COLLEGE

As members of the Dissertation Committee, we certify that we have read the dissertation

prepared by Emanuele Mereghetti

entitled Application of Effective Field Theories to Problems in Nuclear and Hadronic Physics

and recommend that it be accepted as fulfilling the dissertation requirement for the

Degree of Doctor of Philosophy

_____ Date: 5/5/2011
Sean Fleming

_____ Date: 5/5/2011
Bira van Kolck

_____ Date: 5/5/2011
Shufang Su

_____ Date: 5/5/2011
John Rutherfoord

_____ Date: 5/5/2011
Doug Touissant

Final approval and acceptance of this dissertation is contingent upon the candidate's submission of the final copies of the dissertation to the Graduate College.

I hereby certify that I have read this dissertation prepared under my direction and recommend that it be accepted as fulfilling the dissertation requirement.

_____ Date: 5/5/2011
Dissertation Director: Sean Fleming

Statement by Author

This dissertation has been submitted in partial fulfillment of requirements for an advanced degree at The University of Arizona and is deposited in the University Library to be made available to borrowers under rules of the Library.

Brief quotations from this dissertation are allowable without special permission, provided that accurate acknowledgment of source is made. Requests for permission for extended quotation from or reproduction of this manuscript in whole or in part may be granted by the head of the major department or the Dean of the Graduate College when in his or her judgment the proposed use of the material is in the interests of scholarship. In all other instances, however, permission must be obtained from the author.

Signed: Emanuele Mereghetti

Acknowledgements

I am greatly indebted to my advisor, Prof. Sean Fleming, for teaching me Effective Field Theories, for showing me the beauty of this approach to problems in QCD, and its many possible applications. I thank him for his passion and enthusiasm for research, and for the constant encouragement to pursue the physics I liked the most.

Most of the work of this dissertation would have not been possible without Prof. Bira van Kolck. I particularly thank him for opening my eyes to the charms of nuclear physics, and for his intransigent faithfulness to Effective Theories. It has been a real pleasure to learn from him.

I am also grateful for the collaboration of Prof. Rob Timmermans, Claudio Maekawa, and Will Hockings who deserve credit for substantial portions of this dissertation. Particularly important for this work was the collaboration with Jordy de Vries, Bingwei Long and Regina Azevedo I really enjoyed learning nuclear EFTs with Jordy, and I am still in debt for the good time I had in Groningen! I thank Bingwei and Regina not only for the time we spent working together, but especially for their good friendship, which greatly enriched my life as a graduate student. In particular, I am thankful to Regina for bearing with me in PAS 350 for the last four years!

I am particularly grateful to my undergraduate thesis advisor, Nora Brambilla and Antonio Vairo, who gave me the first exposure to Effective Field Theories, back in Milan. I really appreciate their constant interest in my research, and the support they have showed in these years.

My gratitude extends to the entire Nuclear Group at the University of Arizona, which I found a very constructive and friendly environment where to grow and learn. In particular, I want to mention Michael Fickinger (we will sooner or later finish one project together!), Masaoki Kusunoki and his wife Ruriko and Dru Renner and his wife Ali, who immediately made me feel at home in Tucson, Alexei Bazavov and Jimmy Rotureau. A special mention goes to Michael Kruse, for all the work he has done in this years for the graduate students in Physics, and for being a constant and reliable source of information (and gossip) on the life of the department.

In my years as graduate student I had the chance to broaden my knowledge of Quantum Field Theory, especially through the courses of Prof. Shufang Su, Prof. Zackaria Chacko, Prof. Philippe Jacquod and Prof. Jan Wehr. I also appreciated the support of Prof. John Rutherfoord and Alex Cronin, and of Peter Loch in the developing stages of my research work.

This place would be much more boring without graduate students, and I was lucky to cross the path of people like Alan Cooney, Lance Labun, Swati Singh (a particular thanks for supporting Chiara in the comp), Delphine Perrodin, Elizabeth Todd, Arif Erkoca, Fionnbarr O'Grady, and Vaibhav Wasnik.

Outside the dark offices of this building, I cannot forget Julia Arciero, Doug Davis, Marinella Lentis, who were my first family here in Arizona. These years

would have been much emptier without the friendship of Steve and Quyen Skiano, and their beautiful daughters, Monica, Teresa and Maria, Noe Badillo and Elizabeth Riedel, Erica McEvoy (don't ever stop being loud!), Tae Choe, Tony Miller, Luis Hess, Meghan Cassidy, Monica and Marta Grecchi, Anna Dari, Paolo Contu, and Damian Bacich.

Ai miei amici di Milano: Ninja e Maria, Didi e Doni, Chicco e Luisa, Chiaretta e Mules, Paola, Fefe, Maria Elena, Franca e Delo, Maddi e Gimli, Decio, Tossico, Saul, Caggio e Simona (e quei vandali dei vostri figli), Yoyo e Sabina, Giovanni e Simona, e tutti gli altri. Sono grato per la vostra amicizia, quello che ci tiene insieme épiuǵrande delle distanze e della mia infedeltá. Grazie!

I am especially indebted to my dad Gianni, my mom Donata, and my sisters Gloria and Maria, for supporting me always, even in the choice of continuing my studies abroad. My thoughts also go to Nonna Maria e Nonno Carlo, e Nonna Maria e Nonno Luigi, and the love I constantly received from them.

I also have to thank you my father and mother in law, Ambrogio and Pinuccia, for all the help they have given me and Chiara, especially in the last few months

The most beautiful thing of these year in grad school in Tucson are my daughters, Maddie and Cate. I wish them to keep, as they grow up and become young girls, the same simplicity and amazement with which they are taking the early steps of their lives.

And finally, there is Chiara. I have to thank Chiara for spurring me to leave my couch back in Abbiategrasso, Italy, and start this American adventure. I thank her for her company in this journey, and for what she gave up to come here. I thank her for our beautiful daughters, Maddie and Cate, and for her patience.

Dedication

To Chiara, Maddie and Cate

Table of Contents

Table of Contents—*Continued*

Table of Contents—*Continued*

List of Figures

List of Figures—*Continued*

List of Figures—*Continued*

List of Figures—*Continued*

List of Figures—*Continued*

List of Tables

Abstract

The Effective Field Theory formalism is applied to the study of problems in hadronic and nuclear physics. We develop a framework to study the exclusive two-body decays of bottomonium into two charmed mesons and apply it to study the decays of the C-even bottomonia. Using a sequence of effective field theories, we take advantage of the separation between the scales contributing to the decay processes, $2m_b \gg m_c \gg \Lambda_{QCD}$. We prove that, at leading order in the EFT power counting, the decay rate factorizes into the convolution of two perturbative matching coefficients and three non-perturbative matrix elements, one for each hadron. We calculate the relations between the decay rate and non-perturbative bottomonium and D-meson matrix elements at leading order, with next-to-leading log resummation. The phenomenological implications of these relations are discussed. At lower energies, we use Chiral Perturbation Theory and nuclear EFTs to set up a framework for the study of time reversal (T) symmetry in one- and few-nucleon problems. We consider T violation from the QCD $\bar{\theta}$ term and from all the possible dimension 6 operators, expressed in terms of light quarks, gluons and photons, that can be added to the Standard Model Lagrangian. We construct the low energy chiral Lagrangian stemming from different TV sources, and derive the implications for the nucleon Electric Dipole Form Factor and the deuteron T violating electromagnetic Form Factors. Finally, with an eye to applications to nuclei with $A \geq 2$, we construct the T violating nucleon-nucleon potential from different sources of T violation.

Chapter 1
Introduction

Current nuclear and particle physics experiments probe the strong interaction on a large variety of scales — from the MeV scale of nuclear experiments, to the GeV of the B factories, and the TeV of the Large Hadron Collider — offering an extraordinary opportunity to deepen our insight into the dynamics of strong interacting systems. Furthermore, the accurate estimate of the effects of the strong interaction is crucial for understanding the results of these experiments, to precisely constrain the parameters of the Standard Model and to spot evidences of new physics.

The theory of the strong interaction is Quantum Chromodynamics (QCD). The key feature of QCD is asymptotic freedom, the statement that the coupling of quarks and gluons becomes weak at high energy, where a perturbative expansion in the coupling constant α_s is possible. Since its first success in the '70s, the prediction of violation of Bjorken scaling in Deep Inelastic Scattering, QCD in the perturbative regime has been quantitatively tested in several experiments, over a wide range of energies, from bottomonium decays, to e^+e^- annihilation rates into hadrons and jets, to jet production in $p\bar{p}$ and pp collisions at hadron colliders (for an introductory review, see G. Dissertori and G. P. Salam, *Quantum Chromodynamics*, in Ref. [1]). These experimental successes, and its conceptual simplicity and beauty, have firmly established QCD as the correct theory of the strong interaction.

On the other hand, the same asymptotic freedom implies that at low energies, of order of the hadronic scale $\Lambda_{QCD} = 1$ GeV, the theory becomes strongly coupled, and the possibility of a perturbative expansion in α_s is lost.

Furthermore, the strong interaction shows a second striking feature, color confinement. In experiments one does not directly observe quarks and gluons, the degrees of freedom of QCD, but rather hadrons, colorless bound states of quark and gluons.

As a consequence, even processes with large momentum transfer are not entirely describable in perturbation theory, since, at a certain point, the soft, non-perturbative dynamics that governs the structure of the hadrons in the initial and final states kicks in. Perturbation theory is useful only insofar as the perturbative and non-perturbative contributions to a process can be rigorously separated (factorized), and the latter parametrized in terms of universal matrix elements, that can be computed on the lattice or fitted to data.

In the last three decades, Effective Field Theories (EFTs) have emerged as a powerful tool to describe various limits of QCD. The central idea behind EFTs is that the accurate description of the physics at a low energy scale Q does not require the detailed knowledge of what happens at a scale Λ much larger than Q. The EFT approach takes advantage of the separation of scales to focus only on the relevant degrees of freedom at low energy, without, at the same time, losing contact with the fundamental, underlying theory and its symmetries.

In the context of QCD and the strong interaction, EFTs have been developed both in the perturbative and non-perturbative regime.

For problems with one or more high energy scales $\Lambda \gg \Lambda_{QCD}$, the QCD Lagrangian can be used to compute the dynamics of high energy degrees of freedom, which are integrated out in perturbation theory, and contribute to the coefficients of local effective operators. The EFT approach has several advantages. First of all, its focus on the relevant degrees of freedom allows for the simplification of factorization theorems. Secondly, in processes with well separated scales, fixed-order perturbation theory can be invalidated by the presence of large logarithms of their ratio. Renormalization group invariance, a key ingredient of the EFT approach, gives the tools to systematically resum these effects, improving the perturbative expansion. Third, the identification of a second expansion parameter beyond α_s at the high scale — the ratio of the typical momentum of external particles in the problem and the high energy scale — provides an organizational principle (power counting) for non-perturbative

contributions. Finally, the elimination of the high energy scales from the problem simplifies the loop integrals in the EFT, which typically depend on only one scale. At the same time, having only one relevant scale also simplifies the task of simulating non-perturbative matrix elements on the lattice.

EFT techniques have been applied to systems with one heavy quark, like B and D mesons, for which Heavy Quark Effective Theory (HQET) was developed [2, 3, 4]. HQET applies to problems in which the heavy quark exchanges with light degrees of freedom momenta much smaller than its mass m_Q. The HQET Lagrangian consists of an infinite series of operators, organized in an expansion in Λ_{QCD}/m_Q. All the dynamics related to the heavy quark mass (contributions to loop diagrams from the region of integration $k \gtrsim m_Q$, virtual heavy quark-antiquark pairs in loops, *etc*) is encoded in the coefficients of the effective operators, which are computed in perturbation theory by equating (matching) QCD and HQET amplitudes at the high energy scale m_Q. Below m_Q all the physics is non-perturbative, still the power counting provides the rationale for considering only few non-perturbative matrix elements at a given accuracy. Furthermore, in the heavy quark limit, new symmetries — spin and heavy flavor symmetry — become manifest, allowing for the establishment of approximate relations between non-perturbative matrix elements. HQET has been applied to the description of several observables, especially in B physics. For a review, we refer to Ref. [5]

EFT ideas found fertile ground in applications to systems with two heavy quarks, like charmonium and bottomonium. These systems are described by Non Relativistic QCD [6]. Differently from the case with a single heavy quark, the dynamics of non relativistic bound states of a heavy quark and antiquark receives contributions from several scales below m_Q: the relative momentum $m_Q v$, the binding energy $m_Q v^2$ and the hadronic scale Λ_{QCD}. The NRQCD Lagrangian consists of a series of operators organized according to their scaling in the quark-antiquark relative velocity v. In the bilinear sector, the NRQCD Lagrangian has the same form as the HQET Lagrangian,

but the importance of various terms is different. For example, the assumption of an essentially static heavy quark, with kinetic energy of order $E \sim \Lambda_{QCD}$ and recoil $\vec{p}^2/2m_Q \sim \Lambda_{QCD}^2/m_Q$, which works in HQET, does not capture the physics of heavy quarkonium, for which $E \sim p^2/2m_Q \sim m_Q v^2$, and the importance of the respective operators in the EFT Lagrangian has to be readjusted. Furthermore, at scales lower than m_Q, heavy quarkonium annihilation is no longer resolved in the EFT, and it manifests in contact four-quark operators in the NRQCD Lagrangian, with imaginary matching coefficients.

One can further take advantage of the separation between the relative momentum and the binding energy by matching onto lower energy EFTs, potential NRQCD (pNRQCD) [7, 8, 9] or velocity NRQCD (vNRQCD) [10, 11, 12, 13].

Since its first success — the solution of the long-standing problem of infrared divergences in P-wave decays [6] — NRQCD, and lower-energy non relativistic EFTs, have given a fundamental contribution to a better understanding of heavy quarkonium physics, and they are today the standard theoretical tool for the study of heavy quarkonium spectroscopy, production, and decays [14, 15].

A third class of problems to which the EFT approach can be applied are processes with highly energetic, almost light-like hadrons, with one component of the momentum much bigger than the mass. Below the hard scale, typically set by the momentum transfer in hard scattering processes or by the mass of some heavy decaying particle, the degrees of freedom relevant to these problems are collinear and soft quarks and gluons, which are described by Soft Collinear Effective Theory (SCET) [16, 17, 18, 19, 20]. The SCET Lagrangian is organized as an expansion in powers of $\lambda = \sqrt{p^2/s}$, where p^2 is the invariant mass of the hadrons (or jets of hadrons), and s the square of the large energy scale in the problem. One important feature of SCET is the decoupling of soft and collinear degrees of freedom at the Lagrangian level [18], which greatly simplifies factorization theorems.

A first success of SCET is that it allows to recast in a EFT language "classical"

QCD factorization theorems, like those for Deep Inelastic Scattering, or the Drell-Yan process [19]. The strength of the EFT is by no way limited to a reformulation of old results. SCET has been successfully applied to B decays, like $B \to X_s\gamma$, semileptonic and exclusive B meson decays, and to heavy quarkonium decays in particular kinematic limits, where the SCET approach is justified by the large energy released to light degrees of freedom. A very promising direction of development in recent years has been the application of SCET to collider physics, both to specific processes (for example, Higgs production [21, 22, 23]), and as a theoretical tool to understand and improve jet algorithms and event generators [24, 25]. Finally, the key ingredients of the EFT, factorization, resummation and power counting (that is, control of non-perturbative corrections), make it the ideal theoretical tool for high precision extraction of QCD parameters, like the strong coupling constant α_s, from data [26, 27].

In Chapter 2, I will discuss an example that allows me to touch on the basic features of different EFTs, the exclusive decays of the C-even bottomonia χ_b and η_b into two D mesons. The process involves a non-relativistic bound state, the η_b or χ_b, that decays into two fast-moving, but massive, particles. Therefore, it calls for a combination of non-relativistic EFTs (NRQCD, pNRQCD) for the description of the initial state, and effective theories for highly energetic, but massive, particles (SCET, boosted HQET) for the final state. As promised in this introduction, the EFT formalism allows to derive a factorized formula for the decay rate, to resum logarithms of the ratios m_c/m_b and Λ_{QCD}/m_c and to estimate the impact of perturbative and non-perturbative corrections to the decay rate. The work of Chapter 2 has been done in collaboration with R. Azevedo and B. Long, and was published in Ref. [28].

A second type of EFTs has been developed to study the physics at scales Q much smaller than Λ_{QCD}. For these theories, the possibility of a perturbative expansion in the coupling α_s is lost, but the underlying theory and its symmetries still provide a strong constraint on the dynamics of low energy degrees of freedom. This is true in

particular of the approximate chiral symmetry of QCD and its spontaneous breaking, which predict the existence of a almost massless Goldstone boson, the pion, and dictates the form of its interaction to heavier degrees of freedom in the theory, like baryons (nucleon, Delta isobar, ...) and heavy meson (ρ, D, B, ...). These constraints lead to the formulation of an EFT for pions and nucleons, Chiral Perturbation Theory (χPT) [29, 30, 31, 32, 33]. In systems with zero or one nucleon, chiral symmetry and heavy baryon formalism (the baryonic analog of HQET [34]) justify a perturbative expansion of amplitudes in powers of the ratio of the typical momentum Q of external states and the scale $M_{QCD} = 2\pi F_\pi \approx 1$ GeV. χPT has been very successfully applied to pion-pion scattering, pion-nucleon scattering, pion and nucleon electromagnetic form factors, and several other processes with light mesons and one nucleon [33].

For systems with two or more nucleons, where the scale of the nucleon binding energy Q^2/m_N, much smaller than the momentum, becomes relevant, perturbation theory is bound to fail, as signaled by the appearance of shallow bound states, the nuclei [35, 36]. Chiral symmetry and χPT, however, provide the tools to derive and organize contributions to the two- and three-nucleon potential that is to be used in the solution of the few-body Schrödinger equation. In recent years, the accuracy of the EFT potential has reached the level to rival high precision phenomenological potentials, with the advantage, once again, of a closer relation with QCD and the possibility of systematic improvement [37, 38].

In this work, we use the machinery of χPT and nuclear EFTs to study the violation of time reversal symmetry (T) in nuclear physics. The strength of the EFT approach is, first of all, the close relation between the possible sources of T violation at high energy and the form of the T-violating (TV) couplings of nucleons, photons and pions. In particular, the chiral properties of the sources of T violation determine the relative importance of short- and long-distance contributions to TV observables, and the form of the TV pion-nucleon couplings. Secondly, EFT provides a framework that can accomodate at the same time one- and few-nucleon observables, in a consistent

fashion. In this way, we can identify the qualitatively different relations between one- and two-nucleon TV observables that stem from the different chiral properties of high-energy TV sources. If the next generation of EDM experiments will observe a signal for the proton, neutron and deuteron TV electromagnetic moments these relations will be an useful guide to trace TV in nuclear physics back to the fundamental sources at high energy.

The work presented in Chapters 3-7 is the fruit of the collaboration with J. de Vries, W. Hockings, C. Maekawa, R. Timmermans and U. van Kolck, and it is based on the publications [39, 40, 41, 42]. Chapters 3 and 4 expand the discussion of Refs. [39, 40] on the sources of T violation at high energy and the effective chiral Lagrangian they generate, in particular for dimension 6 sources of T violation. Chapter 5 combines the results of Refs. [40, 41] for the nucleon Electric Dipole Moment (EDM) and Electric Dipole Form Factor (EDFF). Chapter 6 is devoted to the deuteron TV electromagnetic moments, and it expands on [42], by including some next-to-leading order corrections to the deuteron EDM. The results of Chapter 7 on the TV nucleon-nucleon potential have not been published yet, and they were obtained in collaboration with C. Maekawa and U. van Kolck.

Chapter 2

Exclusive decays of χ_{bJ} and η_b into two charmed mesons

2.1 Introduction

The exclusive two-body decays of heavy quarkonium into light hadrons have been studied in the framework of perturbative QCD by many authors (for reviews, see [43, 44]). These processes exhibit a large hierarchy between the heavy quark mass, which sets the scale for annihilation processes, and the scales that determine the dynamical structure of the particles in the initial and final states. The large energy released in the annihilation of the heavy quark-antiquark pair and the kinematics of the decay — with the products flying away from the decay point in two back-to-back, almost light-like directions— allow for rigorously deriving a factorization formula for the decay rate at leading twist (for an up-to-date review of the theoretical and experimental status of the exclusive decays into light hadrons, see [14]).

For the bottomonium system, a particularly interesting class of two-body final states is the one containing two charmed mesons. In these cases the picture is complicated by the appearance of an additional intermediate scale, the charm mass m_c, which is much smaller than the bottom mass m_b but is large enough to be perturbative. These decays differ significantly from those involving only light quarks. The creation of mesons that are made up of purely light quarks involves creating two quark-antiquark pairs, with the energy shared between the quark and antiquark in each pair. In the production of two D mesons, however, almost all the energy of the bottomonium is carried away by the heavy c and $\bar{c}$, while the light quark and antiquark, which bind to the $\bar{c}$ and c respectively, carry away (boosted) residual energies.

The existence of well-separated scales in the system and the intuitive picture of the decay process suggest to tackle the problem using a sequence of effective field theories

(EFTs) that are obtained by subsequently integrating out the dynamics relevant to the perturbative scales m_b and m_c.

In the first step, we integrate out the scale m_b by describing the b and $\bar{b}$ with Non-Relativistic QCD (NRQCD) [6], and the highly energetic c and $\bar{c}$ with two copies of Soft-Collinear Effective Theory (SCET) [16, 17, 18, 19, 20] in opposite light-cone directions. In the second step, we integrate out the dynamics manifested at scales of order m_c by treating the quarkonium with potential NRQCD (pNRQCD) [7, 8, 9], and the D mesons with a boosted version of Heavy-Quark Effective Theory (HQET) [2, 3, 4, 45, 46, 47, 48]. The detailed explanation of why the aforementioned EFTs are employed is offered in Sec. 2.2. We will prove that, at leading order in the EFT expansion, the decay rate factors into a convolution of two perturbative matching coefficients and three (one for each hadron) non-perturbative matrix elements. The non-perturbative matrix elements are process-independent and encode information on both the initial and final states.

For simplicity, in this Chapter we focus on the decays of the C-even quarkonia χ_{bJ} and η_b that, at leading order in the strong coupling α_s, proceed via the emission of two virtual gluons. The same method can be generalized to the decays of C-odd states Υ and h_b, which require an additional virtual gluon. We also refrain from processes that have vanishing contributions at leading order in the EFT power counting. So the specific processes studied in this Chapter are $\chi_{b0,2} \to DD$, $\chi_{b0,\,2} \to D^*D^*$, and $\eta_b \to DD^* + \text{c.c.}$ However, the EFT approach developed in this Chapter enables one to systematically include power-suppressed effects, making it possible to go beyond the leading-twist approximation.

The study of the inclusive and exclusive charm production in bottomonium decays and of the role played by the charm mass m_c in such processes have recently drawn renewed attention [49, 50, 51, 52], in connection with the experimental advances spurred in the past few years by the abundance of bottomonium data produced at facilities like BABAR, BELLE, and CLEO. The most notable result was the observation of the

bottomonium ground state η_b, recently reported by the BABAR collaboration [53]. Furthermore, the CLEO collaboration published the first results for several exclusive decays of χ_b into light hadrons [54] and for the inclusive decay of χ_b into open charm [55]. In particular, they measured the branching ratio $\mathcal{B}(\chi_{bJ} \to D^0 X)$, where J is the total angular momentum of the χ_b state, and conclusively showed that for $J = 1$ the production of open charm is substantial: $\mathcal{B}(\chi_{b1}(1P) \to D^0 X) = 12.59 \pm 1.94\%$. For the $J = 0, 2$ states the data are weaker, but the production of open charm still appears to be relevant. The measurements of the CLEO collaboration are in good agreement with the prediction of Bodwin *et al.* [49], where EFT techniques (in particular NRQCD) were for the first time applied to study the production of charm in bottomonium decays.

The double-charm decay channels analyzed here have not yet been observed, so one of our aims is to see if they may be observable given the current data. Unfortunately, the poor knowledge of the D-meson matrix elements prevents us from providing definitive predictions for the decay rates $\Gamma(\chi_{bJ} \to DD)$, $\Gamma(\chi_{bJ} \to D^* D^*)$, and $\Gamma(\eta_b \to DD^* + \text{c.c.})$. As we will show, these rates are indeed strongly dependent on the parameters of the D- and D^*-meson distribution amplitudes, in particular on their first inverse moments λ_D and λ_{D^*}: the rates vary by an order of magnitude in the accepted ranges for λ_D and λ_{D^*}. On the other hand, the factorization formula implies that these channels, if measured with sufficient accuracy, could constrain the form of the D-meson distribution amplitude and the value of its first inverse moment. In turn, the details of the D-meson structure are relevant to other D-meson observables, which are crucial for a model-independent determination of the CKM matrix elements $|V_{cd}|$ and $|V_{cs}|$ [56].

This Chapter is organized as follows. In Sec. 2.2 we discuss the degrees of freedom and the EFTs we use. In Sec. 2.3.1 we match QCD onto NRQCD and SCET at the scale $2m_b$. The renormalization-group equation (RGE) for the matching coefficient is derived and solved in Sec. 2.3.2. In Sec. 2.4.1 the scale m_c is integrated out by

matching NRQCD and SCET onto pNRQCD and bHQET. The renormalization of the low-energy EFT operators is performed in Sec. 2.4.2, with some technical details left to App. A. The decay rates are calculated in Sec. 2.5 using two model distribution amplitudes. In Sec. 2.6 we draw our conclusions.

2.2 Degrees of freedom and the Effective Field Theories

Several well-separated scales are involved in the decays of the C-even bottomonia η_b and χ_{bJ} into two D mesons, making them ideal processes for the application of EFT techniques. The distinctive structures of the bottomonium (a heavy quark-antiquark pair) and the D meson (a bound state of a heavy quark and a light quark) suggest that one needs different EFTs to describe the initial and final states.

We first look at the initial state. The η_b is the ground state of the bottomonium system. It is a pseudoscalar particle, with spin $S = 0$, orbital angular momentum $L = 0$, and total angular momentum $J = 0$. In what follows we will often use the spectroscopic notation $^{2S+1}L_J$, in which the η_b is denoted by $^1S_0$. The χ_{bJ} is a triplet of states with quantum numbers ^3P_J. The η_b and χ_{bJ} are non-relativistic bound states of a b quark and a $\bar{b}$ antiquark. The scales in the system are the b quark mass m_b, the relative momentum of the $b\bar{b}$ pair $m_b w$, the binding energy $m_b w^2$, and $\Lambda_{\rm QCD}$, the scale where QCD becomes strongly coupled. w is the relative velocity of the quark-antiquark pair in the meson, and from the bottomonium spectrum it can be inferred that $w^2 \sim 0.1$. Since $m_b \gg \Lambda_{\rm QCD}$, m_b can be integrated out in perturbation theory and the bottomonium can be described in NRQCD. The degrees of freedom of NRQCD are non-relativistic heavy quarks and antiquarks, with energy and momentum $(E, |\vec{p}|)$ of order $(m_b w^2, m_b w)$, light quarks and gluons. In NRQCD, the gluons can be soft $(m_b w, m_b w)$, potential $(m_b w^2, m_b w)$, and ultrasoft (usoft) $(m_b w^2, m_b w^2)$. The NRQCD Lagrangian is constructed as a systematic expansion in $1/m_b$ whose

first few terms are

$$\mathcal{L}_{\rm NRQCD} = \psi^\dagger \left(iD_0 + \frac{\vec{D}^2}{2m_b} + \frac{\vec{\sigma}\cdot g\vec{B}}{2m_b} + \dots \right) \psi + \chi^\dagger \left(iD_0 - \frac{\vec{D}^2}{2m_b} - \frac{\vec{\sigma}\cdot g\vec{B}}{2m_b} + \dots \right) \chi \ ,$$

where ψ and $\chi^\dagger$ annihilate a b quark and a $\bar{b}$ antiquark respectively, and $\cdots$ denotes higher-order contributions in $1/m_b$. In NRQCD several mass scales are still dynamical and different assumptions on the hierarchy of these scales may lead to different power countings for operators of higher dimensionality. However, as long as $w \ll 1$, higher-dimension operators are suppressed by powers of w (for a critical discussion on the different power countings we refer to [9]).

NRQCD still contains interactions that can excite the heavy quarkonium far from its mass shell, for example, through the interaction of a non-relativistic quark with a soft gluon. In the case $m_b w \gg \Lambda_{\rm QCD}$, we can integrate out these fluctuations, matching perturbatively NRQCD onto a low-energy effective theory, pNRQCD. We are then left with a theory of non-relativistic quarks and ultrasoft gluons, with non-local potentials induced by the integration over soft- and potential-gluon modes. The interactions of the heavy quark with ultrasoft gluons are still described by the NRQCD Lagrangian, with the constraint that all the gluons are ultrasoft. In the weak coupling regime $m_b w \gg \Lambda_{\rm QCD}$, the potentials are organized by an expansion in $\alpha_s(m_b w)$, $1/m_b$, and r, where r is the distance between the quark and antiquark in the quarkonium, $r \sim 1/m_b w$. If we assume $m_b w^2 \sim \Lambda_{\rm QCD}$, each term in the expansion has a definite power counting in w and the leading potential is Coulombic $V \sim \alpha_s(m_b w)/r$.

An alternative approach, which does not require a two-step matching, has been developed in the effective theory vNRQCD [10, 11, 12, 13]. In the vNRQCD approach there is only one EFT below m_b, which is obtained by integrating out all the off-shell fluctuations at the hard scale m_b and introducing different fields for various propagating degrees of freedom (non-relativistic quarks and soft and ultrasoft gluons). In spite of the differences between the two formalisms, pNRQCD and vNRQCD give equivalent final answers in all the known examples in which both theories can be applied.

We now turn to the structure of the D meson. The most relevant features of the D meson are captured by a description in HQET. In HQET, in order to integrate out the inert scale m_c, the momentum of the heavy quark is generically written as [4]

$$p = m_c v + k \ , \tag{2.2.1}$$

where v is the four-velocity label, satisfying $v^2 = 1$, and k is the residual momentum. If one chooses v to be the center-of-mass velocity of the D meson, k scales as $k \sim v\Lambda_{\rm QCD}$. Introducing the light-cone vectors $n^\mu = (1, 0, 0, 1)$ and $\bar{n}^\mu = (1, 0, 0, -1)$, one can express the residual momentum in light-cone coordinates, $k^\mu = \bar{n} \cdot k \, n^\mu/2 + n \cdot k \, \bar{n}^\mu/2 + k_\perp^\mu$ or simply $k = (n \cdot k, \bar{n} \cdot k, \vec{k}_\perp)$. There are two relevant frames. One is the D-meson rest frame, in which v is conveniently chosen as $v_0 = (1, 0, 0, 0)$, and the other is the bottomonium rest frame, in which the D mesons are highly boosted in opposite directions, with v chosen as $v = v_D$, the four-velocity of one of the D mesons. By a simple consideration of kinematics and the scaling $k \sim v\Lambda_{\rm QCD}$, one can work out the scalings for k in the two frames. In the D-meson rest frame, $k \sim \Lambda_{\rm QCD}(1, 1, 1)$, and in the bottomonium rest frame (supposing the D meson moving in the positive z-direction),

$$k \sim \Lambda_{\rm QCD} \left(n \cdot v_D, \bar{n} \cdot v_D, 1\right) \sim \Lambda_{\rm QCD} \bar{n} \cdot v_D \left(\lambda^2, 1, \lambda\right) \ , \tag{2.2.2}$$

where $\bar{n} \cdot v_D \sim 2m_b/m_c$ and $\lambda = m_c/2m_b \ll 1$. It is convenient for the calculation in this Chapter to use the bottomonium rest frame, so we drop the subscript in v_D and we assume $v = v_D$ in the rest of this Chapter. The momentum scaling in Eq. (2.2.2) is called ultracollinear (ucollinear), and boosted HQET (bHQET) is the theory that describes heavy quarks with ultracollinear residual momenta and light degrees of freedom (including gluons and light quarks) with the same momentum scaling.

The bHQET Lagrangian is organized as a series in powers of $\Lambda_{\rm QCD}/m_c$ and, for residual momentum ultracollinear in the n-direction, the leading term is [47]

$$\mathcal{L}_{\rm bHQET} = \bar{h}_n i v \cdot D h_n \ , \tag{2.2.3}$$

where the field h_n annihilates a heavy quark and the covariant derivative D contains ultracollinear and ultrasoft gluons,

$$iD^\mu = \frac{n^\mu}{2}\left(i\bar{n}\cdot\partial + g\bar{n}\cdot A_n\right) + \frac{\bar{n}^\mu}{2}\left(in\cdot\partial + gn\cdot A_n + gn\cdot A_{us}\right) + \left(i\partial_\perp^\mu + gA_{n,\perp}^\mu\right) \ . \tag{2.2.4}$$

The ultrasoft gluons only enter in the small component of the covariant derivative. This fact can be exploited to decouple ultrasoft and ultracollinear modes in the leading-order Lagrangian through a field redefinition reminiscent of the collinear-ultrasoft decoupling in SCET [18, 47]. The ultracollinear-ultrasoft decoupling is an essential ingredient for the factorization of the decay rate.

Therefore, the appropriate EFT to calculate the decay rate is a combination of pNRQCD, for the bottomonium, and two copies of bHQET, with fields collinear to the n and $\bar{n}$ directions, for the D and $\bar{D}$ mesons, symbolically written as $\mathrm{EFT_{II}} \equiv$ pNRQCD + bHQET.

As we mentioned earlier, we plan to describe the bottomonium structure with a two-step scheme QCD $\to$ NRQCD $\to$ pNRQCD. However, at the intermediate stage, where we first integrate out the hard scale $2m_b$ and arrive at the scale $m_b w$, the D meson cannot yet be described in bHQET. This is because the interactions relevant at the intermediate scale $m_b w$ can change the c-quark velocity and leave the D meson off-shell of order $\sim (m_b w)^2 \sim m_c^2 \gg \Lambda_{\mathrm{QCD}}^2$. Highly energetic c and $\bar{c}$ travelling in opposite directions can be described properly by SCET with mass. Thus, at the scale $\mu = 2m_b$, we match QCD onto an intermediate EFT, $\mathrm{EFT_I} \equiv$ NRQCD + SCET, in which the EFT expansion is organized by λ and w. The degrees of freedom of $\mathrm{EFT_I}$ are tabulated in Tab. 2.1.

Then, we integrate out m_c and $m_b w$ at the same time, matching $\mathrm{EFT_I}$ onto $\mathrm{EFT_{II}}$ at the scale $\mu' = m_c$. In $\mathrm{EFT_{II}}$, the low-energy approximation is organized by $\Lambda_{\mathrm{QCD}}/m_c$ and w. The degrees of freedom of $\mathrm{EFT_{II}}$ are summarized in Tab. 2.2. When no subscript is specified in the rest of this Chapter, any reference to EFT applies to both $\mathrm{EFT_I}$ and $\mathrm{EFT_{II}}$. To facilitate the power counting, we adopt $w \sim \lambda \sim \Lambda_{\mathrm{QCD}}/m_c$.

	NRQCD	field	momentum	SCET	field	momentum
quark	b, b	$\psi_b,\ \chi_{\bar{b}}$	$(m_b w^2, m_b w)$	c,	$\xi^c_{\bar{n}}$	$2m_b(1,\lambda^2,\lambda)$
				$\bar{c}$	$\xi^{\bar{c}}_{n}$	$2m_b(\lambda^2,1,\lambda)$
gluon	potential	A^μ	$(m_b w^2, m_b w)$	collinear	$A^\mu_{\bar{n}}$	$2m_b(1,\lambda^2,\lambda)$
					A^μ_{n}	$2m_b(\lambda^2,1,\lambda)$
	soft	A^μ	$(m_b w, m_b w)$	soft	A^μ_s	$2m_b(\lambda,\lambda,\lambda)$
	usoft	A^μ	$(m_b w^2, m_b w^2)$	usoft	A^μ_{us}	$2m_b(\lambda^2,\lambda^2,\lambda^2)$

TABLE 2.1. Degrees of freedom in $\mathrm{EFT_I}$(NRQCD + SCET). w is the $b\bar{b}$ relative velocity in the bottomonium rest frame, while $\lambda \sim m_c/2m_b$ is the SCET expansion parameter. We assume $m_b w \sim m_c$ (or, equivalently, $w \sim \lambda$) and $m_b w^2 \sim m_b\lambda^2 \sim \Lambda_{\mathrm{QCD}}$.

	pNRQCD	field	momentum	bHQET	field	momentum
quark	b, b	$\psi_b,\ \chi_{\bar{b}}$	$(m_b w^2, m_b w)$	c	$h^c_{\bar{n}}$	$Q\,(1,\lambda^2,\lambda)$
				u, d	$\xi_{\bar{n}}$	$Q\,(1,\lambda^2,\lambda)$
gluon	usoft	A^μ	$(m_b w^2, m_b w^2)$	usoft	A^μ_{us}	$Q(\lambda,\lambda,\lambda)$
				ucollinear	$A^\mu_{\bar{n}}$	$Q\,(1,\lambda^2,\lambda)$

TABLE 2.2. Degrees of freedom in $\mathrm{EFT_{II}}$(pNRQCD + bHQET). The scale Q in bHQET is $Q = n\cdot v'\Lambda_{\mathrm{QCD}}$ for the $\bar{n}$-collinear sector and $Q = \bar{n}\cdot v\Lambda_{\mathrm{QCD}}$ for the n-collinear sector. $n\cdot v'$ and $\bar{n}\cdot v$ are the large light-cone components of the D-meson velocities in the bottomonium rest frame, $n\cdot v' \sim \bar{n}\cdot v \sim 2m_b/m_c$. λ and w are defined as in Tab. 2.1. The scaling of quark and gluon fields collinear in the n direction is obtained by exchanging the p^+ and p^- components of $\bar{n}$-collinear fields

As a first study, we will perform in this Chapter the leading-order calculation of the bottomonium decay rates.

2.3 NRQCD + SCET

2.3.1 Matching

In the first step, we integrate out the dynamics related to the hard scale $2m_b$ by matching the QCD diagrams for the production of a $c\,\bar{c}$ pair in the annihilation of a $b\,\bar{b}$ pair onto their $\mathrm{EFT_I}$ counterparts. The tree-level diagrams for the process are shown in Fig. 2.1. The gluon propagator in the QCD diagram has off-shellness of order $q^2 = (2m_b)^2$ and it is not resolved in $\mathrm{EFT_I}$, giving rise to a point-like interaction.

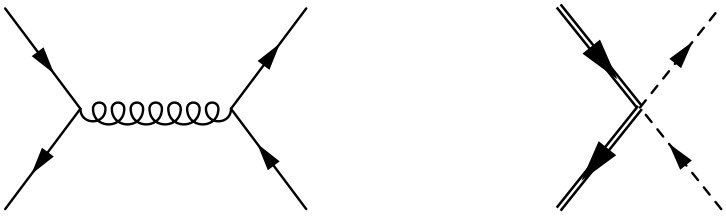

FIGURE 2.1. Matching QCD onto $\mathrm{EFT_I}$. On the r.h.s., the double lines represent the non-relativistic b ($\bar{b}$) (anti)quark, while the dashed lines represent the collinear c ($\bar{c}$) (anti)quark.

We calculate the diagrams on shell, finding

$$iJ_{\rm QCD} = iC(\mu) J_{\rm EFT_I}(\mu) \,, \tag{2.3.1}$$

with, at tree level,

$$J_{\rm EFT_I} = \chi_{\bar{b}}^\dagger \sigma_\perp^\mu t^a \psi_b \; \bar{\chi}_{\bar{n}}^c \, S_{\bar{n}}^\dagger \, \gamma_{\mu\perp} t^a \, S_n \, \chi_n^{\bar{c}} \quad \text{and} \quad C(\mu = 2m_b) = \frac{\alpha_s(2m_b)\pi}{m_b^2} \,, \tag{2.3.2}$$

where t^a are color matrices and the symbol σ^μ denotes the four matrices $\sigma^\mu = (1, \vec{\sigma})$, with $\vec{\sigma}$ the Pauli matrices. The subscript $\perp$ refers to the components orthogonal to the light-cone vectors n^μ and $\bar{n}^\mu$. The fields ψ_b and $\chi_{\bar{b}}^\dagger$ are two-component spinors that annihilate respectively a b quark and a $\bar{b}$ antiquark. $\chi_{n,\,\bar{n}\cdot p}^{\bar{c}}$ and $\chi_{\bar{n},\,n\cdot p}^{c}$ are collinear gauge-invariant fermion fields:

$$\chi_{n,\,\bar{n}\cdot p}^{\bar{c}} \equiv (W_n^\dagger \xi_n^{\bar{c}})_{\bar{n}\cdot p} \,, \qquad \chi_{\bar{n},\,n\cdot p}^{c} \equiv (W_{\bar{n}}^\dagger \xi_{\bar{n}}^{c})_{n\cdot p} \,, \tag{2.3.3}$$

where W_n is defined as

$$W_n \equiv \sum_{\rm perms} \exp\left(-\frac{g}{\bar{n}\cdot\mathcal{P}} \bar{n}\cdot A_n \right) \,. \tag{2.3.4}$$

$W_{\bar{n}}$ has an analogous definition with $n \to \bar{n}$. Collinear fields are labeled by the large component of their momentum. Note, however, we omit in Eq. (2.3.2) the subscripts $n\cdot p$ and $\bar{n}\cdot p$ of the collinear fermion fields, in order to simplify the notation. The operator $\bar{n}\cdot\mathcal{P}$ in the definition (2.3.4) is a label operator that extracts the large component of the momentum of a collinear field, $\bar{n}\cdot\mathcal{P}\,\phi_{n,\,\bar{n}\cdot p} = \bar{n}\cdot p\,\phi_{n,\,\bar{n}\cdot p}$, where

$\phi_{n,\,\bar{n}\cdot p}$ is a generic collinear field. $S_{n(\bar{n})}$ is a soft Wilson line,

$$S_n \equiv \sum_{\text{perms}} \left[\exp\left(-\frac{g}{n\cdot\mathcal{P}} n\cdot A_s\right)\right], \tag{2.3.5}$$

where the operator $n\cdot\mathcal{P}$ acts on soft fields, $n\cdot\mathcal{P}\,\phi_s = n\cdot k\,\phi_s$.

Since in SCET different gluon modes are represented by different fields, we have to guarantee the gauge invariance of the operator J_{EFT_I} under separate soft and collinear gauge transformations. A soft transformation is defined by $V_s(x) = \exp\left(i\beta_s^a t^a\right)$, with $\partial_\mu V \sim 2m_b(\lambda,\lambda,\lambda)$, while a gauge transformation $U(x)$ is n-collinear if $U(x) = \exp\left(i\alpha^a(x)t^a\right)$ and $\partial_\mu U(x) \sim 2m_b(\lambda^2,1,\lambda)$. It has been shown in Ref. [18] that collinear fields do not transform under a soft transformation and that the combination $W_n^\dagger\xi_n$ is gauge invariant under a collinear transformation. Soft fields do not transform under collinear transformations but they do under soft transformations. For example, the NRQCD quark and antiquark fields transform as $\psi_b \to V_s(x)\psi_b$. The soft Wilson line has the same transformation, $S_n \to V_s(x)S_n$. Therefore, $\chi_{\bar{b}}^\dagger\sigma_\perp^\mu t^a\psi_b$ transforms as an octet under soft gauge transformations. Since $\bar{\chi}_{\bar{n}}^c\, S_{\bar{n}}^\dagger\,\gamma_{\mu\,\perp} t^a\, S_n\,\chi_n^{\bar{c}}$ behaves like an octet as well, J_{EFT_I} is invariant. It is worth noting that the soft Wilson lines are necessary to guarantee the gauge invariance of J_{EFT_I}. We have explicitly checked their appearance at one gluon by matching QCD diagrams like the one in Fig. 2.1, with all the possible attachments of an extra soft or collinear gluon, onto four-fermion operators in EFT_I.

2.3.2 Running

The matching coefficient C and the effective operator J_{EFT_I} depend on the renormalization scale μ. Since the effective operator is sensitive to the low-energy scales in EFT_I, logarithms that would appear in the evaluation of J_{EFT_I} are minimized by the choice $\mu \sim m_c$. On the other hand, since the coefficient encodes the high-energy dynamics of the scale $2m_b$, such a choice would induce large logarithms of $m_c/2m_b$ in the matching coefficient. These logarithms can be resummed using RGEs

in NRQCD + SCET.

The μ dependence of $J_{\mathrm{EFT_I}}$ is governed by an equation of the following form [5],

$$\frac{d}{d\ln\mu} J_{\mathrm{EFT_I}}(\mu) = -\gamma_{\mathrm{EFT_I}}(\mu) J_{\mathrm{EFT_I}}(\mu) \ , \tag{2.3.6}$$

where the anomalous dimension $\gamma_{\mathrm{EFT_I}}$ is given by

$$\gamma_{\mathrm{EFT_I}} = Z^{-1}_{\mathrm{EFT_I}} \frac{d}{d\ln\mu} Z_{\mathrm{EFT_I}} \tag{2.3.7}$$

and $Z_{\mathrm{EFT_I}}$ is the counterterm that relates the bare operator $J^{(0)}_{\mathrm{EFT_I}}$ to the renormalized one, $J^{(0)}_{\mathrm{EFT_I}} = Z_{\mathrm{EFT_I}}(\mu) J_{\mathrm{EFT_I}}(\mu)$. Since the l.h.s. of Eq. (2.3.1) is independent of the scale μ, the RGE (2.3.6) can be recast as an equation for the matching coefficient $C(\mu)$,

$$\frac{d}{d\ln\mu} C(\mu) = \gamma_{\mathrm{EFT_I}}(\mu) C(\mu) \ . \tag{2.3.8}$$

The counterterm $Z_{\mathrm{EFT_I}}$ cancels the divergences that appear in Green functions with the insertion of the operator $J_{\mathrm{EFT_I}}$. We calculate $Z_{\mathrm{EFT_I}}$ in the $\overline{\mathrm{MS}}$ scheme by evaluating the divergent part of the four-point Green function at one loop, given by the diagrams in Figs. 2.2 - 2.4.

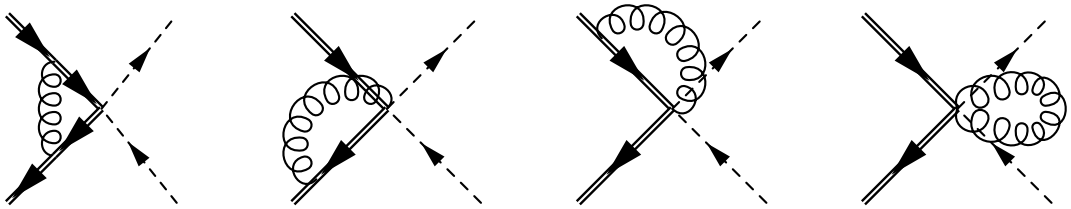

FIGURE 2.2. Soft diagrams at one loop.

Since in NRQCD we do not introduce different gluon fields for different momentum modes, "soft" and "ultrasoft" in Fig. 2.2 and Fig. 2.3 refer to the convention that we impose soft or ultrasoft scaling to the corresponding loop momentum. The potential region, which should be considered in the diagrams of Fig. 2.2, does not give any divergent contribution.

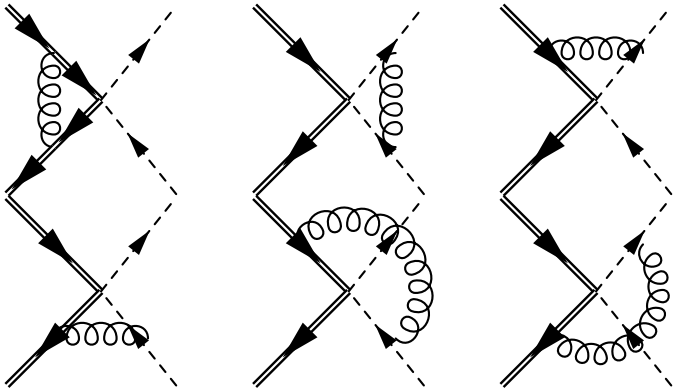

FIGURE 2.3. Ultrasoft diagrams at one loop.

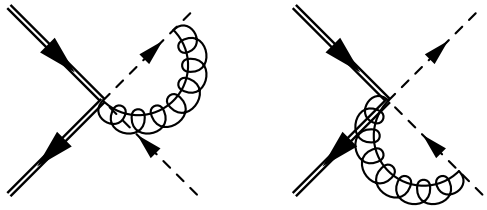

FIGURE 2.4. Collinear diagrams at one loop.

The integrals are evaluated in dimensional regularization, with $d = 4 - 2\varepsilon$. We regulate the infrared divergences by keeping the non-relativistic b and $\bar{b}$ and the collinear c and $\bar{c}$ off-shell: $E_{b,\bar{b}} - \vec{p}^{\,2}_{b,\bar{b}}/2m_b = \Delta_b$, $p_c^2 - m_c^2 = \Delta^2$ and $p_{\bar{c}}^2 - m_c^2 = \bar{\Delta}^2$. We power count the c-quark off-shellness as $\Delta^2 \sim \bar{\Delta}^2 \sim m_b^2\lambda^2$ and the b-quark off-shellness as $\Delta_b \sim m_b w^2$. We also assume Δ^2, $\bar{\Delta}^2 > 0$. To avoid double counting, we define the one-loop integrals with the 0-bin subtraction [57].

Even with an off-shellness, the soft diagrams in Fig. 2.2 do not contain any scale and they are completely canceled by their 0-bin.

The divergent part of the ultrasoft diagrams in Fig. 2.3 is

$$\begin{aligned} i\mathcal{M}_{usoft} = -i\frac{\alpha_s}{4\pi}\,\Bigg\{ & 2C_F\left[\frac{1}{\varepsilon^2} - \frac{1}{\varepsilon}\ln\left(\frac{\Delta^2\,\bar{\Delta}^2}{n\cdot p_c \bar{n}\cdot p_{\bar{c}}\,\mu^2}\right)\right] \\ & + \frac{1}{N_c}\frac{1}{\varepsilon}\ln(-1-i0) - \frac{1}{N_c}\,\frac{1}{\varepsilon}\Bigg\}\, J_{\mathrm{EFT_I}}\,, \end{aligned} \tag{2.3.9}$$

where $C_F = (N_c^2 - 1)/2N_c$ and μ is the $\overline{\mathrm{MS}}$ unit mass, $\mu^2 = 4\pi\mu_{\mathrm{MS}}^2 \exp(-\gamma_E)$. The first term in the curly brackets of Eq. (2.3.9) corresponds to the sum of the

divergences in the second diagram in Fig. 2.3, where an ultrasoft gluon is exchanged between the c and $\bar{c}$ quarks collinear in back-to-back directions, and those in the last four diagrams of the same figure, which contain ultrasoft interactions between the initial and final states. The second term is an extra imaginary piece generated by the second diagram in Fig. 2.3. The $-i0$ prescription in the argument of the logarithm, where 0 is a positive infinitesimal quantity, follows from the prescriptions in the quark propagators and from the choice $\Delta^2, \bar{\Delta}^2 > 0$. The divergences arising from the ultrasoft exchanges between the $b\bar{b}$ pair in the first diagram in Fig. 2.3 are encoded in the last term in Eq. (2.3.9).

The initial and final states cannot interact by exchanging collinear gluons because the emission or absorption of a collinear gluon would give the b quark an off-shellness of order m_b^2, which cannot appear in the effective theory. For the same reason, the c and $\bar{c}$ cannot exchange n or $\bar{n}$-collinear gluons. The only collinear loop diagrams consist of the emission of a $n(\bar{n})$-collinear gluon from the Wilson line $W_{n\,(\bar{n})}$ in $J_{\mathrm{EFT_I}}$ and its absorption by the $\bar{c}(c)$ quark, as shown in Fig. 2.4. The divergent part of the sum of the two collinear diagrams is

$$i\mathcal{M}_{\mathrm{coll}} = i\frac{\alpha_s}{4\pi} 2C_F \left[\frac{2}{\varepsilon^2} + \frac{1}{\varepsilon}\left(2 - \ln\left(\frac{\Delta^2\bar{\Delta}^2}{\mu^2\mu^2}\right)\right)\right] J_{\mathrm{EFT_I}} \,. \tag{2.3.10}$$

The collinear diagrams are calculated with a 0-bin subtraction [57], that is, we subtract from the naive collinear integrals the same integrals in the limit in which the loop momentum is ultrasoft. In this way we avoid double counting between the diagrams in Figs. 2.3 and 2.4.

Summing Eqs. (2.3.9) and (2.3.10) and adding factors of $Z_\psi^{1/2}$ for each field,

$$Z_{\psi_b} = Z_{\chi_b} = 1 + \frac{1}{\varepsilon}\frac{\alpha_s}{2\pi}C_F \,, \qquad Z_{\xi_n} = Z_{\xi_{\bar{n}}} = 1 - \frac{1}{\varepsilon}\frac{\alpha_s}{4\pi}C_F \,,$$

the divergent piece becomes

$$i\mathcal{M}_{\mathrm{div}} = i\frac{\alpha_s}{4\pi}\left\{C_F\left[\frac{2}{\varepsilon^2} + \frac{2}{\varepsilon}\left(\frac{3}{2} - \ln\left(\frac{n\cdot p_c \bar{n}\cdot p_{\bar{c}}}{\mu^2}\right)\right)\right] + \frac{1}{\varepsilon}N_c + \frac{i\pi}{\varepsilon}\frac{1}{N_c}\right\} J_{\mathrm{EFT_I}} \,. \tag{2.3.11}$$

The counterterm $Z_{\mathrm{EFT_I}}$ is chosen so as to cancel the divergence in Eq. (2.3.11),

$$Z_{\mathrm{EFT_I}} = \frac{\alpha_s}{4\pi}\left\{C_F\left[\frac{2}{\varepsilon^2}+\frac{2}{\varepsilon}\left(\frac{3}{2}-\ln\left(\frac{n\cdot p_c\bar{n}\cdot p_{\bar{c}}}{\mu^2}\right)\right)\right]+\frac{1}{\varepsilon}N_c+\frac{i\pi}{\varepsilon}\frac{1}{N_c}\right\}\,. \tag{2.3.12}$$

From the definition (2.3.7), Eq. (2.3.12), and recalling that $d\alpha_s/d\ln\mu = -2\varepsilon\alpha_s + \mathcal{O}(\alpha_s^2)$, the anomalous dimension at one loop is

$$\gamma_{\mathrm{EFT_I}} = -2\frac{\alpha_s(\mu)}{4\pi}\left\{3C_F+N_c+4C_F\ln\left(\frac{\mu}{\sqrt{n\cdot p_c\bar{n}\cdot p_{\bar{c}}}}\right)+i\pi\frac{1}{N_c}\right\}\,. \tag{2.3.13}$$

An important feature of the anomalous dimension (2.3.13) is the presence of a term proportional to $\ln\mu$. Because of this term, the RGE (2.3.8) can be used to resum Sudakov double logarithms. As we will show shortly, the general solution of Eq. (2.3.8) can be written in the following form:

$$C(\mu) = C(\mu_0)\left(\frac{\mu_0}{\sqrt{n\cdot p_c\bar{n}\cdot p_{\bar{c}}}}\right)^{g(\mu_0,\mu)}\exp U(\mu_0,\mu)\,, \tag{2.3.14}$$

where g and U depend on the initial scale μ_0 and the final scale μ that we run down to. For an anomalous dimension of the form (2.3.13), U can be expanded as a series,

$$U(\mu_0,\mu) = \sum_{n=1}^{\infty}\alpha_s^n(\mu_0)\sum_{L=0}^{n+1}u_{n,L}\ln^{n-L+1}\frac{\mu}{\mu_0}\,. \tag{2.3.15}$$

If $\mu/\mu_0 \ll 1$, the most relevant terms in the expansion (2.3.15) are those with $L=0$, which we call "leading logs" (LL). Terms with higher L are subleading; we call the terms with $L=1$ "next-to-leading logs" (NLL), those with $L=2$ "next-to-next-leading logs" (NNLL), and, if $L=m$, we denote them with N^{m}LL. The RGE (2.3.8) determines the coefficients in the expansion (2.3.15). With the anomalous dimensions written as

$$\gamma_{\mathrm{EFT_I}} = -2\left\{\gamma(\alpha_s)+\Gamma(\alpha_s)\ln\left(\frac{\mu}{\sqrt{n\cdot p_c\bar{n}\cdot p_{\bar{c}}}}\right)\right\}\,, \tag{2.3.16}$$

where $\gamma(\alpha_s)$ and $\Gamma(\alpha_s)$ are series in powers of α_s,

$$\gamma(\alpha_s) = \frac{\alpha_s}{4\pi}\gamma^{(0)}+\left(\frac{\alpha_s}{4\pi}\right)^2\gamma^{(1)}+\dots\,,\qquad \Gamma(\alpha_s) = \frac{\alpha_s}{4\pi}\Gamma^{(0)}+\left(\frac{\alpha_s}{4\pi}\right)^2\Gamma^{(1)}+\dots\,,$$

it can be proved that the coefficients of the LL, u_{n0}, are determined by the knowledge of $\Gamma^{(0)}$ and of the QCD β function at one loop. The NLL coefficients u_{n1} are instead completely determined if Γ and β are known at two loops and $\gamma(\alpha_s)$ at one loop.

In the case we are studying, the ratio of the scales $\mu/\mu_0 \sim m_c/2m_b$ is not extremely small. Indeed, as to be seen shortly, the numerical contributions of the LL and NLL terms in the series (2.3.15) are of the same size. It is therefore important to work at NLL accuracy, which requires the calculation of the coefficient of $\ln\mu$ to two loops. The factors of $\ln\mu$ are induced by cusp angles involving light-like Wilson lines and their coefficients are universal $\Gamma(\alpha_s) \propto \Gamma_{\rm cusp}(\alpha_s)$ [58]. The cusp anomalous dimension $\Gamma_{\rm cusp}(\alpha_s)$ is known at two loops [58],

$$\Gamma_{\rm cusp}(\alpha_s) = \frac{\alpha_s}{4\pi}\Gamma^{(0)}_{\rm cusp} + \left(\frac{\alpha_s}{4\pi}\right)^2 \Gamma^{(1)}_{\rm cusp} \,, \tag{2.3.17}$$

with

$$\Gamma^{(0)}_{\rm cusp} = 4C_F \,, \qquad \Gamma^{(1)}_{\rm cusp} = 4C_F\left[\left(\frac{67}{9}-\frac{\pi^2}{3}\right)N_c - \frac{10}{9}n_f\right] \,, \tag{2.3.18}$$

while the constant of proportionality between $\Gamma(\alpha_s)$ and $\Gamma_{\rm cusp}(\alpha_s)$ is fixed by the one-loop calculation. Since we have determined $\gamma^{(0)}$,

$$\gamma^{(0)} = 3C_F + N_c + i\frac{\pi}{N_c} \,, \tag{2.3.19}$$

and the β function is known, we have all the ingredients to provide the NLL approximation for $U(\mu_0,\mu)$ and $g(\mu_0,\mu)$. Taking into account the tree-level initial condition in Eq. (2.3.2), Eq. (2.3.14) determines the leading-order matching coefficient, with NLL resummation.

The solution (2.3.14) can be derived by writing Eq. (2.3.8) as

$$d\ln C = -2\frac{d\alpha}{\beta(\alpha)}\left\{\gamma(\alpha) + \Gamma_{\rm cusp}(\alpha)\left[\ln\left(\frac{\mu_0}{\sqrt{n\cdot p_c \bar{n}\cdot p_{\bar{c}}}}\right) + \int_{\alpha(\mu_0)}^{\alpha}\frac{d\alpha'}{\beta(\alpha')}\right]\right\} \,, \tag{2.3.20}$$

where we have used the definition of the β function, $\beta(\alpha) = d\alpha/d\ln\mu$, to write $\ln\mu$ and $d\ln\mu$ in terms of α. Integrating both sides from μ_0 to μ and exponentiating the

result we find the form given in Eq. (2.3.14), with

$$\begin{aligned} U(\mu_0,\mu) &= -2\int_{\alpha_s(\mu_0)}^{\alpha_s(\mu)}\frac{d\alpha}{\beta(\alpha)}\left\{\gamma(\alpha)+\Gamma_{\rm cusp}(\alpha)\int_{\alpha(\mu_0)}^{\alpha}\frac{d\alpha'}{\beta(\alpha')}\right\}\,, \\ g(\mu_0,\mu) &= -2\int_{\alpha_s(\mu_0)}^{\alpha_s(\mu)}\frac{d\alpha}{\beta(\alpha)}\Gamma_{\rm cusp}(\alpha)\,. \end{aligned} \tag{2.3.21}$$

At NLL, we find

$$\begin{aligned} U(\mu_b,\mu) = \frac{2\pi\Gamma^{(0)}_{\rm cusp}}{\beta_0^2}\left[\frac{r-1-r\ln r}{\alpha_s(\mu)}+\frac{\beta_0\gamma^{(0)}_{\rm Re}}{2\pi\Gamma^{(0)}_{\rm cusp}}\ln r+\left(\frac{\Gamma^{(1)}_{\rm cusp}}{\Gamma^{(0)}_{\rm cusp}}-\frac{\beta_1}{\beta_0}\right)\frac{1-r+\ln r}{4\pi}\right. \\ \left.+\frac{\beta_1}{8\pi\beta_0}\ln^2 r\right]+\frac{\gamma^{(0)}_{\rm Im}}{\beta_0}\ln r\,, \end{aligned} \tag{2.3.22}$$

and

$$g(\mu_b,\mu) = \frac{\Gamma^{(0)}_{\rm cusp}}{\beta_0}\left[\ln r+\left(\frac{\Gamma^{(1)}_{\rm cusp}}{\Gamma^{(0)}_{\rm cusp}}-\frac{\beta_1}{\beta_0}\right)\frac{\alpha_{\rm s}(\mu_b)}{4\pi}(r-1)\right]\,, \tag{2.3.23}$$

where $r=\alpha_s(\mu)/\alpha_s(\mu_b)$ and we have renamed the initial scale μ_b, to denote its connection to the scale $2m_b$. In Eqs. (2.3.22) and (2.3.23) we have used the two-loop beta function,

$$\beta(\alpha_s) = -2\alpha_s\left(\frac{\alpha_s}{4\pi}\beta_0+\left(\frac{\alpha_s}{4\pi}\right)^2\beta_1\right)\,, \tag{2.3.24}$$

with

$$\beta_0 = 11-\frac{2}{3}n_f\,, \qquad \beta_1 = \frac{34}{3}N_c^2-\frac{10}{3}N_cn_f-2C_Fn_f\,. \tag{2.3.25}$$

In Eq. (2.3.22) we have kept the contributions of the real and imaginary part of $\gamma^{(0)}$ separated. The imaginary part of $\gamma^{(0)}$ changes the phase of the matching coefficient $C(\mu)$, but this phase is irrelevant for the calculation of physical observables like the decay rate, which depend on the square modulus of $C(\mu)$. In Sec. 2.5 the factor $U(\mu_b,\mu)$ will be evaluated between the scales $\mu_b=2m_b$ and $\mu=m_c$, with $n_f=4$ active quark flavors. The numerical evaluation shows that the LL term, represented by the first term in the brackets in Eq. (2.3.22), is slightly smaller than and have the opposite sign of the term proportional to $\gamma^{(0)}_{\rm Re}$, which dominates the NLL contribution. This observation confirms, *a posteriori*, the necessity to work at NLL accuracy in the resummation of logarithms of $m_c/2m_b$.

The RGE (2.3.8) and its solution (2.3.14) thus allow us to rewrite Eq. (2.3.1) as

$$J_{\rm QCD} = C(\mu) J_{{\rm EFT_I}}(\mu) = C(\mu_b = 2m_b) \exp U(2m_b, m_c) J_{{\rm EFT_I}}(\mu = m_c) \ ,$$

which avoids the occurrence of any large logarithm in the matching coefficient or in the matrix element of the effective operator.

2.4 pNRQCD + bHQET

2.4.1 Matching

In the second step, we integrate out the soft modes by matching $\mathrm{EFT_I}$ onto $\mathrm{EFT_{II}}$. In NRQCD + SCET, contributions to the exclusive decay processes are obtained by considering time-ordered products of $J_{\mathrm{EFT_I}}$ and the terms in the $\mathrm{EFT_I}$ Lagrangian that contain soft-gluon emissions. The soft gluons have enough virtuality to produce a pair of light quarks travelling in opposite directions with ultracollinear momentum scaling. These light quarks bind to the charm quarks to form back-to-back D mesons. The total momentum of two back-to-back ultracollinear quarks is $2m_b\Lambda_{\rm QCD}/m_c\,(1, 1, \lambda)$ and the invariant mass of the pair is $q^2 \sim (2m_b\Lambda_{\rm QCD}/m_c)^2 \sim m_c^2$: in NRQCD+SCET, only soft gluons have enough energy to produce them. The time-ordered products in NRQCD + SCET are matched onto six-fermion operators in pNRQCD + bHQET, where fluctuations of order m_c^2 cannot be resolved.

We consider the scale $\mu' = m_c$ to be much bigger than $\Lambda_{\rm QCD}$, so the matching can be done in perturbation theory. The Feynman diagrams contributing to the matching are shown in Fig. 2.5. The gluon and the b-quark propagators have off-shellness of order m_c^2, so the two diagrams on the l.h.s. match onto six-fermion operators on the r.h.s.

The amplitude for the decay of a bottomonium with quantum numbers ${}^{2S+1}L_J$ into two D mesons has the following form:

$$\begin{aligned} i\mathcal{M} = iC(\mu) \int \frac{d\omega}{\omega}\frac{d\bar\omega}{\bar\omega} T(\omega, \bar\omega, \mu, \mu'; {}^{2S+1}L_J) F^2(\mu') \\ \langle DA,\, DB | \mathcal{O}_{AB}^{{}^{2S+1}L_J}(\omega, \bar\omega, \mu') | \bar b b({}^{2S+1}L_J)\rangle . \end{aligned} \tag{2.4.1}$$

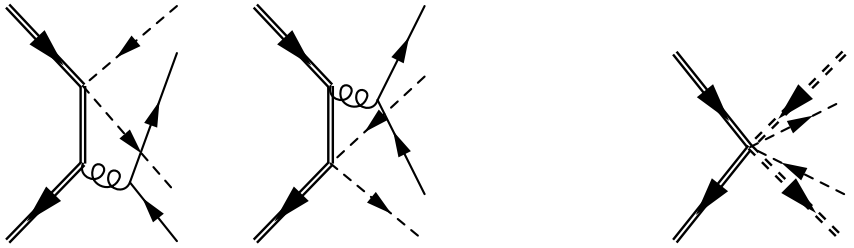

FIGURE 2.5. Matching NRQCD+SCET onto pNRQCD+bHQET. On the r.h.s. the double solid lines represent heavy b ($\bar{b}$) (anti)quarks, the double dashed lines bHQET c ($\bar{c}$) (anti)quarks, and the single dashed lines collinear light quarks.

A and B, which label the final states and the $\mathrm{EFT_{II}}$ operators $\mathcal{O}_{AB}^{^{2S+1}L_J}$, denote the possible parity, spin, and polarization of the D mesons, $A, B = \{P, V_L, V_T\}$, indicating respectively a pseudoscalar D meson, a longitudinally-polarized vector meson D^*, and a transversely-polarized vector meson D^*. Unlike $J_{\mathrm{EFT_I}}$, we have dropped the subscript $\mathrm{EFT_{II}}$ in $\mathcal{O}_{AB}^{^{2S+1}L_J}$ in order to simplify the notation.

The $\mathrm{EFT_{II}}$ operators that contribute to the decay of the P-wave states are

$$\begin{aligned}
F^2(\mu')\,\mathcal{O}^{^3P_J}_{PP}(\omega,\bar{\omega},\mu') &= \chi^\dagger_{\bar{b}}\,\vec{p}_b\cdot\vec{\sigma}_\perp\psi_b\;\bar{\mathcal{H}}^c_{\bar{n}}\,\frac{\bar{n}\!\!\!/}{2}\gamma^5\,\delta\left(-\bar{\omega}-n\cdot\mathcal{P}\right)\chi^{\bar{l}}_{\bar{n}} \\
&\quad\times\bar{\chi}^l_n\delta\left(\omega-\bar{n}\cdot\mathcal{P}^\dagger\right)\,\frac{n\!\!\!/}{2}\gamma^5\,\mathcal{H}^{\bar{c}}_n\,, \\
F^2(\mu')\,\mathcal{O}^{^3P_J}_{V_LV_L}(\omega,\bar{\omega},\mu') &= \chi^\dagger_{\bar{b}}\,\vec{p}_b\cdot\vec{\sigma}_\perp\psi_b\;\bar{\mathcal{H}}^c_{\bar{n}}\,\frac{\bar{n}\!\!\!/}{2}\,\delta\left(-\bar{\omega}-n\cdot\mathcal{P}\right)\chi^{\bar{l}}_{\bar{n}} \\
&\quad\times\bar{\chi}^l_n\delta\left(\omega-\bar{n}\cdot\mathcal{P}^\dagger\right)\,\frac{n\!\!\!/}{2}\,\mathcal{H}^{\bar{c}}_n\,, \\
F^2(\mu')\,\mathcal{O}^{^3P_J}_{V_TV_T}(\omega,\bar{\omega},\mu') &= \chi^\dagger_{\bar{b}}\,p_{b\perp}^{(\mu}\sigma_\perp^{\nu)}\psi_b\;\bar{\mathcal{H}}^c_{\bar{n}}\,\frac{\bar{n}\!\!\!/}{2}\gamma_{\mu\perp}\,\delta\left(-\bar{\omega}-n\cdot\mathcal{P}\right)\chi^{\bar{l}}_{\bar{n}} \\
&\quad\times\bar{\chi}^l_n\delta\left(\omega-\bar{n}\cdot\mathcal{P}^\dagger\right)\,\frac{n\!\!\!/}{2}\gamma_{\nu\perp}\,\mathcal{H}^{\bar{c}}_n,
\end{aligned} \tag{2.4.2}$$

where $p_{b\perp}^{(\mu}\sigma_\perp^{\nu)}$ is a symmetric, traceless tensor,

$$p_{b\perp}^{(\mu}\sigma_\perp^{\nu)} = \frac{1}{2}\left(p_{b\perp}^{\mu}\sigma_\perp^{\nu} + p_{b\perp}^{\nu}\sigma_\perp^{\mu} - g_\perp^{\mu\nu}\vec{p}_b\cdot\vec{\sigma}_\perp\right)\,.$$

At leading order in the $\mathrm{EFT_{II}}$ expansion, the η_b can only decay into a pseudoscalar

and a vector meson, with an operator given by

$$F^2(\mu')\,\mathcal{O}^{^1S_0}_{PV_L}(\omega,\bar\omega,\mu') = \chi_b^\dagger\,\psi_b\,\left[\bar{\mathcal{H}}^c_{\bar n}\,\frac{\not{n}}{2}\gamma^5\,\delta\left(-\bar\omega - n\cdot\mathcal{P}\right)\chi^{\bar l}_{\bar n}\;\bar\chi^l_n\delta\left(\omega-\bar n\cdot\mathcal{P}^\dagger\right)\;\frac{\not{\bar n}}{2}\,\mathcal{H}^{\bar c}_n\right.$$
$$\left. +\;\bar{\mathcal{H}}^c_{\bar n}\,\frac{\not{n}}{2}\,\delta\left(-\bar\omega - n\cdot\mathcal{P}\right)\chi^{\bar l}_{\bar n}\;\bar\chi^l_n\delta\left(\omega-\bar n\cdot\mathcal{P}^\dagger\right)\;\frac{\not{\bar n}}{2}\gamma^5\,\mathcal{H}^{\bar c}_n\right]. \tag{2.4.3}$$

For later convenience, in the definition of the effective operators (2.4.2) and (2.4.3) we have factored out the term $F^2(\mu')$, which is related to the D-meson decay constant. The definition of $F^2(\mu')$ will become clear when we introduce the D-meson distribution amplitudes. The fields χ^l_n and $\chi^{\bar l}_{\bar n}$ are ultracollinear gauge-invariant light-quark fields, while $\mathcal{H}^c_{\bar n} = W^\dagger_{\bar n} h^c_{\bar n}$ and $\mathcal{H}^{\bar c}_n = W^\dagger_n h^{\bar c}_n$ are bHQET heavy-quark fields, which are invariant under an ultracollinear gauge transformation. The Wilson lines W_n and $W_{\bar n}$ have the same definition as in Eq. (2.3.4), with the restriction to ultracollinear gluons. Eqs. (2.4.2) and (2.4.3) allow us to interpret ω as the component of the light-quark momentum along the direction n. Similarly, $\bar\omega$ represents the component of the light-antiquark momentum along $\bar n$. The minus sign in the delta function $\delta(-\bar\omega - n\cdot\mathcal{P})$ is chosen so that $\bar\omega$ is positive.

The tree-level matching coefficients are

$$\begin{aligned} T(\omega,\bar\omega,\mu,\mu'=m_c;\,^3P_J) &= \frac{C_F}{N_c^2}\frac{4\pi\alpha_s(m_c)}{m_b}\frac{1}{\omega+\bar\omega}\,, \\ T(\omega,\bar\omega,\mu,\mu'=m_c;\,^1S_0) &= \frac{C_F}{N_c^2}\frac{4\pi\alpha_s(m_c)}{m_b}\frac{1}{2}\frac{\omega-\bar\omega}{\omega+\bar\omega}\,. \end{aligned} \tag{2.4.4}$$

Note that, at leading order in the $\mathrm{EFT_{II}}$ expansion, the matching coefficient $T(\omega,\bar\omega,\mu,\mu';\,^3P_J)$ is independent of the spin and polarization of the final states, or of the total angular momentum J of the χ_b.

An important feature of bHQET is that the ultracollinear and ultrasoft sectors can be decoupled at leading order in the power counting by a field redefinition reminiscent of the collinear-usoft decoupling in SCET [18, 47]. For bHQET in the n direction, the decoupling is achieved by defining $h^{\bar c}_n \to Y_n h^{\bar c}_n$ and $\bar\xi^l_n \to \bar\xi^l_n Y^\dagger_n$, where Y_n is an

ultrasoft Wilson line,

$$Y_n = \sum_{\text{perms}} \left[\exp\left(-\frac{g}{n\cdot\mathcal{P}} n\cdot A_{us} \right) \right] \ . \tag{2.4.5}$$

An analogous redefinition with $n \to \bar{n}$ decouples ultrasoft from $\bar{n}$-ultracollinear quarks and gluons. These redefinitions do not affect the operators in Eqs. (2.4.2) and (2.4.3) because all the induced Wilson lines cancel out. As a consequence, at leading order in the $\mathrm{EFT_{II}}$ power counting, there is no interaction between the initial and the final states, since the former can only emit and absorb ultrasoft gluons that do not couple to ultracollinear degrees of freedom. Furthermore, fields in the two copies of bHQET, boosted in opposite directions, cannot interact with each other because the interaction with a $\bar{n}$-ultracollinear gluon would give a n-ultracollinear quark or gluon a virtuality of order m_c^2, which, however, cannot appear in $\mathrm{EFT_{II}}$. The matrix elements of the operators $\mathcal{O}_{AB}^{^{2S+1}L_J}(\omega,\bar{\omega},\mu)$, therefore, factorize as

$$\begin{aligned} &F^2(\mu')\langle AB|\mathcal{O}_{A\,B}^{^{2S+1}L_J}(\omega,\bar{\omega},\mu')|\bar{b}b\rangle = \\ &\langle 0|\chi_{\bar{b}}^\dagger T_{AB}^{^{2S+1}L_J}\psi_b|\bar{b}b\rangle \, \langle A|\bar{\mathcal{H}}_{\bar{n}}^c \frac{\bar{n}\!\!\!/}{2}\Gamma_A \, \delta\left(-\bar{\omega}-n\cdot\mathcal{P}\right)\chi_{\bar{n}}^{\bar{l}}|0\rangle \, \langle B|\bar{\chi}_n^l \delta\left(\omega-\bar{n}\cdot\mathcal{P}^\dagger\right) \frac{n\!\!\!/}{2}\Gamma_B \, \mathcal{H}_n^{\bar{c}}|0\rangle \ , \end{aligned} \tag{2.4.6}$$

where $\Gamma_A = \{\gamma_5, 1, \gamma_\perp^\mu\}$ and $T_{AB}^{^{2S+1}L_J} = \{1,\, \vec{p}_b\cdot\vec{\sigma}_\perp,\, p_{b\perp}^{(\mu}\sigma_\perp^{\nu)}\}$. The charge-conjugated contribution is understood in the η_b case.

The quarkonium state and the D mesons in Eq. (2.4.6) have respectively non-relativistic and HQET normalization:

$$\begin{aligned} \langle \chi_{bJ}(E',\vec{p}\,')|\chi_{bJ}(E,\vec{p})\rangle &= (2\pi)^3\delta^{(3)}(\vec{p}-\vec{p}\,') \ , \\ \langle D(v',k')|D(v,k)\rangle &= 2v^0\delta_{v,v'}(2\pi)^3\delta^{(3)}(\vec{k}-\vec{k}\,') \ , \end{aligned}$$

where v^0 is the 0th component of the 4-velocity v^μ.

The D-meson matrix elements can be expressed in terms of the D-meson light-cone distribution amplitudes:

$$\langle P|\bar{\chi}_n^l \frac{\bar{n}\!\!\!/}{2}\gamma^5 \, \delta\left(\omega-\bar{n}\cdot\mathcal{P}^\dagger\right)\mathcal{H}_n^{\bar{c}}|0\rangle = iF_P(\mu')\frac{\bar{n}\cdot v}{2}\phi_P(\omega,\mu') \ , \tag{2.4.7}$$

$$\langle V_L|\bar{\chi}_n^l \frac{\bar{n}\!\!\!/}{2} \, \delta\left(\omega-\bar{n}\cdot\mathcal{P}^\dagger\right)\mathcal{H}_n^{\bar{c}}|0\rangle = F_{V_L}(\mu')\frac{\bar{n}\cdot v}{2}\phi_{V_L}(\omega,\mu') \ , \tag{2.4.8}$$

$$\langle V_T|\bar{\chi}_n^l \frac{\bar{n}\!\!\!/}{2}\gamma_\perp^\mu \, \delta\left(\omega-\bar{n}\cdot\mathcal{P}^\dagger\right)\mathcal{H}_n^{\bar{c}}|0\rangle = F_{V_T}(\mu')\frac{\bar{n}\cdot v}{2}\varepsilon_\perp^\mu\phi_{V_T}(\omega,\mu') \ , \tag{2.4.9}$$

where $\varepsilon_\perp^\mu$ is the transverse polarization of the vector meson. The constants $F_A(\mu')$, with $A = \{P, V_L, V_T\}$, are related to the matrix elements of the local heavy-light currents in coordinate space. In the heavy-quark limit, where D and D^* are degenerate, F_A is the same for all the three states: $F \equiv F_P = F_{V_L} = F_{V_T}$. In this limit,

$$\langle 0|\bar{\xi}_n^{\bar{l}} \frac{\bar{n}\!\!\!/}{2}\gamma^5 h_n^c(0)|P\rangle = -iF(\mu')\frac{\bar{n}\cdot v'}{2} \,. \tag{2.4.10}$$

At tree level, the matrix element is proportional to the D-meson decay constant $f_D = 205.8 \pm 8.5 \pm 2.5$ MeV [59]. More precisely, $F(\mu') = f_D\sqrt{m_D}$, where the factor $\sqrt{m_D}$ is due to HQET normalization. The scale dependence of F is determined by the renormalization of heavy-light HQET currents. At one loop, Ref. [5] showed that

$$\frac{d}{d\ln\mu'}F(\mu') = -\gamma_F F(\mu') = 3C_F\frac{\alpha_s}{4\pi}F(\mu') \,. \tag{2.4.11}$$

The pNRQCD matrix elements can be expressed in terms of the heavy quarkonium wavefunctions. The operator $\chi_{\bar{b}}^\dagger \vec{p}_b \cdot \vec{\sigma}_\perp \psi_b$ contains a component with $J = 0$ and a component with $J = 2$ and $J_z = 0$, so its matrix element has non-vanishing overlap with both χ_{b0} and χ_{b2}. The operator $\chi_{\bar{b}}^\dagger p_b^{(\mu}\sigma_\perp^{\nu)}\psi_b$ instead has only contributions with $J = 2$ and $J_z = \pm 2$ and therefore it only overlaps with χ_{b2}. In terms of the bottomonium wavefunctions, the pNRQCD matrix elements are expressed as

$$\langle 0|\chi_{\bar{b}}^\dagger \vec{p}_b \cdot \vec{\sigma}_\perp \psi_b|\chi_{b0}\rangle = \frac{2}{\sqrt{3}}\sqrt{\frac{3N_c}{2\pi}}R'_{\chi_{b0}}(0,\mu') \,, \tag{2.4.12}$$

$$\langle 0|\chi_{\bar{b}}^\dagger \vec{p}_b \cdot \vec{\sigma}_\perp \psi_b|\chi_{b2}\rangle = -\sqrt{\frac{2}{15}}\sqrt{\frac{3N_c}{2\pi}}R'_{\chi_{b2}}(0,\mu') \,, \tag{2.4.13}$$

$$\langle 0|\chi_{\bar{b}}^\dagger p_b^{(\mu}\sigma_\perp^{\nu)}\psi_b|\chi_{b2}\rangle = (\varepsilon_{\mu\nu}^{(2)} + \varepsilon_{\mu\nu}^{(-2)})\sqrt{\frac{3N_c}{2\pi}}R'_{\chi_{b2}}(0,\mu') \,, \tag{2.4.14}$$

where $R'_{\chi_{bJ}}(0)$ is the derivative of the radial wavefunction of the χ_{bJ} evaluated at the origin. At leading order, the pNRQCD Hamiltonian does not depend on J, so, up to corrections of order w^2, $R'_{\chi_{b2}}(0) = R'_{\chi_{b0}}(0)$. The numerical pre-factors in Eqs. (2.4.12) and (2.4.13) follow from decomposing $\vec{p}_b \cdot \vec{\sigma}_\perp$ into components with definite J_z. $\varepsilon_{\mu\nu}^{(j)}$ is the polarization tensor of the χ_{b2} state, and Eq. (2.4.14) states that, at leading order

in the w^2 expansion, only the particles with polarization $J_z = \pm 2$ contribute to χ_{b2} decay into two transversely-polarized vector mesons. Similarly, one finds

$$\langle 0|\chi_{\bar{b}}^{\dagger}\psi_b|\eta_b\rangle = \sqrt{\frac{N_c}{2\pi}} R_{\eta_b}(0,\mu') \; . \tag{2.4.15}$$

The factorization of the matrix elements (2.4.6) implies that the decay rate also factorizes. For the decays of χ_{b0} and χ_{b2} into two pseudoscalar mesons or two longitudinally-polarized vector mesons, we find

$$\begin{aligned}\Gamma\left(\chi_{b0} \to AA\right) =& \frac{4}{3}\frac{m_D^2\sqrt{m_{\chi_{b0}}^2 - 4m_D^2}}{8\pi m_{\chi_{b0}}}\frac{3N_c}{2\pi}\left|C\left(\mu\right)\right|^2 \left|R'_{\chi_{b0}}(0,\mu')\right|^2 \\ & \left[F^2(\mu')\frac{n\cdot v'}{2}\frac{\bar{n}\cdot v}{2}\int\frac{d\omega}{\omega}\frac{d\bar{\omega}}{\bar{\omega}} T\left(\omega,\bar{\omega},\mu,\mu';\,{}^3P_J\right)\phi_A(\bar{\omega},\mu')\phi_A(\omega,\mu')\right]^2\end{aligned} \tag{2.4.16}$$

and

$$\begin{aligned}\Gamma\left(\chi_{b2} \to AA\right) =& \frac{2}{15}\frac{m_D^2\sqrt{m_{\chi_{b2}}^2 - 4m_D^2}}{8\pi m_{\chi_{b2}}}\frac{3N_c}{2\pi}\left|C\left(\mu\right)\right|^2 \left|R'_{\chi_{b2}}(0,\mu')\right|^2 \\ & \left[F^2(\mu')\frac{n\cdot v'}{2}\frac{\bar{n}\cdot v}{2}\int\frac{d\omega}{\omega}\frac{d\bar{\omega}}{\bar{\omega}} T\left(\omega,\bar{\omega},\mu,\mu';\,{}^3P_J\right)\phi_A(\bar{\omega},\mu')\phi_A(\omega,\mu')\right]^2 ,\end{aligned} \tag{2.4.17}$$

where $A = P, V_L$. For the decay of χ_{b2} into two transversely-polarized vector mesons, one finds the decay rate by summing over the possible transverse polarizations:

$$\begin{aligned}\Gamma\left(\chi_{b2} \to V_T V_T\right) =& \frac{2}{5}\frac{m_D^2\sqrt{m_{\chi_{b2}}^2 - 4m_D^2}}{8\pi m_{\chi_{b2}}}\frac{3N_c}{2\pi}\left|C\left(\mu\right)\right|^2 \left|R'_{\chi_{b2}}(0,\mu')\right|^2 \\ & \left[F^2(\mu')\frac{n\cdot v'}{2}\frac{\bar{n}\cdot v}{2}\int\frac{d\omega}{\omega}\frac{d\bar{\omega}}{\bar{\omega}} T\left(\omega,\bar{\omega},\mu,\mu';{}^3P_J\right)\phi_{V_T}(\bar{\omega},\mu')\phi_{V_T}(\omega,\mu')\right]^2 .\end{aligned} \tag{2.4.18}$$

In the case of η_b decay into a pseudoscalar and a longitudinally-polarized vector meson, we find

$$\begin{aligned}\Gamma\left(\eta_b \to PV_L + \text{c.c.}\right) =& \frac{m_D^2\sqrt{m_{\eta_b}^2 - 4m_D^2}}{8\pi m_{\eta_b}}\frac{N_c}{2\pi}\left|C\left(\mu\right)\right|^2 \left|R_{\eta_b}(0,\mu')\right|^2 \frac{1}{2}\left[F^2(\mu')\frac{n\cdot v'}{2}\frac{\bar{n}\cdot v}{2}\right. \\ & \left.\int\frac{d\omega}{\omega}\frac{d\bar{\omega}}{\bar{\omega}} T\left(\omega,\bar{\omega},\mu,\mu';\,{}^1S_0\right)\left(\phi_{V_L}(\bar{\omega},\mu')\phi_P(\omega,\mu') - \phi_{V_L}(\omega,\mu')\phi_P(\bar{\omega},\mu')\right)\right]^2 .\end{aligned} \tag{2.4.19}$$

Note that we are working in the limit $m_c \to \infty$, where the $m_{D^*} - m_D$ mass splitting vanishes.

The factorized formulas Eqs. (2.4.6) and (2.4.16) - (2.4.19) are the main results of this Chapter. Each decay rate of (2.4.16) - (2.4.19) depends on two calculable matching coefficients, C and T, and three non-perturbative, process-independent matrix elements, namely, two D-meson distribution amplitudes and the bottomonium wavefunction. In Sec. 2.5 we will provide a model-dependent estimate of the decay rates (2.4.16) - (2.4.19) and will discuss the phenomenological implications. We conclude this section by observing that all the non-perturbative matrix elements cancel out in the ratios $\Gamma(\chi_{b0} \to PP)/\Gamma(\chi_{b2} \to PP)$ and $\Gamma(\chi_{b0} \to V_L V_L)/\Gamma(\chi_{b2} \to V_L V_L)$, since the spin symmetry of pNRQCD guarantees $R'_{\chi_{b0}}(0) = R'_{\chi_{b2}}(0)$, at leading order in $\mathrm{EFT_{II}}$. Neglecting the χ_{b0} - χ_{b2} mass difference, we find, up to corrections of order w^2,

$$\Gamma(\chi_{b0} \to AA)/\Gamma(\chi_{b2} \to AA) = \frac{4}{3}\frac{15}{2} = 10 \ , \tag{2.4.20}$$

with $A = P, V_L$.

2.4.2 Running

The dependence of the matching coefficient $T(\omega, \bar{\omega}, \mu, \mu'; {}^{2S+1}L_J)$ and of the operators in Eqs. (2.4.16) - (2.4.19) on the scale μ' is driven by a RGE that can be obtained by renormalizing the $\mathrm{EFT_{II}}$ operators. The RGE for the $\mathrm{EFT_{II}}$ operators, which also defines the anomalous dimension $\gamma_{\mathrm{EFT_{II}}}$, is similar to Eq. (2.3.6),

$$\frac{d}{d\ln\mu'}\left[F^2(\mu')\mathcal{O}_{AB}^{{}^{2S+1}L_J}(\omega,\bar{\omega},\mu')\right] = \\ -\int d\omega' \int d\bar{\omega}' \gamma_{\mathrm{EFT_{II}}}(\omega,\omega';\bar{\omega},\bar{\omega}';\mu') F^2(\mu') \mathcal{O}_{AB}^{{}^{2S+1}L_J}(\omega',\bar{\omega}',\mu') \ . \tag{2.4.21}$$

To calculate the anomalous dimension at one loop, we compute the divergent part of the diagrams in Figs. 2.6 and 2.7. As mentioned in Sec. 2.2, the pNRQCD Lagrangian has the following structure,

$$L_{\mathrm{pNRQCD}} = \int d^3x \, \mathcal{L}^{usoft}_{\mathrm{NRQCD}} + L_{\mathrm{pot}} \ ,$$

where the superscript $usoft$ indicates that the gluons in the NRQCD Lagrangian are purely ultrasoft $(m_b w^2, m_b w^2)$, while $L_{\rm pot}$ contains four-fermions operators, which are non-local in space,

$$L_{\rm pot} = \int d^3x_1 d^3x_2 \psi^\dagger_\alpha(t,\vec{x}_1)\chi_\beta(t,\vec{x}_2)V_{\alpha\beta,\gamma\delta}(\vec{r})\chi^\dagger_\gamma(t,\vec{x}_2)\psi_\delta(t,\vec{x}_1) \; .$$

At leading order in $\alpha_s(m_b w)$ and r, V is the Coulomb potential

$$V_{\alpha\beta,\gamma\delta} = \frac{\alpha_s(m_b w)}{r} t^a_{\alpha\delta} t^a_{\gamma\beta} \; .$$

For the explicit form of higher-order potentials, see, for example, Refs. [9, 13]. Vertices from $L_{\rm pot}$ generate one-loop diagrams as the first diagram in Fig. 2.6. However, these diagrams do not give any contribution to the anomalous dimension at one loop. Indeed, the insertion of the Coulomb potential $1/r$ in Fig. 2.6 does not produce UV divergences. Insertions of the $1/m_b$ potentials yield divergences but the coefficient of the $1/m_b$ potential is proportional to $\alpha_s^2(m_b w)$, so it is not relevant if we are content with a NLL resummation. Insertions of $1/m_b^2$ potentials give divergences proportional to subleading operators, which can be neglected. The second diagram in Fig. 2.6 yields a result completely analogous to the last term in Eq. (2.3.9), with the only difference of a color pre-factor,

$$i\mathcal{M}_{\rm pNRQCD} = -i\frac{\alpha_s}{2\pi}\,\frac{C_F}{\varepsilon}\mathcal{O}^{^{2S+1}L_J}_{AB}(\omega,\bar{\omega},\mu) \; . \tag{2.4.22}$$

This divergence is completely canceled by the b-quark field renormalization constant Z_b, and hence the pNRQCD diagrams in Fig. 2.6 do not contribute to the anomalous dimension at one loop.

On the bHQET side, the third diagram in Fig. 2.7 is convergent, and hence it does not contribute to the anomalous dimension. The first two diagrams give

$$i\mathcal{M}_{\rm bHQET,\bar{n}} = i\int d\omega' d\bar{\omega}' \Delta(\omega,\omega',\,\bar{\omega},\bar{\omega}')\mathcal{O}^{^{2S+1}L_J}_{AB}(\omega',\bar{\omega}',\mu) \; , \tag{2.4.23}$$

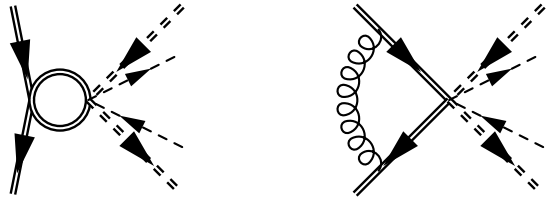

FIGURE 2.6. One-loop diagrams in pNRQCD. The first diagram contains insertions of quark-antiquark potentials. In the second diagram the gluon is ultrasoft.

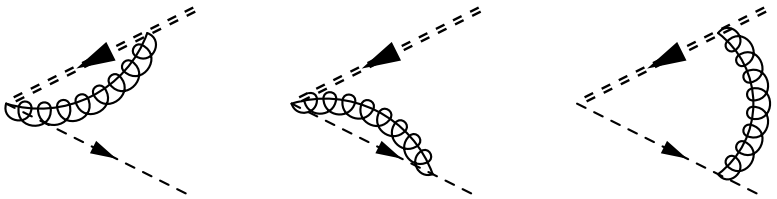

FIGURE 2.7. One-loop diagrams in bHQET. There are three analogous diagrams for the other copy of bHQET.

with

$$\Delta(\omega,\omega',\,\bar\omega,\bar\omega') = \frac{\alpha_s}{2\pi}C_F\delta(\omega-\omega')\left\{\delta\left(\bar\omega-\bar\omega'\right)\left[-\frac{1}{2\varepsilon^2}-\frac{1}{\varepsilon}\ln\left(\frac{\mu' n\cdot v'}{\bar\omega'}\right)+\frac{1}{\varepsilon}\right]\right.$$
$$\left.+\,\frac{1}{\varepsilon}\left[\theta\left(\bar\omega-\bar\omega'\right)\left(\frac{1}{\bar\omega-\bar\omega'}\right)_+ + \theta\left(\bar\omega'-\bar\omega\right)\theta\left(\bar\omega\right)\frac{\bar\omega}{\bar\omega'}\left(\frac{1}{\bar\omega'-\bar\omega}\right)_+\right]\right\}\,. \tag{2.4.24}$$

The diagrams for the bHQET copy in the n-direction give a result analogous to Eqs. (2.4.23) and (2.4.24), with $\bar\omega\to\omega$, $\bar\omega'\to\omega'$, and $n\cdot v'\to\bar n\cdot v$. Extracting $\gamma_{\mathrm{EFT_{II}}}$ from the divergence is again standard, just as we did in the case of $\gamma_{\mathrm{EFT_I}}$. After adding to Eq. (2.4.24) the bHQET field renormalization constants Z_h and Z_ξ for heavy and light quarks

$$Z_h = 1+\frac{1}{\varepsilon}\frac{\alpha_s}{2\pi}C_F\,,\qquad Z_\xi = 1-\frac{1}{\varepsilon}\frac{\alpha_s}{4\pi}C_F\,,$$

we find

$$\gamma_{\mathrm{EFT_{II}}}(\omega,\omega';\bar\omega,\bar\omega';\mu') = 2\gamma_F\,\delta\left(\omega-\omega'\right)\delta\left(\bar\omega-\bar\omega'\right)+\gamma_{\mathcal{O}}(\omega,\omega';\bar\omega,\bar\omega';\mu')\,, \tag{2.4.25}$$

with

$$\begin{aligned}
&\gamma_{\mathcal{O}}(\omega,\omega';\bar\omega,\bar\omega';\mu') \\
&= \frac{\alpha_s}{4\pi}\,4C_F\delta\left(\omega-\omega'\right)\delta\left(\bar\omega-\bar\omega'\right)\left[-1+\ln\left(\frac{\mu' n\cdot v'}{\bar\omega'}\right)+\ln\left(\frac{\mu'\bar n\cdot v}{\omega'}\right)\right] \\
&- \frac{\alpha_s}{4\pi}4C_F\delta\left(\omega-\omega'\right)\left[\theta\left(\bar\omega-\bar\omega'\right)\left(\frac{1}{\bar\omega-\bar\omega'}\right)_+ + \theta\left(\bar\omega'-\bar\omega\right)\theta\left(\bar\omega\right)\frac{\bar\omega}{\bar\omega'}\left(\frac{1}{\bar\omega'-\bar\omega}\right)_+\right] \\
&- \frac{\alpha_s}{4\pi}4C_F\delta\left(\bar\omega-\bar\omega'\right)\left[\theta\left(\omega-\omega'\right)\left(\frac{1}{\omega-\omega'}\right)_+ + \theta\left(\omega'-\omega\right)\theta\left(\omega\right)\frac{\omega}{\omega'}\left(\frac{1}{\omega'-\omega}\right)_+\right] .
\end{aligned} \tag{2.4.26}$$

The term proportional to γ_F in Eq. (2.4.25) reproduces the running of $F^2(\mu')$ (2.4.11). $\gamma_{\mathcal{O}}$ is responsible for the running of the D-meson distribution amplitudes and it agrees with the result found in Ref. [60]. Also, in Eq. (2.4.26) the coefficient of $\ln\mu'$ is proportional to $\Gamma_{\rm cusp}(\alpha_s)$. Note that, since the bHQET Lagrangian is spin-independent, the anomalous dimension does not depend on the spin or on the polarization of the D meson in the final state, at leading order in the power counting.

Using Eqs. (2.4.21) and (2.4.25) we find the following integro-differential RGE for the operator $\mathcal{O}(\omega,\bar\omega,\mu')$:

$$\frac{d}{d\ln\mu'}\mathcal{O}(\omega,\bar\omega,\mu') = -\int d\omega'\int d\bar\omega'\gamma_{\mathcal{O}}(\omega,\omega';\bar\omega,\bar\omega';\mu')\mathcal{O}(\omega',\bar\omega',\mu') \,, \tag{2.4.27}$$

where we have dropped both the subscripts A, B, and the superscript ${}^{2S+1}L_J$, since $\gamma_{\mathcal{O}}$ does not depend on the quantum numbers of the initial or final state. Using the fact that the convolution of $F^2(\mu')\,T(\omega,\bar\omega,\mu,\mu';\,{}^{2S+1}L_J)$ and the operator $\mathcal{O}_{AB}^{{}^{2S+1}L_J}(\omega,\bar\omega,\mu')$ is μ'-independent, we can write an equation for the coefficient,

$$\begin{aligned}
&\frac{d}{d\ln\mu'}[F^2(\mu')\,T(\omega,\bar\omega,\mu,\mu')] \\
&\qquad = \int d\omega'\int d\bar\omega'\frac{\omega}{\omega'}\frac{\bar\omega}{\bar\omega'}F^2(\mu')\,T(\omega',\bar\omega',\mu,\mu')\gamma_{\mathcal{O}}(\omega',\omega;\bar\omega',\bar\omega;\mu') \\
&\qquad = \int d\omega'\int d\bar\omega' F^2(\mu')\,T(\omega',\bar\omega',\mu,\mu')\gamma_{\mathcal{O}}(\omega,\omega';\bar\omega,\bar\omega';\mu') \,,
\end{aligned} \tag{2.4.28}$$

where the last line follows from the property of $\gamma_{\mathcal{O}}$ at one loop,

$$\frac{\omega}{\omega'}\frac{\bar\omega}{\bar\omega'}\gamma_{\mathcal{O}}(\omega',\omega;\bar\omega',\bar\omega;\mu') = \gamma_{\mathcal{O}}(\omega,\omega';\bar\omega,\bar\omega';\mu') \,,$$

as can be explicitly verified from the expression in Eq. (2.4.26).

Eq. (2.4.28) can be solved following the methods described in Ref. [60]. We discuss the details of the solution in App. A, where we derive the analytic expressions for $T(\omega, \bar{\omega}, \mu, \mu'; {}^3P_J)$ and $T(\omega, \bar{\omega}, \mu, \mu'; {}^1S_0)$, with the initial conditions at the scale $\mu'_c = m_c$ expressed in Eq. (2.4.4).

2.5 Decay Rates and Phenomenology

In Sec. 2.4.1 we gave the factorized expressions for the decay rates (2.4.16) - (2.4.19): $\Gamma(\chi_{b0,2} \to PP)$, $\Gamma(\chi_{b0,2} \to V_L V_L)$, $\Gamma(\chi_{b2} \to V_T V_T)$, and $\Gamma(\eta_b \to PV_L + \text{c.c.})$. In Secs. 2.3.2 and 2.4.2 we exploited the RGEs (2.3.8) and (2.4.28) to run the scales μ and μ', respectively, from the matching scales $\mu = 2m_b$ and $\mu' = m_c$ to the natural scales that contribute to the matrix elements, $\mu = m_c$ and $\mu' \sim 1$ GeV, resumming in this way Sudakov logarithms of the ratios $m_c/2m_b$ and $m_c/1$ GeV.

We proceed now to estimate the decay rates (2.4.16) - (2.4.19). In order to do so, we need to evaluate the following ingredients: the light-cone distribution amplitudes of the D meson and of the longitudinally- and transversely-polarized D^* mesons, and the wavefunctions of the states η_b and χ_{bJ}. In principle, these non-perturbative objects could be extracted from other η_b, χ_b, and D-meson observables. In the case of the η_b, the value of the wavefunction at the origin can be obtained from a measurement of the inclusive hadronic width or of the decay rate for the electromagnetic process $\eta_b \to \gamma\gamma$, since they are both proportional to $|R_{\eta_b}(0)|^2$. Unfortunately, at the moment there are not sufficient data on η_b decays. Another way to proceed is to use the spin symmetry of the leading-order pNRQCD Hamiltonian, which implies $R_{\eta_b}(0) = R_\Upsilon(0)$, and to extract the Upsilon wavefunction from $\Gamma(\Upsilon \to e^+e^-) = 1.28 \pm 0.07$ KeV [61]. Using the leading-order expression for $\Gamma(\Upsilon \to e^+e^-)$ [62], one finds $|R_\Upsilon(0)|^2 = 6.92 \pm 0.38\,\text{GeV}^3$, where the error only includes the experimental uncertainty. The above value is in good agreement with the lattice evaluation by Bodwin, Sinclair, and Kim [63] and it falls within the range of values obtained with four different potential

models, as listed in Ref. [64].

$|R'_{\chi_{b0,\,2}}(0)|^2$ can be obtained from the electromagnetic decay $\chi_{b0,2} \to \gamma\gamma$. Unfortunately, such decay rates have not been measured yet. The values listed in Ref. [64] range from a minimum of $|R'_{\chi_{bJ}}(0)|^2 = 1.417$ GeV^5, obtained with the Buchmuller-Tye potential [65], to a maximum of $|R'_{\chi_{bJ}}(0)|^2 = 2.067$ GeV^5, obtained with a Coulomb-plus-linear potential. The lattice value is roughly of the same size, $|R'_{\chi_{bJ}}(0)|^2 = 2.3$ GeV^5, with an uncertainty of about 15% [63]. We use this value in our estimate.

For the pseudoscalar D-meson distribution amplitude we use two model functions widely adopted in the study of B physics. A first possible choice, suggested for example in Ref. [60], is a simple exponential decay:

$$\phi_{P,0}^{\rm Exp}(\omega,\mu' = 1{\rm GeV}) = \theta(\omega)\frac{\omega}{\lambda_{\rm D}^2}\exp\left(-\frac{\omega}{\lambda_{\rm D}}\right) \ . \tag{2.5.1}$$

Another form, suggested in Ref. [66], is

$$\phi_{P,\,0}^{\rm Braun}(\omega,\mu' = 1\,{\rm GeV}) = \theta(\tilde\omega)\frac{4}{\lambda_D\pi}\frac{\tilde\omega}{1+\tilde\omega^2}\left[\frac{1}{1+\tilde\omega^2} - \frac{2(\sigma_D-1)}{\pi^2}\ln\tilde\omega\right] \ , \tag{2.5.2}$$

where $\tilde\omega = \omega/\mu'$. The theta function in Eqs. (2.5.1) and (2.5.2) reflects the fact that the distribution amplitudes $\phi_A(\omega,\mu')$, with $A = \{P, V_L, V_T\}$, have support on $\omega > 0$ [67].

The subscript 0 indicates that these functional forms are valid in the D-meson rest frame, with a HQET velocity-label $v_0 = (1,0,0,0)$. With the definition we adopt in Eq. (2.4.7), the distribution amplitude is not boost-invariant and in the bottomonium rest frame, in which the D meson has a velocity $(n\cdot v, \bar n\cdot v, 0) \sim (m_c/2m_b, 2m_b/m_c, 0)$, it becomes

$$\phi_P(\omega,\mu') = \frac{1}{\bar n\cdot v}\phi_{P,\,0}\left(\frac{\omega}{\bar n\cdot v},\mu'\right) \ , \tag{2.5.3}$$

as shown in App. B. λ_D and σ_D in Eqs. (2.5.1) and (2.5.2) are, respectively, the first inverse moment and the first logarithmic moment of the D-meson distribution amplitude in the D-meson rest frame,

$$\lambda_D^{-1}(\mu') = \int_0^\infty \frac{d\omega}{\omega}\phi_{P,0}(\omega,\mu') \ ,$$

$$\sigma_D(\mu')\lambda_D^{-1}(\mu') = -\int_0^\infty \frac{d\omega}{\omega} \ln\left(\frac{\omega}{\mu'}\right) \phi_{P,0}(\omega,\mu') \ .$$

Furthermore we assume that the vector-meson distribution amplitudes $\phi_{V_L}(\omega)$ and $\phi_{V_T}(\omega)$ have the same functional form as $\phi_P(\omega)$, but with different parameters $\lambda_{D_L^*}$, $\sigma_{D_L^*}$ and $\lambda_{D_T^*}$, $\sigma_{D_T^*}$.

The D-meson distribution amplitude and its moments have not been intensively studied unlike, for example, the B-meson distribution amplitude. Therefore, we invoke heavy-quark symmetry and use the moments of the B-meson distribution amplitude in order to estimate the decay rate. However, the value of λ_B is affected by a noticeable uncertainty. Using QCD sum rules, Braun *et al.* estimated [66] $\lambda_B(\mu' = 1\,\text{GeV}) = 0.460 \pm 0.110$ GeV, where the uncertainty is about 25%. Other authors [68, 69, 70] give slightly different central values and comparable uncertainties, so that λ_B falls in the range $0.350\ \text{GeV} < \lambda_B < 0.600\ \text{GeV}$. The first logarithmic moment σ_D is given in Ref. [66], $\sigma_D = \sigma_B(\mu' = 1\,\text{GeV}) = 1.4 \pm 0.4$. We assume that the moments of the D^*-meson distribution amplitudes fall in the same range as the moments of $\phi_P(\omega)$.

We evaluate numerically the convolution integrals in Eqs. (2.4.16) - (2.4.19). We choose the matching scales μ_b and μ_c' to be $2m_b$ and m_c respectively. Using the RGEs we run the matching coefficients down to the scales $\mu = m_c$ and $\mu' = 1$ GeV. For the b and c quark masses we adopt the 1S mass definition [71],

$$\begin{aligned} m_b(1S) &= \frac{m_\Upsilon}{2} = 4730.15 \pm 0.13 \text{ MeV} \ , \\ m_c(1S) &= \frac{m_{J/\psi}}{2} = 1548.46 \pm 0.01 \text{ MeV} \ . \end{aligned} \tag{2.5.4}$$

The values of α_s at the relevant scales are [61] $\alpha_s(2m_b) = 0.178 \pm 0.005$, $\alpha_s(m_c) = 0.340 \pm 0.020$, and $\alpha_s(1\,\text{GeV}) \sim 0.5$. With these choices, the value of g in Eq. (A.5) is $g(m_c, 1\,\text{GeV}) = -0.12 \pm 0.02$.

The decay rates $\Gamma(\chi_{bJ} \to AA)$ with $A = \{P, V_L, V_T\}$, (2.4.16) - (2.4.18), depend on the masses of the χ_{bJ} and of the D mesons, whose most recent values are reported in Ref. [61]. Since the effects due to the mass splitting of the χ_{bJ} and D multiplets

are subleading in the EFT power counting, we use in the evaluation the average mass of the χ_{bJ} multiplet and the average mass of D and D^* mesons: $m_{\chi_{bJ}} = 9898.87 \pm 0.28 \pm 0.31$ MeV and $m_D = 1973.27 \pm 0.18$ MeV. Therefore, the velocity of the D mesons in χ_{bJ} decay is $\bar{n} \cdot v = n \cdot v' = m_{\chi_{bJ}}/m_D = 5.02$, with negligible error. The decay rate $\Gamma(\eta_b \to PV_L + \text{c.c.})$ (2.4.19) depends on the mass of the η_b, which has been recently measured: $m_{\eta_b} = 9388.9^{+3.1}_{-2.3} \pm 2.7$ MeV [53]. The velocity of the D meson in the η_b decay is $\bar{n} \cdot v = n \cdot v' = m_{\eta_b}/m_D = 4.76$, again with negligible error.

The decay rate $\Gamma(\chi_{b0} \to PP)$ (2.4.16), obtained with ϕ^{Exp} and ϕ^{Braun} separately, is shown in Fig. 2.8. In order to see the impact of resumming Sudakov logarithms, we show for both distribution amplitudes the results with (i) the LL and NLL resummations and (ii) without any resummation at all. In the plots, we call the resummed results NLL-resummed, indicating that Sudakov logarithms are resummed up to NLL. For both distribution amplitudes the resummation does have a relevant effect on the decay rate. In the case of ϕ^{Exp} the resummation decreases the decay rate by a factor of $2 - 1.5$ as λ_D goes from the lowest to the highest value under consideration. In the case of ϕ^{Braun} the decay rate decreases too, for example, by a factor 1.5 when $\sigma_D = 1.4$. In Fig. 2.9 we compare the decay rates obtained with the two distribution amplitudes. Over the range of λ_D we are considering the two decay rates are in rough agreement with each other.

Figs. 2.8 - 2.9 also describe the relation between the decay rate $\Gamma(\chi_{b0} \to V_L V_L)$ and $\lambda_{D_L^*}$. According to Eqs. (2.4.17) and (2.4.18), the processes $\chi_{b2} \to PP$, $\chi_{b2} \to V_L V_L$, and $\chi_{b2} \to V_T V_T$ show an analogous dependence on the first inverse moments of the light-cone distribution amplitudes, and they differ from Figs. 2.8 - 2.9 by constant pre-factors. Therefore, we do not show explicitly their plots.

Qualitatively, Figs. 2.8 - 2.9 show a dramatic dependence of the decay rate on the inverse moment λ_D. Using Eqs. (2.4.16), (2.5.3) and (A.16), one can show that when ϕ^{Braun} is used, the decay rate is proportional to λ_D^{-4}, while it scales as λ_D^{-6-4g} when we adopt ϕ^{Exp}, with g defined in Eq. (A.5). As a consequence, the decay rate

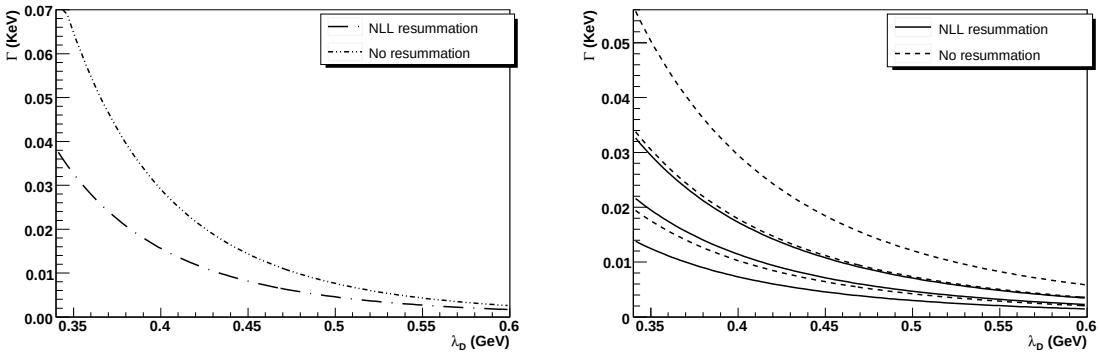

FIGURE 2.8. $\Gamma(\chi_{b0} \to PP)$ as a function of λ_D, calculated with the distribution amplitudes $\phi^{\rm Exp}$ (*left*) and $\phi^{\rm Braun}$ (*right*). The dash dotted and solid lines denote the NLL-resummed decay rate. For comparison, the decay rate without resummation is also shown, denoted by dash double-dotted (*left*) and dashed (*right*) lines. For $\phi^{\rm Braun}$ we vary the parameter σ_D from $\sigma_D = 1$ (lower curve) to $\sigma_D = 1.4$ (middle curve) to $\sigma_D = 1.8$ (upper curve).

drops by an order of magnitude when λ_D goes from 0.350 GeV to 0.600 GeV. The particular sensitivity of exclusive bottomonium decays into two charmed mesons to the light-cone structure of the D meson —much stronger than usually observed in D- and B-decay observables— is due to the dependence of the amplitude on the product of two distributions (one for each meson) and to the non-trivial dependence of the matching coefficient T on the light-quark momentum labels ω and $\bar{\omega}$ at tree level. On one hand, the strong dependence on a relatively poorly known quantity prevents us from predicting the decay rate $\Gamma(\chi_{b0} \to DD)$. On the other hand, however, it suggests that, if the decay rate is measured, this channel could be used to better determine interesting properties of the D-meson distribution amplitude, such as λ_D and σ_D. The viability of this suggestion relies on the control over the theoretical error attached to the curves in Fig. 2.8 and on the actual chances to observe the process $\chi_b \to DD$ at current experiments.

The uncertainty of the decay rate stems mainly from three sources. First, there are corrections coming from subleading EFT operators. In matching NRQCD+SCET onto pNRQCD + bHQET (Sec. 2.4.1), we neglected the subleading EFT_{II} operators

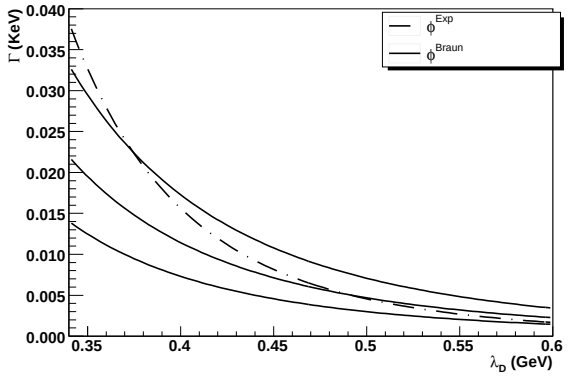

FIGURE 2.9. $\Gamma(\chi_{b0} \to PP)$ as a function λ_D. The dash dotted line denotes the decay rate calculated with $\phi^{\rm Exp}$, while the three solid lines with $\phi^{\rm Braun}$. For $\phi^{\rm Braun}$ we vary the value of the parameter σ_D from $\sigma_D = 1$ (lower curve) to $\sigma_D = 1.4$ (middle curve) to $\sigma_D = 1.8$ (upper curve).

that are suppressed by powers of $\Lambda_{\rm QCD}/m_c$ and w^2, relative to the leading $\text{EFT}_{\rm II}$ operators in Eqs. (2.4.2) and (2.4.3). In matching QCD onto NRQCD + SCET (Sec. 2.3.1), we kept only $J_{\text{EFT}_{\rm I}}$ (2.3.2) and neglected subleading $\text{EFT}_{\rm I}$ operators, suppressed by powers of λ and w^2. These subleading $\text{EFT}_{\rm I}$ operators would match onto subleading $\text{EFT}_{\rm II}$ operators, suppressed by powers of $\Lambda_{\rm QCD}/m_c$ and w^2. Using $w^2 \sim 0.1$ and $\Lambda_{\rm QCD}/m_c \sim 0.3$, we find a conservative estimate for the non-perturbative corrections to be about 30%.

Second, there are perturbative corrections to the matching coefficients C and T. Since $\alpha_s(2m_b) = 0.178$, we expect a 20% correction from the one-loop contributions in matching QCD onto NRQCD + SCET. In the second matching step, similarly, the one-loop corrections to $T(\omega, \bar\omega, \mu, \mu';\, ^{2S+1}L_J)$ would be proportional to $\alpha_s(m_c) \sim 30\%$. We can get an idea of their relevance by estimating the dependence of the decay rate (2.4.16) on the matching scales μ_b and μ_c'. If the matching coefficients C and T and the anomalous dimensions $\gamma_{\text{EFT}_{\rm I}}$ and $\gamma_{\mathcal{O}}(\omega, \omega', \bar\omega, \bar\omega'; \mu')$ were known at all orders, the decay rate would be independent of the matching scales μ_b and μ_c'. However, since we only know the first terms in the perturbative expansions, the decay rate bears a residual renormalization-scale dependence, whose size is determined by the first

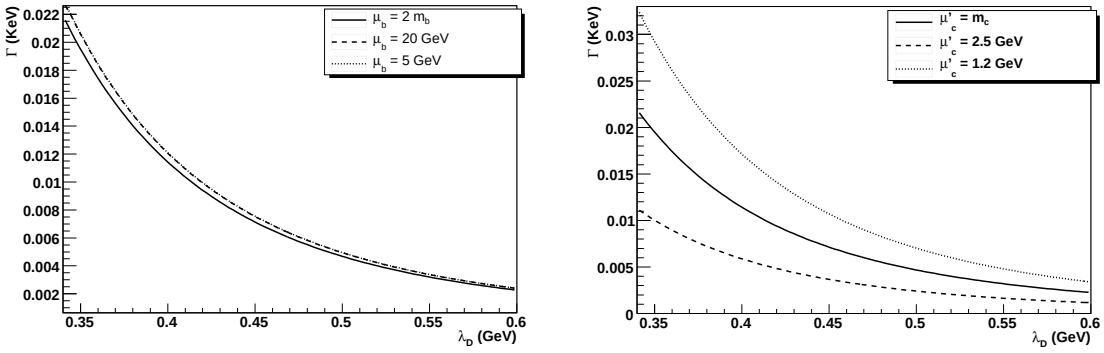

FIGURE 2.10. *Left*: Scale dependence of $\Gamma(\chi_{b0} \to PP)$ on the matching scale μ_b. We vary μ_b from a central value $\mu_b = 2m_b$ (solid line) to a maximum of $\mu_b = 20$ GeV (dashed line) and a minimum of $\mu_b = 5$ GeV (dotted line). The dashed and dotted lines overlap almost perfectly. *Right*: Scale dependence of $\Gamma(\chi_{b0} \to PP)$ on the matching scale μ'_c. We varied μ'_c from a central value of $\mu'_c = m_c$ (solid line) to a maximum of $\mu'_c = 2.5$ GeV (dashed line) and a minimum of $\mu'_c = 1.2$ GeV (dotted line).

neglected terms.

In Fig. 2.10 we show the effect of varying μ_b between $4m_b \sim 20$ GeV and $m_b \sim 5$ GeV on the decay rate, using $\phi^{\rm Braun}$. The solid line represents the choice $\mu_b = 2m_b$, while the dashed and dotted lines, which overlap almost perfectly, correspond respectively to $\mu_b = 20$ GeV and $\mu_b = 5$ GeV. The dependence on μ_b is mild, its effect being a variation of about 5%. We obtain analogous results for the decay rate computed with $\phi^{\rm Exp}$, which are not shown here in order to avoid redundancy.

On the other hand, even after the resummation, the decay rate strongly depends on μ'_c. We vary this scale between 1.2 GeV and 2.5 GeV and we observe an overall variation of about 50%. We expect the scale dependence to be compensated by the one-loop corrections to the matching coefficient $T(\omega, \bar{\omega}, \mu, \mu'; {}^3P_J)$. This observation is reinforced by the fact that the numerical values of the running factors $U(\mu_b, \mu)$ and $V(\mu'_c, \mu')$ (defined respectively in Eqs. (2.3.22) and (A.6)) at NLL accuracy are smaller than expected on the basis of naive counting of the logarithms. As a consequence, the next-to-leading-order corrections to the matching coefficient could be as large as

the effect of the NLL resummation. In the light of Fig. 2.10, the one-loop correction to $T(\omega, \bar{\omega}, \mu, \mu'; {}^3P_J)$ seems to be an important ingredient for a reliable estimate of the decay rate.

A third source of error comes from the unknown functional form of the D-meson distribution amplitude. For the study of the B-meson shape function, an expansion in a complete set of orthonormal functions has recently been proposed and it has provided a systematic procedure to control the uncertainties due to the unknown functional form [72]. The same method should be generalized to the B- and D-meson distribution amplitudes, in order to reduce the model dependence of the decay rate. We leave such an analysis to future work.

To summarize, the calculation of the one-loop matching coefficients and the inclusion of power corrections of order $\Lambda_{\rm QCD}/m_c$ appear to be necessary to provide a decay rate with an accuracy of 10%, that would make the decays $\chi_{bJ} \to D^+D^-$, $\chi_{bJ} \to D^0\bar{D}^0$ competitive processes to improve the determination of λ_D and σ_D, if the experimental decay rate is observed with comparable accuracy.

We estimate the decay rate $\Gamma(\eta_b \to PV_L + \text{c.c.})$ (2.4.19) using $\phi^{\rm Exp}$ and $\phi^{\rm Braun}$ for both ϕ_P and ϕ_{V_L}. In the limit $m_c \to \infty$, spin symmetry of the bHQET Lagrangian would imply the equality of the pseudoscalar and vector distribution amplitudes, $\phi_P = \phi_{V_L}$, and hence the vanishing of the decay rate $\Gamma(\eta_b \to PV_L + \text{c.c.})$. Assuming spin-symmetry violations, the decay rate depends on (i) the two parameters $\bar{\lambda}_D = (\lambda_D + \lambda_{D_L^*})/2$ and $\delta = (\lambda_{D_L^*} - \lambda_D)/(\lambda_D + \lambda_{D_L^*})$, if $\phi^{\rm Exp}$ is used, and on (ii) three parameters $\bar{\lambda}_D$, δ, and $|\sigma_{D_L^*} - \sigma_D|$, if $\phi^{\rm Braun}$ is used.

The two plots in the left column of Fig. 2.11 show the decay rate, computed with $\phi^{\rm Exp}$, as a function of $\bar{\lambda}_D$ with δ adopting various values, and as a function of δ with $\bar{\lambda}_D$ now being the parameter. In the right column, the decay rate computed with $\phi^{\rm Braun}$ is shown. Since in this case the decay rate does not strongly depend on δ, we fix it at $\delta = 0$ and we show the dependence of the decay rate on $\bar{\lambda}_D$ and $|\sigma_{D_L^*} - \sigma_D|$. We "normalize" the difference between the first logarithmic moments by

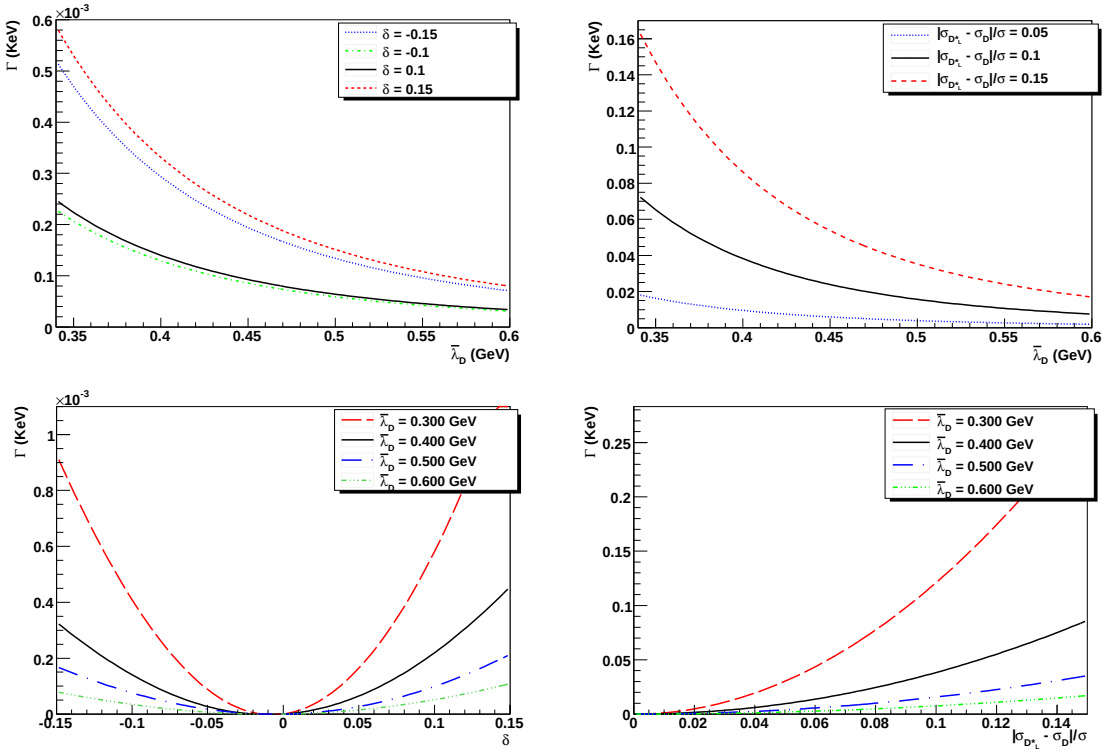

FIGURE 2.11. *Left*: $\Gamma(\eta_b \to PV_L + \text{c.c.})$ as a function of λ_D and δ, computed using exponential distribution amplitudes ϕ_P^{Exp} and $\phi_{V_L}^{\text{Exp}}$. *Right*: $\Gamma(\eta_b \to PV_L + \text{c.c.})$ as a function of λ_D and $|\sigma_{D_L^*} - \sigma_D|/\sigma$, computed with the Braun distribution amplitudes ϕ_P^{Braun} and $\phi_{V_L}^{\text{Braun}}$.

dividing them by $\sigma = 2\sigma_D$.

The most striking feature of Fig. 2.11 is the huge sensitivity to the chosen functional form. Though a precise comparison is difficult, due to the dependence on different parameters, the decay rate increases by two orders of magnitude when we switch from ϕ^{Exp} to ϕ^{Braun}. Once again, this effect hinders our ability to predict $\Gamma(\eta_b \to PV_L + \text{c.c.})$ but it opens up the interesting possibility to discriminate between different model distribution amplitudes.

Using Eqs. (2.4.19) and (A.17), we know that $\Gamma(\eta_b \to PV_L + \text{c.c.})$ goes like $\bar{\lambda}_D^{-4-4g}$ when ϕ^{Exp} used or $\bar{\lambda}_D^{-4}$ when ϕ^{Braun} used. Fig. 2.11 appears to confirm this strong dependence on $\bar{\lambda}_D$. The plots in the lower half of Fig. 2.11 reflect the fact that the decay rate vanishes if one assumes $\phi_P(\omega) = \phi_{V_L}(\omega)$.

We conclude this section with the determination of the branching ratios $\mathcal{B}(\chi_{b0} \to PP) = \Gamma(\chi_{b0} \to PP)/\Gamma(\chi_{b0} \to \text{light hadrons})$ and $\mathcal{B}(\eta_b \to PV_L + \text{c.c.}) = \Gamma(\eta_b \to PV_L + \text{c.c.})/\Gamma(\eta_b \to \text{light hadrons})$. At leading order in pNRQCD, the only non-perturbative parameter involved in the inclusive decay width of the η_b is $|R_{\eta_b}(0)|^2$ [6],

$$\Gamma(\eta_b \to \text{light hadrons}) = \frac{2\text{Im}f_1(^1S_0)}{m_b^2}\frac{N_c}{2\pi}|R_{\eta_b}(0)|^2 \,. \tag{2.5.5}$$

Therefore, $\mathcal{B}(\eta_b \to PV_L + \text{c.c.})$ does not depend on the quarkonium wavefunction and the only non-perturbative parameters in $\mathcal{B}(\eta_b \to PV_L + \text{c.c.})$ are those describing the D-meson distribution amplitudes.

For P-wave states, the inclusive decay rate was obtained in Refs. [6, 73], where the contributions of the configurations in which the quark-antiquark pair is in a color-octet S-wave state were first recognized. In pNRQCD the inclusive decay rate is written as [74, 75]

$$\Gamma(\chi_{b0} \to \text{light hadrons}) = \frac{1}{m_b^4}\frac{3N_c}{\pi}|R'_{\chi_b}(0)|^2\left[\text{Im}f_1(^3P_0) + \frac{1}{9N_c^2}\text{Im}f_8(^3S_1)\mathcal{E}\right] \,, \tag{2.5.6}$$

where the color-octet matrix element has been expressed in terms of the heavy quarkonium wavefunction and of the gluonic correlator $\mathcal{E}$, whose precise definition is given in Ref. [74]. $\mathcal{E}$ is a universal parameter and is completely independent of any particular heavy quarkonium state under consideration. Its value has been obtained by fitting to existing charmonium data and, thanks to the universality, the same value can be used to predict properties of bottomonium decays. It is found in Ref. [74] $\mathcal{E} = 5.3\,^{+3.5}_{-2.2}$. The matching coefficients in Eqs. (2.5.5) and (2.5.6) are known to one loop. For the updated value we refer to Ref. [76] and references therein. For reference, the tree-level values of the coefficients are as follows [6]:

$$\begin{aligned} &\text{Im}f_1(^1S_0) = \alpha_s^2(2m_b)\pi\frac{C_F}{2N_c} \,, \quad \text{Im}f_1(^3P_0) = 3\alpha_s^2(2m_b)\pi\frac{C_F}{2N_c} \,, \\ &\text{Im}f_8(^3S_1) = \frac{n_f}{6}\alpha_s^2(2m_b)\pi \,. \end{aligned} \tag{2.5.7}$$

With the above parameters, we plot $\mathcal{B}(\chi_{b0} \to PP)$ and $\mathcal{B}(\eta_b \to PV_L + \text{c.c.})$ as

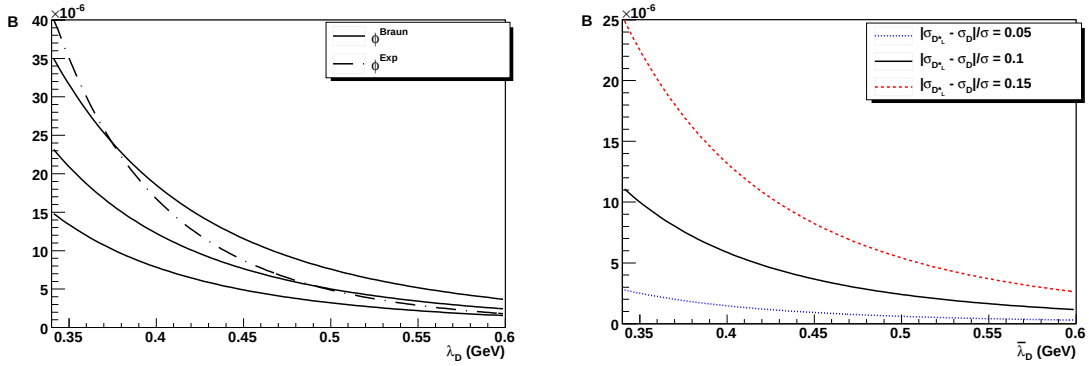

FIGURE 2.12. Branching ratios $\mathcal{B}(\chi_{b0} \to PP)$ (*left*) and $\mathcal{B}(\eta_b \to PV_L + \text{c.c.})$ (*right*). The latter is computed using the distribution amplitude ϕ^{Braun}.

a function of λ_D and $\bar{\lambda}_D$, respectively, in Fig. 2.12. Over the range of λ_D we are considering, $\mathcal{B}(\chi_{b0} \to PP)$ varies between $4 \cdot 10^{-5}$ and $4 \cdot 10^{-6}$; it is approximately one or two orders of magnitude smaller than the branching ratios observed in Ref. [54] for χ_{bJ} decays into light hadrons. $\mathcal{B}(\eta_b \to PV_L + \text{c.c.})$ depends on the choice of the distribution amplitude. Choosing the parameterization ϕ^{Braun} (2.5.2), it appears that, despite the suppression at $|\sigma_{D_L^*} - \sigma_D| = 0$, $\mathcal{B}(\eta_b \to PV_L + \text{c.c.})$ assumes values comparable to $\mathcal{B}(\chi_{b0} \to PP)$ even for a small deviation from the spin-symmetry limit. If ϕ^{Exp} is chosen, the branching ratio is suppressed over a wide range of $|\sigma_{D_L^*} - \sigma_D|$. The branching ratio $\mathcal{B}(\eta_b \to PV_L + \text{c.c.})$ was first estimated in [77]. The authors of [77] assumed that the exclusive decays into DD^* dominate the inclusive decay into charm, $\Gamma(\eta_b \to PV_L + \text{c.c.}) \sim \Gamma(\eta_b \to c\bar{c} + X)$. With this assumption, they estimated the branching ratio to be in the range $10^{-3} < \mathcal{B}(\eta_b \to PV_L + \text{c.c.}) < 10^{-2}$. Our analysis shows that such an assumption does not appear to be justified in the range of $\bar{\lambda}_D$ considered in Fig. 2.12, while it would be appropriate for smaller values of the first inverse moments, for example for $\bar{\lambda}_D \sim 0.200$ GeV if the distribution amplitudes are described by ϕ^{Braun}.

Our estimates indicate that observing the exclusive processes $\eta_b \to DD^* + \text{c.c.}$ and $\chi_b \to DD$ would be extremely challenging. A preliminary analysis for $\chi_b \to D^0\bar{D}^0$ [78] suggests that the number of $\Upsilon(2S)$ produced at BABAR allows for the measurement

of a branching ratio $\mathcal{B}(\chi_{b0} \to D^0 \bar{D}^0) \sim 10^{-3}$, which is two or three orders of magnitude bigger than the values in Fig. 2.12. An even bigger branching ratio would be required for the smaller $\Upsilon(2S)$ sample of CLEO. However, we stress once again the strong dependence of the decay rates on the values of the first inverse moments. In particular, our estimates rely on the relation $\lambda_D = \lambda_B$, which is valid in the limit of $m_b, m_c \to \infty$; even small corrections to the heavy flavor symmetry, if they had the effect of shifting the value of λ_D towards the range $0.250 - 0.350$ GeV, could considerably increase the branching ratios.

2.6 Conclusions

In this Chapter we have analyzed the exclusive decays of the C-even bottomonia into a pair of charmed mesons. We approached the problem using a series of EFTs that lead to the factorization formulas for the decay rates (Eqs. (2.4.16) - (2.4.19)), valid at leading order in the EFT power counting and at all orders in α_s. We improved the perturbative results by resumming Sudakov logarithms of the ratios of the characteristic scales that are germane to the dynamics of the processes.

The decay rates (2.4.16) - (2.4.19) receive both perturbative and non-perturbative corrections. Perturbative corrections come from loop corrections to the matching coefficients C and T, which are respectively of order $\alpha_s(2m_b) \sim 0.2$ and $\alpha_s(m_c) \sim 0.3$. The largest non-perturbative contribution could be as big as $\Lambda_{\rm QCD}/m_c$, which would amount approximately to a 30% correction. Therefore, corrections to the leading-order decay rates could be noticeable, as the strong dependence of the decay rates on the renormalization-scale μ_c' suggests. However, the EFT approach shown in this Chapter allows for a systematic treatment of both perturbative corrections and power-suppressed operators, so that, if the experimental data require, it is possible to extend the present analysis beyond the leading order.

For simplicity, we have focused in this Chapter on the decays of C-even bottomonia, in which cases the decays proceed via two intermediate gluons and both the

matching coefficients C and T are non-trivial at tree level. The same EFT approach can be applied to the decays of C-odd states, in particular, to the decays $\Upsilon \to DD$ and $\Upsilon \to D^*D^*$, with the complication that the matching coefficient T arises only at one-loop level. Moreover, the same EFT formalism developed in this Chapter can be applied to the study of the channels that have vanishing decay rates at leading order in the power counting, such as $\eta_b \to D^*D^*$, $\Upsilon \to DD^* + \text{c.c.}$, and $\chi_{b2} \to DD^* + \text{c.c.}$. Experimental data for the charmonium system show that, for the decays of charmonium into light hadrons, the expected suppression of the subleading twist processes is not seen. It is interesting to see whether such an effect appears in bottomonium decays into two charmed mesons, using the EFT approach of this Chapter to evaluate the power-suppressed decay rates.

Finally, in Sec. 2.5 we used model distribution amplitudes to estimate the decay rates. The most evident, qualitative feature of the decay rates is the strong dependence on the parameters of the D-meson distribution amplitude. Even though this feature may prevent us from giving reliable estimates of the decay rates or of the branching ratios, it makes the channels analyzed here ideal candidates for the extraction of important D-meson parameters, when the branching ratios can be observed with sufficient accuracy.

Chapter 3

T Violation in Nuclear Systems

3.1 Introduction

Time-reversal (T) and CP violation have been a subject of intense interest for nearly half a century. The Standard Model with three families has a natural source of CP violation in the form of a complex phase in the Cabibbo-Kobayashi-Maskawa (CKM) quark-mixing matrix. However, this violation is small in the sense that it comes [79] in a combination of CKM parameters $J_{CP} \simeq 3 \cdot 10^{-5} \ll 1$. Moreover, this mechanism appears to be insufficient for electroweak baryogenesis [80]. As a consequence, it has been hoped that the study of T violation will offer a window into new physics. In this thesis, we study systematically the effects on hadronic and electromagnetic interactions of the lowest-dimension sources of T violation that can be added to the QCD Lagrangian, including all the possible TV operators up to dimension 6.

CP violation has been observed in kaon and B-meson systems at a level consistent with Standard Model expectations [1]. On the other hand, electric dipole moments (EDMs) signal T violation as well, but they are relatively insensitive to the CKM phase because they involve flavor-diagonal CP violation. Indeed, in the Standard Model with $\bar{\theta} = 0$, the neutron EDM, for example, is expected to be very small, $d_n \sim 10^{-32}\, e$ cm [81]. In contrast, the present experimental bound is $|d_n| < 2.9 \cdot 10^{-26}\, e$ cm [82], and plans exist to decrease this limit by one or two orders of magnitude using ultracold neutrons at the Spallation Neutron Source (SNS) of the Oak Ridge National Laboratory [83] and at the UltraCold Neutron Source of the Paul Scherrer Institute [84]. A less strict bound on the proton EDM, $|d_p| < 7.9 \cdot 10^{-25}\, e$ cm, can be extracted from the EDM of the ^{199}Hg atom [85] using a calculation of the contribution of the nuclear Schiff moment [86]. In addition, there exist exciting plans to probe the deuteron EDM in a storage ring at the level of $|d_d| \sim 10^{-29}\, e$ cm [87].

Hadronic and nuclear EDMs are thus sensitive to non-CKM sources of T violation in the strong interactions. (For a review of both experimental and theoretical issues, see, for example, Refs. [88, 81].)

A natural question that arises, if the proposed experiments do measure a non-vanishing hadronic or nuclear EDM, is whether we can identify the dominant mechanism(s) of T violation. In this Thesis we would like to present a step in the direction of answering this question. Calculating hadronic and nuclear properties directly from QCD has proved difficult to say the least. Nevertheless, at low momenta $Q \sim m_\pi \ll M_{QCD}$, where m_π is the pion mass and $M_{QCD} \sim 1$ GeV is the typical mass scale in QCD, these properties can be described in terms of an effective field theory (EFT) involving nucleons, pions and delta isobars, known as chiral perturbation theory (χPT) [29, 30, 31]. In the EFT, all interactions are allowed which transform under Lorentz, parity, time-reversal, and chiral symmetry in the same way as do terms in the QCD Lagrangian. Long-range effects due to the light pions are separated from short-range effects due to all higher-energy degrees of freedom. Observables are systematically expanded in powers of Q/M_{QCD} (times functions of Q/m_π). χPT has been successfully applied to a variety of hadronic and nuclear systems. (For reviews, see for example Refs. [32, 33, 37].) We want to use EFT to analyze T violation in a way similar to what has been done for parity violation [89, 90].

Our first step will be to extend the chiral EFT to include T violation from the lowest-dimension T violating (TV) sources. We include the dimension 4 QCD $\bar{\theta}$ term, and all the possible dimension 6 operators allowed by invariance under the gauge symmetry of the Standard Model, which, when heavy degrees of freedom are integrated out, consist of a quark electric and chromo-electric dipole moment (qEDM and qCEDM), the Weinberg three-gluon operator, which is interpreted as the gluon chromo-EDM (gCEDM), two chiral invariant four-quark operators, and three two-lepton-two-quark operators. The basic idea [92, 91] is that T violation is accompanied at the quark level by a specific form of chiral-symmetry breaking, and thus the inter-

actions among low-energy hadrons and photons break chiral symmetry in the same way. We construct here the TV Lagrangian governing the low-energy interactions of pions and nucleons. (Some of these interactions have already been considered in Refs. [92, 91].) Since various sources of T violation have distinct chiral-symmetry transformation properties, they will generate different interactions at the hadronic level [92]. This, in turn, leads to different relationships among observables.

Since we are interested in low-lying hadronic and nuclear systems, we limit ourselves to two quark flavors, when the chiral symmetry is $SU(2) \times SU(2)$. We dedicate the rest of this Chapter to a summary of the TV sources we are considering, a brief review of χPT and of the T conserving (TC) χPT Lagrangian. In Chapter 4, we construct the TV Chiral Lagrangian. As far as the $\bar{\theta}$ term is concerned, we extend to higher orders in the chiral expansion the pioneering work of Ref. [93]. We do not assume that the strange-quark mass makes a good expansion parameter. With such an assumption more stringent (approximate) relations among observables exist [94, 95, 96, 97, 98, 99]. On the other hand, focusing on $SU(2) \times SU(2)$ will make some intrinsic aspects of the connection between T violation and chiral-symmetry breaking more obvious. For the dimension 6 operators, we construct for the first time the TV Lagrangian that includes all the terms relevant to the calculation of the nucleon EDM, of its momentum dependence, the Electric Dipole Form Factor (EDFF), and of the deuteron EDM at leading order.

The TV Chiral Lagrangian enables us to study various TV nuclear observables in a model independent way. We devote Chapter 5 to the study of the nucleon EDM and its momentum dependence. We find that in the case of TV from $\bar{\theta}$ term and the qCEDM, the leading contributions come from the pion cloud, where the pion couples to the nucleon via a non-derivative isoscalar P- and T-odd interaction, and from shorter-range interactions. At leading order (LO), the $\bar{\theta}$ term and the qCEDM generate an identical signal for the nucleon EDM and EDFF, so that a measurement of the nucleon EDM, or even of its detailed momentum dependence, cannot by itself

discriminate between these two sources of T violation. In the case of the qEDM, gCEDM and of the TV four-quark operators, we find that TV interactions between nucleon and pions play a less important role, and the EDM at LO is completely determined by physics at shorter range. Also the scale of the momentum variation of the EDFF is determined not by m_π, but by the high-energy scale $M_{QCD} \sim 1$ GeV.

A measurement of the proton and neutron EDM can thus be attributed as well to any of the TV sources we consider. The detailed momentum dependence of the EDFF, or at least of its first derivative, would allow to discriminate between TV from the QCD $\bar{\theta}$ term and the qCEDM on the one side and TV from the other dimension 6 operators on the other, but, unfortunately, such a measurement will not be performed in the next generation of EDM experiments. It is clear, then, that nuclear TV observables are of the foremost importance, in the quest to trace the signal from EDM experiments back to the dominant mechanism(s) of T violation at high energy. It is therefore crucial to set up a framework that can consistently accommodate one and few nucleon observables.

Chapter 6 is dedicated to the study of the TV moments of the simplest nucleus, the deuteron. In the one-nucleon sector, we use the Lagrangian developed in Chapter 4, while the complications of the power counting for two nucleon system are addressed using in the "perturbative pion" approach. We find that a measurement of the deuteron EDM in conjunction with the nucleon EDM allows to clearly identify TV from the qCEDM. The measurement of the deuteron Magnetic Quadrupole Moment (MQM) would further allow to separate TV from the $\bar{\theta}$ term from the other TV sources.

Finally in Chapter 7 we study the TV potential stemming from the $\bar{\theta}$ term at next-to-next leading ($\mathrm{N^2LO}$) order, and the LO TV potential from dimension 6 operator. This is the first step towards a description of TV observables for higher nuclei in the same framework used for the calculation of the nucleon EDM. The combination of the TV potential here derived with the TC forces and currents derived in the extension

of χPT to multi-nucleon systems [100, 37, 38] opens the possibility of describing all necessary ingredients in a single framework, which would then allow to use TV parameters extracted from the observation of nucleon and deuteron TV moments to predict in a model-independent and falsifiable way TV moments of light nuclei, like ^{3}He, ^{6}Li or ^{7}Li.

3.2 Sources of T violation

3.2.1 The QCD $\bar{\theta}$ term

Well below the electroweak scale, strong interactions can be described by the most general Lagrangian with Lorentz, color, and electromagnetic gauge invariance among left-handed (q_L) and right-handed (q_R) quarks, gluons (G_μ) and photons (A_μ). The lowest-dimension operators are included in the QCD Lagrangian,

$$\begin{aligned}\mathcal{L}_{QCD} &= -\frac{1}{4}G^{a\,\mu\nu}G^a_{\mu\nu} - g_s^2\frac{\theta}{64\pi^2}\varepsilon^{\mu\nu\alpha\beta}G^a_{\mu\nu}G^a_{\alpha\beta} - \frac{1}{4}F^{\mu\nu}F_{\mu\nu} \\ &\quad +\bar{q}_L i\not{D}\, q_L + \bar{q}_R i\not{D}\, q_R + e\bar{q}_L\not{A}Q\, q_L + e\bar{q}_R\not{A}Q\, q_R \\ &\quad -\bar{q}_R M q_L - \bar{q}_L M^* q_R, \end{aligned} \tag{3.2.1}$$

where $G^a_{\mu\nu}$ and $F_{\mu\nu}$ are the gluon and photon field strengths, respectively; D_μ is the color-gauge covariant derivative; M and Q are the quark mass and charge matrices; e is the electron charge; and θ is a real parameter [101, 102].

The field $q = q_L + q_R$ represents a multiplet of fields, of dimension equal to the number of quark flavors we consider. We work for simplicity with two light flavors, u and d, so

$$q = \begin{pmatrix} u \\ d \end{pmatrix} \tag{3.2.2}$$

is an isospin doublet. Objects in isospin space can be written in terms of the identity and the Pauli matrices $\boldsymbol{\tau}$, for example

$$Q = \frac{1}{3}\begin{pmatrix} 2 & 0 \\ 0 & -1 \end{pmatrix} = \frac{1}{6} + \frac{\tau_3}{2}. \tag{3.2.3}$$

The most general form of the diagonal mass matrix is

$$M = e^{i\rho} \begin{pmatrix} m_u & 0 \\ 0 & m_d \end{pmatrix} = e^{i\rho} \bar{m} \left(1 - \varepsilon \tau_3\right), \tag{3.2.4}$$

with real parameters ρ and $m_{u,d}$, or alternatively

$$\bar{m} = \frac{m_u + m_d}{2} \tag{3.2.5}$$

and

$$\varepsilon = \frac{m_d - m_u}{m_u + m_d}. \tag{3.2.6}$$

An important role is played by rotations in isospin space belonging to the chiral group $SU_L(2) \times SU_R(2) \sim SO(4)$,

$$q \to \exp\left[i\boldsymbol{\theta}_V \cdot \boldsymbol{t} + i\boldsymbol{\theta}_A \cdot \boldsymbol{x}\right] q, \tag{3.2.7}$$

where $\boldsymbol{\theta}_{V,A}$ are real parameters and

$$\boldsymbol{t} = \boldsymbol{\tau}/2, \qquad \boldsymbol{x} = \gamma_5 \boldsymbol{\tau}/2, \tag{3.2.8}$$

the group generators.

The θ term is a total derivative, but it contributes to physical processes through extended, spacetime-dependent field configurations known as instantons [103, 104]. The θ term can be eliminated from the Lagrangian by performing transformations on the quark field. The most general transformation that leaves M diagonal is a combination of a chiral transformation (3.2.7) with $\boldsymbol{\theta}_V = (0, 0, \beta)$ and $\boldsymbol{\theta}_A = (0, 0, \alpha)$, and two $U(1)$ transformations,

$$q \to \exp\left[i\theta_V^0 + i\theta_A^0 \gamma_5\right] q, \tag{3.2.9}$$

with arbitrary parameters $\theta_{V,A}^0$. The axial $U(1)$ transformation has an anomaly [105] and induces a transformation in the integration measure in the path integral that is equivalent to a modification of the θ term in the QCD Lagrangian. With the choice $\theta_A^0 = -\theta/4$, the θ term can be eliminated and the QCD Lagrangian can be written as

$$\mathcal{L}_{QCD} = -\frac{1}{4} G^{a\,\mu\nu} G^a_{\mu\nu} - \frac{1}{4} F^{\mu\nu} F_{\mu\nu} + \bar{q}_L i \not{D} q_L + \bar{q}_R i \not{D} q_R + \mathcal{L}_e + \mathcal{L}_\alpha, \tag{3.2.10}$$

where

$$\mathcal{L}_e = eA_\mu \bar{q}\gamma^\mu Q q = eA_\mu \left(\frac{1}{6} I^\mu + T^\mu_{34}\right) \tag{3.2.11}$$

is the electromagnetic interaction, and

$$\begin{aligned}
\mathcal{L}_\alpha &= -\bar{q}_R e^{i\frac{\bar{\theta}}{2}} \begin{pmatrix} m_u e^{i\alpha} & 0 \\ 0 & m_d e^{-i\alpha} \end{pmatrix} q_L + \text{H.c.} \\
&= -\bar{m}\cos\alpha\cos\frac{\bar{\theta}}{2}\left\{\left[1+\varepsilon\tan\alpha\tan\frac{\bar{\theta}}{2}\right] S_4 - \left[\varepsilon+\tan\alpha\tan\frac{\bar{\theta}}{2}\right] P_3 \right. \\
&\qquad \left. + \left[\varepsilon\tan\alpha-\tan\frac{\bar{\theta}}{2}\right] P_4 + \left[\tan\alpha-\varepsilon\tan\frac{\bar{\theta}}{2}\right] S_3 \right\}
\end{aligned} \tag{3.2.12}$$

is a family of CP-violating mass terms labeled by the angle α and parametrized by $\bar{\theta} = 2\rho - \theta$. We have expressed the mass and electromagnetic Lagrangians in terms of two $SO(4)$ vectors, a Lorentz scalar

$$S = \begin{pmatrix} -i\bar{q}\gamma^5 \boldsymbol{\tau} q \\ \bar{q} q \end{pmatrix} \tag{3.2.13}$$

and a Lorentz pseudoscalar

$$P = \begin{pmatrix} \bar{q}\,\boldsymbol{\tau} q \\ i\bar{q}\gamma^5 q \end{pmatrix}, \tag{3.2.14}$$

and two Lorentz vectors, an $SO(4)$ scalar,

$$I^\mu = \bar{q}\gamma^\mu q, \tag{3.2.15}$$

and an $SO(4)$ antisymmetric tensor,

$$T^\mu = \frac{1}{2}\begin{pmatrix} \varepsilon_{ijk}\bar{q}\gamma^\mu\gamma^5\tau_k q & \bar{q}\gamma^\mu\tau_i q \\ -\bar{q}\gamma^\mu\tau_j q & 0 \end{pmatrix}. \tag{3.2.16}$$

3.2.2 Dimension 6 TV operators

The current bound on the neutron EDM, as discussed more in detail in Chapter 5, can be interpreted as a bound on $\bar{\theta}$, $\bar{\theta} \lesssim 2.5\cdot 10^{-10}$. $\bar{\theta}$ is thus unnaturally small, and its smallness leaves room for other sources of T violation in the strong interaction. The next-to-lowest-dimension TV operators involving quark and gluon fields that one can

add to the QCD Lagrangian have effective dimension 6 [106, 107, 108, 109, 110, 111]. At this level, in the flavor diagonal sector, we encounter the quark electric dipole moment, which couples quarks and photons; the quark chromoelectric dipole moment, which couples quarks and gluons; the Weinberg operator, which couples three gluons and can be identified as the gluon chromoelectric dipole moment, and two TV chiral invariant four-quark operators. Extending our attention to leptons, we also consider electron and muon EDMs and three two-lepton-two-quark operators.

These higher-dimension operators have their origin in an ultraviolet-complete theory at a high-energy scale, such as, for example, supersymmetric extensions of the Standard Model. We assume that T violation arises in this theory at a characteristic scale, $M_{\not T}$. Well below the scale $M_{\not T}$ we expect TV effects to be captured by the lowest-dimension interactions among Standard Model fields that respect the theory's $SU_c(3) \times SU_L(2) \times U_Y(1)$ gauge symmetry.

The complete list of gauge-invariant operators with dimension up to 6 is given in Refs. [106, 111] (the CP violating operators are also listed in Ref. [107, 110]). Above the electroweak scale, only one gauge invariant, dimension 5 operator can be written. After electroweak symmetry breaking, it generates neutrino masses and mixing, and we neglect it in the rest of our analysis.

TV effects are encoded in several dimension 6 operators, that, following Ref. [111], we organize according to their field content: three-gluon (ggg), two quarks and a scalar ($qq\varphi$), two fermions, a scalar, and a vector boson ($qq\varphi$ v), four quarks ($qqqq$), and two leptons and two quarks ($llqq$). Since our goal is to study the low energy manifestations of T violation in nuclear systems, we focus here on those operators that, after electroweak symmetry breaking, can be expressed in terms of light degrees of freedom; light quarks, leptons, photons and gluons. We neglect, for example, TV in the Higgs sector, operators that represent the W boson electric dipole and magnetic quadrupole moment, or flavor non-diagonal CP violating four-quark operators containing both heavy and light quark fields. These operators are listed in [106, 107, 111], to which we

refer the interested reader. In the EFT spirit, they are integrated out in matching the CP violating Lagrangian at the electroweak scale onto the CP violating Lagrangian at scales of order 1 GeV, and their contribution is hidden in the coupling constants (matching coefficients) of the operators that appear in the latter.

The dimension 6 operators relevant to our discussion of T violation are

$$\mathcal{L}_{6,\,qq\varphi} = -2\frac{\varphi^\dagger\varphi}{v^2}\left(\frac{\sqrt{2}}{v}\bar{q}_L\tilde{\varphi}M'_u u_R + \frac{\sqrt{2}}{v}\bar{q}_L\varphi M'_d d_R + g_s^2\frac{\theta'}{64\pi^2}\varepsilon^{\mu\nu\alpha\beta}G^a_{\mu\nu}G^a_{\alpha\beta}\right) + \text{h.c.}. \tag{3.2.17}$$

$$\mathcal{L}_{6,\,\text{ggg}} = \frac{d_W}{6}f^{abc}\varepsilon^{\mu\nu\alpha\beta}G^a_{\alpha\beta}G^b_{\mu\rho}G^{c\,\rho}_{\nu}. \tag{3.2.18}$$

$$\begin{aligned}\mathcal{L}_{6,\,qq\varphi\text{v}} = &-\frac{1}{\sqrt{2}}\bar{q}_L\sigma^{\mu\nu}\tilde{\Gamma}^u\lambda^a\frac{\tilde{\varphi}}{v}\,u_R G^a_{\mu\nu} - \frac{1}{\sqrt{2}}\bar{q}_L\sigma^{\mu\nu}\tilde{\Gamma}^d\lambda^a\frac{\varphi}{v}\,d_R G^a_{\mu\nu}\\ &-\frac{1}{\sqrt{2}}\bar{q}_L\sigma^{\mu\nu}\left(\Gamma^u_B B_{\mu\nu} + \Gamma^u_W\boldsymbol{\tau}\cdot\mathbf{W}_{\mu\nu}\right)\frac{\tilde{\varphi}}{v}\,u_R\\ &-\frac{1}{\sqrt{2}}\bar{q}_L\sigma^{\mu\nu}\left(\Gamma^d_B B_{\mu\nu} + \Gamma^d_W\boldsymbol{\tau}\cdot\mathbf{W}_{\mu\nu}\right)\frac{\varphi}{v}d_R\\ &-\frac{1}{\sqrt{2}}\bar{l}_L\sigma^{\mu\nu}\left(\Gamma^e_B B_{\mu\nu} + \Gamma^e_W\boldsymbol{\tau}\cdot\mathbf{W}_{\mu\nu}\right)\frac{\varphi}{v}\,e_R + \text{h.c.}\end{aligned} \tag{3.2.19}$$

$$\mathcal{L}_{6,\,qqqq} = \Sigma_1\left(\bar{q}^J_L u_R\right)\,\varepsilon_{JK}\,\left(\bar{q}^K_L d_R\right) + \Sigma_8\left(\bar{q}^J_L\lambda^a u_R\right)\,\varepsilon_{JK}\,\left(\bar{q}^K_L\lambda^a d_R\right) + \text{h.c.} \tag{3.2.20}$$

$$\begin{aligned}\mathcal{L}_{6,\,llqq} = &\,\Sigma_{lq\,1}\left(\bar{l}^J_L e_R\right)\left(\bar{d}_R q^J_L\right) + \Sigma_{lq\,2}\left(\bar{l}^J_L e_R\right)\,\varepsilon_{JK}\,\left(\bar{q}^K_L u_R\right)\\ &+\Sigma_{lq\,3}\left(\bar{l}^J_L\sigma^{\mu\nu}e_R\right)\,\varepsilon_{JK}\,\left(\bar{q}^K_L\sigma_{\mu\nu}u_R\right) + \text{h.c.}\end{aligned} \tag{3.2.21}$$

In Eqs. (3.2.17)-(3.2.21), $G^a_{\mu\nu}$ is the gluon field strength, λ^a the Gell-Man matrices and f^{abc} the structure constants. $W^i_{\mu\nu}$ and $B_{\mu\nu}$ are the fields strengths of the $SU_L(2)$ and $U(1)$ gauge boson,

$$W^i_{\mu\nu} = \partial_\mu W^i_\nu - \partial_\nu W^i_\mu - g\varepsilon^{ijk}W^j_\mu W^i_\nu, \qquad B_{\mu\nu} = \partial_\mu B_\nu - \partial_\nu B_\mu. \tag{3.2.22}$$

We recall that W^3_μ and B_μ can be expressed in terms of the physical photon and Z boson fields

$$\begin{aligned}W^3_\mu &= \cos\theta_w Z_\mu + \sin\theta_w A_\mu,\\ B_\mu &= \cos\theta_w A_\mu - \sin\theta_w Z_\mu,\end{aligned} \tag{3.2.23}$$

and, in terms of the electric charge e and of weak mixing angle θ_w, the $SU_L(2)$ and $U(1)$ gauge coupling g and g' are

$$g = \frac{e}{\sin\theta_w}, \qquad g' = \frac{e}{\cos\theta_w}. \tag{3.2.24}$$

The scalar field φ is a doublet under $SU(2)$, and it has hypercharge $Y = +1/2$. The electroweak symmetry is spontaneously broken by the vacuum expectation value of the field φ

$$\langle\varphi\rangle = \frac{1}{\sqrt{2}}\begin{pmatrix} 0 \\ v \end{pmatrix}, \tag{3.2.25}$$

with $v = 247$ GeV. The Higgs boson represents fluctuations around the vacuum Eq. (3.2.25), in a unitary gauge

$$\varphi = \frac{1}{\sqrt{2}}\begin{pmatrix} 0 \\ v + h(x) \end{pmatrix}. \tag{3.2.26}$$

Eqs. (3.2.17) and (3.2.19) thus also generate CP violating couplings of the Higgs to gluons, vector bosons and fermions, with coefficients fixed by gauge symmetry. Since in the rest of our work we are interested in low-energy observables, we do not further consider these couplings, which are carefully analyzed for example in [107]. We denote with the symbol $\tilde{\varphi}^I = \varepsilon^{IJ}\varphi^J$, where ε^{IJ} is the antisymmetric tensor in two dimension, and $\varepsilon^{12} = 1$.

The fields l_L and q_L denote the left-handed doublets

$$l_L = \begin{pmatrix} \nu_L \\ e_L \end{pmatrix}, \qquad \bar{q}_L = \begin{pmatrix} u_L \\ d_L \end{pmatrix}, \tag{3.2.27}$$

while e_R, u_R and d_R are right-handed fermion fields, singlet under $SU(2)$. For simplicity, we do not explicitly show the family indices in Eqs. (3.2.17)-(3.2.21). In this Section, we use the symbol u to indicate the fields of the u, c and t quarks, while d stands in general for d, s and b. Similarly e and ν denotes electron, muon and tau fields, and their respective neutrinos. In a second step, we will integrate out the tau and the heavy quarks, and concentrate only on the light lepton and quark flavors.

The coupling constants in Eqs. (3.2.17)-(3.2.21) are all proportional to two inverse powers of the new physics scale M_T. For example the coefficient of the three-gluon

operator is

$$d_W = \mathcal{O}\left(4\pi\frac{w}{M_{\not T}^2}\right), \tag{3.2.28}$$

with w a dimensionless constant. For reasons that will be clear in a moment, we choose to rescale the scalar field by the Higgs vacuum expectation value. With this choice, $M'_{u,d}$ in Eq. (3.2.17) have dimension of mass, while θ' is dimensionless:

$$\theta' = \mathcal{O}\left(\frac{v^2}{M_{\not T}^2}\right), \qquad M'_{u,d} = \mathcal{O}\left(\frac{1}{\sqrt{2}}\lambda'_{u,d} v \frac{v^2}{M_{\not T}^2}\right), \tag{3.2.29}$$

In full generality $M'_{u,d}$ should be interpreted as 3×3 complex-valued matrices in flavor space. We assume them to be proportional to the Yukawa couplings of the Higgs to quarks and leptons, so that in the basis of the mass eigenstates $M'_{u,d}$ are diagonal.

Similarly, in the most general case, the couplings in Eq. (3.2.19) $\Gamma^e_{B,W}$, $\Gamma^u_{B,W}$, $\Gamma^d_{B,W}$, $\tilde{\Gamma}^u$ and $\tilde{\Gamma}^d$ are 3×3 complex-valued matrices. Also in this case, since the applications we will investigate are most sensitive to flavor-diagonal CP violation, we assume these matrices to be proportional to the Yukawa couplings in the Standard Model Lagrangian, so in the basis of the mass eigenstates, the couplings in Eq. (3.2.19) are diagonal. Non-diagonal elements of the matrices Γ are also interesting, and they give rise to flavor-changing neutral current that contribute, for example, to processes like $K_0 \to \mu^+\mu^-$, $B_0 \to \mu^+\mu^-$, or $b \to s\gamma$ and $b \to d\gamma$. Since these processes receive small contributions from the Standard Model, they are particularly sensitive to new physics, and the subject of much theoretical and experimental interest.

With our assumption,

$$\begin{aligned}
\Gamma^e_{W(B)} &= \mathcal{O}\left(g^{(\prime)}\delta_e \frac{v\lambda^e}{M_{\not T}^2}\right), \quad \Gamma^u_{W(B)} = \mathcal{O}\left(g^{(\prime)}\delta_u \frac{v\lambda^u}{M_{\not T}^2}\right), \quad \Gamma^d_{W(B)} = \mathcal{O}\left(g^{(\prime)}\delta_d \frac{v\lambda^d}{M_{\not T}^2}\right), \\
\tilde{\Gamma}^u &= \mathcal{O}\left(4\pi\tilde{\delta}_u \frac{v\lambda^u}{M_{\not T}^2}\right), \quad \tilde{\Gamma}^d = \mathcal{O}\left(4\pi\tilde{\delta}_d \frac{v\lambda^d}{M_{\not T}^2}\right),
\end{aligned} \tag{3.2.30}$$

where λ^e, λ^u and λ^d are the Yukawa couplings that generate lepton and quark masses, $m_e = v\lambda^e/\sqrt{2}$, $m_{u,d} = v\lambda^{u,d}/\sqrt{2}$, and $\tilde{\delta}_{u,d}$ and $\delta_{u,d}$ are dimensionless constants.

The couplings Σ in Eqs. (3.2.20) and (3.2.21) are four-index complex-valued tensors in flavor space, labeled by the family-index of the quark and lepton fields. In practice, we are mainly interested in operators containing the lightest quarks u and d, and in what follow we ignore the possibility of complicated flavor structures. The four-quark and two-quark-two-lepton couplings scale as

$$\Sigma_{1,8} = \mathcal{O}\left(\frac{(4\pi)^2\sigma_{1,8}}{M_{\not T}^2}\right), \qquad \Sigma_{lq\,i} = \mathcal{O}\left(e^2\frac{\sigma_{lq\,i}}{M_{\not T}^2}\right), \tag{3.2.31}$$

where $\sigma_{1,8}$ and $\sigma_{lq,\,i}$ are dimensionless constants.

After electroweak symmetry breaking, Eq. (3.2.17) becomes

$$\mathcal{L}_{6,qq\varphi} = -\left(\bar{u}_L M'_u u_R + \bar{d}_L M'_d d_R + \frac{\theta'}{64\pi^2}\varepsilon^{\mu\nu\alpha\beta}G^a_{\mu\nu}G^a_{\alpha\beta}\right) + \text{h.c.} + \ldots, \tag{3.2.32}$$

where the dots denote operators with quark-Higgs and gluon-Higgs interactions. Comparing Eq. (3.2.32) and (3.2.1), it is apparent that $M'_{u,d}$ and θ' are $\mathcal{O}\left(v^2/M_{\not T}^2\right)$ corrections to the light quark masses and to the $\bar{\theta}$ term, where the size of v is determined by the electroweak scale $v \approx M_W$.

Eqs. (3.2.18) and (3.2.19) are more interesting. The operator in Eq. (3.2.18) is the Weinberg three-gluon operators, which represents the chromo-EDM of the gluon. Other purely gluonic TV operators, like the gluon chromo-MQM, have higher dimension.

After electroweak symmetry breaking, and integrating out the W, Z and Higgs bosons, Eq. (3.2.19) can be expressed in terms of quark and lepton magnetic and chromo-magnetic dipole moments (MDM and CMDM) and electric and chromo-electric dipole moments. In the assumptions that the matrices $\Gamma^{e,d,u}$ are diagonal in the mass eigenstate basis, Eq. (3.2.19) reduces to

$$\begin{aligned}
\mathcal{L}_{6,\,qq\varphi\text{v}} \;=\; & -\frac{c_e}{2}\,\bar{e}\,\sigma^{\mu\nu}\left(1 + i\tan\phi_e\gamma^5\right)e\,F_{\mu\nu} - \frac{c_0}{2}\,\bar{q}\,\sigma^{\mu\nu}\left(1 + i\tan\phi_0\gamma^5\right)q\,F_{\mu\nu} \\
& -\frac{c_3}{2}\,\bar{q}\sigma^{\mu\nu}\left(1 + i\tan\phi_3\gamma^5\right)\,\tau_3 q\,F_{\mu\nu} - \frac{\tilde{c}_0}{2}\,\bar{q}\,\sigma^{\mu\nu}\left(1 + i\tan\tilde{\phi}_0\gamma^5\right)\lambda^a q\,G^a_{\mu\nu} \\
& -\frac{\tilde{c}_3}{2}\,\bar{q}\sigma^{\mu\nu}\left(1 + i\tan\tilde{\phi}_3\gamma^5\right)\lambda^a\,\tau_3 q\,G^a_{\mu\nu},
\end{aligned} \tag{3.2.33}$$

where the quark field q is defined as in Eq. (3.2.2), and family indices are, as usual, suppressed.

The coefficients in Eq. (3.2.33) are combinations of those introduced in Eq. (3.2.19), for example, in the case of the qCMDM and qCEDM

$$\tilde{c}^f_{0,3} = \mathrm{Re}\left[\tilde{\Gamma}^u \pm \tilde{\Gamma}^d\right]_{ff}, \tag{3.2.34}$$

$$\tan\tilde{\phi}^f_{0,3} = \frac{\mathrm{Im}\left[\tilde{\Gamma}^u \pm \tilde{\Gamma}^d\right]_{ff}}{\mathrm{Re}\left[\tilde{\Gamma}^u \pm \tilde{\Gamma}^d\right]_{ff}}, \tag{3.2.35}$$

where f is the family index. Similar relations hold for the lepton and quark EDM operators, with the slight complication that Eq. (3.2.23) has to be used to express the operators in terms of the photon and Z boson fields.

Since our focus are the manifestations of the effects of the Lagrangian (3.2.33) in nuclear physics, for which the lightest quarks are the most relevant, we integrate out the heavy quarks t, b and c (and the s quark as well), and we match Eq. (3.2.33) onto an effective Lagrangian at a scale just above the typical QCD scale $M_{QCD} \sim 1$ GeV, which only contains MDM and EDM of electron, muon, and u and d quarks. The form of the Lagrangian is the same as Eq. (3.2.33), where now only light degrees of freedom appear. The coefficients of the MDM and EDM operators receive contributions from the coefficients Γ in Eq. (3.2.19), and, via loops, also from all the Standard Model TV operators that are no longer explicit in the theory (EDM of heavy quarks, EDM and MQM of the W boson, CP violation in the Higgs sector, ...).

The breaking of electroweak symmetry does not affect the form of the four-fermion operators Eqs. (3.2.20) and (3.2.21). For convenience, we rewrite Eq. (3.2.20) in

terms of quark doublets q

$$\begin{aligned}\mathcal{L}_{6,\,qqqq} &= \frac{1}{8}\mathrm{Re}\Sigma_1\left(\bar{q}q\,\bar{q}q - \bar{q}\boldsymbol{\tau}q\cdot\bar{q}\boldsymbol{\tau}q + \bar{q}\gamma^5 q\,\bar{q}\gamma^5 q - \bar{q}\gamma^5\boldsymbol{\tau}q\cdot\bar{q}\gamma^5\boldsymbol{\tau}q\right)\\ &+\frac{1}{4}\mathrm{Im}\Sigma_1\left(\bar{q}q\,\bar{q}i\gamma^5 q - \bar{q}\boldsymbol{\tau}q\,\cdot\bar{q}\boldsymbol{\tau}i\gamma^5 q\right)\\ &+\frac{1}{8}\mathrm{Re}\Sigma_8\left(\bar{q}\lambda^a q\,\bar{q}\lambda^a q - \bar{q}\boldsymbol{\tau}\lambda^a q\cdot\bar{q}\boldsymbol{\tau}\lambda^a q + \bar{q}\gamma^5\lambda^a q\,\bar{q}\gamma^5\lambda^a q\right.\\ &\left.-\bar{q}\gamma^5\boldsymbol{\tau}\lambda^a q\cdot\bar{q}\gamma^5\boldsymbol{\tau}\lambda^a q\right)\\ &+\frac{1}{4}\mathrm{Im}\Sigma_8\left(\bar{q}\lambda^a q\,\bar{q}i\gamma^5\lambda^a q - \bar{q}\boldsymbol{\tau}\lambda^a q\,\cdot\bar{q}\boldsymbol{\tau}i\gamma^5\lambda^a q\right), \qquad (3.2.36)\end{aligned}$$

where as usual we are dropping flavor indices. The TC and TV operators in Eq. (3.2.36) are invariant under the chiral group $SU_L(2)\otimes SU_R(2)$, as it can be seen either by directly applying the transformation (3.2.7) to Eq. (3.2.36), or by realizing that the operators in (3.2.36) are constructed as scalar product of the chiral vectors S and P defined in Eq. (3.2.13) and (3.2.14).

The two-lepton-two-quark operators can be rewritten in terms of the quark field q and of the electron field $e = e_R + e_L$. Neglecting the part of the operator which contains neutrino-quark interactions, we find

$$\begin{aligned}\mathcal{L}_{6,\,llqq} &= \mathrm{Re}\Sigma'_{lq\,1}\left(\bar{e}e\,\bar{q}q + \bar{e}\gamma^5 e\,\bar{q}\gamma^5 q\right) + \mathrm{Im}\Sigma'_{lq\,1}\left(\bar{e}i\gamma^5 e\,\bar{q}q + \bar{e}e\,\bar{q}i\gamma^5 q\right)\\ &+\mathrm{Re}\Sigma'_{lq\,2}\left(\bar{e}e\,\bar{q}\tau_3 q + \bar{e}\gamma^5 e\,\bar{q}\tau_3\gamma^5 q\right) + \mathrm{Im}\Sigma'_{lq\,2}\left(\bar{e}i\gamma^5 e\,\bar{q}\tau_3 q + \bar{e}e\,\bar{q}i\gamma^5\tau_3 q\right)\\ &+\mathrm{Re}\Sigma_{lq\,3}\,\bar{e}\sigma^{\mu\nu}e\,\bar{q}\sigma_{\mu\nu}(1+\tau_3)q + \mathrm{Im}\Sigma_{lq\,3}\left(\bar{e}\sigma^{\mu\nu}e\,\bar{q}i\sigma_{\mu\nu}\gamma^5(1+\tau_3)q\right), \qquad (3.2.37)\end{aligned}$$

where $\Sigma'_{lq\,1,2}$ are linear combinations of $\Sigma_{lq\,1,2}$. For our applications, once again, we integrate out the heavy fields and express Eqs. (3.2.36) and (3.2.37) in terms of electron, muon, u and d fields. The scaling of the coefficients of Eqs. (3.2.36) and (3.2.37) is given in Eq. (3.2.31).

The goal of the current generation of lepton, nuclear and atomic EDM experiments is to constrain the coefficients of the TV operators in Eqs. (3.2.18), (3.2.33), (3.2.36), and (3.2.37), and, by doing so, to attain information on the new physics mechanism(s)

responsible for T violation. From Eqs. (3.2.30) the scaling of the electron and muon EDM is

$$d_e = c_e \tan\phi_e = \mathcal{O}\left(e\delta_e \frac{m_e}{M_{\not T}^2}\right), \quad d_\mu = c_\mu \tan\phi_\mu = \mathcal{O}\left(e\delta_\mu \frac{m_\mu}{M_{\not T}^2}\right). \tag{3.2.38}$$

The factors $\delta_{e,\mu}$ depend on the particular extension of the Standard Model under consideration, and on the details of T violation. The minimal assumption is $\delta_e = \mathcal{O}(1)$. In the Minimal SuperSymmetric extension of the Standard Model (MSSM), $\delta_{e,\mu}$ receives further suppression from the electroweak coupling constant $\delta_e \sim \alpha_{\rm em}/(4\pi \sin\theta_w^2)$ (for the detailed results, we refer to the reviews [81, 112] and references therein). In the Standard Model, the CKM phase generates a contribution to the $d_{e,\mu}$ of the order $d_e \sim 10^{-25}\, e$ fm, which is way smaller than the current experimental limits, and entirely negligible.

Experimentally, bounds on d_e can be extracted by experiments that investigate EDMs of paramagnetic atoms. The most accurate bound is extracted from the Thallium EDM experiment [113], which gives

$$d_e = (0.069 \pm 0.074) \cdot 10^{-13}\, e\,\text{fm}. \tag{3.2.39}$$

For the ratio of the parameter δ_e and the scale of new physics $M_{\not T}$, Eq. (3.2.39) implies

$$\frac{\delta_e}{M_{\not T}^2} \lesssim (100\ \text{TeV})^{-2}. \tag{3.2.40}$$

A less stringent bound on d_μ was found by the $g-2$ experiment at Brookhaven National Laboratory (BNL) [114]

$$d_\mu = -(0.1 \pm 0.9) \cdot 10^{-6}\, e\,\text{fm}, \tag{3.2.41}$$

which translates in

$$\frac{\delta_\mu}{M_{\not T}^2} \lesssim (100\ \text{GeV})^{-2}. \tag{3.2.42}$$

The same $g-2$ experiment sets the current limit on contributions of Beyond the Standard Model physics to the muon MDM c_μ [115].

$$\frac{m_\mu c_\mu^{BSM}}{e} = \Delta_\mu \frac{m_\mu^2}{M_{\not T}^2} = (255 \pm 63 \pm 49) \times 10^{-11}, \tag{3.2.43}$$

where we have defined $\delta_\mu = \Delta_\mu \tan\phi_\mu$. Eq. (3.2.43) set the ratio of Δ_μ and the new physics scale to be

$$\frac{\Delta_\mu}{M_{\not T}^2} \sim (2\ \text{TeV})^{-2}. \tag{3.2.44}$$

The success of the $g-2$ experiment, which, though optimized to measure the muon anomalous magnetic moment, has improved the existing bound on d_μ by a factor of 5, has spurred plans for a dedicated muon EDM experiment [116], which could lower the bound on the muon EDM by four or five orders of magnitude and thus allow to probe $\delta_\mu/M_{\not T}^2$ with the same accuracy as Eq. (3.2.44).

The size of the qEDM, $d_{0,3}$, and of the qCEDM, $\tilde{d}_{0,3}$, can be estimated from Eqs. (3.2.30), and (3.2.34) and (3.2.35).

$$d_{0,3} \equiv c_{0,3}\tan\phi_{0,3} = \mathcal{O}\left(e\delta_{0,3}\frac{\bar{m}}{M_{\not T}^2}\right), \quad \tilde{d}_{0,3} \equiv \tilde{c}_{0,3}\tan\tilde{\phi}_{0,3} = \mathcal{O}\left(4\pi\tilde{\delta}_{0,3}\frac{\bar{m}}{M_{\not T}^2}\right), \tag{3.2.45}$$

with the average light quark mass $\bar{m}$ defined in Eq. (3.2.5). As we have already remarked, the EDM and CEDM of light quarks receive contributions from the integration of the heavy flavors, in which case we expect the heavy quark mass, rather than $\bar{m}$, to appear in Eq. (3.2.45). In most models, however, such enhancements is compensated by the smallness of the flavor-changing parameters, so that we expect Eq. (3.2.45) to still capture the size of the quark EDM and CEDM.

The sizes of $\delta_{0,3}$, $\tilde{\delta}_{0,3}$ and w depend on the exact mechanisms of electroweak and T breaking and on the running to the low energies where non-perturbative QCD effects take over. The minimal assumption is that they are $\mathcal{O}(1)$, $\mathcal{O}(g_s/4\pi)$ and $\mathcal{O}((g_s/4\pi)^3)$, respectively, with g_s the strong-coupling constant. However they can be much smaller (when parameters encoding T violation beyond the Standard Model are small) or much larger. In the Standard Model itself, where $M_{\not T} = M_W$, $\delta_{0,3}$, $\tilde{\delta}_{0,3}$ and w are suppressed not only by the Jarlskog parameter [79] $J_{CP} \simeq 3\cdot 10^{-5}$, but also by additional powers of the TV scale, in this case equal to M_W, and by small gauge coupling constants. For example, in the Standard Model, the qEDM and gCEDM

both receive their first contribution at three loops [81, 117, 118]

$$\delta_d = \frac{2}{27} J_{CP} \frac{\alpha_{\rm em}^2}{(4\pi)^2 \sin^4\theta_w} \frac{\alpha_s}{4\pi} \frac{m_c^2}{M_W^2} \ln^2 \frac{m_b^2}{m_c^2} \ln \frac{M_W^2}{m_b^2}, \tag{3.2.46}$$

$$w = \frac{1}{12} \left(\frac{g_s}{4\pi}\right)^3 J_{CP} \frac{\alpha_{\rm em}^2}{(4\pi)^2 \sin^4\theta_w} \frac{m_b^2 m_c^2 m_s^2}{M_W^6} \ln \frac{m_b^2}{m_s^2} \ln \frac{M_W^2}{m_b^2}, \tag{3.2.47}$$

and δ and w are much smaller of the naive expectation.

In supersymmetric models with various simplifying, universality assumptions of a soft-breaking sector with a common scale M_{SUSY}, one has $M_{\not T} = M_{SUSY}$ and the size of the dimensionless parameters is given by the minimal assumption times a factor which is [81, 112], roughly (neglecting electroweak parameters), $A_{CP} = (g_s/4\pi)^2 \sin\phi$, with ϕ a phase encoding T violation. Allowing for non-diagonal terms in the soft-breaking sfermion mass matrices, enhancements of the type $m_b/m_d \sim 10^3$ or even $m_t/m_u \sim 10^5$ are possible, although they are usually associated with other, smaller phases [81].

The coefficients $\Sigma_{1,8}$ and $\Sigma_{lq\,i}$ have not received much attention in the literature. In many models of Beyond the Standard Model physics, the gauge-invariant, dimension 6 operators in Eqs. (3.2.36) and (3.2.37) have vanishing matching coefficient, while other, chiral violating four-fermion TV operators, are effectively dimension 8, and each flip of chirality costs a power of the light quark or lepton mass [119, 120, 121]. For example, in the MSSM, with certain simplifying assumptions, an operator similar to $\mathrm{Im}\Sigma_{lq\,1}$ receives a coefficient of order $\alpha_{\rm em} m_e m_q/(4\pi) M_W^2 M_{\not T}^2$, suppressed by a further $m_e m_q/M_W^2$ and a loop factor $(4\pi)^2$ with respect to Eq. (3.2.31) [119] .

The examples of this section emphasize that the dimensionless coefficients $\delta_{0,3}$, $\tilde{\delta}_{0,3}$, w, $\sigma_{1,8}$ and $\sigma_{lq\,i}$ that we have introduced, and their relative size, strongly depend on the particular model of Beyond the Standard Model physics, making it difficult to compare the relative contribution of different TV sources to the same observable in a way that is independent of the details of the physics at the high energy scale $M_{\not T}$. Our analysis of nuclear TV observables in Chapters 5 and 6 will rather try to identify, for each TV source, a characteristic pattern of relations between different

observables, specific of each source and rooted in its transformation properties under chiral symmetry. The observation of such pattern in the current generation of nuclear EDM experiments would then effectively pinpoint the dominant TV mechanism at high energy. On the other hand, the formalism we develop can be easily adjusted to specific extensions of the Standard Model. Once the values of $\delta_{0,3}$, $\tilde{\delta}_{0,3}$, w, $\sigma_{1,8}$ and $\sigma_{lq\,i}$ in a given model, and their running from $M_{\not T}$ to $M_{\rm QCD}$, are known, then the relative importance of the interactions constructed in Chapter 4 can be reassessed to accommodate, for instance, a large hierarchy between these parameters.

Below the hadronic scale M_{QCD}, the dimension 6 sources of T violation generate further effective interactions, which break chiral symmetry in their own ways. Introducing the $SO(4)$ singlets

$$
\begin{aligned}
I_W &= \frac{1}{6}\epsilon^{\mu\nu\lambda\sigma} f^{abc} G^a_{\mu\rho} G^{b,\rho}_{\nu} G^c_{\lambda\sigma}, && (3.2.48)\\
I^{(1)}_{qq} &= \frac{1}{4}\left(\bar{q}q\,\bar{q}i\gamma^5 q - \bar{q}\boldsymbol{\tau}q\cdot\bar{q}\boldsymbol{\tau}i\gamma^5 q\right), && (3.2.49)\\
I^{(8)}_{qq} &= \frac{1}{4}\left(\bar{q}\lambda^a q\,\bar{q}i\gamma^5\lambda^a q - \bar{q}\boldsymbol{\tau}\lambda^a q\cdot\bar{q}\boldsymbol{\tau}i\gamma^5\lambda^a q\right) && (3.2.50)
\end{aligned}
$$

and the $SO(4)$ vectors

$$
W = \tfrac{1}{2}\begin{pmatrix} -i\bar{q}\sigma^{\mu\nu}\gamma^5\boldsymbol{\tau}q \\ \bar{q}\sigma^{\mu\nu}q \end{pmatrix} F_{\mu\nu}, \qquad V = \tfrac{1}{2}\begin{pmatrix} \bar{q}\sigma^{\mu\nu}\boldsymbol{\tau}q \\ i\bar{q}\sigma^{\mu\nu}\gamma^5 q \end{pmatrix} F_{\mu\nu}, \tag{3.2.51}
$$

and

$$
\tilde{W} = \tfrac{1}{2}\begin{pmatrix} -i\bar{q}\sigma^{\mu\nu}\gamma^5\boldsymbol{\tau}\lambda^a q \\ \bar{q}\sigma^{\mu\nu}\lambda^a q \end{pmatrix} G^a_{\mu\nu}, \qquad \tilde{V} = \tfrac{1}{2}\begin{pmatrix} \bar{q}\sigma^{\mu\nu}\boldsymbol{\tau}\lambda^a q \\ i\bar{q}\sigma^{\mu\nu}\gamma^5\lambda^a q \end{pmatrix} G^a_{\mu\nu}, \tag{3.2.52}
$$

Eq. (3.2.33) and (3.2.36) can be written as

$$
\begin{aligned}
\mathcal{L}_6 &= -d_0 V_4 + c_3 V_3 + d_3 W_3 + c_0 W_4 - \tilde{d}_0\tilde{V}_4 + \tilde{c}_3\tilde{V}_3 + \tilde{d}_3\tilde{W}_3 + \tilde{c}_0\tilde{W}_4 \\
&\quad + d_W I_W + \mathrm{Im}\Sigma_1\, I^{(1)}_{qq} + \mathrm{Im}\Sigma_8\, I^{(8)}_{qq}. && (3.2.53)
\end{aligned}
$$

Similarly, introducing the vector P and S as in Eq. (3.2.13) and (3.2.14), and the $SO(4)$ vector, Lorentz tensors

$$
S^{\mu\nu} = \begin{pmatrix} -\bar{q}i\sigma^{\mu\nu}\gamma^5\boldsymbol{\tau}q \\ \bar{q}\sigma^{\mu\nu}q \end{pmatrix}, \quad P^{\mu\nu} = \begin{pmatrix} \bar{q}\sigma^{\mu\nu}\boldsymbol{\tau}q \\ \bar{q}i\sigma^{\mu\nu}\gamma^5 q \end{pmatrix}, \tag{3.2.54}
$$

the lepton-quark Lagrangian can be expressed by

$$\begin{aligned}\mathcal{L}_{6,\,llqq} &= \bar{e}i\gamma^5 e\,\left(\mathrm{Im}\Sigma'_{lq\,1}S_4 + \mathrm{Re}\Sigma'_{lq\,2}S_3 + \mathrm{Im}\Sigma'_{lq\,2}P_3 - \mathrm{Re}\Sigma'_{lq\,1}P_4\right)\\ &\quad +\bar{e}e\,\left(\mathrm{Im}\Sigma'_{lq\,1}P_4 + \mathrm{Re}\Sigma'_{lq\,2}P_3 - \mathrm{Im}\Sigma'_{lq\,2}S_3 + \mathrm{Re}\Sigma'_{lq\,1}S_4\right)\\ &\quad +\bar{e}\sigma^{\mu\nu}e\,\left[2\mathrm{Re}\Sigma_{lq\,3}\left(S_{4\,\mu\nu} + P_{3\,\mu\nu}\right) + 2\mathrm{Im}\Sigma_{lq\,3}\left(P_{4\,\mu\nu} - S_{3\,\mu\nu}\right)\right]. \quad (3.2.55)\end{aligned}$$

The TV effective Lagrangian corresponding to Eqs. (3.2.53) and (3.2.55) can be constructed by writing down all terms that transform in the same way under Lorentz, P, T, and chiral symmetry as the terms in Eq. (3.2.53) and (3.2.55). This will be the focus of Chapter 4.

3.3 Chiral Lagrangian

The low-energy EFT that describes interactions among pions and nucleons (and delta isobars, since $m_\Delta - m_N \sim 2m_\pi$) at low momentum $Q \sim m_\pi \ll M_{QCD}$ is χPT. At such momenta we can resolve pion propagation, but not details of its structure. Pions must explicitly be accounted for in the theory, while other mesons can be integrated out. The special role of the pion is a consequence of the approximate invariance of the QCD Lagrangian under chiral symmetry. Because it is not manifest in the spectrum, which only exhibits approximate isospin symmetry, chiral symmetry must be spontaneously broken down to its diagonal subgroup $SU_{L+R}(2) \sim SO(3)$. From Goldstone's theorem, one expects to find in the spectrum massless Goldstone bosons that live on the "chiral circle" $S^3 \sim SO(4)/SO(3)$. There are, of course, infinite ways to parametrize the chiral circle. Here we use stereographic coordinates, whose dimensionless fields we denote by an isovector field $\boldsymbol{\zeta}$. We can identify these degrees of freedom with canonically normalized pion fields $\boldsymbol{\pi} = F_\pi\boldsymbol{\zeta}$, where $F_\pi \simeq 186$ MeV, called the pion decay constant, is the diameter of the chiral circle. Such fields transform in a complicated way under chiral symmetry. However, a pion covariant derivative can be defined by

$$D_\mu\boldsymbol{\pi} = D^{-1}\partial_\mu\boldsymbol{\pi}, \quad (3.3.1)$$

with

$$D = 1 + \frac{\boldsymbol{\pi}^2}{F_\pi^2}, \tag{3.3.2}$$

which transforms under chiral transformations as under an isospin transformation, but with a field-dependent parameter (see App. C). One can also construct the covariant derivative of this covariant derivative,

$$\mathcal{D}_\nu D_\mu \boldsymbol{\pi} = \partial_\nu D_\mu \boldsymbol{\pi} + \frac{2}{F_\pi^2} \left(\boldsymbol{\pi}\, D_\nu \boldsymbol{\pi} \cdot D_\mu \boldsymbol{\pi} - D_\nu \boldsymbol{\pi}\, \boldsymbol{\pi} \cdot D_\mu \boldsymbol{\pi} \right), \tag{3.3.3}$$

and so on.

Nucleons are described by an isospin-1/2 field N, and we can define a nucleon covariant derivative

$$\mathcal{D}_\mu N = \left(\partial_\mu + \frac{i}{F_\pi^2} \boldsymbol{\tau} \cdot (\boldsymbol{\pi} \times D_\mu \boldsymbol{\pi}) \right) N, \tag{3.3.4}$$

where τ_i, $i = 1, 2, 3$, are the Pauli matrices in isospin space. We also define $\mathcal{D}^\dagger$ through $\bar{N}\mathcal{D}^\dagger = \overline{\mathcal{D}N}$, and use the shorthand notation

$$\mathcal{D}^\mu_\pm \equiv \mathcal{D}^\mu \pm \mathcal{D}^{\dagger\mu}, \qquad \mathcal{D}^\mu_\pm \mathcal{D}^\nu_\pm \equiv \mathcal{D}^\mu \mathcal{D}^\nu + \mathcal{D}^{\dagger\nu} \mathcal{D}^{\dagger\mu} \pm \mathcal{D}^{\dagger\mu} \mathcal{D}^\nu \pm \mathcal{D}^{\dagger\nu} \mathcal{D}^\mu \tag{3.3.5}$$

and

$$\tau_i \mathcal{D}^\mu_\pm \equiv \tau_i \mathcal{D}^\mu \pm \mathcal{D}^{\dagger\,\mu} \tau_i, \quad \tau_i \mathcal{D}^\mu_\pm \mathcal{D}^\nu_\pm \equiv \tau_i \mathcal{D}^\mu \mathcal{D}^\nu + \mathcal{D}^{\dagger\nu} \mathcal{D}^{\dagger\mu} \tau_i \pm \mathcal{D}^{\dagger\mu} \tau_i \mathcal{D}^\nu \pm \mathcal{D}^{\dagger\nu} \tau_i \mathcal{D}^\mu. \tag{3.3.6}$$

At $Q \sim m_\pi \ll m_N$, nucleons are essentially non-relativistic; as such, the only coordinate with which their fields vary rapidly is $v \cdot x$, where v is the velocity. For simplicity, we employ a heavy-nucleon field from which this fast variation has been removed [34]. This simplifies the gamma matrix algebra, since only the spin S^μ remains. (This procedure can be easily generalized to include a heavy-delta field.) Below we use the subscript $\perp$ to denote the component of a four-vector perpendicular to the velocity, for example

$$\mathcal{D}_{\mu\perp} \equiv \mathcal{D}_\mu - v_\mu\, v \cdot \mathcal{D}. \tag{3.3.7}$$

The first step in describing QCD at low energies is to construct the most general Lagrangian that transforms under the symmetries of QCD in the same way as QCD itself. Along with this, one needs a power-counting scheme so that interactions can be ordered according to the expected size of their contributions. The Lagrangian contains an infinite number of terms that we group using an integer "chiral index" Δ and the (even) number of fermion fields f:

$$\mathcal{L} = \sum_{\Delta=0}^{\infty} \sum_{f/2} \mathcal{L}_f^{(\Delta)}. \tag{3.3.8}$$

The technology for constructing the Lagrangian is well known, see, for example, Ref. [32]. When we neglect $\mathcal{L}_e$, Eq. (3.2.11), $\mathcal{L}_\alpha$, Eq. (3.2.12), $\mathcal{L}_6$, Eq. (3.2.53), and $\mathcal{L}_{6,\,llqq}$, Eq. (3.2.55), the EFT Lagrangian includes all interactions made out of $D_\mu \boldsymbol{\pi}$, N, and their covariant derivatives that are chiral invariant. In this case interactions have index

$$\Delta = d + f/2 - 2 \geq 0, \tag{3.3.9}$$

in terms of the number d of derivatives (and powers of $m_\Delta - m_N$). For example, in leading order the chiral-invariant Lagrangians are

$$\mathcal{L}^{(0)}_{\chi,f=0} = \frac{1}{2} D_\mu \boldsymbol{\pi} \cdot D^\mu \boldsymbol{\pi} \tag{3.3.10}$$

and (omitting delta isobars)

$$\mathcal{L}^{(0)}_{\chi,f=2} = \bar{N} \left(iv \cdot \mathcal{D} - \frac{2 g_A}{F_\pi} S^\mu \boldsymbol{\tau} \cdot D_\mu \boldsymbol{\pi} \right) N, \tag{3.3.11}$$

where $g_A \simeq 1.267$ is the pion-nucleon axial-vector coupling.

Explicit chiral symmetry breaking can be systematically included in the χPT Lagrangian. $\mathcal{L}_\alpha$, Eq. (3.2.12), and $\mathcal{L}_e$, Eq. (3.2.11), break chiral symmetry: $\mathcal{L}_\alpha$ as third and fourth components of the vectors (3.2.13) and (3.2.14), and $\mathcal{L}_e$ as the third and fourth components of the antisymmetric tensor (3.2.16). In the EFT they generate interactions, now involving $\boldsymbol{\pi}$ directly and A_μ, that transform as these vectors and tensors, and their tensor products. These terms are proportional to powers of $m_{u,d}$ and e.

Operators proportional to the light-quark masses are power counted with the same chiral index Δ as in eq. (3.3.9), where the definition of d is extended to count powers of the quark mass. For power counting purposes, we count the average quark mass and the quark mass difference in the same way, that is, we consider $\varepsilon = \mathcal{O}(1)$.

Explicit chiral symmetry breaking in the form of isospin violation is also present in the electromagnetic terms from Eq. (3.2.11). They generate two classes of interactions. In one class, hadrons interact with soft photons (those with momenta below M_{QCD}) in a gauge-invariant way. We can minimally couple charged pions and nucleons to the photon by modifying their covariant derivatives,

$$\begin{aligned} (D_\mu \boldsymbol{\pi})_a &\rightarrow (D_{\mu,\,\mathrm{em}}\boldsymbol{\pi})_a = \frac{1}{D}\left(\partial_\mu \delta_{ab} - eA_\mu \varepsilon_{3ab}\right)\pi_b \\ \mathcal{D}_\mu N &\rightarrow \mathcal{D}_{\mu,\,\mathrm{em}} N = \left[\partial_\mu + \frac{i}{F_\pi^2}\boldsymbol{\tau}\cdot(\boldsymbol{\pi}\times D_{\mu,\mathrm{em}}\boldsymbol{\pi}) - ieA_\mu \frac{1}{2}\left(1+\tau_3\right)\right] N \\ &\quad . \end{aligned} \tag{3.3.12}$$

(For simplicity, in the text that follows we drop the subscript "em" in covariant derivatives.) In addition, we can couple the photon through the field strength $F_{\mu\nu}$. The other class of interactions consists of purely hadronic interactions from the exchange of hard photons (momenta above M_{QCD}), which can be integrated out, giving rise to operators with no explicit photon fields. The first class of interactions is very important because of EDMs; the second class competes with interactions from Eq. (3.2.12). We thus construct the low-energy interactions from Eq. (3.2.11) as well.

The index Δ defined in Eq. (3.3.9) can be generalized to label electromagnetic operators. If the operator contains soft photons, the definition of d is enlarged to count also the number of photon fields, which, having dimension one, require compensating powers of M_{QCD} in their coefficients. Operators generated by the integration of hard photons — sometimes called indirect electromagnetic operators — are proportional to powers of e^2. Typically, an extra inverse power of $4\pi^2$ appears in a loop, leading to a factor of α_{em}/π. Since the numerical value of α_{em}/π is very close to $\varepsilon\, m_\pi^3/M_{QCD}^3$ (using $M_{QCD} \sim m_\rho$, the mass of the rho meson), we can still use Δ to label this class

of operators, provided that each power of $\alpha_{\rm em}/\pi$ increases the chiral index by 3 [122].

The interactions stemming from the dimension 6 TV sources in Eq. (3.2.53) and (3.2.55) can be organized according to a chiral index analogous to Eq. (3.3.9), with the only difference that the coefficients of low-energy realizations of Eq. (3.2.53) and (3.2.55) must contain two powers of the high energy scale $M_{\mathcal{T}}$, which replace two powers of M_{QCD}. The powers of M_{QCD} in a coefficient are therefore counted by

$$\Delta_6 = d + f/2 - 4 \geq -2, \tag{3.3.13}$$

where d counts derivative and powers of the quark mass as described above.

For processes with at most one nucleon, $A = 0, 1$, all momenta and energies are typically $\sim Q$. The contribution of a diagram with L loops and C separately connected pieces to the amplitude T can then be estimated by

$$T \propto Q^\nu \mathcal{F}(Q/\mu), \tag{3.3.14}$$

where $\mathcal{F}$ is a calculable function, μ is a renormalization scale, and the counting index ν is

$$\nu = 4 - A + 2(L - C) + \sum_i \Delta_i. \tag{3.3.15}$$

Here, i counts the number of insertions of vertices from $\mathcal{L}_f^{(\Delta)}$. From Eq. (3.3.15) it is apparent that diagrams with increasingly higher number of loops and non-vanishing-index interactions are increasingly suppressed, leading to a perturbative expansion. Assigning to loops a characteristic factor $Q^2/(4\pi)^2$ and using naive dimensional analysis (NDA) to estimate the EFT parameters [123], the suppression scale is $M_{QCD} \sim 2\pi F_\pi$. Note that in this sector of the theory nucleon recoil is a subleading effect: the nucleon is nearly static.

The χPT power counting formula (3.3.15) cannot directly be applied to processes with $A \geq 2$ [35, 36, 37, 100, 38]. Indeed, in diagrams in which the intermediate state consists purely of propagating nucleons —which are called "reducible"— the contour of integration for integrals over the 0th components of loop momenta cannot be deformed in way to avoid the poles of the nucleon propagators, thus picking up energies

$\sim Q^2/m_N$ from nucleon recoil, no longer a subleading effect, rather than $\sim Q$. There is also an extra factor of 4π. These diagrams are therefore enhanced by factors of $4\pi m_N/Q$ with respect to the χPT power counting that assigns $Q^2/(4\pi)^2$ to a loop, and the need to resum them leads to the appearance of shallow bound states in systems with two or more nucleons, nuclei. Diagrams whose intermediate states contain interacting nucleons and pions —"irreducible"— do not suffer from this infrared enhancement, and in them nucleon recoil remains a small effect. Reducible diagrams are thus obtained by patching together irreducible diagrams with intermediate states consisting of A free-nucleon propagators. Calling V the sum of all irreducible diagrams, an amplitude for a process with $A \geq 2$ can be written schematically as

$$T = V + VG_0V + VG_0VG_0V + \ldots = V + VG_0T, \tag{3.3.16}$$

where G_0 is the free-nucleon, non-relativistic Green's function. Equation (3.3.14) is just the Lippmann-Schwinger equation, which is formally equivalent to a Schrödinger equation with a potential V.

Naive dimensional analysis suggests [35, 36] that irreducible diagrams follow the χPT power counting rule (3.3.15). While this is true for pion-exchange diagrams, the situation is more complicated for contact interactions. In fact, it can be shown that the iteration of the singular one-pion exchange requires for renormalization at the same order a finite number of $f = 4$ interactions, some of which are less suppressed than expected on the basis of naive dimensional analysis [124, 125, 126] (see also Refs. [127, 128] for further discussion). On the other hand, corrections, which should be perturbative, are expected to still conform to dimensional analysis [129, 130]. Since the TV potential, the quantity we focus on in the $f \geq 4$ sector, is very small and it can be treated as a perturbation, it should be amenable to an expansion in powers of Q/M_{QCD}, with different contributions organized according to their chiral index ν, or, equivalently, according to the number of inverse powers of M_{QCD}.

3.3.1 The TC χPT Lagrangian

We give here the TC chiral invariant terms of the χPT Lagrangian. The leading TC chiral Lagrangian has chiral index $\Delta = 0$ and is given by

$$\mathcal{L}^{(0)}_{\chi,\, f\leq 2} = \frac{1}{2} D_\mu \boldsymbol{\pi} \cdot D^\mu \boldsymbol{\pi} - \frac{m_\pi^2}{2D} \boldsymbol{\pi}^2 + \bar{N} \left(iv \cdot \mathcal{D} - \frac{2 g_A}{F_\pi} D_\mu \boldsymbol{\pi} \cdot \boldsymbol{\tau} S^\mu \right) N, \tag{3.3.17}$$

where g_A is the pion-nucleon axial coupling, $g_A \simeq 1.27$. Electromagnetic interactions at LO arise purely from the covariant derivatives D_μ and $\mathcal{D}_\mu$, defined in Eq. (3.3.12). For ease of reference, we have included in Eq. (3.3.17) the pion mass term, which, though chiral symmetry breaking, has nonetheless chiral index $\Delta = 0$.

Neglecting chiral-symmetry breaking from the quark masses, which will be extensively treated in Chapter 4, at order $\Delta = 1$ the relevant Lagrangian consists of

$$\begin{aligned} \mathcal{L}^{(1)}_{\chi,\, f=2} \;=\; & -\frac{1}{2m_N} \bar{N} \mathcal{D}_\perp^2 N + \frac{g_A}{F_\pi m_N} \left(iv \cdot D \boldsymbol{\pi} \right) \cdot \bar{N} \boldsymbol{\tau}\, S \cdot \mathcal{D}_- N \\ & + \frac{e}{4m_N} \epsilon_{\mu\nu\rho\sigma} \bar{N} \Bigg\{ (1+\kappa_0) \\ & + (1+\kappa_1) \left[\tau_3 - \frac{2}{F_\pi^2 D} \left(\boldsymbol{\pi}^2 \tau_3 - \pi_3 \boldsymbol{\pi} \cdot \boldsymbol{\tau} \right) \right] \Bigg\} v^\mu S^\nu N F^{\rho\sigma}, \end{aligned} \tag{3.3.18}$$

where $\varepsilon^{\mu\nu\rho\sigma}$ is the completely antisymmetric tensor in four dimension, with $\varepsilon^{0123} = -1$. Here the first two terms are the nucleon kinetic energy and a relativistic correction to the pion-nucleon coupling. The coefficients of both operators are fixed by Galilean invariance. The third and fourth terms represent the isoscalar and isovector magnetic dipole moment of the nucleon, and the anomalous nucleon-photon couplings κ_0 and κ_1 have the values $\kappa_0 = -0.12$ and $\kappa_1 = 3.7$. At the next chiral order, $\Delta = 2$,

$$\begin{aligned} \mathcal{L}^{(2)}_{\chi,\, f=2} \;=\; & + \frac{g_A}{4 F_\pi m_N^2} D_\mu \boldsymbol{\pi} \cdot \bar{N} \boldsymbol{\tau} \left(S^\mu \mathcal{D}^2_{\perp,-} - \mathcal{D}^\mu_{\perp,-}\, S \cdot \mathcal{D}_{\perp,-} \right) N \\ & - \frac{c_1}{F_\pi} D_\mu \boldsymbol{\pi} \cdot \bar{N} \boldsymbol{\tau}\, S^\mu \mathcal{D}^2_{\perp,+} N \\ & + \frac{e}{8m_N^2} i \varepsilon_{\mu\nu\alpha\beta} \bar{N} S^\nu \mathcal{D}^\mu_{\perp,-} \left[\left(1 + \kappa_0 - \frac{1}{2} \right) + \tau_3 \left(1 + \kappa_1 - \frac{1}{2} \right) \right] N F_{\alpha\beta}. \end{aligned} \tag{3.3.19}$$

The first term represents further relativistic corrections to the g_A term in Eq. (3.3.17). The constraints imposed by Lorentz invariance on Eqs. (3.3.18) and (3.3.19) are obtained following the method outlined in App. I, they do agree with the results of Ref. [131, 132], once a field redefinition is used to eliminate time derivatives acting on the nucleon field from the subleading $\Delta = 1$ and $\Delta = 2$ Lagrangians. The operator with coefficient $c_1 = \mathcal{O}\left(1/M_{QCD}^2\right)$ in Eq. (3.3.19) is a contribution to the square radius of the pion-nucleon form factor. The last two terms in Eq. (3.3.19) are the isoscalar and isovector spin-orbit couplings of the nucleon to the photon. Their coefficients is fixed by Lorentz invariance.

In the $f = 4$ sector, four-nucleon operators with no derivatives or insertion of the pion mass have the lowest chiral index $\Delta = 0$ [35, 36]

$$\mathcal{L}^{(0)}_{\chi,\, f=4} = -\frac{C_{11}}{2}\bar{N}N\bar{N}N - \frac{C_{\tau\tau}}{2}\bar{N}\boldsymbol{\tau}N\cdot\bar{N}\boldsymbol{\tau}N, \tag{3.3.20}$$

where, by naive dimensional analysis [123], the coefficients scale as $C_{11,\tau\tau} = \mathcal{O}(1/F_\pi^2)$. The combinations $C_{0s} = C_{11} - 3C_{\tau\tau}$ and $C_{0t} = C_{11} + C_{\tau\tau}$ contribute, respectively, to the to the isospin-singlet ($^3S_1$) and the isospin-triplet ($^1S_0$) scattering lengths. As we mentioned at the end of the previous Section, the iteration of the singular one-pion exchange potential requires for renormalization the promotion of some contact P-wave operators in the leading order $f = 4$ Lagrangian [124, 125, 126]. We will discuss four-nucleon operators and their power counting in some more detail in Chapters 6 and 7.

Explicit chiral-symmetry breaking and isospin-breaking operators in the chiral Lagrangian [122] stem from the average quark mass $\bar{m}$, the quark mass difference $m_d - m_u = 2\bar{m}\varepsilon$, and from the quark coupling to photons through the fine-structure constant $\alpha_{\rm em}$. We devote most of Chapter 4 to the inclusion of operators proportional to the quark mass in the χPT Lagrangian. Here, we list the most important isospin-breaking operators from electromagnetism. We count $\varepsilon \sim 1/3$ as $\mathcal{O}(1)$ and $\alpha_{\rm em}/\pi$ as $\mathcal{O}(\varepsilon m_\pi^3/M_{QCD}^3)$, since numerically $\alpha_{\rm em}/\pi \sim \varepsilon m_\pi^3/(2\pi F_\pi)^3$. Isospin-violating terms first contribute to the $\Delta = 1$ Lagrangian in the pion sector, and to the $\Delta = 2$

Lagrangian in the pion nucleon sector,

$$\mathcal{L}^{(1)}_{I,\,f=0,\,\mathrm{em}} = -\frac{\breve{\delta}m_\pi^2}{2D^2}\left(\boldsymbol{\pi}^{\,2}-\pi_3^2\right), \tag{3.3.21}$$

$$\mathcal{L}^{(2)}_{I,\,f=2,\,\mathrm{em}} = \frac{\breve{\delta}m_N}{2}\bar{N}\left[\tau_3+\frac{2}{F_\pi^2 D}\left(\pi_3\boldsymbol{\pi}\cdot\boldsymbol{\tau}-\boldsymbol{\pi}^{\,2}\tau_3\right)\right]N. \tag{3.3.22}$$

Here $\breve{\delta}m_\pi^2 = \mathcal{O}\left(\alpha_{\mathrm{em}}M_{QCD}^2/\pi\right)$ is the leading electromagnetic contribution to the pion mass splitting, while the quark-mass-difference contribution δm_π^2, which is defined in Sec. 4.1.1, is smaller by a power of $\varepsilon m_\pi/M_{QCD}$. The pion mass splitting, $m_{\pi^\pm}^2 - m_{\pi^0}^2 = \breve{\delta}m_\pi^2 + \delta m_\pi^2 = (35.5\text{ MeV})^2$, is dominated by the electromagnetic contribution. The nucleon mass splitting, $m_n - m_p = \delta m_N + \breve{\delta}m_N = 1.29$ MeV [1] also receives contributions from electromagnetism and from the quark masses. In this case, the quark-mass contribution δm_N is expected to be the largest. By dimensional analysis $\delta m_N = \mathcal{O}(\varepsilon m_\pi^2/M_{QCD})$, and lattice simulations estimate it to be $\delta m_N = 2.26 \pm 0.57 \pm 0.42 \pm 0.10$ MeV [133], which is in agreement with an extraction from charge-symmetry breaking in the $pn \to d\pi^0$ reaction [134, 135, 136]. The electromagnetic contribution is $\breve{\delta}m_N = \mathcal{O}\left(\alpha_{\mathrm{em}}M_{QCD}/\pi\right)$, that is, $\mathcal{O}\left(\varepsilon m_\pi^3/M_{QCD}^2\right)$ and about the 20% of δm_N. Using the Cottingham sum rule, $\breve{\delta}m_N = -(0.76 \pm 0.30)$ MeV [137], which is consistent with dimensional analysis.

We will extensively treat isospin violation from the quark mass difference in Chapter 4. For many applications it is convenient to eliminate the nucleon mass difference $m_n - m_p = \delta m_N + \breve{\delta}m_N$ from the nucleon propagator and from asymptotic states. This result can be accomplished through a field redefinition, defined in Ref. [138], which we summarize in App. G.

3.4 Vacuum Alignment

Explicit breaking of chiral symmetry can be systematically implemented as a small perturbation on the chiral invariant Lagrangian of Sec. 3.3 only if the true vacuum of the theory, which is selected by the explicit breaking terms, is aligned with the vacuum that was implicitly chosen in the construction of the χPT Lagrangian [32]

(see also the discussion and the simple example, in the case of linear realization of the symmetry group, in App. E). The S_3 term in Eq. (3.2.12) is actually unphysical because it gives rise to terms in the low-energy effective Lagrangian that make the vacuum unstable under small fluctuations. At leading order a term would arise that is linear in the pion fields (*i.e.* π_3). The vacuum would then be unstable because it could always produce mesons to lower its energy. The problem of such leading-order tadpoles, which signal vacuum misalignment, is discussed below in Subsec. 3.4.1.

There are two approaches to removing these spurious terms. One approach [139] is to impose, at quark level, the condition that TV interactions should not cause vacuum instability. This has been done [140] to first-order in symmetry-breaking interactions, and we review this argument in Subsec. 3.4.2. Then we derive in Chapter 4 the corresponding low-energy EFT, which will not contain terms which cause vacuum instability.

The other approach is to derive the low-energy EFT without putting any conditions on how the resulting interactions affect the vacuum, then employ field redefinitions on the fields at the hadronic level to eliminate terms that affect the stability of the vacuum. It is the second approach that we follow in Subsec. 3.4.3. For most of this section we neglect $\mathcal{L}_e$, Eq. (3.2.11), but we consider the field redefinitions in the presence of electromagnetism in Subsec. 3.4.4. Such an alternative procedure will help to understand what kind of interactions can be removed from the chiral Lagrangian. As we will see in Sec. 4.1.1, further pion tadpoles appear in subleading orders but pose no problems. They can also be eliminated with a field redefinition of the form discussed in this section.

The dimension 6 TV Lagrangian in Eq. (3.2.53) also contains terms which generate pion tadpoles. Because of their small coupling constant, however, they do not cause vacuum instability, and they can be treated in perturbation theory.

3.4.1 The need for vacuum alignment

To illustrate the importance of vacuum alignment for the construction of the EFT, let us suppose we do not align the vacuum at the quark level. One can construct the low-energy interactions induced by Eq. (3.2.12) following the method sketched in App. D. Among the various types of terms are the ones that are linear in the symmetry-breaking parameters. These are the infinitely many operators that transform as third and fourth components of S and P type vectors:

$$\begin{aligned}\mathcal{L}_\alpha &= \sum_n \{C_{4n} S_{4n}[\boldsymbol{\pi}, N] + C_{3n} S_{3n}[\boldsymbol{\pi}, N]\} \\ &\quad + \sum_n \{D_{3n} P_{3n}[\boldsymbol{\pi}, N] + D_{4n} P_{4n}[\boldsymbol{\pi}, N]\} + \ldots,\end{aligned} \tag{3.4.1}$$

where n runs over all $S[\boldsymbol{\pi}, N]$ and $P[\boldsymbol{\pi}, N]$ that can be obtained using Eq. (D.5), and "..." stand for higher-rank tensors. The coefficient $C_{\alpha n}$ or $D_{\alpha n}$ of each term depends on details of the QCD dynamics, and cannot at present be determined. However, chiral symmetry fixes the ratio of coefficients of components of the same object, which is given by Eq. (3.2.12). Thus

$$\begin{aligned}\frac{C_{3n}}{C_{4n}} &= \frac{\tan\alpha - \varepsilon \tan\frac{\bar\theta}{2}}{1 + \varepsilon \tan\alpha \tan\frac{\bar\theta}{2}} = \tan\left[\alpha - \arctan\left(\varepsilon \tan\frac{\bar\theta}{2}\right)\right], \\ \frac{D_{4n}}{D_{3n}} &= -\frac{\varepsilon\tan\alpha - \tan\frac{\bar\theta}{2}}{\varepsilon + \tan\alpha\tan\frac{\bar\theta}{2}} = -\tan\left[\alpha - \arctan\left(\frac{1}{\varepsilon}\tan\frac{\bar\theta}{2}\right)\right].\end{aligned} \tag{3.4.2}$$

The simplest symmetry breaking operator comes from $S[0, N] = (\mathbf{0}\ v_0)^T$, in which case a piece in Eq. (3.4.1) is

$$\mathcal{L}_{m_\pi^2} = \frac{\tilde m_\pi^2 F_\pi^2}{4} - \frac{\tilde m_\pi^2}{2D}\boldsymbol{\pi}^2 + \frac{g\tilde m_\pi^2 F_\pi}{2D}\pi_3, \tag{3.4.3}$$

where the bare pion mass is

$$\tilde m_\pi^2 = \frac{4v_0}{F_\pi^2}\bar m \cos\alpha\cos\frac{\bar\theta}{2}\left[1 + \varepsilon\tan\alpha\tan\frac{\bar\theta}{2}\right], \tag{3.4.4}$$

and the coupling of the neutral pion to the vacuum is

$$g = \tan\left[\alpha - \arctan\left(\varepsilon\tan\frac{\bar\theta}{2}\right)\right]. \tag{3.4.5}$$

The first term in Eq. (3.4.3) is a constant that is irrelevant for our purposes. The second term is a mass term, which together with the pion kinetic term in Eq. (3.3.10) generates a pion propagator of conventional form,

$$\frac{i\delta_{ab}}{p^2 - \tilde{m}_\pi^2 + i\varepsilon}, \tag{3.4.6}$$

when the pion momentum is p. Due to the non-linear realization of chiral symmetry, both this term and the pion kinetic term in Eq. (3.3.10) generate also pion self-interactions. The third term in Eq. (3.4.3) is T violating and allows neutral pions to disappear into the vacuum. It generates both tadpoles and interactions among an odd number of pions. Together, these two effects change pion propagation, since the full pion propagator includes now an arbitrary number of π_3s that disappear into vacuum. Examples are illustrated in Fig. 3.1, where we draw all the diagrams that contribute to the pion propagator up to order g^4.

The physical pion mass $m_\pi^2 = m_\pi^2(\tilde{m}_\pi^2, g)$ is given by the pole of the two-point Green's function. The difficulty is that the contributions of all the diagrams in Fig. 3.1 to the two-point Green's function are comparable to the one of the propagator. Indeed, the first two diagrams in Fig. 3.1 give a contribution of order $g^2\tilde{m}_\pi^2/(p^2-\tilde{m}_\pi^2)^2$, while the other diagrams in Fig. 3.1 scale as $g^4\tilde{m}_\pi^2/(p^2 - \tilde{m}_\pi^2)^2$ or $g^4\tilde{m}_\pi^4/(p^2 - \tilde{m}_\pi^2)^3$, where we take $p \sim \tilde{m}_\pi$. These translate into contributions of relative order g^2 and g^4, respectively, to the pion mass. Since g depends on α and is *a priori* not small, these diagrams have the same power counting as the propagator (3.4.6): to calculate the two-point Green's function at tree level we need to sum all the diagrams of the type in Fig. 3.1 with an arbitrary number of tadpoles. That is, the pion two-point function in the presence of explicit chiral symmetry breaking in the form (3.4.1) cannot be calculated in perturbation theory.

Notice that the vectors $\tilde{W}_3$ and W_3 (and $\tilde{V}_4$, when combined with the antysimmetric tensor T_{34} generated by an hard photon) in Eq. (3.2.53) also generate pion tadpoles. However, as we will see in Sec. 4.1.1, in this case the coupling constant g

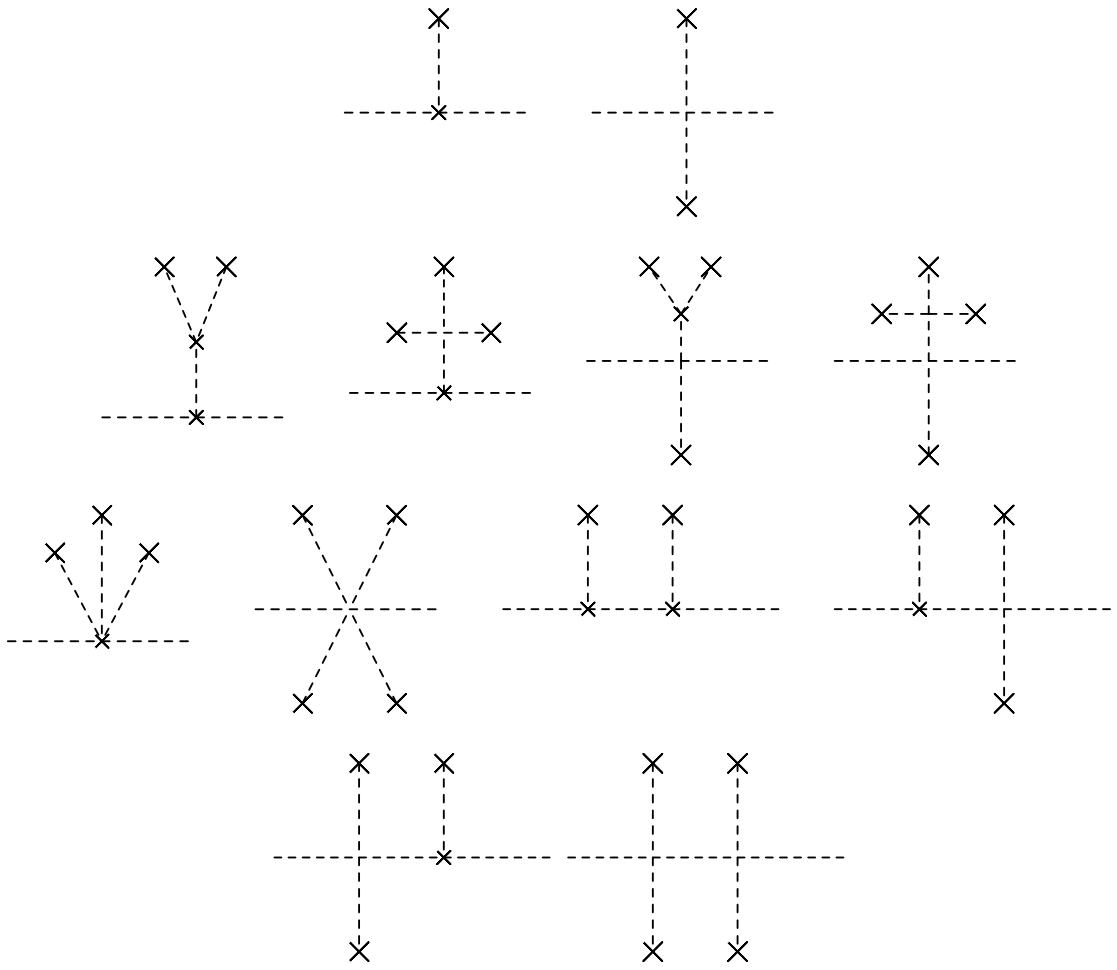

FIGURE 3.1. Contributions of order g^2 (first line) and g^4 (next three lines) to the pion two-point Green's function. A dashed line stands for a pion propagator, Eq. (3.4.6). A cross denotes a vertex coming from the third term in Eq. (3.4.3). Other vertices arise from Eq. (3.3.10) and the second term in Eq. (3.4.3).

is small, being suppressed by two powers of $M_{QCD}/M_{\mathcal{T}}$

$$g = \mathcal{O}\left((\delta_3 + \delta_0)\,\frac{\alpha_{\rm em}}{\pi}\left(\frac{M_{QCD}}{M_{\mathcal{T}}}\right)^2,\ \tilde{\delta}_3\left(\frac{M_{QCD}}{M_{\mathcal{T}}}\right)^2\right). \tag{3.4.7}$$

Eq. (3.4.7) allows to treat pion tadpoles stemming from the dimension 6 sources in perturbation theory, and no further alignment is needed.

The example of the pion mass can be extended to other observables, for example pion-pion or pion-nucleon scattering cross sections: at any order in Q/M_{QCD}, an infinite number of diagrams in which zero-momentum neutral pions disappear into the vacuum contribute to the physical process. When explicit and spontaneous symmetry breaking are badly misaligned, explicit symmetry breaking is not just a perturbation. In App. E we show this in a simple example.

The resummation of pion tadpoles can be performed explicitly in diagrams. We show in App. F how to do so in the case of the pion two-point Green's function at tree level. Although calculations can be carried out with arbitrary α, it is unpractical to do so for all quantities and at every order. We are thus led to impose at least approximate vacuum alignment.

3.4.2 Alignment at quark level

Explicit symmetry-breaking terms provide a preferred direction for spontaneous symmetry breaking [139]. The construction of the effective Lagrangian only relies on the fact that the symmetry group is broken to one of its subgroups, for example, $SO(4)$ broken to $SO(3)$. However, in the absence of explicit symmetry-breaking terms, there is no way to say which particular subgroup it is broken to. We choose the $SO(3)$ subgroup of rotations in the three-dimensional space orthogonal to the vector $n = (\mathbf{0}\ 1)^T$, but any other choice of n would be equivalent. Explicit symmetry-breaking terms force a particular choice of vacuum, "aligned" with the breaking terms.

Here we consider alignment in first order in chiral-symmetry-breaking parameters, as originally done by Baluni [140]. The chiral-symmetry-breaking Lagrangian (3.2.12)

generates at tree level an effective potential

$$V_1 = c_4 S_4 + d_3 P_3 + d_4 P_4 + c_3 S_3. \tag{3.4.8}$$

The vacuum alignment condition (see Eq. (E.5)) is

$$\begin{aligned} \sum_{\alpha=1}^{4} \left(\mathcal{T}^a \bar{S}\right)_\alpha \frac{\partial V_1}{\partial S_\alpha} + \sum_{\alpha=1}^{4} \left(\mathcal{T}^a \bar{P}\right)_\alpha \frac{\partial V_1}{\partial P_\alpha} = 0, \\ \sum_{\alpha=1}^{4} \left(\mathcal{X}^a \bar{S}\right)_\alpha \frac{\partial V_1}{\partial S_\alpha} + \sum_{\alpha=1}^{4} \left(\mathcal{X}^a \bar{P}\right)_\alpha \frac{\partial V_1}{\partial P_\alpha} = 0, \end{aligned} \tag{3.4.9}$$

where the bar means we are considering the vacuum expectation value, and $\mathcal{T}^a$ and $\mathcal{X}^a$ are the $SO(4)$ generators. Using the explicit expression (C.2) of the generators, the vacuum alignment condition (3.4.9) reads

$$\begin{aligned} d_3 \bar{P}_1 + c_3 \bar{S}_1 = 0, \qquad d_3 \bar{P}_2 + c_3 \bar{S}_2 = 0, \\ d_4 \bar{P}_1 + c_4 \bar{S}_1 = 0, \qquad d_4 \bar{P}_2 + c_4 \bar{S}_2 = 0, \end{aligned} \tag{3.4.10}$$

and

$$c_4 \bar{S}_3 + d_4 \bar{P}_3 - d_3 \bar{P}_4 - c_3 \bar{S}_4 = 0. \tag{3.4.11}$$

Assuming that the vacuum does not break isospin [141, 142] and parity [143],

$$\bar{S} = \begin{pmatrix} \mathbf{0} \\ v \end{pmatrix}, \qquad \bar{P} = \begin{pmatrix} \mathbf{0} \\ 0 \end{pmatrix}, \tag{3.4.12}$$

with $v \neq 0$ a real number, which we can choose to be positive. Plugging in this guess for the vacuum, Eq. (3.4.11) becomes

$$c_3 v = 0, \tag{3.4.13}$$

which is satisfied only if the coefficient of the third component of the S vector in Eq. (3.2.12) vanishes, $c_3 = 0$. We can rephrase this result by saying that TV terms can be implemented as small perturbations in the usual chiral Lagrangian if the freedom to choose the parameter α in Eq. (3.2.12) is used to make the TV interaction an isospin singlet [139, 144, 140]. Explicitly, the condition $c_3 = 0$ is

$$\tan\alpha = \varepsilon \tan\frac{\bar{\theta}}{2}. \tag{3.4.14}$$

This choice automatically kills all coefficients C_{3n} (see Eq. (3.4.2)), and in particular the strength g of the pion tadpole (see Eq. (3.4.5)).

Substituting Eq. (3.4.14) into Eq. (3.2.12), we obtain

$$\mathcal{L}_m = -\bar{m}\, r(\bar{\theta})\, S_4 + \varepsilon \bar{m}\, r^{-1}(\bar{\theta})\, P_3 + m_\star \sin\bar{\theta}\, r^{-1}(\bar{\theta})\, P_4, \tag{3.4.15}$$

where we introduced the standard parameter

$$m_\star = \frac{m_u m_d}{m_u + m_d} = \frac{\bar{m}}{2}\left(1 - \varepsilon^2\right) \tag{3.4.16}$$

and the function

$$r(\bar{\theta}) = \left(\frac{1 + \varepsilon^2 \tan^2\frac{\bar{\theta}}{2}}{1 + \tan^2\frac{\bar{\theta}}{2}}\right)^{1/2}. \tag{3.4.17}$$

The last term in Eq. (3.4.15) is T violating. As it is well known, this source of T violation is small for $\bar{\theta}$ near 0 or near π. If $|\bar{\theta}| \ll 1$, then $r(\bar{\theta}) = 1 + \mathcal{O}(\bar{\theta}^2)$ and [140, 93]

$$\mathcal{L}_m = -\bar{m}\, S_4 + \varepsilon \bar{m}\, P_3 + m_\star \bar{\theta}\, P_4 + \mathcal{O}\left(\bar{\theta}^2\right). \tag{3.4.18}$$

On the other hand, for $|\bar{\theta} - \pi| \ll 1$, $r(\bar{\theta}) = |\varepsilon| + \mathcal{O}((\bar{\theta} - \pi)^2)$ and [93]

$$\mathcal{L}_m = -\bar{m}|\varepsilon|\, S_4 + \frac{\varepsilon}{|\varepsilon|}\bar{m}\, P_3 + \frac{m_\star}{|\varepsilon|}\left(\pi - \bar{\theta}\right)\, P_4 + \mathcal{O}\left((\pi - \bar{\theta})^2\right). \tag{3.4.19}$$

3.4.3 Alignment at hadronic level

In the previous section we exploited the freedom in the choice of the parameter α in Eq. (3.2.12) to write the TV term in the QCD Lagrangian in a way compatible with the usual choice of the vacuum, which respects parity and isospin symmetry. In this section we follow a different approach: we start from the EFT Lagrangian (3.4.1) that reflects Eq. (3.2.12) before alignment, and we look for a rotation within the EFT that enforces the vacuum alignment condition (3.4.13).

We define a new field $\boldsymbol{\zeta}'$ for the pion through

$$\zeta_i = \frac{1}{d'}\left\{\zeta'_i - \delta_{i3}\left[2C\zeta'_3 + S\left(1 - \boldsymbol{\zeta}'^2\right)\right]\right\}, \tag{3.4.20}$$

where

$$d' = 1 - C\left(1 - \boldsymbol{\zeta}'^2\right) + 2S\zeta_3', \tag{3.4.21}$$

and

$$C = \frac{1}{2}(1 - \cos\varphi), \qquad S = \frac{1}{2}\sin\varphi, \tag{3.4.22}$$

in terms of an angle φ. Although this transformation is complicated, the pion covariant derivative simply rotates,

$$D_\mu \pi_i = \sum_j O'_{ij} D'_\mu \pi'_j \tag{3.4.23}$$

with a matrix

$$O'_{ij} = \delta_{ij} - \frac{2}{d'}\left\{C\left[\left(\boldsymbol{\zeta}'^2 - \zeta_3'^2\right)\delta_{ij} - \varepsilon_{3ik}\zeta'_k\varepsilon_{3jl}\zeta'_l\right] + \left(C\zeta_3' + S\right)\left(\zeta'_i\delta_{3j} - \zeta'_j\delta_{3i}\right)\right\} \tag{3.4.24}$$

that is orthogonal,

$$\sum_l O'_{il}O'_{jl} = \delta_{ij}. \tag{3.4.25}$$

Analogously, we define a new field N' for the nucleon via

$$N = U'N', \tag{3.4.26}$$

with a matrix

$$U' = \frac{1}{\sqrt{d'}}\left[\sqrt{1-C} + \sqrt{C}\left(\zeta_3' + 2i\varepsilon_{3jk}\zeta'_j t_k\right)\right] \tag{3.4.27}$$

that is unitary,

$$U'^\dagger U' = 1. \tag{3.4.28}$$

One can show that the covariant derivative of the nucleon is indeed covariant under this field redefinition,

$$\mathcal{D}_\mu N = U'\mathcal{D}'_\mu N'. \tag{3.4.29}$$

As a consequence, nucleon bilinears change under this field redefinition as under isospin; for example,

$$\begin{aligned} \bar{N}N &= \bar{N}'N', \\ \bar{N}t_i N &= \sum_j O'_{ij}\bar{N}'t_j N'. \end{aligned} \tag{3.4.30}$$

More generally then, a generic pionless isoscalar and isovector operator, constructed with nucleon fields, their covariant derivatives and covariant derivatives of the pion, transforms under (3.4.26) like

$$\begin{aligned} V_4[0,N] &= V'_4[0,N'], \\ V_i[0,N] &= \sum_j O'_{ij} V'_j[0,N']. \end{aligned} \tag{3.4.31}$$

The chiral-invariant part of the Lagrangian, for example Eqs. (3.3.10) and (3.3.11), is built out of isoscalar combinations of chiral-covariant objects. The properties (3.4.25) and (3.4.28) thus ensure that the chiral-invariant Lagrangian is invariant under the field redefinitions (3.4.20) and (3.4.26).

This is not true of the chiral-variant interactions (3.4.1). After the redefinitions (3.4.20) and (3.4.26),

$$\begin{aligned} \mathcal{L}_\alpha \;=\; & \sum_n \left\{ C'_{4n} S_{4n}[\boldsymbol{\pi}', N'] + C'_{3n} S_{3n}[\boldsymbol{\pi}', N'] \right\} \\ & + \sum_n \left\{ D'_{3n} P_{3n}[\boldsymbol{\pi}', N'] + D'_{4n} P_{4n}[\boldsymbol{\pi}', N'] \right\} + \ldots, \end{aligned} \tag{3.4.32}$$

with

$$\begin{aligned} C'_{3n} &= (1-2C)\, C_{3n} + 2S C_{4n}, \qquad & C'_{4n} &= (1-2C)\, C_{4n} - 2S C_{3n}, \\ D'_{3n} &= (1-2C)\, D_{3n} + 2S D_{4n}, \qquad & D'_{4n} &= (1-2C)\, D_{4n} - 2S D_{3n}. \end{aligned} \tag{3.4.33}$$

All S_{3n} can be eliminated from the Lagrangian by choosing

$$\tan\varphi = \frac{2S}{1-2C} = -\frac{C_{3n}}{C_{4n}} = -\tan\left[\alpha - \arctan\left(\varepsilon \tan\frac{\bar\theta}{2}\right)\right], \tag{3.4.34}$$

that is, by

$$\tan(\varphi+\alpha) = \varepsilon \tan\frac{\bar\theta}{2}. \tag{3.4.35}$$

In this case,

$$\begin{aligned} C'_{3n} &= 0, \qquad & C'_{4n} &= -\bar m\, r(\bar\theta), \\ D'_{3n} &= \varepsilon\, \bar m\, r^{-1}(\bar\theta), \qquad & D'_{4n} &= m_\star \sin\bar\theta\, r^{-1}(\bar\theta), \end{aligned} \tag{3.4.36}$$

just as it results from Eq. (3.4.15).

Equation (3.4.35) is the counterpart of Eq. (3.4.14), which was found by imposing the vacuum alignment condition at the level of the QCD Lagrangian. What the field redefinitions (3.4.20) and (3.4.26) do is to realize in the EFT a chiral rotation that, composed with the rotation in Eq. (3.2.12), changes the angle $\alpha \to \alpha + \varphi$. After the field redefinition, there are no leading-order tadpoles; we have effectively resummed in one go all terms generated by the third term in Eq. (3.4.3) and by all other S_3s.

3.4.4 Alignment in the presence of electromagnetism

We now show that the transformations (3.4.20) and (3.4.26) do not change the realization of isospin-breaking operators generated by the electromagnetic interaction of the quarks.

In the presence of electromagnetism, the covariant derivatives change according to Eq. (3.3.12). This does not change the results (3.4.23) and (3.4.29),

$$D_{\mu,\,\mathrm{em}}\pi_i = \sum_j O'_{ij} D'_{\mu,\,\mathrm{em}}\pi'_j \tag{3.4.37}$$

and

$$\mathcal{D}_{\mu,\,\mathrm{em}}N = U'\mathcal{D}'_{\mu,\,\mathrm{em}}N'. \tag{3.4.38}$$

As a consequence, chiral-invariant operators constructed with the minimally coupled pion and nucleon covariant derivatives are unchanged by the field redefinitions (3.4.20) and (3.4.26).

Following the method of App. D, the chiral-variant operators involving electromagnetism can be constructed from the components of $SO(4)$ antisymmetric tensors: the 4-i component, $T_{4i}[0, N]$, which is an isovector, and under the field redefinitions (3.4.20) and (3.4.26) transforms like Eq. (3.4.31); and the i-j component, $T_{ij}[0, N]$, which transforms as

$$T_{ij}[0, N] = \sum_{l,m} O'_{il} O'_{jm} T'_{lm}[0, N']. \tag{3.4.39}$$

Since under the redefinitions (3.4.20) and (3.4.26)

$$\left[\frac{1}{D}\left(1-\frac{\boldsymbol{\pi}^2}{F_\pi^2}\right)\delta_{3i}+\frac{2\pi_3\pi_i}{F_\pi^2 D}\right]T_{4i}[0,N]=\left[\frac{1}{D}\left(1-\frac{\boldsymbol{\pi}'^2}{F_\pi^2}\right)\delta_{3i}+\frac{2\pi'_3\pi'_i}{F_\pi^2 D'}\right]T'_{4i}[0,N'] \tag{3.4.40}$$

and

$$\frac{2}{F_\pi D}\left(\delta_{3j}\pi_i-\pi_j\delta_{3i}\right)T_{ij}[0,N]=\frac{2}{F_\pi D'}\left(\delta_{3j}\pi'_i-\pi'_j\delta_{3i}\right)T'_{ij}[0,N'], \tag{3.4.41}$$

the tensor is also invariant.

Chapter 4

The T Violating χPT Lagrangian

4.1 Hadronic Interactions

In this section we construct the most important operators in the low-energy EFT with the same chiral properties as Eqs. (3.4.15), (3.2.53) and (3.2.55). We start from studying Eq. (3.4.15).

The first class of interactions originates entirely from the average quark mass $\bar{m}$, the first term in Eq. (3.4.15). These interactions break $SO(4)$ explicitly down to the $SO(3)$ of isospin. They are well known, and examples are given in App. D. The most important effect is an S_4 that gives rise to the pion mass,

$$\mathcal{L}^{(0)}_{\not\chi, f=0} = \frac{m_\pi^2 F_\pi^2}{4} - \frac{m_\pi^2}{2D}\boldsymbol{\pi}^2, \tag{4.1.1}$$

where $m_\pi^2 = \mathcal{O}(r(\bar{\theta})\bar{m}M_{QCD})$. Also relevant for what follows is a similar S_4 but containing two nucleon fields, the nucleon sigma term

$$\mathcal{L}^{(1)}_{\not\chi,\, f=2} = \Delta m_N \bar{N} N \left(1 - \frac{2\boldsymbol{\pi}^2}{F_\pi^2 D}\right), \tag{4.1.2}$$

where the nucleon mass correction $\Delta m_N = \mathcal{O}\left(r(\bar{\theta})\bar{m}\right) = \mathcal{O}\left(m_\pi^2/M_{QCD}\right)$. There is, of course, an infinite number of other S_4s, all of which will bring in interactions $\propto \bar{m}$. An example in the $\Delta = 2$ Lagrangian is

$$\mathcal{L}^{(2)}_{\not\chi,\, f=2} = \frac{\beta_2}{F_\pi}\left(1 - \frac{2\boldsymbol{\pi}^{\,2}}{F_\pi^2 D}\right) D_\mu \boldsymbol{\pi} \cdot \bar{N}\boldsymbol{\tau} S^\mu N, \tag{4.1.3}$$

where $\beta_2 = \mathcal{O}\left(m_\pi^2/M_{QCD}^2\right)$ is a chiral-symmetry-breaking correction to g_A [145], the so-called Goldberger-Treiman discrepancy. In addition, there are interactions from tensor products of S_4s proportional to higher powers of $\bar{m}$. For example, $S_4 \otimes S_4$ with the same S_4 that generates Eq. (4.1.1) produces

$$\mathcal{L}^{(2)}_{\not\chi, f=0} = \frac{F_\pi^2\, \Delta m_\pi^2}{8} - \frac{\Delta m_\pi^2}{2D^2}\boldsymbol{\pi}^2, \tag{4.1.4}$$

where Δm_π^2 is an $\mathcal{O}(m_\pi^4/M_{QCD}^2)$ contribution to the pion mass. All such chiral-variant interactions have strengths proportional to powers of m_π^2 times appropriate powers of M_{QCD}. Since by all evidence $r(\bar{\theta})$ is not small, the dimensionless factors are expected to be of $\mathcal{O}(1)$. When we are interested in processes with typical momenta $Q \sim m_\pi$, the power counting of $f \leq 2$ interactions, Eq. (3.3.9), can be straightforwardly generalized by defining d to count powers of m_π as well.

More interesting are the low-energy interactions stemming from the other two terms in Eq. (3.4.15). The second breaks the $SO(3)$ of isospin down to $SO(2)$ of rotations in the 1-2 plane in $\boldsymbol{\zeta}$ space. In particular, it is also charge-symmetry breaking (CSB) —charge symmetry is a discrete isospin rotation of π around the 2 axis that exchanges (up to a phase) the u and d quarks [146, 147]. The third term is P and T violating but also breaks $SO(4)$. The crucial point is that these two terms are linked because they break chiral symmetry through components of the *same* chiral four-vector. Therefore, T violation from the $\bar{\theta}$ term is intrinsically linked to CSB because of chiral symmetry: for each TV hadronic interaction with an odd (even) number of pions from a P_4, there is a CSB interaction with an even (odd) number of pions from the associated P_3. The ratio between the coefficients of the P_4 and P_3 components is fixed by the ratio in Eq. (3.4.15),

$$\frac{T \text{ violation}}{\text{isospin violation}} = \frac{m_\star}{\varepsilon \bar{m}} \sin\bar{\theta} = \frac{1-\varepsilon^2}{2\varepsilon} \sin\bar{\theta} \equiv \rho(\bar{\theta}, \epsilon). \tag{4.1.5}$$

This ratio ρ is small when $\sin\bar{\theta} \simeq \bar{\theta}$ for $|\bar{\theta}| \ll 1$ and $\sin\bar{\theta} \simeq \pi - \bar{\theta}$ for $|\pi - \bar{\theta}| \ll 1$.

Unfortunately this link becomes ineffective when sufficiently complicated tensor products have to be included. We show in App. H that in the pion-nucleon sector of the purely hadronic Lagrangian this problem only appears when considering operators suppressed by m_π^4/M_{QCD}^4 relative to the leading TV interaction. As we will see in Sec. 4.2, the electromagnetic interaction makes this problem more acute, so that Eq. (4.1.5) is ineffective already for the leading short-distance contributions to the nucleon EDM.

Relations analogous to Eq. (4.1.5) can be established for the operators stemming

from the dimension 6 qEDM and qMDM, and qCEDM and qCMDM. From Eq. (3.2.54), one sees that the isoscalar (isovector) qEDM breaks chiral symmetry as the fourth (third) component V_4 (W_3) of a chiral four-vector V (W), whose third (fourth) component V_3 (W_4) represents the isovector (isoscalar) qMDM. In analogy to Eq. (4.1.5), we thus introduce the factors ρ_0 and ρ_3 to express, respectively, the ratio between the coefficients of the V_4 and V_3 components and W_3 and W_4 components

$$\begin{aligned} \frac{\text{isoscalar qEDM}}{\text{isovector qMDM}} &= -\frac{d_0}{c_3} = -\frac{c_0}{c_3}\tan\phi_0 \equiv \rho_0, \\ \frac{\text{isovector qEDM}}{\text{isoscalar qMDM}} &= \frac{d_3}{c_0} = \frac{c_3}{c_0}\tan\phi_3 \equiv \rho_3. \end{aligned} \tag{4.1.6}$$

Similarly, for the qCEDM and qCMDM, the ratios between the coefficients of $\tilde{V}_4$ and $\tilde{V}_3$ and $\tilde{W}_3$ and $\tilde{W}_4$ are given by $\tilde{\rho}_0$ and $\tilde{\rho}_3$, with

$$\tilde{\rho}_0 \equiv -\frac{\tilde{c}_0}{\tilde{c}_3}\tan\tilde{\phi}_0, \quad \tilde{\rho}_3 \equiv \frac{\tilde{c}_3}{\tilde{c}_0}\tan\tilde{\phi}_3. \tag{4.1.7}$$

In the case of the qEDM and qCEDM, the formal link with the coefficients of the operators generated by the qMDM and qCMDM carries little relevance. As we will see from the explicit realization of Eq. (3.2.53) in the EFT, the low energy manifestations of the qCMDM and qMDM amount to small corrections, suppressed by $\mathcal{O}(M_{QCD}^2/M_T^2)$, to the coefficients of chiral-symmetry breaking and isospin-symmetry breaking operators, whose leading contribution is given by the quark average mass and quark mass difference terms in Eq. (3.4.15). It is therefore impossible to extract the coefficients of the effective operators that realize the qCMDM and qMDM in χPT from TC observables, and thus the ability of Eqs. (4.1.6) and (4.1.7) to express the coefficients of TV operators in terms of a function of parameters of the Lagrangian only ($\rho_{0,3}$ and $\tilde{\rho}_{0,3}$) and a strong interaction contributions, fitted to data for TC observables, is lost.

For the two-lepton-two-quark operators, the ratio of the coefficients of TV and TC lepton-quark operators is expressed by $\rho_{lq\,1,2,3}$, with

$$\rho_{lq\,1} \equiv \frac{\text{Im}\,\Sigma'_{lq\,1}}{\text{Re}\Sigma_{eq\,2}}, \quad \rho_{lq\,2} \equiv -\frac{\text{Im}\,\Sigma'_{lq\,2}}{\text{Re}\Sigma_{eq\,1}}, \quad \rho_{lq\,3} \equiv \frac{\text{Im}\,\Sigma'_{lq\,3}}{\text{Re}\Sigma_{eq\,3}}. \tag{4.1.8}$$

We now proceed to build the low-energy interactions that arise from Eqs. (3.4.15), (3.2.53) and (3.2.55). As for the chiral-variant but isospin- and T-symmetric terms, we will for simplicity take $r(\bar{\theta})$ to be $\mathcal{O}(1)$ for power-counting purposes. Note that mixed operators that combine symmetry breaking from various sources have to be included. Since the chiral-symmetry-breaking operators involving only S_4s do not directly affect the link (4.1.5), we do not list all of them, but only those relevant to our discussion.

We consider here only the lower chiral-index Δ operators, classified according to the number f of nucleon fields. As d and f increase, interactions decrease in importance [33, 37], but obviously the procedure can be continued *ad nauseum*. As we will show, non-aligned operators, like pion tadpoles, appear in power-suppressed terms in the Lagrangian, but they can be dealt with in perturbation theory.

4.1.1 Pion sector

We start by discussing the leading interactions generated by the quark mass, the quark mass difference and the $\bar{\theta}$ term that involve only pion fields, that is, with $f = 0$. As it turns out, one cannot construct any terms that transform as P_3 and P_4. Higher-order terms have the same transformation properties as the third and fourth components of $SO(4)$ tensors that correspond to tensor products of the different symmetry-breaking sources in the QCD Lagrangian (3.4.15).

The chiral-symmetry-breaking Lagrangian with $\Delta = 2$ could receive contributions from the tensor products $S_4 \otimes P_b$ and $P_a \otimes P_b$. No purely-pionic operator of the first type can be constructed, while the tensor $P_a \otimes P_b$ can be reduced to a chiral invariant and a two-index symmetric tensor, $P_a \otimes P_b = \delta_{ab} I + S_{ab}$. In the pion sector the invariant is a constant, and can be discarded. The 3-3 component of the symmetric tensor yields an isospin-breaking correction to the pion mass, the 4-4 component a chiral-breaking but isospin-conserving correction to the mass, while the

3-4 component breaks isospin, parity and time reversal:

$$\mathcal{L}^{(2)}_{\not\chi,f=0} = \frac{\rho^2 F_\pi^2\,\delta m_\pi^2}{8} + \frac{\delta m_\pi^2}{2D^2}\left[\pi_3^2 - \rho^2\boldsymbol{\pi}^2 + \rho F_\pi\left(1-\frac{\boldsymbol{\pi}^2}{F_\pi^2}\right)\pi_3\right], \tag{4.1.9}$$

where we introduced the coefficient

$$\delta m_\pi^2 = \mathcal{O}\left(\frac{\varepsilon^2 m_\pi^4}{r^4(\bar\theta) M_{QCD}^2}\right), \tag{4.1.10}$$

which is the largest quark-mass contribution to the pion-mass splitting [122]. Since the latter receives a much larger electromagnetic contribution (see Eq. (3.3.21)) $\breve{\delta} m_\pi^2 = \mathcal{O}\left(\alpha_{\rm em} M_{QCD}^2/\pi\right)$ [122, 145], it is unlikely that this term is of any phenomenological use in itself.

However, Eq. (4.1.9) presents a simple illustration of the link between isospin and T violation. It also has the interesting feature that, even after we chose to align the vacuum linearly in the chiral-symmetry breaking parameters, non-aligned operators appear in the power-suppressed Lagrangian. We discuss the role of such tadpoles in Sec. 4.3.

Pion tadpoles are generated also by indirect electromagnetic effects. If we count $\alpha_{\rm em}/\pi \sim \varepsilon m_\pi^3/M_{QCD}^3$, these term are booked in the $\Delta = 3$ Lagrangian, and have the form

$$\mathcal{L}^{(3)}_{\not\chi,f=0,{\rm em}} = \frac{\breve{\delta}^{(3)} m_\pi^2\, F_\pi^2}{4} - \frac{\breve{\delta}^{(3)} m_\pi^2}{2D}\left(\boldsymbol{\pi}^2 + \rho F_\pi\,\pi_3\right), \tag{4.1.11}$$

the two terms corresponding to the tensor products $P_4 \otimes T_{34}$ and $P_3 \otimes T_{34}$. Here the coefficient

$$\breve{\delta}^{(3)} m_\pi^2 = \mathcal{O}\left(\frac{\alpha_{\rm em}}{\pi}\frac{\varepsilon m_\pi^2}{r^2(\bar\theta)}\right). \tag{4.1.12}$$

Equation (4.1.11) is exactly of the form of Eq. (3.4.3). The only TV operator is the pion tadpole (and its associated interactions). Since $\breve{\delta}^{(3)} m_\pi^2 \ll m_\pi^2$, it does not signal vacuum instability and can be treated in perturbation theory. Because these are already small terms, we do not bother to consider higher orders.

The dimension 6 sources in Eq. (3.2.53) also generate pion tadpoles. At lowest order, $\Delta_6 = -2$, tadpoles come from the isovector qCEDM, which transforms as

the third component of a $SO(4)$ vector $\tilde{W}_3$, and from combining the effects of the chiral-invariant TV operators, the gCEDM and the two four-quark operators in Eq. (3.2.36), with isospin violation from the quark mass difference. At $\Delta = -2$, we find

$$\mathcal{L}^{(-2)}_{6,\,f=0} = \frac{F_\pi^2}{4}\tilde{\Delta}_q m_\pi^2 - \tilde{\Delta}_q m_\pi^2 \frac{\boldsymbol{\pi}^2}{2D} + \left(\tilde{\rho}_3 \tilde{\Delta}_q m_\pi^2 + \bar{\Delta}_w m_\pi^2\right) \frac{F_\pi \pi_3}{2D}, \tag{4.1.13}$$

where, from the rules of NDA [123],

$$\tilde{\rho}_3\, \tilde{\Delta}_q m_\pi^2 = \mathcal{O}\left(\tilde{\delta}_3 \frac{m_\pi^2 M_{QCD}^2}{M_{\not T}^2}\right), \quad \bar{\Delta}_w m_\pi^2 = \mathcal{O}\left(w\varepsilon \frac{m_\pi^2 M_{QCD}^2}{M_{\not T}^2}\right). \tag{4.1.14}$$

From here on, we always use the symbol w to denote collectively the dimensionless constant w, defined in Eq. (3.2.28), and $\sigma_{1,8}$ in Eq. (3.2.31); $w \in \{w, \sigma_1, \sigma_8\}$. The operators in Eq. (4.1.13) also receive a contribution from the quark EDM and MDM, which is suppressed by one power of $\alpha_{\rm em}/\pi$, and appears in the $\Delta_6 = 1$ Lagrangian.

At $\Delta_6 = 0$, pion tadpoles emerge from considering operators that transform as tensor product of the mass term in Eq. (3.4.15) and the qCEDM and qCMDM operators in Eq. (3.2.53). Purely pionic operators are generated by the tensor products $\bar{m} S_4 \otimes (c_0 \tilde{W}_4 + d_3 \tilde{W}_3)$ and $\bar{m}\varepsilon P_3 \otimes (c_3 \tilde{V}_3 - d_0 \tilde{V}_4)$, and we find

$$\mathcal{L}^{(0)}_{6,\,f=0} = \frac{\tilde{\delta}_3 m_\pi^2}{2D^2}\left[-\boldsymbol{\pi}^2 + \tilde{\rho}_3 F_\pi \pi_3 \left(1 - \frac{\boldsymbol{\pi}^2}{F_\pi^2}\right)\right] + \frac{\tilde{\delta}_0 m_\pi^2}{2D^2}\left[\pi_3^2 + \tilde{\rho}_0 F_\pi \pi_3 \left(1 - \frac{\boldsymbol{\pi}^2}{F_\pi^2}\right)\right], \tag{4.1.15}$$

where the new low-energy constants scale as

$$\tilde{\rho}_3\, \tilde{\delta}_3 m_\pi^2 = \mathcal{O}\left(\tilde{\delta}_3 \frac{m_\pi^4}{M_{\not T}^2}\right), \qquad \tilde{\rho}_0\, \tilde{\delta}_0 m_\pi^2 = \mathcal{O}\left(\tilde{\delta}_0 \varepsilon \frac{m_\pi^4}{M_{\not T}^2}\right). \tag{4.1.16}$$

The gCEDM and the TV four-quark operators generate operators identical to the TV part of Eq. (4.1.9) through the tensor products $d_w \bar{m}^2 \varepsilon S_4 \otimes P_3 \otimes I$, with the replacement $\delta m_\pi^2 \rho \to \bar{\delta}_w m_\pi^2$

$$\bar{\delta}_w m_\pi^2 = \mathcal{O}\left(w\varepsilon \frac{m_\pi^4}{M_{\not T}^2}\right). \tag{4.1.17}$$

Contributions from the qEDM are suppressed by a power of $\alpha_{\rm em}/\pi$, and we do not consider them explicitly.

In Eqs. (4.1.14), (4.1.16) and (4.1.17), we have assumed $\bar{\theta}$ to be small, in which case $r(\bar{\theta}) \sim 1$. For generic $\bar{\theta}$, the scaling of the coefficients can be obtained by replacing ε with $\varepsilon/r^2(\bar{\theta})$ in Eqs. (4.1.16) and (4.1.17). Notice that for generic $\bar{\theta}$, one should also construct TV operators that transform like tensor products of the $\bar{\theta}$ term and the TC qCMDM, $m_\star \sin\bar{\theta} P_4 \otimes (c_0\tilde{W}_4 + c_3\tilde{V}_3)$. In the purely pionic sector, the second tensor product gives an additional contribution to the coefficient of the tadpole in Eq. (4.1.15) of order

$$\mathcal{O}\left(\tilde{\delta}_0 \frac{\tan\bar{\theta}}{\tan\phi_0}\frac{\cos\bar{\theta}}{r^2(\bar{\theta})}\frac{m_\pi^4}{M_T^2}\right). \tag{4.1.18}$$

Now, the rationale for considering TV from dimension 6 operators along side with the dimension 4 $\bar{\theta}$ term is that the M_T^2 suppression of the former is somehow balanced by CP violating phases much bigger than $\bar{\theta}$, that is $\tan\bar{\theta} \ll \tan\phi_0$. Consequently, the contribution of Eq. (4.1.18) can be safely neglected.

The TC operators in Eqs. (4.1.13) and (4.1.15) are a first example of the impossibility to differentiate the low-energy manifestations of the qCMDM from the effects of the quark mass term, at least in an approach which, as χPT, solely relies on the symmetry properties of the quark-gluon operators. The correction to the pion mass $\tilde{\Delta}_q m_\pi^2$ in Eq. (4.1.13) has exactly the same structure as the pion mass term in Eq. (4.1.1), to which it gives a small correction of order M_{QCD}^2/M_T^2. Similarly, $\tilde{\delta}_3 m_\pi^2$ and $\tilde{\delta}_0 m_\pi^2$ in Eq. (4.1.15) are respectively identical to the correction to the pion mass Δm_π^2 in Eq. (4.1.4) and the correction to the neutral pion mass δm_π^2 in Eq. (4.1.9). Once again, the only effect of the qCMDM is to give a correction of order M_{QCD}^2/M_T^2 to these coefficients.

4.1.2 Pion-nucleon sector. The QCD $\bar{\theta}$ term.

In the case of T violation from the QCD $\bar{\theta}$ term interactions with $f = 2$ are potentially the most important for TV phenomenology, because they appear at the lowest chiral index. Already at $\Delta = 1$ we can find a P_a vector, whose third and fourth components give the operators

$$\mathcal{L}^{(1)}_{\chi,f=2} = \frac{\delta m_N}{2}\left\{\bar{N}\tau_3 N - \frac{2\pi_3}{F_\pi^2 D}\bar{N}\boldsymbol{\tau}\cdot\boldsymbol{\pi}N - \frac{2\rho}{F_\pi D}\bar{N}\boldsymbol{\tau}\cdot\boldsymbol{\pi}N\right\}. \tag{4.1.19}$$

These operators provide the leading isospin-breaking [122] and TV [93] pion-nucleon interactions, respectively. The low-energy constant

$$\delta m_N = \mathcal{O}\left(\frac{\varepsilon m_\pi^2}{r^2(\bar{\theta})M_{QCD}}\right) \tag{4.1.20}$$

is the main quark-mass contribution to the nucleon mass splitting [122, 145]. Equation (4.1.19) links the leading TV pion-nucleon coupling to the strong nucleon mass splitting δm_N via the characteristic factor ρ, Eq. (4.1.5). We return to this issue in Sec. 4.4.

Considering $\Delta = 2$, we can construct operators that contain one covariant derivative,

$$\mathcal{L}^{(2)}_{\chi,f=2} = \frac{\beta_1}{F_\pi}\left\{D_\mu\pi_3 - \frac{2\pi_3}{F_\pi^2 D}\boldsymbol{\pi}\cdot D_\mu\boldsymbol{\pi} - \frac{2\rho}{F_\pi D}\boldsymbol{\pi}\cdot D_\mu\boldsymbol{\pi}\right\}\bar{N}S^\mu N, \tag{4.1.21}$$

with

$$\beta_1 = \mathcal{O}\left(\frac{\varepsilon m_\pi^2}{r^2(\bar{\theta})M_{QCD}^2}\right). \tag{4.1.22}$$

The subleading TV interaction thus consists of a seagull vertex (and its chiral partners) [91], which is related to isospin violation in the pion-nucleon coupling constant [122, 145, 148, 149].

Increasing the index by one, we find terms with two covariant derivatives and two powers of symmetry-breaking parameters. We write

$$\mathcal{L}^{(3)}_{\chi,f=2} = \mathcal{L}^{(3)}_{\chi^1,f=2} + \mathcal{L}^{(3)}_{\chi^2,f=2}. \tag{4.1.23}$$

With two covariant derivatives we find

$$\begin{aligned}
\mathcal{L}^{(3)}_{\chi^1,f=2} \;=\; & \left\{ \frac{\zeta_1}{F_\pi} \left(D_\nu \boldsymbol{\pi}\right) \cdot \bar{N} \left[S^\mu, S^\nu\right] \boldsymbol{\tau} \mathcal{D}_{\mu\,-} N + \frac{\zeta_2}{F_\pi} \left(v \cdot \mathcal{D}\, v \cdot D\, \boldsymbol{\pi}\right) \cdot \bar{N} \boldsymbol{\tau} N \right. \\
& \left. + \frac{\zeta_3}{F_\pi} \left(\mathcal{D}_{\mu\,\perp} D^\mu_\perp\, \boldsymbol{\pi}\right) \cdot \bar{N} \boldsymbol{\tau} N + \frac{2\zeta_4}{F_\pi^2} \left(D_\mu \boldsymbol{\pi} \times v \cdot D \boldsymbol{\pi}\right) \cdot \bar{N} S^\mu \boldsymbol{\tau} N \right\} \\
& \frac{1}{2D} \left[\frac{2\pi_3}{F_\pi} + \rho \left(1 - \frac{\boldsymbol{\pi}^2}{F_\pi^2}\right) \right] \\
& + \left\{ -\frac{\zeta_5}{4} \bar{N} \tau_i\, v \cdot \mathcal{D}^2_- N - \frac{\zeta_6}{4} \bar{N} \tau_i\, \mathcal{D}^2_{\perp,-} N + \frac{\zeta_7}{F_\pi} \bar{N} S^\mu \left(\boldsymbol{\tau} \times \left(v \cdot \mathcal{D} D_\mu \boldsymbol{\pi}\right)\right)_i N \right. \\
& + \frac{i\zeta_8}{F_\pi} \left(v \cdot D \pi_i\right) \bar{N} S \cdot \mathcal{D}_- N + \frac{2i\zeta_9}{F_\pi^2} \left(D_\mu \boldsymbol{\pi} \times D_\nu \boldsymbol{\pi}\right)_i \bar{N} [S^\mu, S^\nu] N \\
& + \frac{\zeta_{10}}{F_\pi^2} \left(D_\mu \pi_i\right) \left(D^\mu \boldsymbol{\pi}\right) \cdot \bar{N} \boldsymbol{\tau} N + \frac{\zeta_{11}}{F_\pi^2} \left(v \cdot D \pi_i\right) \left(v \cdot D \boldsymbol{\pi}\right) \cdot \bar{N} \boldsymbol{\tau} N \\
& \left. + \frac{\zeta_{12}}{F_\pi^2} \left(D_\mu \boldsymbol{\pi}\right)^2 \bar{N} \tau_i N + \frac{\zeta_{13}}{F_\pi^2} \left(v \cdot D \boldsymbol{\pi}\right)^2 \bar{N} \tau_i N \right\} \frac{1}{2} \left(\delta_{i3} - \frac{2\pi_3\, \pi_i}{F_\pi^2 D} - \frac{2\rho \pi_i}{F_\pi D} \right),
\end{aligned} \tag{4.1.24}$$

where the coefficients

$$\zeta_i = \mathcal{O}\left(\frac{\varepsilon m_\pi^2}{r^2(\bar{\theta}) M^3_{QCD}} \right). \tag{4.1.25}$$

Again, we see that the TV terms have an extra factor of ρ compared to their isospin-breaking partners.

Lorentz invariance relates the coefficients of some of the operators in Eq. (4.1.24) to δm_N and β_1. We discuss such relations in App. I, where we find

$$\zeta_1 = \zeta_6 = \frac{\delta m_N}{2 m_N^2}, \qquad \zeta_8 = \frac{g_A \delta m_N}{m_N^2} - \frac{\beta_1}{m_N}. \tag{4.1.26}$$

The relation between ζ_6 and δm_N is in agreement with the one found in Ref. [145]. Equation (4.1.26) reproduces the relations in Ref. [150], once a field redefinition is used to eliminate time derivatives acting on the nucleon field from the subleading chiral Lagrangian [151].

Contributions to $\mathcal{L}^{(3)}_{\chi,f=2}$ that do not contain derivatives come from consideration of the tensor products $P_a \otimes P_b$ and $S_4 \otimes P_b$. As noticed earlier, the representation of $P_a \otimes P_b$ contains a chiral invariant and a symmetric tensor. In the pion-nucleon

sector, the chiral-invariant operator gives an inconsequential correction to the nucleon mass, while the symmetric tensor yields a P- and T-conserving isospin-breaking term from its 3-3 component, a P- and T-violating isospin-breaking term ($\propto \rho$) from its 3-4 component, and a P- and T-conserving chiral-symmetry breaking but isospin-conserving term ($\propto \rho^2$) from its 4-4 component. The tensor product $S_4 \otimes P_b$, in turn, contributes the 3-4 (which is isospin-breaking) and 4-4 (which is P- and T-violating and down by a factor of ρ) components of a symmetric tensor, and the 3-4 component (which is isospin-breaking) of an antisymmetric tensor. We thus find the additional $\Delta = 3$ terms,

$$\begin{aligned}
\mathcal{L}^{(3)}_{\chi^2,f=2} &= c_1^{(3)}\left[\frac{4\pi_3^2}{F_\pi^2 D^2}+\rho^2\left(1-\frac{4\boldsymbol{\pi}^2}{F_\pi^2 D^2}\right)+\frac{4\rho\pi_3}{F_\pi D^2}\left(1-\frac{\boldsymbol{\pi}^2}{F_\pi^2}\right)\right]\bar{N}N \\
&\quad +\frac{\delta_1^{(3)} m_N}{2}\left\{\bar{N}\left[\tau_3-\frac{2}{F_\pi^2 D}\left(6\pi_3\left(1-\frac{4\boldsymbol{\pi}^2}{3F_\pi^2 D}\right)\boldsymbol{\pi}\cdot\boldsymbol{\tau}-\boldsymbol{\pi}^2\tau_3\right)\right]N\right. \\
&\quad \left.+\frac{4\rho}{F_\pi D^2}\left(1-\frac{\boldsymbol{\pi}^2}{F_\pi^2}\right)\bar{N}\boldsymbol{\pi}\cdot\boldsymbol{\tau}N\right\} \\
&\quad +\frac{\delta_2^{(3)} m_N}{2}\bar{N}\left[\tau_3+\frac{2}{F_\pi^2 D}\left(\pi_3\boldsymbol{\pi}\cdot\boldsymbol{\tau}-\boldsymbol{\pi}^2\tau_3\right)\right]N, \qquad (4.1.27)
\end{aligned}$$

where we can estimate the coefficients,

$$c_1^{(3)} = \mathcal{O}\left(\frac{\varepsilon^2 m_\pi^4}{r^4(\bar{\theta})M_{QCD}^3}\right), \qquad \delta_{1,2}^{(3)} m_N = \mathcal{O}\left(\frac{\varepsilon m_\pi^4}{r^2(\bar{\theta})M_{QCD}^3}\right). \qquad (4.1.28)$$

The TV interaction associated to $\delta_1^{(3)} m_N$ is similar to the leading TV pion-nucleon interaction in Eq. (4.1.19), and it is also linked to a contribution to the nucleon mass splitting, but it is suppressed by an extra m_π^2/M_{QCD}^2. More interesting is the TV interaction associated to $c_1^{(3)}$, since it involves only the neutral pion. Because of its isospin character, it contributes differently to observables than the leading TV pion-nucleon interaction. As one can see, it is suppressed with respect to the latter by a factor $\varepsilon m_\pi^2/M_{QCD}^2$, and it is linked to an isospin-breaking two-neutral-pion-nucleon seagull interaction. Note that there is no TV operator directly associated to $\delta_2^{(3)} m_N$. This term has exactly the same form as the main electromagnetic contribution to

the nucleon mass difference, Eq. (3.3.21), and can only be distinguished by the dependence of its coefficient on m_π^2; in our power counting, it is suppressed by one power of m_π/M_{QCD}.

One can of course continue the procedure to higher orders. It is hard to imagine they would have much phenomenological use, but they are not entirely devoid of structural interest. For example, it is from tensor products of three vectors (at $\Delta = 5$) that the first non-electromagnetic $\pi_3\bar{N}\tau_3 N$ interaction appears. Also, at this point the connection between isospin and T violation ceases to be useful. These tensor products are discussed in App. H.

4.1.3 Pion-nucleon sector. Dimension 6 sources.

The leading contributions from dimension 6 operators to the $f = 2$ Lagrangian come from the isoscalar and isovector qCEDM and from the chiral invariant gCEDM and TV four-quark operators. From Eq. (3.3.13), one finds that, being $\tilde{d}_{0,3}$ proportional to the light quark mass, in the case of the qCEDM pion-nucleon interactions first appear in the $\Delta_6 = -1$ Lagrangian. As far as the chiral invariant operators are concerned, it turns out that, in the $f = 2$ sector, it is impossible to build any chiral invariant, TV operator with zero or one derivative. The first possible operators then have two derivatives, or contain an insertion of the light quark mass, and thus also the chiral invariant TV operators first contribute at $\Delta_6 = -1$. We find

$$\begin{aligned}
\mathcal{L}^{(-1)}_{6,\,f=2} \;=\;& \frac{\tilde{\delta}_q m_N}{2}\left\{\bar{N}\tau_3 N - \frac{2\pi_3}{F_\pi^2 D}\bar{N}\boldsymbol{\tau}\cdot\boldsymbol{\pi}N - \frac{2\tilde{\rho}_0}{F_\pi D}\bar{N}\boldsymbol{\tau}\cdot\boldsymbol{\pi}N\right\} \\
& -\frac{\tilde{\Delta}_q m_N}{2}\left\{\left(1 - \frac{2\boldsymbol{\pi}^2}{DF_\pi^2}\right)\bar{N}N + \frac{2\tilde{\rho}_3}{F_\pi D}\pi_3\bar{N}N\right\} \\
& -\frac{\bar{g}_{0\,w}}{F_\pi D}\bar{N}\boldsymbol{\tau}\cdot\boldsymbol{\pi}N - \frac{\bar{g}_{1\,w}}{F_\pi D}\pi_3\bar{N}N - \frac{\bar{\imath}_{0\,w}}{F_\pi^2}(v\cdot D\boldsymbol{\pi}\times D_\mu\boldsymbol{\pi})\cdot\bar{N}S^\mu\boldsymbol{\tau}N.
\end{aligned} \tag{4.1.29}$$

The first two operators in Eq. (4.1.29) are induced by the qCEDM and they have coefficients

$$\tilde{\delta}_q m_N \tilde{\rho}_0 = \mathcal{O}\left(\tilde{\delta}_0 \frac{m_\pi^2}{M_T^2} M_{QCD}\right), \quad \tilde{\Delta}_q m_N \tilde{\rho}_3 = \mathcal{O}\left(\tilde{\delta}_3 \frac{m_\pi^2}{M_T^2} M_{QCD}\right). \tag{4.1.30}$$

The other three operators in Eq. (4.1.29) stem from the gCEDM and the TV four-quark operators; their coefficients are

$$\begin{aligned} \bar{g}_{0\,w} &= \mathcal{O}\left(w \frac{m_\pi^2}{M_T^2} M_{QCD}\right), \qquad \bar{g}_{1\,w} = \mathcal{O}\left(w\varepsilon \frac{m_\pi^2}{M_T^2} M_{QCD}\right), \\ \bar{\imath}_{0\,w} &= \mathcal{O}\left(\frac{w}{M_T^2} M_{QCD}\right), \end{aligned} \tag{4.1.31}$$

where, as in the previous section, we use the shorthand $w \in \{w, \sigma_1, \sigma_8\}$, and we assumed $r(\bar{\theta}) \approx 1$.

The qEDM generates indirect electromagnetic contributions, which are suppressed by a power of $\alpha_{\rm em}/\pi$ with respect to the operators in Eq. (4.1.29), and do not play an important role for the observables we are interested in.

Eq. (4.1.29) shows a first important difference between TV from dimension 6 operators and the QCD $\bar{\theta}$ term, namely the presence of a TV and isospin breaking coupling already at leading order in the $f = 2$ Lagrangian. The implications of this difference are particularly relevant for the TV electromagnetic moments of deuteron, and we will further discuss them in Chapter 6.

The calculation of the nucleon EDM generated by the qCEDM at NLO requires the knowledge of the $\Delta_6 = 0$ Lagrangian. In the case of the gCEDM and of the TV four-quark operators, which also generate $\Delta_6 = 0$ pion-nucleon interactions, short-range physics plays a more important role than long-range physics mediated by pions, thus making the derivation of pion-nucleon couplings at sub-leading orders irrelevant.

The qCEDM contribution to the $\Delta_6 = 0$ Lagrangian is

$$\begin{aligned}\mathcal{L}^{(0)}_{6,f=2} &= \frac{\tilde{\beta}_{q\,1}}{F_\pi}\left\{D_\mu\pi_3 - \frac{2\pi_3}{F_\pi^2 D}\boldsymbol{\pi}\cdot D_\mu\boldsymbol{\pi} - \frac{2\tilde{\rho}_0}{F_\pi D}\boldsymbol{\pi}\cdot D_\mu\boldsymbol{\pi}\right\}\bar{N}S^\mu N \\ &+\frac{\tilde{\beta}_{q\,2}}{F_\pi}\left\{\left(1-\frac{2\boldsymbol{\pi}^2}{F_\pi^2 D}\right)+\tilde{\rho}_3\frac{2\pi_3}{F_\pi D}\right\}\bar{N}S^\mu\boldsymbol{\tau}\cdot D_\mu\boldsymbol{\pi}N \\ &+\frac{\tilde{\beta}_{q\,3}}{F_\pi}\left\{-\frac{2\pi_i}{F_\pi D}+\tilde{\rho}_3\left(\delta_{i3}-\frac{2\pi_i\pi_3}{F_\pi^2 D}\right)\right\}\bar{N}\left(\boldsymbol{\tau}\times v\cdot D\boldsymbol{\pi}\right)_i N, \quad (4.1.32)\end{aligned}$$

with the scaling of the coupling constant determined by

$$\tilde{\beta}_{q\,1}\,\tilde{\rho}_0 = \mathcal{O}\left(\tilde{\delta}_0\frac{m_\pi^2}{M_{\not\pi}^2}\right), \qquad \tilde{\beta}_{q\,2,3}\,\tilde{\rho}_3 = \mathcal{O}\left(\tilde{\delta}_3\frac{m_\pi^2}{M_{\not\pi}^2}\right). \quad (4.1.33)$$

At $\Delta_6 = 1$ we can construct operators with two covariant derivatives, or one insertion of the light quark mass. With two covariant derivatives, the isoscalar component of the qCEDM, and its chiral partner, the isovector qCMDM, generate interactions identical to Eq. (4.1.24), with the replacement $\zeta_i \to \tilde{\zeta}_{q\,i}$ and $\rho \to \tilde{\rho}_0$. The coefficients go as

$$\tilde{\zeta}_{q\,i}\,\tilde{\rho}_0 = \mathcal{O}\left(\tilde{\delta}_0\frac{m_\pi^2}{M_{\not\pi}^2 M_{QCD}}\right). \quad (4.1.34)$$

The constraints imposed by Lorentz invariance on $\tilde{\zeta}_{q\,1}$, $\tilde{\zeta}_{q\,6}$ and $\tilde{\zeta}_{q\,8}$ are identical to Eq. (4.1.26).

The isovector qCEDM generates TV interactions with two derivatives that also violate isospin symmetry, accompanied by chiral-symmetry breaking, but isospin in-

variant, TC operators stemming from the isoscalar qCMDM

$$\begin{aligned}
\mathcal{L}^{(1)}_{6,f=2} \;=\; & \left\{ \frac{\tilde{\xi}_{q\,1}}{F_\pi} D_\nu \pi_i \bar{N} \left[S^\mu, S^\nu\right] \mathcal{D}_{\mu\,-} N + \frac{\tilde{\xi}_{q\,2}}{F_\pi} (v\cdot\mathcal{D} v \cdot D\pi_i) \bar{N} N \right. \\
& + \frac{\tilde{\xi}_{q\,3}}{F_\pi} \left(\mathcal{D}^\mu_\perp D_{\mu\perp} \pi_i\right) \bar{N} N + \frac{2\tilde{\xi}_{q\,4}}{F_\pi^2} (D_\mu \boldsymbol{\pi} \times v\cdot D\boldsymbol{\pi})_i \, \bar{N} S^\mu N \\
& \left. + i \frac{\tilde{\xi}_{q\,5}}{F_\pi} \bar{N} \left((D^\mu \boldsymbol{\pi}) \times \boldsymbol{\tau}\right)_i \mathcal{D}_{\mu\,\perp,\,-} N \right\} \left[-\frac{2\pi_i}{F_\pi D} + \tilde{\rho}_3 \left(\delta_{3i} - \frac{2}{D} \frac{\pi_3 \pi_i}{F_\pi^2} \right) \right] \\
& + \left\{ -\frac{\tilde{\xi}_{q\,6}}{4} \bar{N} v\cdot \mathcal{D}^2_- N - \frac{\tilde{\xi}_{q\,7}}{4} \bar{N} \mathcal{D}^2_{\perp,\,-} N_v + \frac{i\tilde{\xi}_{q\,8}}{2F_\pi} (v\cdot D\boldsymbol{\pi}) \cdot \bar{N} \boldsymbol{\tau}\, S\cdot \mathcal{D}_- N \right. \\
& + \frac{i\tilde{\xi}_{q\,9}}{2F_\pi^2} (D_\mu \boldsymbol{\pi} \times D_\nu \boldsymbol{\pi}) \cdot \bar{N} [S^\mu, S^\nu] \boldsymbol{\tau} N + \frac{\tilde{\xi}_{q\,10}}{F_\pi^2} (D^\mu \boldsymbol{\pi}\,)^2 \bar{N} N \\
& \left. + \frac{\tilde{\xi}_{q\,11}}{F_\pi^2} (v\cdot D\boldsymbol{\pi}\,)^2 \bar{N} N \right\} \left[\left(1 - \frac{2\boldsymbol{\pi}^2}{F_\pi^2 D} \right) + \tilde{\rho}_3 \frac{2\pi_3}{F_\pi D} \right] \qquad (4.1.35)
\end{aligned}$$

The scaling of the coefficients $\tilde{\xi}_{q\,i}$ is

$$\tilde{\xi}_{q\,i}\, \tilde{\rho}_3 = \mathcal{O}\left(\tilde{\delta}_3 \frac{m_\pi^2}{M_T^2} \frac{1}{M_{QCD}} \right). \qquad (4.1.36)$$

Reparameterization invariance constrains some of the coefficients in Eq. (4.1.35). At order $1/m_N^2$, we find the following relations:

$$\tilde{\xi}_{q\,1} = -\tilde{\xi}_{q\,7} = \frac{\tilde{\Delta}_q m_N}{4m_N^2}, \quad \tilde{\xi}_{q\,5} = \frac{\tilde{\beta}_{q\,3}}{2m_N}, \quad \tilde{\xi}_{q\,8} = -\frac{g_A}{m_N^2} \tilde{\Delta}_q m_N - \frac{\tilde{\beta}_{q\,2}}{m_N}. \qquad (4.1.37)$$

At the same order, we consider insertion of the quark mass. The resulting operators transform as the tensor product of the QCD mass term and the qCEDM and

qCMDM: $(\bar{m}S_4 - \epsilon\bar{m}P_3) \otimes \left(-\tilde{d}_0\tilde{V}_4 + \tilde{c}_3\tilde{V}_3 + \tilde{d}_3\tilde{W}_3 + \tilde{c}_0\tilde{W}_4\right)$

$$\begin{aligned}
\mathcal{L}^{(1)}_{6,f=2} \;=\; & \left[\left(\tilde{c}^{(1)}_1\tilde{\rho}_3 + \tilde{c}^{(1)}_2\tilde{\rho}_0\right)\frac{4\pi_3}{F_\pi D^2}\left(1 - \frac{\boldsymbol{\pi}^2}{F_\pi^2}\right) + \tilde{c}^{(1)}_1\left(1 - \frac{4\boldsymbol{\pi}^2}{F_\pi^2 D^2}\right) + \tilde{c}^{(1)}_2\frac{4\pi_3^2}{F_\pi^2 D^2}\right]\bar{N}N \\
& + \frac{\tilde{\delta}^{(1)}_1 m_N + \tilde{\delta}^{(1)}_2 m_N}{2}\bar{N}\left[\tau_3 - \frac{2}{F_\pi^2 D}\left(6\pi_3\left(1 - \frac{4}{3}\frac{\boldsymbol{\pi}^2}{F_\pi^2 D}\right)\boldsymbol{\pi}\cdot\boldsymbol{\tau} - \boldsymbol{\pi}^2\tau_3\right)\right]N \\
& - \tilde{\rho}_0\tilde{\delta}^{(1)}_1 m_N\frac{2}{F_\pi D}\left(1 - \frac{2\boldsymbol{\pi}^2}{F_\pi^2 D}\right)\bar{N}\boldsymbol{\pi}\cdot\boldsymbol{\tau}N \\
& - \tilde{\rho}_3\tilde{\delta}^{(1)}_2 m_N\frac{2\pi_3}{F_\pi D}\bar{N}\left(\tau_3 - \frac{2\pi_3}{F_\pi^2 D}\boldsymbol{\pi}\cdot\boldsymbol{\tau}\right)N \\
& + \frac{\tilde{\delta}^{(1)}_3 m_N + \tilde{\delta}^{(1)}_4 m_N}{2}\bar{N}\left[\tau_3 + \frac{2}{F_\pi^2 D}\left(\pi_3\boldsymbol{\pi}\cdot\boldsymbol{\tau} - \boldsymbol{\pi}^2\tau_3\right)\right]N. \qquad (4.1.38)
\end{aligned}$$

At this order, all three possible non-derivative pion-nucleon TV couplings receive contribution from the qCEDM. The first TV operator in Eq. (4.1.38) represent a correction to the isovector TV coupling in Eq. (4.1.29), from which it only differs for observables with three or more pions. It receives a contribution from two tensor products $\bar{m}\tilde{d}_3 S_4 \otimes \tilde{W}_3$ and $\bar{m}\varepsilon\tilde{d}_0 P_3 \otimes \tilde{V}_4$, which are encoded in the two coefficients $\tilde{c}^{(1)}_1$ and $\tilde{c}^{(1)}_2$. They scale as

$$\tilde{c}^{(1)}_1\tilde{\rho}_3 = \mathcal{O}\left(\tilde{\delta}_3\frac{m_\pi^2}{M_T^2 M_{QCD}}\right), \qquad \tilde{c}^{(1)}_2\tilde{\rho}_0 = \mathcal{O}\left(\tilde{\delta}_0\varepsilon\frac{m_\pi^2}{M_T^2 M_{QCD}}\right). \qquad (4.1.39)$$

The chiral partners of $\tilde{c}^{(1)}_1\tilde{\rho}_3$ and $\tilde{c}^{(1)}_2\tilde{\rho}_0$ transform, respectively, as the products $\bar{m}\tilde{c}_0$ $S_4 \otimes \tilde{W}_4$ and $\bar{m}\varepsilon\tilde{c}_3 P_3 \otimes \tilde{V}_3$. The first represents a isospin invariant correction to the nucleon mass, which however has different multi-pion structure with respect to the term $\tilde{\Delta}_q m_N$ in Eq. (4.1.29). The second operator violates isospin symmetry, and it contributes to the scattering of neutral pion off the nucleon. The TV operator with coefficient $\tilde{\rho}_0\tilde{\delta}^{(1)}_1 m_N$ provides a correction to the isoscalar TV coupling $\bar{N}\boldsymbol{\pi}\cdot\boldsymbol{\tau}N$ in Eq. (4.1.29), while $\tilde{\rho}_3\tilde{\delta}^{(1)}_2 m_N$ is the first contribution of the qCEDM to the isospin breaking coupling $\pi_3\bar{N}\tau_3 N$. These two operators realize the tensor products $\bar{m}\tilde{d}_0 S_4 \otimes \tilde{V}_4$ and $\bar{m}\varepsilon\tilde{d}_3 P_3 \otimes \tilde{W}_3$ in the effective Lagrangian, and their coefficients go as

$$\tilde{\delta}^{(1)}_1 m_N\tilde{\rho}_0 = \mathcal{O}\left(\tilde{\delta}_0\frac{m_\pi^4}{M_T^2 M_{QCD}}\right), \qquad \tilde{\delta}^{(1)}_2 m_N\tilde{\rho}_3 = \mathcal{O}\left(\tilde{\delta}_3\varepsilon\frac{m_\pi^4}{M_T^2 M_{QCD}}\right). \qquad (4.1.40)$$

The chiral partner of both $\tilde{\rho}_0\tilde{\delta}_1^{(1)}m_N$ and $\tilde{\rho}_3\tilde{\delta}_2^{(1)}m_N$ is the operator in the third line of Eq. (4.1.38). Such operator contributes to the nucleon mass difference, and, at least in principle, it can be distinguished from the operator proportional to $\tilde{\delta}_q m_N$ in Eq. (4.1.29) if observables with two or more pions are considered. However, here we see a first failure of the link between TC and TV operators we established in Eqs. (4.1.6) and (4.1.7). Even in the purely hypothetical scenario that the coefficient of the third operator in Eq. (4.1.38) could be extracted independently of $\delta_1^{(3)}m_N$ in Eq. (4.1.27), this coefficient would carry information only on the sum $\tilde{\delta}_1^{(1)}m_N + \tilde{\delta}_2^{(1)}m_N$, and thus it would not provide any constraint on the coefficients of TV operators, which depend on the individual value of $\tilde{\delta}_1^{(1)}m_N$ and $\tilde{\delta}_2^{(1)}m_N$. Finally, the tensor products $\bar{m}\tilde{c}_3 S_4 \otimes \tilde{V}_3$ and $\bar{m}\varepsilon\tilde{c}_0 P_3 \otimes \tilde{W}_4$ also generate two TC operators without TV partners. These operators contribute to the nucleon mass difference in exactly the same form as the electromagnetic contribution $\breve{\delta}m_N$ in Eq. (3.3.22). The coefficients $\tilde{\delta}_3^{(1)}m_N$ and $\tilde{\delta}_4^{(1)}m_N$ scale as

$$\tilde{\delta}_3^{(1)}m_N = \mathcal{O}\left(\frac{\tilde{\delta}_0}{\tan\tilde{\phi}_0}\frac{m_\pi^4}{M_T^2 M_{QCD}}\right), \quad \tilde{\delta}_4^{(1)}m_N = \mathcal{O}\left(\varepsilon\frac{\tilde{\delta}_3}{\tan\tilde{\phi}_3}\frac{m_\pi^4}{M_T^2 M_{QCD}}\right). \quad (4.1.41)$$

4.1.4 Four-nucleon sector.

We discuss here the TV four-nucleon operators that stem from the QCD $\bar{\theta}$ term and the dimension 6 sources of T violation. In this Section, different TV four-nucleon operators are organized according to the chiral index Δ, defined in Eq. (3.3.9) for the $\bar{\theta}$ term and in Eq. (3.3.13) for the dimension 6 sources. Modifications of the power counting of four-nucleon operators that account for the unnatural size of the nucleon-nucleon scattering lengths are discussed in Chapter 6.

In the case of the QCD $\bar{\theta}$ term, the first contribution to the $f = 4$ sector of the

Lagrangian comes at $\Delta = 2$,

$$\begin{aligned}\mathcal{L}^{(2)}_{\not\chi, f=4} &= \frac{\gamma_s}{2}\bar{N}\left\{\left(\tau_3 - \frac{2\pi_3}{F_\pi^2 D}\boldsymbol{\pi}\cdot\boldsymbol{\tau}\right) - \frac{\rho}{F_\pi D}\boldsymbol{\pi}\cdot\boldsymbol{\tau}\right\} N\,\bar{N}N \\ &\quad +2\gamma_\sigma\bar{N}\left\{\left(\tau_3 - \frac{2\pi_3}{F_\pi^2 D}\boldsymbol{\pi}\cdot\boldsymbol{\tau}\right) - \frac{\rho}{F_\pi D}\boldsymbol{\pi}\cdot\boldsymbol{\tau}\right\} S^\mu N\,\bar{N}S_\mu N, \quad (4.1.42)\end{aligned}$$

in terms of two TV parameters $\gamma_{s,\sigma}$, which by naive dimensional analysis scale as

$$\gamma_{s,\sigma} = \mathcal{O}\left(\frac{1}{F_\pi^2}\frac{\varepsilon m_\pi^2}{r^2(\bar{\theta})M_{QCD}^2}\right). \quad (4.1.43)$$

Just as for $f \leq 2$, here too TV operators are linked to isospin-violating operators, which in this case generates the dominant contributions to the short-range isospin-violating two-nucleon potential [122, 145]. The isospin-violating coefficients γ_i can be seen as low-energy remnants of ρ-ω mixing [145] and a_1-f_1 mixing [152]. The TV operators in Eq. (4.1.42) are not relevant for the nuclear potential to the order we work in Chapter 7, but contribute to the three-nucleon TV potential at next order.

The first operators relevant to the calculation of the TV potential are

$$\begin{aligned}\mathcal{L}^{(3)}_{\not\chi, f=4} &= C_1\left[\frac{2\pi_3}{F_\pi^2 D} + \rho\left(1 - \frac{2\boldsymbol{\pi}^2}{F_\pi^2 D}\right)\right]\bar{N}N\partial_\mu(\bar{N}S^\mu N) \\ &\quad +C_2\left[\frac{2\pi_3}{F_\pi^2 D} + \rho\left(1 - \frac{2\boldsymbol{\pi}^2}{F_\pi^2 D}\right)\right]\bar{N}\boldsymbol{\tau}N\cdot\mathcal{D}_\mu(\bar{N}\boldsymbol{\tau}S^\mu N), \quad (4.1.44)\end{aligned}$$

where the $\bar{C}_i = \rho C_i$ are two new TV parameters. The covariant derivative in the operator C_2 is meant to be in the adjoint representation, that is, the isospin matrix in Eq. (3.3.4) is replaced by $(t^j)_{ik} = i\varepsilon^{ijk}$. The coefficients scale as

$$C_{1,2} = \mathcal{O}\left(\frac{1}{F_\pi^2}\frac{\varepsilon m_\pi^2}{r^2(\bar{\theta})M_{QCD}^3}\right), \quad (4.1.45)$$

and therefore, in the case of the QCD $\bar{\theta}$ term, TV four-nucleon effects are smaller than those induced by the leading TV pion-nucleon coupling, in Eq. (4.1.19). For example, we will see in Chapter 7 that TV one-pion-exchange (OPE) gives the biggest contribution to the TV nucleon-nucleon potential. The contribution of $\bar{C}_{1,2}$ to the TV potential is suppressed by two powers of m_π/M_{QCD}, and it arises at the same

level as the TV two-pion-exchange potential and subleading OPE potentials from $\mathcal{O}(m_\pi^2/M_{QCD}^2)$ corrections to leading TC and TV pion-nucleon couplings. Since the contribution of the largest four-nucleon operators to TV observables is already small, we do not construct corrections to Eq. (4.1.44).

The coefficients C_i could in principle be determined from pion production in the two-nucleon system and/or from isospin-violating three-nucleon forces. However, even lower-order isospin-violating three-nucleon forces are very small [153, 154], so prospects for extracting C_i from TC data are grim.

For the chiral-symmetry breaking qCEDM, the relative importance of four-nucleon interactions and pion exchanges is the same as for the $\bar{\theta}$ term, even if the isospin structure of the four-nucleon interactions is richer. The first four-nucleon operators appear at $\Delta_6 = 0$. The isoscalar qCEDM and the isovector qCMDM generate interactions with the same form as those in Eq. (4.1.42), with the replacement $\gamma_{s,\sigma} \to \tilde{\gamma}_{s,\sigma}$ and $\rho \to \tilde{\rho}_0$. The isovector qCEDM generates

$$\begin{aligned}\mathcal{L}^{(0)}_{6,\,f=4} &= \tilde{\gamma}'_s \left[\left(1 - \frac{2\boldsymbol{\pi}^2}{F_\pi^2 D}\right) + \tilde{\rho}_3 \frac{2\pi_3}{F_\pi D}\right] \bar{N}N\,\bar{N}N \\ &\quad + 4\tilde{\gamma}'_\sigma \left[\left(1 - \frac{2\boldsymbol{\pi}^2}{F_\pi^2 D}\right) + \tilde{\rho}_3 \frac{2\pi_3}{F_\pi D}\right] \bar{N}S^\mu N\,\bar{N}S_\mu N. \end{aligned} \tag{4.1.46}$$

In terms of the qCEDM parameters $\tilde{\delta}_0$ and $\tilde{\delta}_3$, the coefficients $\tilde{\gamma}_{s,\sigma}$ and $\tilde{\gamma}'_{s,\sigma}$ are

$$\tilde{\rho}_0\tilde{\gamma}_{s,\sigma} = \mathcal{O}\left(\tilde{\delta}_0 \frac{m_\pi^2}{F_\pi^2 M_{\not T}^2}\right), \qquad \tilde{\rho}_3\tilde{\gamma}'_{s,\sigma} = \mathcal{O}\left(\tilde{\delta}_3 \frac{m_\pi^2}{F_\pi^2 M_{\not T}^2}\right). \tag{4.1.47}$$

As in the case of the $\bar{\theta}$ term, the interactions in Eq. (4.1.46) contribute to the largest TV three-body force.

Four-nucleon interactions from qCEDM that start with no pions first appear at $\Delta_6 = 1$, that is, two orders down with respect to the leading pion-nucleon coupling in Eq. (4.1.29). Once again, the interactions from the isoscalar qCEDM are already contained in Eq. (4.1.44), with $C_{1,2}$ replaced by $\tilde{C}_{1,2}$ and ρ replaced by $\tilde{\rho}_0$. The

isovector qCEDM is responsible for TV and isospin breaking four-nucleon operators

$$\begin{aligned}\mathcal{L}^{(1)}_{6,f=4} &= \tilde{C}_3\bar{N}\left[-\frac{2}{F_\pi D}\boldsymbol{\pi}\cdot\boldsymbol{\tau}+\tilde{\rho}_3\left(\tau_3-\frac{2\pi_3}{F_\pi^2 D}\boldsymbol{\pi}\cdot\boldsymbol{\tau}\right)\right]N\,\partial_\mu\left(\bar{N}S^\mu N\right)\\ &\quad -\tilde{C}_4\bar{N}\left[-\frac{2}{F_\pi D}\boldsymbol{\pi}\cdot\boldsymbol{\tau}+\tilde{\rho}_3\left(\tau_3-\frac{2\pi_3}{F_\pi^2 D}\boldsymbol{\pi}\cdot\boldsymbol{\tau}\right)\right]S^\mu N\,\partial_\mu\left(\bar{N}N\right)\end{aligned} \tag{4.1.48}$$

The TV low-energy constants $\tilde{\bar{C}}_{1,2}=\tilde{\rho}_0\tilde{C}_{1,2}$ and $\tilde{\bar{C}}_{3,4}=\tilde{\rho}_3\tilde{C}_{3,4}$ scale as

$$\tilde{\bar{C}}_{1,2}=\mathcal{O}\left(\tilde{\delta}_0\frac{m_\pi^2}{F_\pi^2 M_{\mathcal{T}}^2 M_{QCD}}\right),\qquad \tilde{\bar{C}}_{3,4}=\mathcal{O}\left(\tilde{\delta}_3\frac{m_\pi^2}{F_\pi^2 M_{\mathcal{T}}^2 M_{QCD}}\right). \tag{4.1.49}$$

Four-nucleon operators play a more relevant role in the case of the chiral-invariant gCEDM and TV four-quark operators. In this case, four-nucleon operators appear already in the $\Delta_6=-1$ Lagrangian, that is at the same level as the pion-nucleon couplings in Eq. (4.1.29). We find

$$\mathcal{L}^{(-1)}_{6,\,f=4}=\bar{C}_{w1}\bar{N}N\partial_\mu(\bar{N}S^\mu N)+\bar{C}_{w2}\bar{N}\boldsymbol{\tau}N\cdot\mathcal{D}_\mu(\bar{N}\boldsymbol{\tau}S^\mu N), \tag{4.1.50}$$

with coefficients

$$\bar{C}_{w1,2}=\mathcal{O}\left(w\frac{M_{QCD}}{F_\pi^2 M_{\mathcal{T}}^2}\right). \tag{4.1.51}$$

As usual, w includes the effects of the gCEDM, and of two four-quark operators in Eq. (3.2.37), $w\in\{w,\sigma_1,\sigma_8\}$. The four-nucleon interactions in Eq. (4.1.50) are thus responsible for a TV nucleon-nucleon potential of the same order as OPE from Eq. (4.1.29). We will further discuss the implications of this observation for the TV electromagnetic moments of the deuteron in Chapter 6. The chiral invariant and TV dimension 6 operators contribute to the $\Delta=0$ and $\Delta=1$ four-nucleon Lagrangian. Since these operators are not needed for the calculation of the observables discussed in Chapters 5 and 6, we do not explicitly construct them.

The qEDM generates four-nucleon TV operators, which are, however, suppressed by a factor of $\alpha_{\rm em}/\pi$ with respect to Eq. (4.1.46) and (4.1.48) and thus completely negligible.

4.2 Electromagnetic Interactions

In this section we are interested in studying how the combined effects of the electromagnetic interaction of quarks and of the sources of T violation we are studying manifest themselves in the low-energy Lagrangian. As we have mentioned, we have to consider interactions of two types, with and without soft photons. The former provide short-range contributions to EDMs. The latter involve the exchange of at least one hard photon, which cannot be resolved in the low-energy EFT and is therefore integrated out —these interactions are purely hadronic and sometimes called indirect electromagnetic effects. Such indirect effects include pion-nucleon TV vertices, which result from a TV interaction accompanied by a hard-photon exchange.

As far as the QCD $\bar{\theta}$ term is concerned, the simplest operators are linear in the chiral-breaking parameters $\bar{m}$ and e, and thus necessarily involve a soft photon. Under $SO(4)$, these operators have the transformation properties of tensor products of the chiral-symmetry-breaking terms in $\mathcal{L}_m$, Eq. (3.4.15), and $\mathcal{L}_e$, Eq. (3.2.11),

$$\left[\bar{m}r(\bar{\theta})S_4 - \bar{m}\varepsilon r^{-1}(\bar{\theta})\left(P_3 + \rho P_4\right)\right] \otimes eA_\mu \left(\frac{I^\mu}{6} + T^\mu_{34}\right). \tag{4.2.1}$$

We have therefore to construct operators that transform as components of $SO(4)$ vectors, S_4 and P_a, or components of tensor products, $S_4 \otimes T_{34}$ and $P_a \otimes T_{34}$, with $a = 3, 4$. The tensor product of the antisymmetric tensor T_{ab} and the vector P_c gives rise to a vector $(\boldsymbol{V}, V_4)$ and a three-index tensor $Z_{ab,c}$, antisymmetric in the first two indices. As far as parity and time reversal are concerned, the vector $(\boldsymbol{V}, V_4)$ has the same properties as $(\boldsymbol{S}, S_4)$: V_4 is P and T even while $\boldsymbol{V}$ is P and T odd. On the other hand, the tensor product $T_{ab} \otimes S_c$ generates a vector with the same properties as P and a three-index tensor. For soft-photon interactions, our index Δ counts also the number of photon fields and their derivatives.

The analysis of dimension 6 sources proceeds along similar lines. A quark chromo-EDM and its chiral partner, a quark anomalous chromo-magnetic moment, induce

soft-photon interactions via tensor products with $\mathcal{L}_e$ of the form

$$\left(-\tilde{d}_0\tilde{V}_4+\tilde{c}_3\tilde{V}_3+\tilde{d}_3\tilde{W}_3+\tilde{c}_0\tilde{W}_4\right)\otimes eA_\mu\left(\frac{I^\mu}{6}+T^\mu_{34}\right), \tag{4.2.2}$$

while TV electromagnetic operators from the chiral invariant TV sources have the same transformations as $\mathcal{L}_e$. The qEDM and qMDM already have a soft photon, therefore they yield nucleon-photon operators that transforms like the fourth and third components of the vectors V and W in Eq. (3.2.51).

Another possibility is to construct operators that have higher powers of e. Those with odd (even) powers of e generate operators with odd (even) number of external photons. For example, for the $\bar{\theta}$ term, the simplest of the indirect electromagnetic effects come from operators that under the group $SO(4)$ have the transformation properties of tensor product of

$$\left[\bar{m}r(\bar{\theta})S_4-\bar{m}\varepsilon r^{-1}(\bar{\theta})\left(P_3+\rho P_4\right)\right]\otimes\, eA_\mu\left(\frac{I^\mu}{6}+T^\mu_{34}\right)\otimes\, eA_\nu\left(\frac{I^\nu}{6}+T^\nu_{34}\right), \tag{4.2.3}$$

in which the photon is integrated out. In this case we need components of $SO(4)$ vectors, S_4 and P_a, and of tensor products, $S_4\otimes T_{34}$, $P_a\otimes T_{34}$, $S_4\otimes T_{34}\otimes T_{34}$, and $P_a\otimes T_{34}\otimes T_{34}$. These contributions are proportional to the electromagnetic fine-structure constant $\alpha_{\rm em}$. Typically, there is also an extra inverse factor of π, so for power counting purposes we assign them a factor of $\alpha_{\rm em}/\pi$. Recall that we enlarge the chiral index to count also powers of $\alpha_{\rm em}/\pi$, with the assumption $\alpha_{\rm em}/\pi\sim\varepsilon m_\pi^3/M_{QCD}^3$. With this assumption, it turns out that indirect electromagnetic operators are negligible, at the order we are working at. For example, pion-nucleon indirect couplings only appear in the $\Delta=4$ Lagrangian, three orders down with respect to the leading TV coupling from the $\bar{\theta}$ term. We derive these operators, in particular the first electromagnetic contribution to the vertex $\pi_3\bar{N}\tau_3N$ in Ref. [39]. Similarly, in the case of the qEDM or qCEDM, the first indirect pion-nucleon coupling has $\Delta_6=2$, which means it contributes to the nucleon EDM at N^{3}LO, which is far beyond the accuracy of our analysis.

Clearly, more complicated operators can be constructed, which involve either more external photons and/or more powers of $\bar{m}$ and $\alpha_{\rm em}/\pi$. Operators with two photons have been discussed in Ref. [156] in connection with nucleon Compton scattering; since they give small contributions even to atomic EDMs [119], we do not list here operators with more than a single soft photon. Higher-order terms in the Lagrangian can also be realized by building operators with the transformation properties above that contain covariant derivatives of the nucleon and pion fields or higher-dimension gauge-invariant operators.

In the following we catalog the most important TV interactions with one external photon, classifying them by the number of nucleon fields f. For the QCD $\bar{\theta}$ term these interactions are always linked to operators from quark mass difference, according to Eq. (4.1.5). Below we list these partners together. Unlike the operators in Sec. 4.1, however, here the S_4s play an important role: although the interactions they generate are of course T conserving, when combined with T_{34}s they lead to isospin-breaking interactions that spoil the link (4.1.5) between operators from $\bar{\theta}$ and the quark mass difference already for the leading electromagnetic terms. For the other chiral symmetry breaking sources, the qEDM and qCEDM, as in the case of purely hadronic interaction, the links (4.1.6) and (4.1.7) are irrelevant because of the impossibility to isolate the effects of the quark anomalous magnetic moment or chromo-magnetic moment from those of the quark mass terms. We discuss in further detail the link between TC and TV operators in Sec. 4.4

4.2.1 Photon-nucleon sector. The QCD $\bar{\theta}$ term

Interactions with soft photons can be obtained using the $U(1)$-gauge covariant derivatives (3.3.12) in existing operators. More interesting are the interactions that arise through the field strength $F_{\mu\nu}$, which we describe here. Since the pion has spin 0, we cannot construct an EDM operator in the $f = 0$ sector. In contrast, there are plenty of TV interactions in the $f = 2$ sector.

The first contributions from the QCD $\bar{\theta}$ term come at $\Delta = 3$. TV appears in

$$\begin{aligned}
\mathcal{L}^{(3)}_{\not\chi,f=2,\mathrm{em}} &= 2D_0^{(3)}\left[\frac{2\pi_3}{F_\pi D}+\rho\left(1-\frac{2\boldsymbol{\pi}^2}{F_\pi^2 D}\right)\right]\bar{N}S^\mu\left(v^\nu+\frac{i\mathcal{D}^\nu_{\perp -}}{2m_N}\right)N\,F_{\mu\nu} \\
&\quad +E_1^{(3)}\bar{N}\left(\tau_3-\frac{2\pi_3}{F_\pi^2 D}\boldsymbol{\pi}\cdot\boldsymbol{\tau}-\frac{2\rho}{F_\pi D}\boldsymbol{\pi}\cdot\boldsymbol{\tau}\right)i\left[S^\mu,S^\nu\right]N\,F_{\mu\nu} \\
&\quad +2D_1^{(3)}\bar{N}\left[\frac{2}{F_\pi D}\boldsymbol{\pi}\cdot\boldsymbol{\tau}+\rho\left(\tau_3-\frac{2\pi_3}{F_\pi^2 D}\boldsymbol{\pi}\cdot\boldsymbol{\tau}\right)\right]S^\mu\left(v^\nu+\frac{i\mathcal{D}^\nu_{\perp -}}{2m_N}\right)N\,F_{\mu\nu} \\
&\quad +E_0^{(3)}\left(1-\frac{2\boldsymbol{\pi}^2}{F_\pi^2 D}-\frac{2\rho\pi_3}{F_\pi D}\right)\bar{N}i\left[S^\mu,S^\nu\right]N\,F_{\mu\nu} \\
&\quad +2D_1'^{(3)}\left[\frac{2\pi_3}{F_\pi D}+\rho\left(1-\frac{2\boldsymbol{\pi}^2}{F_\pi^2 D}\right)\right] \\
&\qquad \bar{N}\left[\left(1-\frac{2\boldsymbol{\pi}^2}{F_\pi^2 D}\right)\tau_3+\frac{2\pi_3}{F_\pi^2 D}\boldsymbol{\pi}\cdot\boldsymbol{\tau}\right]S^\mu\left(v^\nu+\frac{i\mathcal{D}^\nu_{\perp -}}{2m_N}\right)N\,F_{\mu\nu}. \qquad (4.2.4)
\end{aligned}$$

Here the first two sets of interactions have the transformation properties of P_3 and P_4, while the other three represent the tensor product $T_{34}\otimes P_a$. The TV operator with coefficient $\bar{D}_0^{(3)} = D_0^{(3)}\rho$ contributes to the isoscalar nucleon EDM, while $\bar{D}_1^{(3)} = D_1^{(3)}\rho$ and $\bar{D}_1'^{(3)} = D_1'^{(3)}\rho$ are isovector contributions. With coefficients $E_0^{(3)}$ and $E_1^{(3)}$, we find isoscalar and isovector contributions to the nucleon magnetic dipole moment, suppressed by m_π^2/M_{QCD}^2 with respect to Eq. (3.3.18). They are associated to TV interactions that contribute to pion photoproduction. The coefficients in Eq. (4.2.4) scale as

$$D_{0,1}^{(3)}, D_1'^{(3)}, E_{0,1}^{(3)} = \mathcal{O}\left(e\frac{\varepsilon m_\pi^2}{r^2(\bar{\theta})M_{QCD}^3}\right). \qquad (4.2.5)$$

For convenience, the EDM operators in Eq. (4.2.5) include a recoil correction, which will be needed in the calculation of the nucleon EDM at NLO. Other electromagnetic interactions with $\Delta = 4$ are constructed in Ref. [39].

At the same order $\Delta = 3$, more TC electromagnetic operators are generated by

tensor products involving the quark mass term S_4 in Eq. (3.4.15). They are

$$\begin{aligned}\mathcal{L}^{(3)}_{S,f=2,\mathrm{em}} &= 2F_0^{(3)}\frac{2\pi_3}{F_\pi D}\bar{N}S^\mu v^\nu N\,F_{\mu\nu} + 2F_1^{(3)}\frac{2}{F_\pi D}\bar{N}\boldsymbol{\pi}\cdot\boldsymbol{\tau}S^\mu v^\nu N\,F_{\mu\nu} \\ &+ \bar{N}i\left[S^\mu,S^\nu\right]\left\{G_0^{(3)}\left(1-\frac{2\boldsymbol{\pi}^2}{F_\pi^2}\right)+G_1^{(3)}\left(\tau_3-\frac{2\pi_3}{F_\pi^2 D}\boldsymbol{\pi}\cdot\boldsymbol{\tau}\right)\right. \\ &+ \left. G_1'^{(3)}\left(1-\frac{2\boldsymbol{\pi}^2}{F_\pi^2 D}\right)\bar{N}\left[\left(1-\frac{2\boldsymbol{\pi}^2}{F_\pi^2 D}\right)\tau_3+\frac{2\pi_3}{F_\pi^2 D}\boldsymbol{\pi}\cdot\boldsymbol{\tau}\right]\right\}N\,F_{\mu\nu}. \end{aligned} \tag{4.2.6}$$

Notice that the operators $F_0^{(3)}$ and $F_1^{(3)}$ have exactly the same form as the TC partners of the isoscalar and isovector EDM operators with coefficients $D_0^{(3)}$ and $D_1^{(3)}$, while $G_0^{(3)}$ and $G_1^{(3)}$ are identical to the TC operators $E_0^{(3)}$ and $E_1^{(3)}$. Therefore experimental data on TC pion photoproduction, or on the nucleon magnetic moment can at best provide information on the sum of coefficients $D_{0,1}^{(3)}+F_{0,1}^{(3)}$ and $E_{0,1}^{(3)}+G_{0,1}^{(3)}$, but not on the value of the individual coefficients. Since the short-distance contribution to the nucleon EDM only depend on $D_{0,1}^{(3)}$, this destroys our ability to extract information about the TV operators from their TC partners.

4.2.2 Photon-nucleon sector. Dimension 6 sources.

We now consider the dimension 6 sources of T violation in Eq. (3.2.53). The chiral-invariant sources, the gCEDM and the TV four-quark operators in Eq. (3.2.37), generate the interaction with the lowest chiral index, $\Delta_6=-1$.

$$\begin{aligned}\mathcal{L}^{(-1)}_{6,\,f=2,\,\mathrm{em}} &= \bar{N}\left\{2\bar{D}^{(-1)}_{w\,0}+2\bar{D}^{(-1)}_{w\,1}\left[\tau_3+\frac{2}{F_\pi^2 D}\left(\pi_3\boldsymbol{\pi}\cdot\boldsymbol{\tau}-\boldsymbol{\pi}^{\,2}\tau_3\right)\right]\right\} \\ &\quad S^\mu\left(v^\nu+\frac{i\mathcal{D}^\nu_-}{2m_N}\right)NF_{\mu\nu}, \end{aligned} \tag{4.2.7}$$

where, as before, we included a recoil correction in the $\Delta_6=-1$ Lagrangian. The scaling of the coefficient is

$$\bar{D}^{(-1)}_{w\,0,1}=\mathcal{O}\left(ew\frac{M_{QCD}}{M_{\mathcal{T}}^2}\right), \tag{4.2.8}$$

with $w \in \{w, \sigma_1, \sigma_8\}$. Notice that, differently from TV from the $\bar{\theta}$ term, for chiral invariant TV sources the short-distance EDM operators have the same chiral index as the leading pion-nucleon coupling, Eq. (4.1.29). Since the latter contributes to the nucleon EDM only via loops, which pick up a further Q^2/M_{QCD}^2 suppression, it follows that, for chiral invariant sources, the nucleon EDM is mainly determined by short-distance physics.

A second consequence of the enhancement of short-distance vs. long-distance physics for chiral invariant sources is that the nucleon EDFF does not depend on the momentum transfer at leading order in χPT. Momentum dependence only arises at next-to-next leading order (N^{2}LO). At this accuracy we need to consider the power-suppressed, $\Delta = 1$ Lagrangian

$$\begin{aligned}
\mathcal{L}^{(1)}_{w,\, f=2,\,\mathrm{em}} \;=\;& 2\bar{N}\left[\bar{D}^{(1)}_{w\,0}\left(1-\frac{2\boldsymbol{\pi}^2}{F_\pi^2 D}\right)+\bar{D}^{(1)}_{w\,1}\left(\tau_3-\frac{2\pi_3}{F_\pi^2 D}\boldsymbol{\pi}\cdot\boldsymbol{\tau}\right)\right] S^\mu N\, v^\nu F_{\mu\nu} \\
& +2\bar{D}^{(1)'}_{w\,1}\left(1-\frac{2\boldsymbol{\pi}^2}{F_\pi^2 D}\right)\bar{N}\left[\tau_3+\frac{2}{F_\pi^2 D}\left(\pi_3\boldsymbol{\pi}\cdot\boldsymbol{\tau}-\boldsymbol{\pi}^2\tau_3\right)\right] S^\mu N\, v^\nu F_{\mu\nu} \\
& -\frac{1}{4m_N^2}\bar{N}\left\{2\bar{D}^{(-1)}_{w\,0}+2\bar{D}^{(-1)}_{w\,1}\left[\tau_3+\frac{2}{F_\pi^2 D}\left(\pi_3\boldsymbol{\pi}\cdot\boldsymbol{\tau}-\boldsymbol{\pi}^{\,2}\tau_3\right)\right]\right\} \\
& S\cdot\mathcal{D}_{\perp-}\mathcal{D}^\mu_{\perp-} N\, v^\nu F_{\mu\nu} \\
& -\bar{N}\left(\bar{S}'^{(1)}_{w\,0}+\bar{S}'^{(1)}_{w\,1}\tau_3\right)\left(S\cdot\mathcal{D}_{\perp+}\mathcal{D}^\mu_{\perp+}+S^\mu\mathcal{D}^2_{\perp+}\right) N\, v^\nu F_{\mu\nu}+\ldots
\end{aligned} \tag{4.2.9}$$

The first three operators in Eq. (4.2.9) are proportional to the quark mass, while the fourth and fifth are relativistic corrections to $\bar{D}^{(-1)}_{w\,0}$ and $\bar{D}^{(-1)}_{w\,1}$. Finally, the two operators in the last line are short-distance contributions to the first derivative of the nucleon EDFF. The scaling of the coefficients is

$$\bar{D}^{(1)}_{w\,0,1}, \bar{D}'^{(1)}_{w\,1} = \mathcal{O}\left(ew\frac{m_\pi^2}{M_T^2}\frac{1}{M_{QCD}}\right), \quad \bar{S}^{(1)}_{w\,0,1} = \mathcal{O}\left(ew\frac{1}{M_T^2}\frac{1}{M_{QCD}}\right). \tag{4.2.10}$$

Eq. (4.2.9) only contains the operators relevant to the calculation of the momentum dependence of the EDFF, the full $\Delta_6 = 1$, electromagnetic Lagrangian stemming from the gCEDM and four-quark TV operators is given in Ref. [155].

The qCEDM and qCMDM generate electromagnetic interactions very similar to those stemming from the QCD $\bar{\theta}$ term and the quark mass difference. Also in this

case, chiral symmetry breaking from electromagnetism spoils the relation between TV operators and their TC chiral partners, which, for convenience, we list separately in Eqs. (4.2.11) and (4.2.12). Since $\tilde{d}_0$ and $\tilde{d}_3$ are proportional to the light quark mass, the first TV operators with soft photons appears at $\Delta = 1$. They are

$$\begin{aligned}
\mathcal{L}^{(1)}_{\mathrm{qCEDM},f=2,\mathrm{em}} &= 2\bar{N}\left\{\tilde{\bar{D}}^{(1)}_{q\,0}\left(1-\frac{2\boldsymbol{\pi}^2}{F_\pi^2 D}\right)+\tilde{\bar{D}}^{(1)}_{q\,1}\left(\tau_3-\frac{2\pi_3}{F_\pi^2 D}\boldsymbol{\pi}\cdot\boldsymbol{\tau}\right)\right. \\
&\quad \left.+\,\tilde{\bar{D}}'^{(1)}_{q\,1}\left(1-\frac{2\boldsymbol{\pi}^2}{F_\pi^2 D}\right)\left[\tau_3-\frac{2}{F_\pi^2 D}\left(\boldsymbol{\pi}^2\tau_3-\pi_3\boldsymbol{\pi}\cdot\boldsymbol{\tau}\right)\right]\right\} \\
&\quad S^\mu\left(v^\nu+\frac{i\mathcal{D}^\nu_{\perp\,-}}{2m_N}\right)N\,F_{\mu\nu} \\
&\quad -\bar{N}\left\{\tilde{\bar{E}}^{(1)}_{q\,1}\,\frac{2\boldsymbol{\pi}\cdot\boldsymbol{\tau}}{F_\pi D}+\frac{2\pi_3}{F_\pi D}\left[\tilde{\bar{E}}^{(1)}_{q\,0}\right.\right. \\
&\quad \left.\left.-\,\tilde{\bar{E}}'^{(1)}_{q\,1}\left(\tau_3-\frac{2}{F_\pi^2 D}\left(\boldsymbol{\pi}^2\tau_3-\pi_3\boldsymbol{\pi}\cdot\boldsymbol{\tau}\right)\right)\right]\right\}\,i\,[S^\mu,S^\nu]\,N\,F_{\mu\nu}.
\end{aligned} \tag{4.2.11}$$

As usual, we have introduced recoil corrections to the isoscalar and isovector EDMs in the leading Lagrangian. As in the case of the QCD $\bar{\theta}$ term, the largest short-distance electromagnetic interactions are contributions to the isoscalar and isovector EDMs and to TV in pion photoproduction, and they appear with chiral index which is two units bigger than the leading pion-nucleon TV coupling. The TC partners of the operators in Eq. (4.2.11), generated by the isoscalar and isovector qCMDM, are

$$\begin{aligned}
\mathcal{L}^{(1)}_{\mathrm{qCMDM},f=2,\mathrm{em}} &= 2\bar{N}\left\{\frac{2\pi_3}{F_\pi D}\left[\tilde{D}^{(1)}_{q\,0}+\tilde{D}'^{(1)}_{q\,1}\left(\tau_3-\frac{2}{F_\pi^2 D}\left(\boldsymbol{\pi}^2\tau_3-\pi_3\boldsymbol{\pi}\cdot\boldsymbol{\tau}\right)\right)\right]\right. \\
&\quad \left.+\,\tilde{D}_{q\,1}\frac{2}{F_\pi D}\boldsymbol{\pi}\cdot\boldsymbol{\tau}\right\}S^\mu\left(v^\nu+\frac{i\mathcal{D}^\nu_{\perp-}}{2m_N}\right)N\,F_{\mu\nu} \\
&\quad +\bar{N}\left\{\tilde{E}^{(1)}_{q\,1}\left(\tau_3-\frac{2\pi_3}{F_\pi^2 D}\boldsymbol{\pi}\cdot\boldsymbol{\tau}\right)+\left(1-\frac{2\boldsymbol{\pi}^2}{F_\pi^2 D}\right)\right. \\
&\quad \left.\left[\tilde{E}^{(1)}_{q\,0}+\tilde{E}'^{(1)}_{q\,1}\left(\tau_3-\frac{2}{F_\pi^2 D}\left(\boldsymbol{\pi}^2\tau_3-\pi_3\boldsymbol{\pi}\cdot\boldsymbol{\tau}\right)\right)\right]\right\}\,i\,[S^\mu,S^\nu]\,N\,F_{\mu\nu}.
\end{aligned} \tag{4.2.12}$$

and, as in the case of $\bar{\theta}$, they do constitute small corrections to the isoscalar and isovector nucleon MDM and to TC pion photoproduction off the nucleon.

The operators $\tilde{\bar{D}}^{(1)}_{q\,0}$, $\tilde{\bar{D}}^{(1)}_{q\,1}$, $\tilde{\bar{E}}^{(1)}_{q\,0}$ and $\tilde{\bar{E}}^{(1)}_{q\,1}$ transform as third and fourth components of chiral four vectors. They all receive contributions from both the isoscalar and isovector qCEDM. Schematically, we write the scaling of these coefficients

$$\tilde{\bar{D}}^{(1)}_{q\,0,1},\ \tilde{\bar{E}}^{(1)}_{q\,0,1} = \mathcal{O}\left(e\left(\tilde{\delta}_0 + \tilde{\delta}_3\right)\frac{m_\pi^2}{M_{\not T}^2 M_{QCD}}\right), \tag{4.2.13}$$

where the "+" should not be interpreted literally, but simply as an indication of the existence of two contributions to the coefficients. $\tilde{\bar{D}}^{\prime(1)}_{q\,1}$ and $\tilde{\bar{E}}^{\prime(1)}_{q\,1}$ respectively come from the realization of the product $\tilde{d}_0\tilde{V}_4 \otimes T_{34}$ and $\tilde{d}_3\tilde{W}_3 \otimes T_{34}$. Consequently, they scale as

$$\tilde{\bar{D}}^{\prime(1)}_{q\,1} = \mathcal{O}\left(e\tilde{\delta}_0\frac{m_\pi^2}{M_{\not T}^2 M_{QCD}}\right), \qquad \tilde{\bar{E}}^{\prime(1)}_{q\,1} = \mathcal{O}\left(e\tilde{\delta}_3\frac{m_\pi^2}{M_{\not T}^2 M_{QCD}}\right). \tag{4.2.14}$$

The scaling of the TC coefficient in Eq. (4.2.12) can be inferred from Eqs. (4.2.13) and (4.2.14).

Finally, the qEDM only generates operators that transform as vector,

$$\begin{aligned}
\mathcal{L}^{(1)}_{\text{qEDM},f=2,\text{em}} &= 2D^{(1)}_{q\,0}\bar{N}\left[\frac{2\pi_3}{F_\pi D} + \rho_0\left(1 - \frac{2\boldsymbol{\pi}^2}{F_\pi^2 D}\right)\right] S^\mu\left(v^\nu + \frac{i\mathcal{D}^\nu_{\perp -}}{2m_N}\right) N\, F_{\mu\nu} \\
&+ 2D^{(1)}_{q\,1}\bar{N}\left[\frac{2}{F_\pi D}\boldsymbol{\pi}\cdot\boldsymbol{\tau} + \rho_3\left(\tau_3 - \frac{2\pi_3}{F_\pi^2 D}\boldsymbol{\pi}\cdot\boldsymbol{\tau}\right)\right] S^\mu\left(v^\nu + \frac{i\mathcal{D}^\nu_{\perp -}}{2m_N}\right) N\, F_{\mu\nu} \\
&+ E^{(1)}_{q\,1}\bar{N}\left[\left(\tau_3 - \frac{2\pi_3}{F_\pi^2 D}\boldsymbol{\pi}\cdot\boldsymbol{\tau}\right) - \rho_0\frac{2}{F_\pi D}\boldsymbol{\pi}\cdot\boldsymbol{\tau}\right] i\left[S^\mu, S^\nu\right] N\, F_{\mu\nu} \\
&+ E^{(1)}_{q\,0}\left[\left(1 - \frac{2\boldsymbol{\pi}^2}{F_\pi^2 D}\right) - \rho_3\frac{2\pi_3}{F_\pi D}\right]\bar{N} i\left[S^\mu, S^\nu\right] N\, F_{\mu\nu},
\end{aligned} \tag{4.2.15}$$

with coefficients

$$\left(D^{(1)}_{q\,0}, E^{(1)}_{q\,1}\right)\rho_0 = \mathcal{O}\left(e\delta_0\frac{m_\pi^2}{M_{\not T}^2}\frac{1}{M_{QCD}}\right), \quad \left(D^{(1)}_{q\,1}, E^{(1)}_{q\,0}\right)\rho_3 = \mathcal{O}\left(e\delta_3\frac{m_\pi^2}{M_{\not T}^2}\frac{1}{M_{QCD}}\right). \tag{4.2.16}$$

In the case of TV from the qEDM, long-range physics is suppressed by powers of α_{em} and TV observables like the neutron and deuteron TV electromagnetic moments are dominated by short-range effects. As in the case of TV from chiral-invariant operators,

the scale of the momentum variation of the nucleon EDFF is thus determined not by m_π, but by M_{QCD}, and, consequently, we have to construct the power suppressed $\Delta = 3$ Lagrangian. As usual, we find operators with two more covariant derivatives, or one extra insertion of the light quark mass. Neglecting the TC operators, and using barred symbols to denote TV coefficients

$$\begin{aligned}\mathcal{L}^{(3)}_{6,\,f=2\,\mathrm{em}} &= 2\bar{N}\left(\bar{D}^{(3)}_{q\,0}+\bar{D}^{(3)}_{q\,1}\tau_3\right)S^\mu N\,v^\nu F_{\mu\nu}\\ &\quad -\frac{1}{4m_N^2}\bar{N}\left(\bar{D}^{(1)}_{q\,0}+\bar{D}^{(1)}_{q\,1}\tau_3\right)S\cdot\mathcal{D}_{\perp-}\mathcal{D}^\mu_{\perp-}N\,v^\nu F_{\mu\nu}\\ &\quad -\bar{N}\left(\bar{S}'^{(3)}_{q\,0}+\bar{S}'^{(3)}_{q\,1}\tau_3\right)\left(S\cdot\mathcal{D}_{\perp+}\mathcal{D}^\mu_{\perp+}+S^\mu\mathcal{D}^2_{\perp+}\right)N\,v^\nu F_{\mu\nu}+\ldots \end{aligned} \tag{4.2.17}$$

with

$$\begin{aligned}\bar{D}^{(3)}_{q\,0} &= \mathcal{O}\left(e(\delta_0+\delta_3\varepsilon)\frac{m_\pi^4}{M_I^2M_{\rm QCD}^3}\right),\\ \bar{D}^{(3)}_{q\,1} &= \mathcal{O}\left(e(\delta_0\varepsilon+\delta_3)\frac{m_\pi^4}{M_I^2M_{\rm QCD}^3}\right),\\ \bar{S}'^{(3)}_{q\,0} &= \mathcal{O}\left(e\delta_0\frac{m_\pi^2}{M_I^2M_{\rm QCD}^3}\right),\quad \bar{S}'^{(3)}_{q\,1}=\mathcal{O}\left(e\delta_3\frac{m_\pi^2}{M_I^2M_{\rm QCD}^3}\right).\end{aligned} \tag{4.2.18}$$

Once again, the "+" in the power counting estimate of $\bar{D}^{(3)}_{q\,0,1}$ indicates the presence of different contributions. The dots in Eq. (4.2.17) denote multi-pion components of the listed operator, and operators which start at one pion, which are not relevant to our discussion.

4.2.3 Four-nucleon currents

The study of TV electromagnetic moments of the deuteron and other nuclei requires the construction of four-nucleon TV currents, which, as discussed in Chapter 6, can play a role, especially for those TV sources, like the qEDM or the chiral invariant gCEDM and TV four-quark operators, for which short-distance effects tend to dominate. We construct in this Section the most important four-nucleon currents, which appear with index $\Delta = 4$ for the QCD $\bar{\theta}$ term, $\Delta_6 = 2$ for the qEDM and qCEDM

and $\Delta_6 = 0$ in the case of chiral invariant TV sources. Modifications to the power counting of four-nucleon currents in the Kaplan, Savage and Wise power counting are discussed in Chapter 6.

In the case of $\bar{\theta}$ term, at $\Delta = 4$ we find

$$\begin{aligned}
\mathcal{L}^{(4)}_{\not\chi,\, f=4,\mathrm{em}} &= \bar{D}_{NN}\left(1-\frac{2\boldsymbol{\pi}^2}{F_\pi^2 D}\right)\bar{N}S^\mu v^\nu N\,\bar{N}NF_{\mu\nu} \\
&\quad + \left[\bar{L}_1\left(\delta_{i3}-\frac{2\pi_i\pi_3}{F_\pi^2 D}\right)+\bar{L}_2\left(1-\frac{2\boldsymbol{\pi}^2}{F_\pi^2 D}\right)\left(\delta_{i3}-\frac{2}{F_\pi^2 D}\left(\boldsymbol{\pi}^2-\pi_3\pi_i\right)\right)\right] \\
&\quad \left[\bar{N}S^\mu v^\nu \tau_i\, N\,\bar{N}N - \bar{N}S^\mu v^\nu\, N\,\bar{N}\tau_i N\right]F_{\mu\nu} \\
&\quad + \left[\bar{L}_3\left(\delta_{i3}-\frac{2\pi_i\pi_3}{F_\pi^2 D}\right)+\bar{L}_4\left(1-\frac{2\boldsymbol{\pi}^2}{F_\pi^2 D}\right)\left(\delta_{i3}-\frac{2}{F_\pi^2 D}\left(\boldsymbol{\pi}^2-\pi_3\pi_i\right)\right)\right] \\
&\quad \left[\bar{N}S^\mu v^\nu \tau_i\, N\,\bar{N}N + \bar{N}S^\mu v^\nu\, N\,\bar{N}\tau_i N\right]F_{\mu\nu} + \ldots, \qquad (4.2.19)
\end{aligned}$$

where the first operator $\bar{D}_{NN}$ transforms like the vector P_4, $\bar{L}_{1,3}$ and $\bar{L}_{2,4}$ as the vector and the tensor in the representation of $P_4 \otimes T_{34}$. The dots in Eq. (4.2.19) stand for other TV operators with $\Delta = 4$ that start with one pion. Since they do not contribute to the deuteron EDM, we do not construct them explicitly. We also omitted the TC partners of the operators $\bar{D}_{NN}$ and $\bar{L}_i$, since, as in the case of electromagnetic operators with $f = 2$, the link is no longer useful. By naive dimensional analysis, the coefficients of the four-nucleon currents in Eq. (4.2.19) are

$$\bar{D}_{NN}, \bar{L}_i = \mathcal{O}\left(e\bar{\theta}\frac{m_\pi^2}{r^2(\bar{\theta})F_\pi^2 M_{QCD}^4}\right). \qquad (4.2.20)$$

The operator $\bar{D}_{NN}$ represents a short-distance contribution to the deuteron EDM. In the perturbative pion approach, its scaling is modified, and the operator is enhanced with respect to (4.2.20). Nonetheless, we find that it does not contribute to the deuteron EDM at LO, but it is important at NLO. The operators $\bar{L}_1$ and $\bar{L}_2$ contribute to the radiative capture process $n + p \to d + \gamma$, and the inverse process, the photodissociation of the deuteron $d + \gamma \to n + p$, with the neutron and proton in a ${}^1S_0$ configuration. The operators $\bar{L}_3$ and $\bar{L}_4$ do not contribute to S waves.

The qCEDM generates exactly the same operators as (4.2.19), with coefficients

$$\tilde{\bar{D}}_{q\,NN}, \tilde{\bar{L}}_{q\,1,2} = \mathcal{O}\left(e(\tilde{\delta}_0+\tilde{\delta}_3)\frac{m_\pi^2}{F_\pi^2 M_{\cal T}^2 M_{QCD}^2}\right) \tag{4.2.21}$$

$$\tilde{\bar{L}}_{q\,3,4} = \mathcal{O}\left(e\tilde{\delta}_0\frac{m_\pi^2}{F_\pi^2 M_{\cal T}^2 M_{QCD}^2}\right), \tag{4.2.22}$$

while the qEDM only contributes to the operators that transform like vectors, $\bar{D}_{NN}$, $\bar{L}_1$ and $\bar{L}_3$

$$\bar{D}_{q\,NN} = \mathcal{O}\left(e\delta_0\frac{m_\pi^2}{F_\pi^2 M_{\cal T}^2 M_{QCD}^2}\right), \quad \bar{L}_{q\,1,3} = \mathcal{O}\left(e\delta_3\frac{m_\pi^2}{F_\pi^2 M_{\cal T}^2 M_{QCD}^2}\right). \tag{4.2.23}$$

The operators stemming from chiral invariant gCEDM and TV four-quark operators differ from those in Eq. (4.2.19) only in their chiral structure. They appear in the $\Delta = 0$ Lagrangian

$$\begin{aligned}\mathcal{L}^{(0)}_{6,\,f=4,\mathrm{em}} = {} & \bar{D}_{w\,NN}\bar{N}S^\mu v^\nu N\,\bar{N}NF_{\mu\nu} \\ & + \left(\delta_{i3} - \frac{2}{F_\pi^2 D}\left(\boldsymbol{\pi}^2 - \pi_3\pi_i\right)\right)\left[\bar{L}_{w\,1}\left(\bar{N}S^\mu v^\nu\tau_i\,N\,\bar{N}N - \bar{N}S^\mu v^\nu\,N\,\bar{N}\tau_i N\right)\right. \\ & \left. + \bar{L}_{w\,2}\left(\bar{N}S^\mu v^\nu\tau_i\,N\,\bar{N}N + \bar{N}S^\mu v^\nu\,N\,\bar{N}\tau_i N\right)\right]F_{\mu\nu},\end{aligned} \tag{4.2.24}$$

with coefficients given by

$$\bar{D}_{w\,NN}, \bar{L}_{w\,1,2} = \mathcal{O}\left(e\frac{w}{F_\pi^2 M_{\cal T}^2}\right). \tag{4.2.25}$$

For the qEDM and the chiral invariant TV sources, it is interesting to go one order further, and construct short-range contributions to the deuteron MQM. We find

$$\mathcal{L}^{(n+1)}_{6,\,f=4,\mathrm{em}} = \varepsilon^{\mu\nu\alpha\beta}v_\alpha\bar{N}S_\beta N\,\bar{N}S_\lambda N\,\partial^\lambda F_{\mu\nu}\left[\bar{M}_w + \bar{M}_q\left(1 - \frac{2\boldsymbol{\pi}^2}{F_\pi^2 D}\right)\right] + \ldots \tag{4.2.26}$$

where the dots denote other TV operators at this order that do not contribute to the deuteron MQM. The chiral index n is $n = 2$ for the qEDM and $n = 0$ for the gCEDM

and the TV four-quark operators. Consequently, the scaling of the coefficient is

$$\bar{M}_w = \mathcal{O}\left(ew\frac{1}{F_\pi^2 M_{\mathcal{T}}^2 M_{QCD}}\right), \quad \bar{M}_q = \mathcal{O}\left(e\delta_0\frac{m_\pi^2}{F_\pi^2 M_{\mathcal{T}}^2 M_{QCD}^3}\right). \tag{4.2.27}$$

Once again, these scalings are modified if we want to account for the fine tuning in nuclear physics, as we discuss in Chapter 6.

4.2.4 Lepton-nucleon operators

Finally, we take into account the lepton-nucleon operators stemming from the two-lepton-two-quark operators in Eq. (3.2.55). At leading order in the χPT power counting, we obtain

$$\begin{aligned}
\mathcal{L}^{(0)}_{llNN} \;=\; & \Sigma_1^{(0)}\bar{e}i\gamma^5 e\,\bar{N}N\left[\frac{2\pi_3}{F_\pi D}+\rho_{lq\,1}\left(1-\frac{2\boldsymbol{\pi}^2}{F_\pi^2 D}\right)\right] \\
& +\Sigma_2^{(0)}\bar{e}i\gamma^5 e\,\bar{N}\tau^i N\left[-\frac{2\pi_i}{F_\pi D}+\rho_{lq\,2}\left(\delta_{i3}-\frac{2\pi_i\pi_3}{F_\pi^2 D}\right)\right] \\
& +\Sigma_3^{(0)}\bar{e}e\,\bar{N}\tau_i N\left[\left(\delta_{i3}-\frac{2\pi_i\pi_3}{F_\pi^2 D}\right)-\rho_{lq\,1}\frac{2\pi^i}{F_\pi D}\right] \\
& +\Sigma_4^{(0)}\bar{e}e\,\bar{N}N\left[\left(1-\frac{2\boldsymbol{\pi}^2}{F_\pi^2 D}\right)+\rho_{lq\,2}\frac{2\pi_3}{F_\pi D}\right] \\
& +\Sigma_5^{(0)}\bar{e}\sigma^{\mu\nu}e\,\bar{N}\,S_\mu v_\nu N\left[\frac{2\pi_3}{F_\pi D}+\rho_{lq\,3}\left(1-\frac{2\boldsymbol{\pi}^2}{F_\pi^2 D}\right)\right] \\
& +\Sigma_6^{(0)}\bar{e}\sigma^{\mu\nu}e\,\bar{N}\tau^i S_\mu v_\nu N\left[-\frac{2\pi_i}{F_\pi D}+\rho_{lq\,3}\left(\delta_{i3}-\frac{2\pi_i\pi_3}{F_\pi^2 D}\right)\right] \\
& +\Sigma_7^{(0)}\bar{e}\sigma^{\mu\nu}e\,\bar{N}\tau_i i\left[S_\mu,S_\nu\right]N\left[\left(\delta_{i3}-\frac{2\pi_i\pi_3}{F_\pi^2 D}\right)-\rho_{lq\,3}\frac{2\pi^i}{F_\pi D}\right] \\
& +\Sigma_8^{(0)}\bar{e}\sigma^{\mu\nu}e\,\bar{N}i\left[S_\mu,S_\nu\right]N\left[\left(1-\frac{2\boldsymbol{\pi}^2}{F_\pi^2 D}\right)+\rho_{lq\,3}\frac{2\pi_3}{F_\pi D}\right],
\end{aligned} \tag{4.2.28}$$

to which we assign the coefficients

$$\Sigma_i^{(0)} = \mathcal{O}\left(e^2\frac{\sigma_{lq}}{M_{\mathcal{T}}^2}\right). \tag{4.2.29}$$

Increasing the chiral order by one, at $\Delta_6 = 1$ there are operators with one covariant derivative, for example with the form (neglecting chiral partners and isospin)

$\bar{e}e\bar{N}S\cdot\mathcal{D}_+N$ and coefficients of order $\mathcal{O}(e^2\sigma_{lq}/M_T^2M_{QCD})$. We do not construct them explicitly.

The QCD $\bar{\theta}$ term, and the other dimension 6 sources of T violation in Eq. (3.2.53) can also generate couplings of the form (4.2.28), when hard photon exchanges between quark and leptons are integrated out. However, the chiral violating structures $\bar{e}e$, $\bar{e}i\gamma_5 e$ and $\bar{e}\sigma^{\mu\nu}$ in the lepton sector can only be generated by insertions of the lepton mass, and require the exchange of at least two hard photons, leading to tiny coefficients. Long-range contributions to lepton-nucleon interactions of the form (4.2.28) are less suppressed, and arise from TV operators with two nucleons and two photons, still their contribution to atomic EDM appears to be small [119], and we do not explicitly calculate them here. The largest lepton-nucleon couplings from the $\bar{\theta}$ term and the dimension 6 sources of TV comes from the radius of the Electric Dipole Form Factor, which we discuss in detail in Chapter 5.

Operators of the form (4.2.28) are important for the EDMs of paramagnetic atoms. For example, in the case of ^{205} Tl it is found that [81, 119]

$$d_{Tl} = -585 d_e - e(43\,\mathrm{GeV})\left(\Sigma_1^{(0)} - 1/5\Sigma_2^{(0)}\right) \tag{4.2.30}$$

which, with our estimates (3.2.38) and (4.2.29), and neglecting $\Sigma_2^{(0)}$

$$d_{Tl} \approx -e\frac{m_e}{M_T^2}\left(585\,\delta_e + \frac{43\,\mathrm{GeV}}{m_e}e^2\sigma_{lq\,1}\right). \tag{4.2.31}$$

If, as in the majority of the models, $\sigma_{lq\,1}$ is proportional to m_e/M_T, then the contribution of short-distance lepton-nucleon operators is negligible, and experimental constraints on the Thallium EDM are immediately translated in bounds on d_e. On the other hand, if there exist models in which $\sigma_{lq\,1}$ is not suppressed by the lepton mass, as could be the case of certain two Higgs doublet models, $\Sigma_1^{(0)}$ and $\Sigma_2^{(0)}$ can contribute significantly to d_{Tl}, polluting the extraction of d_e.

4.3 Role of tadpoles

In Sec. 3.4 we discussed how the quark mass term, in presence of T violation, can cause vacuum instability and we imposed vacuum alignment in first order in the symmetry-breaking parameters by choosing φ according to Eq. (3.4.35) so that no S_3 was present in the leading Lagrangian. Yet, non-aligned terms, tadpoles in particular, germinate in second order in the symmetry breaking parameters, or when higher dimension TV sources are added to the mix.

In this Section we show how the subleading tadpoles do not constitute a problem. Because of the smallness of their coupling constant, they can be dealt with in perturbation theory, meaning that, for any given TV observable at a given accuracy only a finite number of neutral pion disappearing into the vacuum must be considered. For the applications we discuss in Chapters 5 and 7 it is more convenient to eliminate the pion tadpoles from the mesonic Lagrangian. This result can be achieved with field redefinitions of the form (3.4.20) and (3.4.26) and an appropriate choice of the rotation angle φ. The field redefinitions do not induce new TV interactions. Their net effect is to modify the dependence of the coefficients of the TV operators constructed of Secs. 4.1 and 4.2 on the parameters ε (3.2.6), and $\tilde{\delta}_{0,3}$ (3.2.45). Since in the previous Section we kept track of the dependence of the low energy constants on ε and $\tilde{\delta}_{0,3}$, here we show in detail how such dependence is modified by the elimination of the tadpoles.

For the reader not interested in the details, we can summarize the main result of this Section by noting that the elimination of the leading tadpole from dimension 6 sources, in Eq. (4.1.13) causes an ineffectual shift of the coefficients of the operators generated by the isovector qCEDM, while it produces an additional contribution, proportional to $\tilde{\delta}_3$ and to the quark mass difference ε, to the EFT operators that represent the isoscalar qCEDM. Schematically, the effect of the elimination of the leading tadpole can be obtained by replacing $\tilde{\delta}_0$ with $\tilde{\delta}_0 + \varepsilon\tilde{\delta}_3$ in the scaling formulas in Secs. 4.1 and 4.2.

Now the details. The chiral symmetry breaking Lagrangian in the purely mesonic sector, including operators with Δ up to 2 in the case of chiral symmetry breaking from the quark masses, and $\Delta_6 = 0$ for dimension 6 sources was constructed in Eqs. (4.1.1), (4.1.4), (4.1.9), (4.1.13), (4.1.15). We summarize it here.

$$\begin{aligned}\mathcal{L}_{\rm tadpole} &= \frac{m_\pi^2 F_\pi^2}{4}\left(1+\frac{\Delta m_\pi^2}{2m_\pi^2}\right) - \frac{m_\pi^2}{2D}\left(1+\frac{\Delta m_\pi^2}{m_\pi^2 D}\right)\boldsymbol{\pi}^2 + \frac{\delta m_\pi^2}{2D^2}\pi_3^2 \\ &+F_\pi \frac{\delta m_\pi^2 \rho}{2D}\left(1-\frac{2\boldsymbol{\pi}^2}{F_\pi^2 D}\right)\pi_3 + \left(\tilde{\rho}_3\tilde{\Delta}_q m_\pi^2 + \bar{\Delta}_w m_\pi^2\right)\frac{F_\pi \pi_3}{2D} \\ &+F_\pi \frac{\tilde{\delta}_3 m_\pi^2 \tilde{\rho}_3 + \tilde{\delta}_0 m_\pi^2 \tilde{\rho}_0 + \bar{\delta}_w m_\pi^2}{2D}\left(1-\frac{2\boldsymbol{\pi}^2}{F_\pi^2 D}\right)\pi_3. \end{aligned} \tag{4.3.1}$$

The quark masses are responsible for the TC operators in the first line of Eq. (4.3.1), while $\bar{\theta}$ causes the $\Delta = 2$ tadpole. We have

$$\Delta m_\pi^2 = \mathcal{O}\left(\frac{m_\pi^4}{M_{QCD}^2}\right), \qquad \delta m_\pi^2 = \mathcal{O}\left(\frac{\varepsilon^2 m_\pi^4}{r^4(\bar{\theta}) M_{QCD}^2}\right). \tag{4.3.2}$$

The qCEDM and the chiral invariant TV sources produce tadpoles in the $\Delta_6 = -2$ and $\Delta_6 = 0$ Lagrangian,

$$\tilde{\rho}_3\tilde{\Delta}_q m_\pi^2 = \mathcal{O}\left(\tilde{\delta}_3 \frac{m_\pi^2 M_{QCD}^2}{M_{\not T}^2}\right), \quad \bar{\Delta}_w = \mathcal{O}\left(w\varepsilon \frac{m_\pi^2 M_{QCD}^2}{M_{\not T}^2}\right), \tag{4.3.3}$$

and

$$\tilde{\rho}_3\tilde{\delta}_3 m_\pi^2 = \mathcal{O}\left(\tilde{\delta}_3 \frac{m_\pi^4}{M_{\not T}^2}\right), \quad \tilde{\rho}_0\tilde{\delta}_0 m_\pi^2 = \mathcal{O}\left(\tilde{\delta}_0 \varepsilon \frac{m_\pi^4}{M_{\not T}^2}\right), \quad \bar{\delta}_w m_\pi^2 = \mathcal{O}\left(w\varepsilon \frac{m_\pi^4}{M_{\not T}^2}\right). \tag{4.3.4}$$

In Eq. (4.3.1) we have not written the TC operators in Eq. (4.1.13) and (4.1.15), whose variation is negligible at the accuracy we are working, and we also neglect terms proportional to ρ^2, which are small for small $\bar{\theta}$.

The suppressed non-aligned tadpole operators in Eq. (4.3.1) can be dealt with in perturbation theory and do not constitute *per se* a problem. This can be seen, for example, in the case of the two-point pion Green's function, already discussed in Sec. 3.4.1. The Lagrangian (4.3.1) generates Feynman diagrams similar to those in Fig. 3.1. If we limit ourselves to power counting and neglect the details of the diagrams,

the tadpole term generates interactions analogous to those in Eq. (3.4.3), with the replacement

$$g \sim \rho \frac{\delta m_\pi^2}{m_\pi^2} = \mathcal{O}\left(\frac{\rho \varepsilon^2 m_\pi^2}{r^4(\bar{\theta}) M_{QCD}^2}\right) \tag{4.3.5}$$

in the case of the $\bar{\theta}$ term, and

$$g \sim \tilde{\rho}_3 \frac{\tilde{\Delta}_q m_\pi^2}{m_\pi^2} + \frac{\bar{\Delta}_w m_\pi^2}{m_\pi^2} = \mathcal{O}\left(\tilde{\delta}_3 \frac{M_{QCD}^2}{M_{\not T}^2}\right) + \mathcal{O}\left(w\varepsilon \frac{M_{QCD}^2}{M_{\not T}^2}\right) \tag{4.3.6}$$

for the largest tadpoles generated by dimension 6 sources.

In the present case g is much smaller than one, suppressed by two powers of m_π/M_{QCD} or $M_{QCD}/M_{\not T}$. The subleading tadpoles generated by dimension 6 sources yield an even smaller g, of the size of $m_\pi^2/M_{\not T}^2$. Therefore, the tadpoles in Eq. (4.3.1) do not cause vacuum instability, that is, the choice of vacuum done in the construction of the chiral Lagrangian is still viable and the explicit symmetry-breaking terms can be handled in χPT. A toy model that illustrates this fact can be found in App. E.

However, generally pion tadpoles need to be considered when calculating any observable. Due to the smallness of their coefficients, only a manageable number of them contribute to the calculation of an observable at a given accuracy in the expansion in powers of Q/M_{QCD}. A concrete example where tadpoles play a role is the TV pion-nucleon form factor at relative $\mathcal{O}(Q^2/M_{QCD}^2)$, which will be discussed in App. J.

Still, one can rotate the tadpoles away using Eqs. (3.4.20) and (3.4.26). With the choice

$$\tan\varphi = -\frac{\tilde{\rho}_3 \tilde{\Delta}_q m_\pi^2 + \bar{\Delta}_w m_\pi^2}{m_\pi^2} = \mathcal{O}\left(\tilde{\delta}_3 \frac{M_{QCD}^2}{M_{\not T}^2}\right) + \mathcal{O}\left(w\varepsilon \frac{M_{QCD}^2}{M_{\not T}^2}\right) \tag{4.3.7}$$

we can eliminate the tadpoles that transform like S_3 from Eq. (4.3.1). Since the angle is small, $\tan\varphi \approx \varphi$, and from here on we keep only terms linear in φ. The fact that the angle φ scales as $M_{QCD}^2/M_{\not T}^2$ implies that the transformation of chiral variant operators generated from the quark mass at $\Delta = n + 2$ contributes to TV operators from dimension 6 TV sources at $\Delta_6 = n$. The variation of TV operators

from $\bar{\theta}$ generates a TC contribution proportional to $\bar{\theta}$ and to $1/M_T^2$, which, for the same argument of Sec. 4.1.1, is small, while the variation of TC operators from the TC and chiral breaking dimension 6 sources generates TV operators proportional to $1/M_T^4$, which are also negligible. Chiral invariant operators are not modified by the redefinitions (3.4.20) and (3.4.26).

The effect of the rotation (3.4.20), with angle (4.3.7), on the mesonic Lagrangian is to cancel the tadpoles with transformation properties of a chiral vector, and to modify the coefficients of the tensor:

$$\begin{aligned}\mathcal{L}_{\rm tadpole} &= \frac{m_\pi^2 F_\pi^2}{4}\left(1+\frac{\Delta m_\pi^2}{2m_\pi^2}\right)-\frac{m_\pi^2}{2D}\left(1+\frac{\Delta m_\pi^2}{m_\pi^2 D}\right)\boldsymbol{\pi}^2+\frac{\delta m_\pi^2}{2D^2}\pi_3^2 \\ &\quad +\frac{F_\pi}{2D}\left(\delta m_\pi^2\rho+\tilde{\delta}_3' m_\pi^2\tilde{\rho}_3+\tilde{\delta}_0' m_\pi^2\tilde{\rho}_0+\bar{\delta}_w' m_\pi^2\right)\left(1-\frac{2\boldsymbol{\pi}^2}{F_\pi^2 D}\right)\pi_3, \qquad (4.3.8)\end{aligned}$$

with

$$\tilde{\delta}_3' m_\pi^2\tilde{\rho}_3 = \tilde{\delta}_3 m_\pi^2\tilde{\rho}_3-\tilde{\Delta}_q m_\pi^2\tilde{\rho}_3\frac{\Delta m_\pi^2}{m_\pi^2}, \qquad (4.3.9)$$

$$\tilde{\delta}_0' m_\pi^2\tilde{\rho}_0 = \tilde{\delta}_0 m_\pi^2\tilde{\rho}_0+\tilde{\Delta}_q m_\pi^2\tilde{\rho}_3\frac{\delta m_\pi^2}{m_\pi^2}, \qquad (4.3.10)$$

$$\bar{\delta}_w' m_\pi^2 = \bar{\delta}_w m_\pi^2-\bar{\Delta}_w m_\pi^2\left(\frac{\Delta m_\pi^2-\delta m_\pi^2}{m_\pi^2}\right). \qquad (4.3.11)$$

The new terms come from the transformation of the TC operators in Eqs. (4.1.4) and (4.1.9). We can thus rotate away the tadpole without introducing new interactions in the meson Lagrangian. The net effect of the rotation is only to change the dependence of the coefficients on the parameters $\tilde{\delta}_0$, $\tilde{\delta}_3$, and ε. The rotation indeed replaces Eqs. (4.1.16) and (4.1.17) with

$$\tilde{\rho}_3\tilde{\delta}_3' m_\pi^2 = \mathcal{O}\left(\tilde{\delta}_3\frac{m_\pi^4}{M_T^2}\right), \qquad (4.3.12)$$

$$\tilde{\rho}_0\tilde{\delta}_0' m_\pi^2 = \mathcal{O}\left(\varepsilon(\tilde{\delta}_0+\varepsilon\tilde{\delta}_3)\frac{m_\pi^4}{M_T^2}\right), \qquad (4.3.13)$$

$$\bar{\delta}_w' m_\pi^2 = \mathcal{O}\left(w\varepsilon(1+\varepsilon^2)\frac{m_\pi^4}{M_T^2}\right), \qquad (4.3.14)$$

where, as usual, the "+" in power counting estimates is used to indicate the presence of different contributions to the coefficients.

The remaining tadpole in Eq. (4.3.8) can eliminated by a second rotation, now with angle

$$\varphi' = -\frac{1}{m_\pi^2}\left(\delta m_\pi^2 \rho + \tilde{\delta}'_3 m_\pi^2 \tilde{\rho}_3 + \tilde{\delta}'_0 m_\pi^2 \tilde{\rho}_0 + \bar{\delta}'_w m_\pi^2\right). \tag{4.3.15}$$

In this case, the size of φ' implies that the variation of TC, chiral breaking operators generated by the quark mass at order $\Delta = n$ yields new TV contributions to the $\Delta = n+2$ Lagrangian from the $\bar{\theta}$ term and $\Delta_6 = n$ Lagrangian from the dimension 6 sources.

In the mesonic sector, we are left with

$$\begin{aligned}\mathcal{L}_{\text{tadpole}} &= \frac{m_\pi^2 F_\pi^2}{4}\left(1+\frac{\Delta m_\pi^2}{2m_\pi^2}\right) - \frac{m_\pi^2}{2D}\left(1+\frac{\Delta m_\pi^2}{m_\pi^2 D}\right)\boldsymbol{\pi}^2 + \frac{\delta m_\pi^2}{2D^2}\pi_3^2 \\ &\quad -\frac{F_\pi}{2D}\left(\delta m_\pi^2 \rho + \tilde{\delta}'_3 m_\pi^2 \tilde{\rho}_3 + \tilde{\delta}'_0 m_\pi^2 \tilde{\rho}_0 + \bar{\delta}'_w m_\pi^2\right)\frac{2\boldsymbol{\pi}^2}{F_\pi^2 D}\pi_3, \end{aligned} \tag{4.3.16}$$

Since the tadpole generated by the rotation (3.4.20) and the one in Eq. (4.3.8) have different chiral properties, residual TV interactions involving an odd number of pions are left behind. In many processes they will only contribute at loop level and, consequently, at high order.

The two rotations that allow to eliminate the tadpoles affect the other sectors of the Lagrangian as well. Also in this case, no new interactions are introduced, but the dependence of the coefficients of TV operators on the parameters of the quark-gluon Lagrangian $\tilde{\delta}_{0,3}$, and ε becomes more complicated.

For the $\bar{\theta}$ term, the rotation with angle φ' turns Eqs. (4.1.2), (4.1.19) and (4.1.27) into

$$\begin{aligned}\mathcal{L}^{(\Delta\leq 3)}_{\not\chi,\, f=2} &= \Delta m_N \bar{N} N\left(1-\frac{2\boldsymbol{\pi}^2}{F_\pi^2 D}\right) + \frac{\delta m_N}{2}\left\{\bar{N}\tau_3 N - \frac{2\pi_3}{F_\pi^2 D}\bar{N}\boldsymbol{\tau}\cdot\boldsymbol{\pi} N\right\} \\ &\quad -\frac{\rho}{F_\pi D}\delta m_N\left(1+\frac{\delta m_\pi^2}{m_\pi^2}\right)\bar{N}\boldsymbol{\tau}\cdot\boldsymbol{\pi} N + c_1^{(3)}\frac{4\pi_3^2}{F_\pi^2 D^2}\bar{N}N \\ &\quad +\frac{4\rho}{F_\pi D}\left[c_1^{(3)} - \frac{\Delta m_N}{2}\frac{\delta m_\pi^2}{m_\pi^2} - \frac{2c_1^{(3)}\boldsymbol{\pi}^2}{F_\pi^2 D}\right]\pi_3 \bar{N} N + \ldots \end{aligned} \tag{4.3.17}$$

where we neglected terms quadratic in ρ, and ... denotes the remaining terms in Eq. (4.1.27), which are not affected by the rotation. Eliminating the tadpoles amounts to a $\mathcal{O}(\varepsilon^2 m_\pi^2/M_{QCD}^2)$ shift in the $\bar{\theta}$ contribution to $\bar{g}_0$, and a shift in the $\pi_3\bar{N}N$ coupling. Recall that the $c_1^{(3)}$ term originated in the symmetric tensor contained in a $P_a \otimes P_b$ structure just like the tadpole, as it is obvious from the form of the corresponding terms. However, since there is no *a priori* relation between $c_1^{(3)}/\Delta m_N$ and $\delta m_\pi^2/2m_\pi^2$, the $\pi_3\bar{N}N$ coupling is not eliminated when we rotate the tadpole away. The new contribution to the isovector coupling $\bar{g}_1^{(3)}$ has the same scaling as $c_1^{(3)}$. Notice, however, that the two contributions differ in their multi-pion structure, and, at least in principle, the two coefficients $c_1^{(3)}$ and $\Delta m_N \delta m_\pi^2/m_\pi^2$ can be extracted independently.

The elimination of the tadpole has more consequences for the dimension 6 operators. In the pion-nucleon sector, the rotation with an angle $\varphi = \mathcal{O}\left(M_{QCD}^2/M_T^2\right)$ transforms the TV part of Eq. (4.1.29) into

$$\begin{aligned}\mathcal{L}^{(-1)}_{6,\,f=2} &= -(\bar{g}'_{0\,q} + \bar{g}'_{0\,w})\frac{1}{F_\pi D}\bar{N}\boldsymbol{\tau}\cdot\boldsymbol{\pi}N - (\bar{g}'_{1\,q} + \bar{g}'_{1\,w})\frac{1}{F_\pi D}\pi_3\bar{N} \\ &\quad -\frac{\bar{\imath}_{0w}}{F_\pi^2}(v\cdot D\boldsymbol{\pi}\times D_\mu\boldsymbol{\pi})\cdot\bar{N}S^\mu\boldsymbol{\tau}N. \qquad (4.3.18)\end{aligned}$$

with

$$\bar{g}'_{0\,q} = \tilde{\delta}_q m_N\tilde{\rho}_0 + \delta m_N\tilde{\rho}_3\frac{\tilde{\Delta}_q m_\pi^2}{m_\pi^2} \qquad (4.3.19)$$

$$\bar{g}'_{0\,w} = \bar{g}_{0\,w} + \delta m_N\frac{\bar{\Delta}_w m_\pi^2}{m_\pi^2} \qquad (4.3.20)$$

$$\bar{g}'_{1\,q} = \tilde{\Delta}_q m_N\tilde{\rho}_3 - 2\Delta m_N\tilde{\rho}_3\frac{\tilde{\Delta}_q m_\pi^2}{m_\pi^2} \qquad (4.3.21)$$

$$\bar{g}'_{1\,w} = \bar{g}_{1\,w} - 2\Delta m_N\frac{\bar{\Delta}_w m_\pi^2}{m_\pi^2}. \qquad (4.3.22)$$

From Eqs. (4.1.14) and the scaling of $\Delta m_N = m_\pi^2/M_{QCD}$, we see that the shift in the isovector couplings $\bar{g}_{1\,q}$ and $\bar{g}_{1\,w}$ is inconsequential, their scaling is still the same as Eqs. (4.1.30) and (4.1.31). Instead, for the isoscalar couplings, the behavior in Eqs.

(4.1.30) and (4.1.31) is replaced, after the rotation, by

$$\bar{g}'_{0\,q} = \mathcal{O}\left(\left(\tilde{\delta}_0 + \varepsilon\tilde{\delta}_3\right)\frac{m_\pi^2}{M_{\not\pi}^2}M_{QCD}\right), \quad \bar{g}'_{0\,w} = \mathcal{O}\left(w(1+\varepsilon^2)\frac{m_\pi^2}{M_{\not\pi}^2}M_{QCD}\right). \tag{4.3.23}$$

The rotation used to eliminate the subleading tadpole induces a further, small, shift in the qCEDM and gCEDM contributions to $\bar{g}_0$ and $\bar{g}_1$ in Eqs. (4.3.18). Such a shift contributes at $\Delta_6 = 1$ in the pion-nucleon sector, for which we only considered qCEDM contributions. We find that $\bar{g}'_{0,1}$ is replaced by $\bar{g}'_{0,1} + \delta\bar{g}'_{0,1}$, with

$$\delta\bar{g}'_{0\,q} = \frac{\delta m_N}{m_\pi^2}\left(\tilde{\delta}'_3 m_\pi^2\tilde{\rho}_3 + \tilde{\delta}'_0 m_\pi^2\tilde{\rho}_0\right) \tag{4.3.24}$$

$$\delta\bar{g}'_{1\,q} = -2\frac{\Delta m_N}{m_\pi^2}\left(\tilde{\delta}'_3 m_\pi^2\tilde{\rho}_3 + \tilde{\delta}'_0 m_\pi^2\tilde{\rho}_0\right). \tag{4.3.25}$$

The rotation with angle φ' does not affect, at the order we are working, the nucleon-nucleon and nucleon-photon Lagrangian from the qCEDM and from the gCEDM and four-quark operators.

On the contrary, the rotation used to eliminate the leading tadpole from dimension 6 sources also affects the subleading pion-nucleon Lagrangian, and the nucleon-nucleon and nucleon-photon Lagrangian. In the subleading pion-nucleon Lagrangian, for operators that transform as $\tilde{W}_3$, like $\tilde{\beta}_{q\,2}$ and $\tilde{\beta}_{q\,3}$ in Eq. (4.1.32) and all the operators in Eq. (4.1.35) the effects of the rotation can be absorbed in a redefinition of the coefficients, whose scaling is still determined by Eqs. (4.1.33) and (4.1.36). For operators that transform as $\tilde{V}_4$, the scaling of the coefficients is modified.

$$\tilde{\rho}_0\tilde{\beta}'_{q\,1} = \tilde{\rho}_0\tilde{\beta}_{q\,1} + \tilde{\rho}_3\beta_1\frac{\tilde{\Delta}_q m_\pi^2}{m_\pi^2} = \mathcal{O}\left(\left(\tilde{\delta}_0 + \varepsilon\tilde{\delta}_3\right)\frac{m_\pi^2}{M_{\not\pi}^2}\right) \tag{4.3.26}$$

$$\tilde{\rho}_0\tilde{\zeta}'_{q\,i} = \tilde{\rho}_0\tilde{\zeta}_{q\,i} + \tilde{\rho}_3\zeta_i\frac{\tilde{\Delta}_q m_\pi^2}{m_\pi^2} = \mathcal{O}\left(\left(\tilde{\delta}_0 + \varepsilon\tilde{\delta}_3\right)\frac{m_\pi^2}{M_{\not\pi}^2 M_{QCD}}\right). \tag{4.3.27}$$

For the tensors (4.1.38), the shift in the coefficient $\tilde{\delta}_2^{(1)} m_N$ is inconsequential. The coefficients of the isoscalar and isovector couplings $\bar{N}\boldsymbol{\pi}\cdot\boldsymbol{\tau}N$ and $\pi_3\bar{N}N$ receive an

additional contribution:

$$\tilde{\rho}_3\tilde{c}_1^{\prime(1)} + \tilde{\rho}_0\tilde{c}_2^{\prime(1)} = \left(\tilde{\rho}_3\tilde{c}_1^{(1)} + \tilde{\rho}_0\tilde{c}_2^{(1)} + \tilde{\rho}_3 c_1^{(3)}\frac{\tilde{\Delta}_q m_\pi^2}{m_\pi^2}\right) \tag{4.3.28}$$

$$\tilde{\rho}_0\tilde{\delta}_1^{\prime(1)} m_N = \tilde{\rho}_0\tilde{\delta}_1^{(1)} m_N + \tilde{\rho}_3\delta_1^{(3)} m_N \frac{\tilde{\Delta}_q m_\pi^2}{m_\pi^2} \tag{4.3.29}$$

where the new contributions to the coefficients go as $\varepsilon^2\tilde{\delta}_3$ and $\varepsilon\tilde{\delta}_3$. Once again, they can be obtained by replacing $\tilde{\delta}_0$ with $\tilde{\delta}_0 + \varepsilon\tilde{\delta}_3$ in Eqs. (4.1.39) and (4.1.40).

The same replacement in Eqs. (4.1.47) and (4.1.49) takes care of the effects of the elimination of the tadpoles in the four-nucleon sector. Notice in particular that the coefficient of the chiral invariant operators in Eq. (4.1.50) are not changed by the field redefinition.

The same argument applies to electromagnetic operators. The elimination of the leading tadpole generated by the qCEDM modifies to coefficients in Eq. (4.2.11) in a way that can be schematically summarized by the replacement $\tilde{\delta}_0 \to \tilde{\delta}_0 + \varepsilon\tilde{\delta}_3$ in Eqs. (4.2.13) and (4.2.14) (and also Eq. (4.2.21) and (4.2.22)). The rotation of the leading tadpole generated by the chiral invariant gCEDM and TV four-quark operators does not modify the coefficients of the electromagnetic operators with $\Delta_6 = -1$ in Eqs. (4.2.7), while it changes the chiral breaking operators $\bar{D}^{(1)}_{w,0,1}$ in Eq. (4.2.9) in a way that corresponds to shifting $w \to w(1+\varepsilon^2)$.

Since in EFT a field redefinition does not change the result for any observable, it is our choice whether to keep or eliminate tadpoles. We give an example of this flexibility in App. J.

4.4 Discussion

In Secs. 4.1 and 4.2 we constructed the lowest orders of the TV chiral Lagrangian involving pions and up to four nucleons, which is generated by dimension 4 and dimension 6 TV sources. Tab. 4.1 summarizes the accuracy of our results in the pion-nucleon, nucleon-photon and nucleon-nucleon sector. The coefficients of TV operators

	Correction	pion-nucleon	photon-nucleon $\times Q^2$	nucleon-nucleon $\times F_\pi^2 Q$
θ term, qCEDM	leading	1	Q^2/M_{QCD}^2	Q/M_{QCD}
	derivative	Q/M_{QCD}	Q^3/M_{QCD}^3	Q^2/M_{QCD}^2
	derivative^2	Q^2/M_{QCD}^2	—	—
	mass	m_π^2/M_{QCD}^2	—	—
gCEDM 4-quark	leading	1	1	1
	derivative	—	Q/M_{QCD}	—
	derivative^2	—	Q^2/M_{QCD}^2	—
	mass	—	m_π^2/M_{QCD}^2	—
qEDM	leading	$\alpha_{\rm em}/\pi$	Q^2/M_{QCD}^2	$\alpha_{\rm em}Q/\pi M_{QCD}$

TABLE 4.1. Size of the coefficients of the TV terms in the Lagrangian constructed in Secs. 4.1 and 4.2. Operators stemming from the $\bar{\theta}$ term are measured in units of $\bar{\theta}m_\pi^2/M_{QCD}$, while operators generated by the dimensions 6 TV sources in units of $(\tilde{\delta},\, \delta,\, w)m_\pi^2 M_{QCD}/M_T^2$ for the qCEDM, qEDM and chiral invariant respectively. To compare quantity of the same dimension, photon-nucleon and nucleon-nucleon coefficients are multiplied by Q^2 and $F_\pi^2 Q$, where Q is the momentum of external particles, of the order of the pion mass.

stemming from the $\bar{\theta}$ term are measured in units of $\bar{\theta}m_\pi^2/M_{QCD}$, while for dimension 6 sources we are using units of $(\tilde{\delta},\, \delta,\, w)m_\pi^2 M_{QCD}/M_T^2$ for the qCEDM, qEDM and for the chiral invariant dimension 6 sources respectively. In order to compare objects with the same dimension, we have multiplied the photon-nucleon coefficients by Q^2 and the nucleon-nucleon by $F_\pi^2 Q$, where Q denotes the typical momentum of external particles, and it is of order of the pion mass.

Even before delving into the details of the calculation of some TV nuclear observables, which is the subject of Chapters 5 and 6, we can already draw some qualitative conclusion from Tab. 4.1.

For the dimension 4 QCD $\bar{\theta}$ term, the first noticeable aspect is that all interactions are proportional to negative powers of the large scale M_{QCD}. This is a simple consequence of two facts: *i)* the $\bar{\theta}$ term can be traded for a mass term, which then brings at least one power of m_π^2 in the EFT; *ii)* no P vector can be constructed out of pion fields alone. Time reversal is an accidental symmetry, in the sense that it only

appears in the subleading effective Lagrangian, even though it is (for $\bar{\theta} \neq 0$) a leading interaction (that is, represented by a dimension-four operator) in the underlying theory. T violation would thus be somewhat suppressed at low energies, even if $\bar{\theta}$ had natural size. The same is true of isospin violation and ε [122].

Extending the analysis to the dimension 6 operators, we notice that the different chiral properties of the $\bar{\theta}$ term and the qCEDM on the one side and the gCEDM and four-quark operators on the other imply very different relations between long-distance and short-distance TV effects. The $\bar{\theta}$ term and the qCEDM both violate chiral symmetry, and thus they can generate TV pion-nucleon interactions in which the pion couples to the nucleon non-derivatively (see App. D). As a consequence, the first TV pion-nucleon couplings appear in the Lagrangian two orders before short-range contributions to the nucleon EDM, and to the first nucleon-nucleon interaction which contributes to the TV nucleon-nucleon potential. For the nucleon EDM and EDFF, this fact implies that even though pion-nucleon TV couplings can only contribute to the nucleon EDM via loops, which bring in a $m_\pi^2/(2\pi F_\pi)^2$ suppression, they are still as important as the short-distance operators [93, 91]. For higher nuclei, the most important contribution to TV electromagnetic moments comes from the one-pion-exchange TV potential, which causes the nucleus wavefunction to mix with states of different parity, unless the admixed component has quantum numbers that cause the dipole matrix element to vanish. We will discuss in detail the example of the deuteron EDM and MQM in Chapter 6. The application of chiral EFT to study the effects of $\bar{\theta}$ term and the qCEDM in few nucleon systems with $A \geq 2$ is thus particularly promising, since TV observables are likely to depend on few low energy constants, in the $f = 2$ TV Lagrangian. Once these constants are fixed in TV experiments, one is in the position to make testable, model independent predictions.

For the chiral invariant sources of T violation, instead, the pion-nucleon TV coupling appear in the Lagrangian at the same order as short-distance nucleon EDM operators and four-nucleon TV operators. This happens because it is not possible

to write a TV chiral invariant pion-nucleon coupling with only one derivative. The first chiral invariant TV pion-nucleon coupling must have two derivatives, while non-derivative couplings can be generated by considering the combined effects of chiral invariant TV sources and the chiral-breaking quark mass; in any case, pion-nucleon couplings receive a further suppression of Q^2/M_{QCD}^2. This difficulty does not affect the nucleon-photon and nucleon-nucleon sector, where chiral invariant operators with a minimal number of derivatives can be constructed.

The consequence for the nucleon EDM is that it is dominated in this case by short-distance contributions. For higher nuclei, TV corrections to the wavefunction now are not only due to TV pion-exchange, but also to short-distance operators. More in general, we will see in the concrete examples of Chapters 5 and 6 that the increased role of short-distance interactions in the case of chiral invariant TV operators reduces the predictive power of our analysis, because of the appearance of more low energy constant.

Finally, pion physics is suppressed also in the case of TV from the qEDM. In this case the suppression comes from the need to integrate out the photon in the qEDM, which leads to the factor of $\alpha_{\rm em}/\pi$ in Tab. 4.1. Also in this case, the predominance of short-distance effects poses a serious limitation to our predictive power.

		$\bar{g}_0$	$\bar{g}_1$	$\bar{g}_2$
θ term	LO	θ	—	—
	$\mathrm{N^2LO}$	$\bar{\theta}\,(1,\varepsilon^2)\ m_\pi^2/M_{QCD}^2$	$\bar{\theta}\varepsilon\, m_\pi^2/M_{QCD}^2$	—
qCEDM	LO	$\tilde{\delta}_0,\ \varepsilon\tilde{\delta}_3$	$\tilde{\delta}_3$	—
	$\mathrm{N^2LO}$	$(\tilde{\delta}_0, \varepsilon\tilde{\delta}_3, \varepsilon^2\tilde{\delta}_0, \varepsilon^3\tilde{\delta}_3)$ $\times m_\pi^2/M_{QCD}^2$	$(\tilde{\delta}_3,\ \varepsilon\tilde{\delta}_0,\ \varepsilon^2\tilde{\delta}_3)$ $\times m_\pi^2/M_{QCD}^2$	$\varepsilon\tilde{\delta}_3$ $\times m_\pi^2/M_{QCD}^2$
gCEDM	LO	$w, w\varepsilon^2$	$w\varepsilon$	—

TABLE 4.2. List of possible non-derivative TV pion-nucleon vertices, up to $\mathcal{O}(m_\pi^2/M_{QCD}^2)$ w.r.t. the leading pion-nucleon coupling. We give the size of the contributions to the interaction strengths in units of m_π^2/M_{QCD} for the $\bar{\theta}$ term and of $m_\pi^2 M_{QCD}/M_T^2$ for the dimension 6 TV sources. For simplicity we assumed $\bar{\theta} \ll 1$.

We can now look more in detail to the structure of the TV pion-nucleon vertex.

Traditionally [157, 158, 159, 160, 161], implications of T violation in nuclear physics have been drawn from the possible isospin structures of non-derivative pion-nucleon interactions, without prejudice about their relative sizes:

$$\mathcal{L}_{\not{T},\pi N} = -\frac{\bar{g}_0}{F_\pi}\bar{N}\boldsymbol{\pi}\cdot\boldsymbol{\tau}N - \frac{\bar{g}_1}{F_\pi}\pi_3\bar{N}N - \frac{\bar{g}_2}{F_\pi}\bar{N}\left(3\pi_3\tau_3 - \boldsymbol{\pi}\cdot\boldsymbol{\tau}\right). \tag{4.4.1}$$

In Tab. 4.2 we list the estimated sizes of the non-derivative TV pion-nucleon couplings found in Sec. 4.1.2 for different sources of T violation.

Since the $\bar{\theta}$ term breaks chiral symmetry, but not isospin symmetry, at leading order it only contributes to the isoscalar coupling $\bar{g}_0$ via Eq. (4.1.19) which is nothing but the pion-nucleon interaction of Ref. [93] with its chiral partners, in stereographic coordinates. From Eq. (4.1.19)

$$\bar{g}_{0\,\bar{\theta}} = \delta m_N \rho. \tag{4.4.2}$$

This coupling receives hadronic corrections of $\mathcal{O}(m_\pi^2/M_{QCD}^2)$, and, after the elimination of the tadpoles, from Eqs. (4.1.27) and (4.3.17) one gets

$$\delta\bar{g}_{0\,\bar{\theta}} = 2\rho\left(-\delta_1^{(3)}m_N + \delta m_N\frac{\delta m_\pi^2}{2m_\pi^2}\right). \tag{4.4.3}$$

$\bar{g}_{0\,\bar{\theta}}$ also receives electromagnetic corrections, which are suppressed by $\alpha_{\rm em}/\pi$, and are not explicitly constructed here.

The isospin breaking coupling $\pi_3\bar{N}N$ is suppressed by two powers of m_π/M_{QCD}:

$$\bar{g}_{1\,\bar{\theta}} = -4\rho\left(c_1^{(3)} - \Delta m_N\frac{\delta m_\pi^2}{2m_\pi^2}\right). \tag{4.4.4}$$

It also receives corrections of order $\alpha_{\rm em}/\pi$, which we do not explicitly list here. Numerically $\alpha_{\rm em}/\pi \sim \varepsilon m_\pi^3/M_{QCD}^3$ (using $M_{QCD} \sim m_\rho$, the mass of the rho-meson), so the most important contribution is presumably the hadronic one. Finally, the most relevant contribution to $\bar{g}_2$ has electromagnetic origin and is suppressed by $\alpha_{\rm em}/\pi$ with respect to $\bar{g}_0$ [39]. Hadronic contributions to $\pi_3\bar{N}\tau_3 N$ are suppressed by m_π^4/M_{QCD}^4, as shown in App. H.

It is clear then that the calculation of TV observables that are mostly sensitive to $\bar{g}_1$ requires, at least for TV from the QCD $\bar{\theta}$ term, the construction of the full N^{2}LO

TV Lagrangian, which contains not only non-derivative pion-nucleon couplings of the form (4.4.1), but also derivative pion-nucleon couplings and short-range interactions. We will return on this subject in Chapter 7.

In the case of the qCEDM, if we assume that the isoscalar and isovector qCEDM have the same size, $\tilde{\delta}_0 \approx \tilde{\delta}_3$, the isospin conserving and isospin breaking couplings $\bar{g}_0$ and $\bar{g}_1$ both are present at leading order, and, after the rotation of the tadpole they are (dropping the primes in Eqs. (4.3.19) and (4.3.21))

$$\bar{g}_{0\,q} = \tilde{\delta}_q m_N \tilde{\rho}_0 + \delta m_N \tilde{\rho}_3 \frac{\tilde{\Delta}_q m_\pi^2}{m_\pi^2} \tag{4.4.5}$$

$$\bar{g}_{1\,q} = \tilde{\Delta}_q m_N \tilde{\rho}_3 - 2\Delta m_N \tilde{\rho}_3 \frac{\tilde{\Delta}_q m_\pi^2}{m_\pi^2}. \tag{4.4.6}$$

Two orders down, we encounter hadronic corrections to $\bar{g}_0$ and $\bar{g}_1$, and the first hadronic contribution to $\bar{g}_2$. Dropping for a moment the assumption $\tilde{\delta}_0 \approx \tilde{\delta}_3$, a predominantly isoscalar qCEDM, $\tilde{\delta}_0 \gg \tilde{\delta}_3$ will not be distinguishable from the $\bar{\theta}$ term in low energy observables. In particular, as far as pion-nucleon couplings are concerned one would find in this case that $\bar{g}_0 \gg \bar{g}_1$. A predominantly isovector qCEDM, $\tilde{\delta}_3 \gg \tilde{\delta}_0$ would instead yield $\bar{g}_0$ and $\bar{g}_1$ of approximately the same order, with the extra factor of ε in the isoscalar coupling suggesting $\bar{g}_1 \gtrsim \bar{g}_0$.

The chiral invariant TV sources give rise to the same relations between the non-derivative couplings $\bar{g}_0$, $\bar{g}_1$ and $\bar{g}_2$ as the qCEDM, even though in this case, derivative couplings appear already at leading order.

The fact that different sources of TV are responsible for different hierarchies between the non-derivative TV couplings $\bar{g}_0$, $\bar{g}_1$ and $\bar{g}_2$ has important implications for the TV electromagnetic moments of nuclei. In Chapter 6, we will explore them more in detail in the simplest possible example, the calculation of the EDM and MQM of the deuteron.

4.4.1 Connection to TC operators

As we have shown, in the purely hadronic sector of the theory, chiral symmetry links the coefficients of the leading TV operators to those of TC operators. This relation is particularly important for TV from the $\bar{\theta}$ term, on which we focus in the first part of this Section. We will briefly discuss the operators induced by the TC partners of the qCEDM and qEDM at the end of the Section.

TV from the $\bar{\theta}$ term is linked, in particular, to isospin breaking from the quark mass difference. Therefore, the measurement of TC but isospin-breaking observables can determine the contribution of the QCD dynamics to TV coupling constants. Since isospin violation that is linear in the quark masses always breaks charge symmetry, while this is not necessarily true of indirect electromagnetic interactions, it is in CSB observables that we have the best chance of making inferences about T violation from the $\bar{\theta}$ term. If we consider the latter as the only source of T violation, this link would leave $\bar{\theta}$ as the only parameter to be determined in the direct observation of T violation.

The most important example of the link to isospin violation is in the lowest-order terms [93, 92, 163]: Eq. (4.1.19) links the leading TV interaction

$$\mathcal{L}^{(1)}_{\not{T},\pi N} = -\frac{\bar{g}_0}{F_\pi D}\bar{N}\boldsymbol{\tau}\cdot\boldsymbol{\pi}N \tag{4.4.7}$$

to the quark-mass contribution to the nucleon mass splitting δm_N:

$$\bar{g}_0 = \rho\,\delta m_N = \mathcal{O}\left(\frac{\rho\varepsilon m_\pi^2}{r^2(\bar{\theta})M_{QCD}}\right). \tag{4.4.8}$$

It is well-known that this interaction produces the dominant long-range contribution to the nucleon EDM and form factor [93, 94, 95, 96, 162, 97, 91, 98, 99]. With δm_N known, a determination of $\bar{g}_0$ would allow one to obtain the value of $\bar{\theta}$ via Eq. (4.1.5).

Now, δm_N cannot be determined solely from the observed mass splitting, since the latter also receives an indirect electromagnetic contribution of similar size $\breve{\delta} m_N = \mathcal{O}(\alpha_{\rm em} M_{QCD}/\pi)$ [122, 145], given in Eq. (3.3.22). One can use models for higher-energy physics in order to extract $\breve{\delta} m_N$ from the Cottingham sum rule, $\breve{\delta} m_N =$

$-(0.76 \pm 0.30)$ MeV [137], thus inferring δm_N. There is also a lattice calculation, $\delta m_N = 2.26 \pm 0.57 \pm 0.42 \pm 0.10$ MeV [133]. Alternatively, one would like to determine δm_N directly from low-energy data. This is in principle possible [122] because $\breve{\delta} m_N$ originates from a chiral tensor, and thus generates different interactions between the nucleon and an even number of pions than does Eq. (4.1.19). In fact, CSB observables in pion production reactions such as $pn \to d\pi^0$ [134, 135, 136] and $dd \to \alpha\pi^0$ [164, 165] are quite sensitive to δm_N. Unfortunately they are also sensitive to other CSB parameters and the calculation of the strong interactions themselves are not easy, so that at present there is room for improvement in the extraction of δm_N from data [166, 167]. This should, nevertheless, be possible as we hone our theoretical and experimental tools [147]. The link with T violation should serve as an extra motivation for this program.

The connection with CSB is in no way limited to leading order. The first correction in the pion-nucleon sector [91],

$$\mathcal{L}^{(2)}_{\not T,2\pi N} = -\frac{2\bar{h}_0}{F_\pi^2 D}\boldsymbol{\pi}\cdot D_\mu\boldsymbol{\pi}\bar{N}S^\mu N, \tag{4.4.9}$$

has a coefficient related by Eq. (4.1.21) to the quark-mass contribution to isospin breaking in the pion-nucleon coupling constant,

$$\bar{h}_0 = \rho\beta_1 = \mathcal{O}\left(\frac{\rho\varepsilon m_\pi^2}{r^2(\bar{\theta})M_{QCD}^2}\right). \tag{4.4.10}$$

At present there are only bounds on β_1. For example, from a phase-shift analysis of two-nucleon data [145, 148, 149], $\beta_1 = 0(9)\cdot 10^{-3}$, which is comparable to estimates of β_1 from π-η mixing.

Note that when we face interactions that are no longer linear in ε, the connection is not necessarily to CSB; it might be merely to more general isospin violation. For example, the new TV structure $\pi_3\bar{N}N$ in Eq. (4.1.27),

$$\mathcal{L}^{(3)}_{\not T,\pi N} = \frac{\bar{g}_1^{(3)}}{F_\pi D}\left(1 - \frac{2\boldsymbol{\pi}^2}{F_\pi^2 D}\right)\pi_3\bar{N}N + \ldots, \tag{4.4.11}$$

with

$$\bar{g}_1^{(3)} = 4\rho c_1^{(3)} = \mathcal{O}\left(\frac{\rho\varepsilon^2 m_\pi^4}{r^4(\bar{\theta})M_{QCD}^3}\right), \tag{4.4.12}$$

has a partner that is isospin-breaking but does respect charge symmetry. The parameter $c_1^{(3)}$ can in principle be extracted from isospin violation in pion-nucleon scattering, but it is not easy: even the very sophisticated, state-of-the-art analysis of Ref. [168] stops one order shy of it, at which level many other poorly determined parameters already appear.

We can thus obtain information about some strong-interaction matrix elements that appear in T violation from an analysis of isospin violation. However, at higher orders in the strong-interaction sector this connection disappears. The consideration of subleading TV interactions requires the construction of operators that transform as tensor products of the chiral-breaking terms in the QCD Lagrangian. In this case, the relation (4.1.5) applies to the ratio of the coefficients of the TV and TC components of the tensors. In general, however, the tensors thus obtained belong to some reducible representation of $SO(4)$, and they have to be decomposed as the sum of independent operators belonging to irreducible representations of the group. High-order tensor products may generate operators that have the same chiral properties as the vectors S and P in the QCD Lagrangian. T violation is still in P_4s and S_3s proportional to ρ, but their number might no longer match those of T-conserving S_4s and P_3s.

One example, given in App. H, is that of a TV operator with the same transformation properties as S_3, which is linked by Eq. (4.1.5) to a chiral-breaking operator that transforms as S_4. This S_4 is merely a subleading correction to another S_4, the nucleon sigma term, which does not have a TV partner. The correction cannot be separated experimentally from the lower-order term; it could potentially be separated theoretically via lattice simulations with varying quark masses (although if it is necessary to appeal to lattice calculations then one could calculate the strong-interaction coefficient of the TV operator directly). Worse still, another S_4 without TV partner can appear at the same order as the S_4 we are interested in, which is in fact the

case of the example in App. H. In this case, the connection with a TC observable is completely lost.

Similarly, in another App. H example, only part of a P_4 is linked to a P_3, which is a correction to the nucleon mass splitting. As a consequence, the connection between the coefficient of a $\bar{N}\boldsymbol{\pi}\cdot\boldsymbol{\tau}N$ interaction and δm_N, shown in leading order in Eq. (4.4.8), no longer holds four orders down in the m_π/M_{QCD} expansion.

As soon as the electromagnetic interaction is turned on, the combined isospin-breaking effects of the electromagnetic coupling and of the quark-mass difference destroy the validity of the relation (4.1.5). Here the most important example is the case of the short-distance contributions to the nucleon EDM, extracted from Eq. (4.2.4):

$$\begin{aligned}\mathcal{L}^{(3)}_{\not{T},N\gamma} &= 2\bar{N}\left[\bar{D}_0^{(3)}+\left(\bar{D}_1^{(3)}+\bar{D}_1'^{(3)}\right)\tau_3+\frac{2}{F_\pi^2}\left(\frac{\bar{D}_1'^{(3)}}{D}-\frac{\bar{D}_1^{(3)}}{2-D}\right)\right.\\ &\left.\left(\pi_3\boldsymbol{\pi}\cdot\boldsymbol{\tau}-\boldsymbol{\pi}^2\tau_3\right)\right]S^\mu\left(v^\nu+\frac{i\mathcal{D}^\nu_{\perp -}}{2m_N}\right)NeF_{\mu\nu}\left(1-\frac{2\boldsymbol{\pi}^2}{F_\pi^2 D}\right),\end{aligned} \tag{4.4.13}$$

with coefficients

$$\bar{D}_i^{(3)}=\rho D_i^{(3)}=\mathcal{O}\left(\frac{\rho\varepsilon m_\pi^2}{r^2(\bar{\theta})M_{QCD}^3}\right). \tag{4.4.14}$$

Since by power counting they should be comparable to the EDM generated by a pion loop [93, 94, 95, 96, 97, 91, 98, 99], the nucleon EDM up to next-to-leading order depends on three TV parameters: $\bar{g}_0$, $\bar{D}_0^{(3)}$, and $\bar{D}_1^{(3)}+\bar{D}_1'^{(3)}$.

These operators are linked by Eq. (4.2.5) to operators that contribute to pion photoproduction on the nucleon. (We do not see here a direct link to anomalous magnetic moments [169].) However, the coefficients cannot be extracted from the measurement of isospin violation in pion photoproduction due to the existence in Eq. (4.2.6) of operators with the same chiral properties as $D_0^{(3)}$ and $D_1^{(3)}$ that are not linked to TV operators. Even if one assumes TV to arise solely from the $\bar{\theta}$ term, the measurement of the neutron and proton EDMs alone would not be sufficient to fix

$\bar{g}_0$ (and thus extract the value of the angle $\bar{\theta}$ using δm_N), unless the short-distance operators are calculated in lattice QCD.

These conclusions are obtained by considering the chiral group $SU(2)_L \times SU(2)_R$. If one assumes the strange quark mass to provide a suitable expansion parameter, one works with $SU(3)_L \times SU(3)_R$ instead. This larger symmetry increases our ability to extract strong-interaction matrix elements needed for an analysis of T violation from TC measurements [93, 94, 95, 96, 97, 98, 99]. The limitation of this approach comes, of course, from the poorer convergence of the chiral expansion in the $SU(3)_L \times SU(3)_R$ case.

In Sec. 4.1.1 we pointed out that the isoscalar and isovector qCEDM break chiral symmetry as components of two chiral four-vectors whose TC components represent the anomalous quark chromo-magnetic dipole moment. Therefore, we introduced the parameters $\tilde{\rho}_0$ and $\tilde{\rho}_3$ and we could establish relations analogous to Eq. (4.1.5). We also noticed that, unfortunately, such a relation carries no practical effect, since the contribution of the quark anomalous chromo-magnetic moment to TC low-energy observables can never be isolated from other, more relevant chiral breaking effects, in particular the effects of the quark mass and the quark mass difference.

We can more concretely see this in the realization of the Lagrangian from the qCMDM in Secs. 4.1 and 4.2. Eq. (4.1.29) contains the leading interactions in the pion-nucleon sector. We can see the the qCMDM generates a contribution to the nucleon mass difference, $\tilde{\delta}_q m_N$, and a contribution to the sigma term, $\tilde{\Delta}_q m_N$, which have the exact same form as Eqs. (4.1.19) and (4.1.2) and are suppressed by M_{QCD}^2/M_T^2 with respect to δm_N and Δm_N. In the nucleon-photon sector, the contributions to the isoscalar and isovector nucleon magnetic moment $\tilde{E}_{q0}^{(1)}$, $\tilde{E}_{q\,1}$and $\tilde{E}_{q\,1}^{\prime\,(1)}$ are $\mathcal{O}(M_{QCD}^2/M_T^2)$ corrections to $E_0^{(3)} + G_0^{(3)}$, $E_1^{(3)} + G_1^{(3)}$ and $G_1^{\prime\,(3)}$, which are already smaller by m_π^2/M_{QCD}^2 with respect to the leading contributions to the anomalous magnetic moments in Eq. (3.3.18). The same can be said for the pion photoproduction operators in Eq. (4.2.12), and also for the electromagnetic operators from the

qMDM. Thus we see that the symmetry properties of the qCMDM and qMDM are not sufficient to allow us to identify their contributions to low-energy observables in nuclear physics, and to disentangle them from those of other operators that have the same chiral properties.

If on the one hand chiral symmetry is not sufficient to fully constrain the QCD dynamics that enters the TV couplings, on the other hand it is a powerful tool to organize the TV Lagrangian as a series of terms suppressed by more and more powers of m_π/M_{QCD} and Q/M_{QCD}. It can be used to extrapolate lattice calculations, in this case the nucleon EDM [170, 171, 172], to realistic values of m_π, and to take one-nucleon information, experimental or numerical, into nuclear systems [37].

Chapter 5

The Nucleon Electric Dipole Moment

5.1 Introduction

The electric dipole form factor (EDFF) completely specifies the parity (P) and time-reversal (T) -violating coupling of a spin 1/2 particle to a single photon [91, 92]. Together with the well-known parity P and T-preserving electric and magnetic form factors and the P-violating, T-preserving anapole form factor, the P- and T-violating EDFF completely specifies the Lorentz covariant electromagnetic current of a particle with spin 1/2. At zero momentum, it reduces to the nucleon electric dipole moment (EDM). Although the full momentum dependence of a nuclear EDFF will not be measured anytime soon, the radius of the form factor provides a contribution to the Schiff moment (SM) of the corresponding atom, because it produces a short-range electron-nucleus interaction. Furthermore, it can be used in lattice simulations to extract the EDM by extrapolation from a finite-momentum calculation [173] (in addition to the required extrapolations in quark masses and volume [163]).

There has been some recent interest [91, 92, 174, 175, 99, 40] in the nucleon EDFF motivated by prospects of experiments that aim to improve the current bound on the neutron EDM, $|d_n| < 2.9 \cdot 10^{-13}\, e$ fm [82], by nearly two orders of magnitude [83], and to constrain the proton and deuteron EDMs at similar levels [87]. We would like to understand the implications of a possible signal in these measurements to the sources of T violation at the quark level, which include, in order of increasing dimension, the QCD $\bar{\theta}$ term, the quark color-EDM (qCEDM) and EDM, the gluon color-EDM, TV four-quark operators *etc.* [107, 108, 110, 111]. Unfortunately, as with other low-energy observables, both the EDM and the SM of hadrons and nuclei are difficult to calculate directly in QCD. However, long-range contributions from pions can, to some extent, be calculated using Chiral Perturbation Theory, in particular the TV

Lagrangian constructed in Chapters 3 and 4.

The TV current-current nucleon-electron interaction is of the form

$$iT = -ie\,\bar{e}(l')\gamma^{\mu}e(l)\,D_{\mu\nu}(q)\,\bar{N}(p')J^{\nu}_{ed}(q,K)N(p), \tag{5.1.1}$$

where $e(l)$ ($N(p)$) is an electron (nucleon) spinor with momentum l (p) and $D_{\mu\nu}(q) = -i(\eta_{\mu\nu}/q^2+\ldots)$ is the photon propagator with $q^2 = (p-p')^2 \equiv -Q^2 < 0$. The nucleon electric dipole current J^{μ}_{ed} can be expressed in terms of $q = p-p'$ and $K = (p+p')/2$ as an expansion in powers of Q/m_N that reads [91, 39, 40]

$$\begin{aligned} J^{\mu}_{ed}(q,K) &= 2\left(F_0(Q^2)+F_1(Q^2)\tau_3\right)\Big[S^{\mu}v\cdot q - S\cdot q v^{\mu} \\ &+ \frac{1}{m_N}\left(S^{\mu}q\cdot K - S\cdot q K^{\mu}\right) + \frac{1}{2m_N^2}S\cdot K\left(K\cdot q v^{\mu} - K^{\mu}v\cdot q\right)\Big], \end{aligned} \tag{5.1.2}$$

where $F_0(Q^2)$ and $F_1(Q^2)$ are the isoscalar and isovector EDFF of the nucleon. We will write

$$F_i(Q^2) = D_i - S_i'\,Q^2 + H_i(Q^2), \tag{5.1.3}$$

where D_i is the EDM, S_i' the Schiff moment

$$S_i' = -\frac{dF_i(Q^2)}{dQ^2}, \tag{5.1.4}$$

and $H_i(Q^2)$ accounts for the remaining Q^2 dependence of the form factor. The form factor itself can be expanded in powers of Q/M_{QCD}. In Sec. 5.2 we compute the nucleon EDFF generated by the $\bar{\theta}$ term and the qCEDM, at next-to-leading order (NLO) in Q/M_{QCD}. In Sec. 5.3 we turn our attention to the other dimension 6 sources. In this case, the momentum dependence of the EDFF only arises at next-to-next LO (N^{2}LO), and we work at this accuracy. Finally, in Sec. 5.4 we discuss how the nucleon EDFF partially reflects the source of T violation at the quark level.

5.2 The Nucleon EDFF. QCD $\bar{\theta}$ and qCEDM

The leading-order contribution to the EDM from the QCD $\bar{\theta}$ term has been known for a long time [93]. It includes loop diagrams made out of the leading TV pion-nucleon

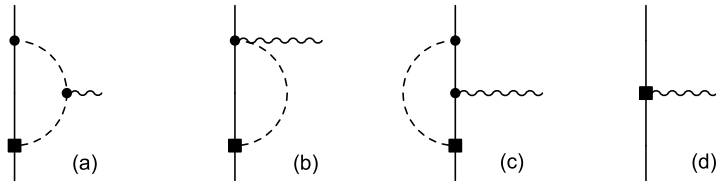

FIGURE 5.1. Tree level and one-loop diagrams contributing to the nucleon electric dipole form factor from the $\bar{\theta}$ and qCEDM in leading order. Solid, dashed and wavy lines represent nucleons, pions and (virtual) photons, respectively; single filled circles stand for interactions from $\mathcal{L}^{(0)}_{\chi,\, f\leq 2}$ in Eq. (3.3.17), squares represent the TV vertices from the leading TV pion-nucleon and nucleon-photon Lagrangian, $\mathcal{L}^{(1)}_{\chi,\, f=2}$ (4.1.19) and $\mathcal{L}^{(3)}_{\chi,\, f=2,\mathrm{em}}$ (4.2.4), and $\mathcal{L}^{(-1)}_{6,\, f=2}$ (4.1.29) and $\mathcal{L}^{(1)}_{\mathrm{qCEDM},f=2,\mathrm{em}}$ (4.2.7). For simplicity only one possible ordering is shown here.

interaction $\bar{g}_0$ in $\mathcal{L}^{(1)}_{\chi,f=2}$ in Eq. (4.1.19) and the unknown short-range contributions in $\mathcal{L}^{(3)}_{\chi,\, f=2,\mathrm{em}}$ in Eq. (4.2.4). We depict these contributions in Fig. 5.1. Both the one-loop diagram and the short-range operators contribute to the TV electromagnetic current at the order $\mathcal{O}\left(em_\pi^2 Q/M_{QCD}^3\right)$, where M_{QCD} is the typical hadronic scale, $M_{QCD} = 2\pi F_\pi$. More recently, the calculation has been extended to the nucleon SM [162], and to the full momentum dependence of the EDFF [91]

In this Section, we extend the analysis to the nucleon EDM and EDFF generated by the qCEDM, and, for both sources, we carry out the calculation of the EDFF to NLO in the χPT power counting.

We remarked in Chapter 4 that the relative importance of long- and short-distance physics is similar for TV from qCEDM and the $\bar{\theta}$ term, and that the main difference between the two sources is that, in leading order, the QCD $\bar{\theta}$ term only contributes to the isoscalar non-derivative pion-nucleon coupling $\bar{g}_0$, while the qCEDM induces contributions to $\bar{g}_0$ and $\bar{g}_1$ at the same level. Consequently, we find that also in the case of the qCEDM the leading contributions to the EDFF come from pion loops, with the leading TV couplings given in Eq. (4.1.29), and from the short-distance EDM operators that appear in the $\Delta_6 = 1$ Lagrangian, in Eq. (4.2.11). In this case,

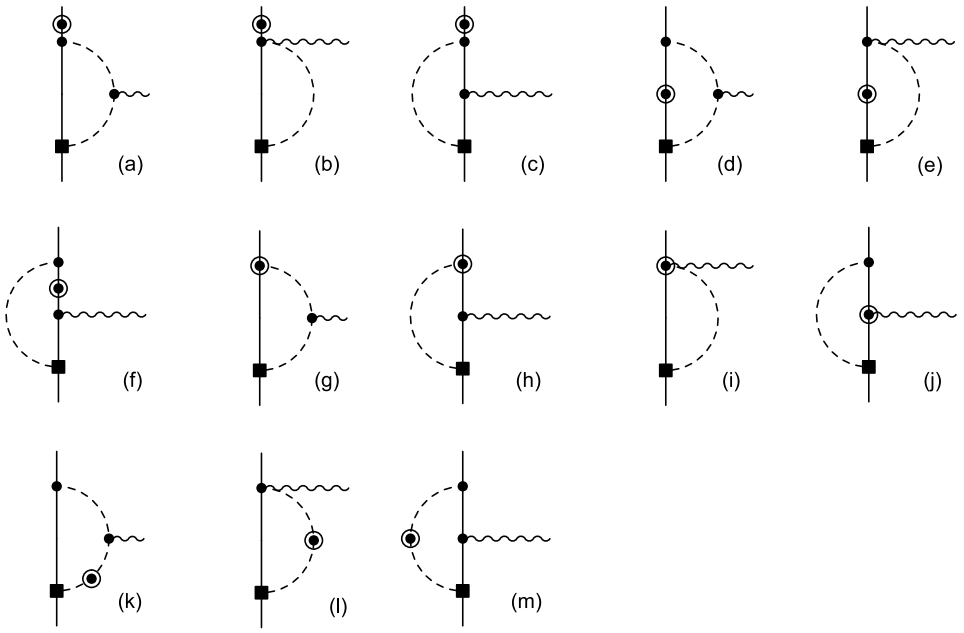

FIGURE 5.2. One-loop diagrams contributing to the nucleon electric dipole form factor in sub-leading order coming from one insertion of an $\mathcal{L}^{(1)}_{f=2}$ operator. Solid, dashed and wavy lines represent nucleons, pions and (virtual) photons, respectively; single filled circles stand for interactions from $\mathcal{L}^{(0)}_{\chi,f=2}$ while double circles for TC chiral invariant and chiral breaking interactions from $\mathcal{L}^{(1)}_{\chi,f=2}$ (3.3.18), and $\mathcal{L}^{(1)}_{\not\chi,f=2}$, given in Eqs. (4.1.2) and (4.1.19). Squares represent the TV vertices from $\mathcal{L}^{(1)}_{\not\chi,\,f=2}$ (4.1.19) and $\mathcal{L}^{(-1)}_{6,\,f=2}$ (4.1.29) for the $\bar{\theta}$ and qCEDM, respectively. For simplicity only one possible ordering is shown here.

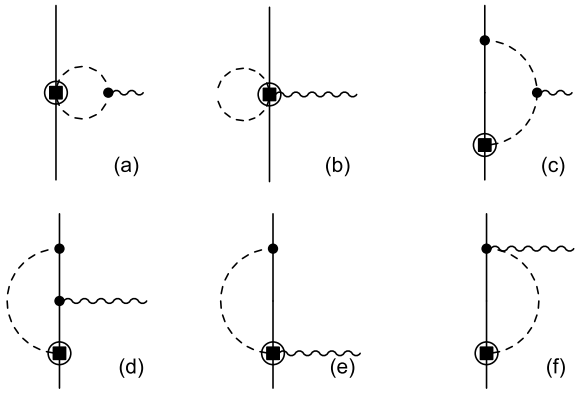

FIGURE 5.3. Diagrams contributing to the nucleon electric dipole form factor in subleading order coming from one insertion of the subleading TV vertices, represented by the circled square. The form of the interaction is given in $\mathcal{L}^{(2)}_{\chi,\,f=2}$ (4.1.21) and $\mathcal{L}^{(0)}_{6,\,f=2}$ (Eq. (4.1.29)) for the $\bar{\theta}$ and qCEDM, respectively. Other symbols are as in Fig. 5.2. For simplicity only one possible ordering is shown here.

the contribution to the current is of the order $\mathcal{O}\left(em_\pi^2 Q/M_T^2 M_{QCD}\right)$.

The explicit calculation of the diagrams in Fig. 5.1 shows that the only one loop diagram that does not vanish in leading order is diagram 5.1(a). Since only charged pions contribute to the diagram, it turns out that the nucleon EDM in leading order is sensitive only to $\bar{g}_0$, while $\bar{g}_1$, which couples the nucleon the a neutral pion, does not play any role in LO. As a consequence, the nucleon EDM and EDFF induced by the QCD $\bar{\theta}$ term and by the qCEDM have identical form, at least in leading order.

At NLO, there are no new, unknown short-range parameters appearing at tree level, the recoil corrections in $\mathcal{L}^{(4)}_{\chi,\,f=2,\,\mathrm{em}}$ and $\mathcal{L}^{(2)}_{6,\,f=2,\,\mathrm{em}}$ (which we included in Eqs. (4.2.4) and (4.2.11)) simply ensuring —together with the relativistic corrections in $\mathcal{L}^{(1)}_{\chi,\,f=2}$ (3.3.18) — the form (5.1.1) of the current.

The loop diagrams contributing to the nucleon EDFF in NLO are shown in Figs. 5.2 and 5.3, classified according to the combination of couplings that they contain. All other contributions to the EDFF are formally of higher order: they come from more powers of momenta in diagrams with the same number of loops, or from extra

loops.

The NLO diagrams of Fig. 5.2 are built from the leading TV interaction, in Eq. (4.1.19) for $\bar{\theta}$ and Eq. (4.1.29) for the qCEDM, the leading TC interactions in Eq. (3.3.17), plus one insertion of an operator from the subleading TC Lagrangian, Eq. (3.3.18). Diagrams 5.2(a,b,c) represent a correction to the external energies,

$$v \cdot q = -\frac{q \cdot K}{m_N}, \tag{5.2.1}$$

$$v \cdot K = -\frac{1}{2m_N}\left(K^2 + \frac{q^2}{4}\right) \mp \frac{\delta m_N}{2}, \tag{5.2.2}$$

of a proton ($-$ sign) or neutron ($+$ sign) in LO diagrams. (In the remaining NLO diagrams, we set the right-hand side of these equations to zero.) Analogous insertions in the nucleon propagator are represented by diagrams 5.2(d,e,f). Diagrams 5.2(g,h,i) originate in the recoil correction in pion emission/absorption, while diagram 5.2(j) arises from the magnetic photon-nucleon interaction. Diagrams 5.2(k,l,m) represent an insertion of the pion mass splitting in pion propagation. These one-loop diagrams contribute to the current at order $\mathcal{O}(e\bar{g}_i Q^2/(2\pi F_\pi)^2 m_N)$.

The NLO diagrams in Fig. 5.3 are built from the leading interactions in Eq. (3.3.17) with one insertion of an operator from the TV subleading Lagrangian, Eqs. (4.1.21) and (4.1.32) for $\bar{\theta}$ and qCEDM. The $\bar{\theta}$ term only contribute to diagrams 5.3(a,b), which, in the case of $\bar{\theta}$ are only proportional to the coupling $\bar{h}_0$. The qCEDM contributes to all the diagrams in Fig. 5.3, diagrams 5.3(a,b) stem from the sub-leading pion-nucleon couplings $\bar{h}_0 = \tilde{\beta}_{q\,1}\tilde{\rho}_0$ and $\bar{h}_1 = \tilde{\beta}_{q\,2}\tilde{\rho}_3$, and diagrams 2(c,d,e,f) from the sub-leading coupling $\bar{h}_2 = \tilde{\beta}_{q\,2}\tilde{\rho}_3$. These one-loop diagrams contribute to the current at order $\mathcal{O}(e\bar{h}_i Q^2/(2\pi F_\pi)^2)$, which is precisely the same order as the diagrams in Fig. 5.2.

The diagrams in Figs. 5.1, 5.2 and 5.3 can be evaluated in a straightforward way. We use regularization in d spacetime dimensions, and define

$$L \equiv \frac{2}{4-d} - \gamma_E + \ln 4\pi, \tag{5.2.3}$$

where $\gamma_E = 0.557\ldots$ is the Euler constant. The LO loop contributions depend on a renormalization scale μ but this dependence is compensated for by the contribution from the short-range interactions in Eq. (4.2.4) and (4.2.11). The NLO diagrams are finite in this regularization scheme.

Most of the diagrams actually vanish when the on-shell conditions (5.2.1) and (5.2.2) are consistently enforced. Diagrams (a,b) in Fig. 5.3 vanish due to isospin. Since diagrams 5.3(c,d,e,f) vanish too, the EDFF to this order depends only on the leading TV parameters $\bar{g}_{0,1}$ through Fig. 5.2. Diagram 5.2(j) vanishes due to its spin structure and therefore the EDFF does not depend on the anomalous magnetic moments, either. Diagram 5.2(h) gives both isoscalar and isovector contributions. The remaining non-vanishing diagrams are 5.2(a,d,k). Neglecting TC isospin violation, these diagrams give purely isovector results. In the case of $\bar{\theta}$, the results are proportional to $eg_A\bar{g}_0/(2\pi F_\pi)^2$, as in LO [91], times the recoil suppression factor m_π/m_N. For qCEDM, there is an additional momentum-independent contribution proportional to $\bar{g}_1$.

We have checked each of the isospin-breaking contributions in two ways. The contributions from $\breve{\delta}m_\pi^2$ come through diagrams 5.2(k,l,m). Because the LO EDFF originates entirely in charged-pion diagrams, these contributions can be obtained alternatively by evaluating the LO EDFF with $m_\pi^2 + \breve{\delta}m_\pi^2$, then expanding in powers of $\breve{\delta}m_\pi^2/m_\pi^2$:

$$F_1(Q^2)|_{m_\pi^2+\breve{\delta}m_\pi^2} = F_1(Q^2)|_{m_\pi^2} + \breve{\delta}m_\pi^2 \left.\frac{\partial F_1(Q^2)}{\partial m_\pi^2}\right|_{m_\pi^2} + \ldots \tag{5.2.4}$$

The resulting EDFF is thus isovector. Including the nucleon mass difference δm_N, diagrams 5.2(a,d) generate an additional isoscalar contribution. As a check, we have performed the field redefinition of Ref. [138], which amounts here to adding to the isospin breaking Lagrangian Eq. (4.1.19)

$$\Delta\mathcal{L}^{(1)} \;=\; -\frac{\delta m_N}{2}\bar{N}\tau_3 N - \delta m_N\,(\boldsymbol{\pi}\times v\cdot D\boldsymbol{\pi})_3\,. \tag{5.2.5}$$

The first term eliminates δm_N from the internal nucleon lines and from the asymptotic

states (and thus from Eq. (5.2.2)), but the second term generates extra contributions $\propto \delta m_N$ in diagrams 5.2(k,l,m) and a new isospin-breaking photon-pion coupling, which appears in a diagram with the same topology as diagram 5.2(d). The same final result is obtained.

The diagrams in Fig. 5.2 contribute to both isoscalar and isovector EDMs. Taking the NLO contributions, together with the LO from Ref. [91], we have

$$D_0 = \bar{D}_0 + \frac{e g_A \bar{g}_0}{(2\pi F_\pi)^2}\,\pi\left[\frac{3m_\pi}{4m_N}\left(1+\frac{\bar{g}_1}{3\bar{g}_0}\right)-\frac{\delta m_N}{m_\pi}\right], \tag{5.2.6}$$

$$D_1 = \bar{D}_1 + \bar{D}_1' + \frac{e g_A \bar{g}_0}{(2\pi F_\pi)^2}\left[L - \ln\frac{m_\pi^2}{\mu^2} + \frac{5\pi}{4}\frac{m_\pi}{m_N}\left(1+\frac{\bar{g}_1}{5\bar{g}_0}\right) - \frac{\breve{\delta} m_\pi^2}{m_\pi^2}\right]. \tag{5.2.7}$$

The meaning of the low-energy-constants in Eq. (5.2.7) is as follows. In the case of the $\bar{\theta}$ term, $\bar{g}_0 = \bar{g}_{0\,\bar{\theta}}$, defined in Eqs. (4.1.19) and (4.4.2). The coupling $\bar{g}_1$ is suppressed, and it can be neglected at NLO accuracy. The isoscalar and isovector short-distance EDM operators are defined in Eq. (4.2.4) and we have $\bar{D}_0 = D_0^{(3)}\rho$, $\bar{D}_1 = D_1^{(3)}\rho$ and $\bar{D}_1' = D_1'^{(3)}\rho$, with scaling given by Eq. (4.2.5). For the qCEDM, $\bar{g}_0 = \bar{g}_{0\,q}$ and $\bar{g}_1 = \bar{g}_{1\,q}$. The two couplings have roughly the same size, given in Eq. (4.3.19) and (4.3.21). The short-distance contributions to the isoscalar EDM are given in Eq. (4.2.11). The TC couplings in Eqs. (5.2.6) and (5.2.7) are all defined in Sec. 3.3.1

The LO piece in Eq. (5.2.7), which depends on $\bar{g}_0$ and is non-analytic in m_π^2, is, with the use of the Goldberger-Treiman relation, the result of Ref. [93], which holds also for the qCEDM. The short-range isovector combination $\bar{D}_1 + \bar{D}_1'$ absorbs the divergence and μ dependence of the LO loop. The short- and long-range contributions to the EDM are in general of the same size, but a cancellation is unlikely due to the non-analytic dependence on m_π of the pion contribution. The isoscalar parameter $\bar{D}_0$ is not needed for renormalization at this order, but there is no apparent reason to assume its size to be much smaller than NDA either.

At NLO, the EDM receives finite non-analytic corrections, which depend also on $\bar{g}_1$ for qCEDM. From Eqs. (5.2.6) and (5.2.7) we see that, as usual in baryon χPT, the

NLO contributions are enhanced by π over NDA. However, the other dimensionless factors are not large enough to overcome the m_π/m_N suppression. Setting μ to m_N as a representative value for the size of D_1 [93], the NLO term in Eq. (5.2.7) (Eq. (5.2.6)) is about 15% (10%) of the leading non-analytic term in Eq. (5.2.7), indicating good convergence of the chiral expansion. The isovector character of the LO non-analytic terms is approximately preserved at NLO. Isospin-breaking contributions, although formally NLO, are pretty small, amounting to 15-20% of the total NLO contribution.

In the case of $\bar{\theta}$ we can use Eq. (4.1.5) and expect

$$\begin{aligned} |d_n| = |D_0 - D_1| &\gtrsim \frac{eg_A}{(2\pi F_\pi)^2}\frac{\delta m_N}{2\varepsilon}\left[\ln\frac{m_N^2}{m_\pi^2} + \frac{\pi}{2}\frac{m_\pi}{m_N} - \frac{\breve{\delta} m_\pi^2}{m_\pi^2} + \pi\frac{\delta m_N}{m_\pi}\right]\bar{\theta} \\ &\simeq (1.99 + 0.12 - 0.04 + 0.03)\cdot 10^{-3}\ \bar{\theta}\, e\,\mathrm{fm} \end{aligned} \tag{5.2.8}$$

for the neutron EDM and

$$\begin{aligned} |d_p| = |D_0 + D_1| &\gtrsim \frac{eg_A}{(2\pi F_\pi)^2}\frac{\delta m_N}{2\varepsilon}\left[\ln\frac{m_N^2}{m_\pi^2} + 2\pi\frac{m_\pi}{m_N} - \frac{\breve{\delta} m_\pi^2}{m_\pi^2} - \pi\frac{\delta m_N}{m_\pi}\right]\bar{\theta} \\ &\simeq (1.99 + 0.46 - 0.04 - 0.03)\cdot 10^{-3}\ \bar{\theta}\, e\,\mathrm{fm} \end{aligned} \tag{5.2.9}$$

for the proton EDM, using the lattice QCD value $\delta m_N/2\varepsilon = 2.8$ MeV [133]. Non-analytic NLO corrections are therefore somewhat larger for the proton EDM, but this difference is unlikely to be significant in light of our ignorance about the size of short-range contributions.

The non-analytic terms in Eq. (5.2.6) represent a lower-bound estimate for the size of the nucleon isoscalar EDM, as the short-range contribution $\bar{D}_0$ is nominally of lower order. The expected lower bound on the nucleon isoscalar EDM might have implications for proposed experiments on EDMs of light nuclei. In these cases, there will be additional many-nucleon contributions, which could be dominant, but the average of the one-nucleon contributions still provides a lower bound for the expected nuclear EDM. For the deuteron, the average one-nucleon contribution is exactly $2D_0$ and, in the case of $\bar{\theta}$, we expect for the deuteron EDM

$$|d_d| \gtrsim 2\frac{eg_A}{(2\pi F_\pi)^2}\frac{\delta m_N}{2\varepsilon}\,\pi\left[\frac{3m_\pi}{4m_N} - \frac{\delta m_N}{m_\pi}\right]\bar{\theta} \simeq (3.4 - 0.6)\cdot 10^{-4}\,\bar{\theta}\, e\,\mathrm{fm}. \tag{5.2.10}$$

Therefore, if there are no cancellations, a deuteron EDM signal from $\bar{\theta}$ is expected to be larger than about 15% of the neutron EDM signal.

Note that short- and long-range physics cannot be separated with a measurement of the neutron and proton EDMs alone. On the other hand, the momentum dependence of the EDFF is completely determined, to the order we are working, by long-range contributions generated by $\bar{g}_0$. It is therefore the same for $\bar{\theta}$ and qCEDM. It turns out that the isoscalar form factor receives momentum dependence only from isospin-breaking terms, while there is a non-vanishing correction to the isovector momentum dependence also from isospin-conserving terms.

The variation of the form factor with Q^2 can be characterized at very small momenta by the electromagnetic contribution to the nucleon SM, the leading and subleading contributions of which we find to be

$$S_0' = -\frac{e g_A \bar{g}_0}{6(2\pi F_\pi)^2 m_\pi^2} \frac{\pi}{2} \frac{\delta m_N}{m_\pi}, \tag{5.2.11}$$

$$S_1' = \frac{e g_A \bar{g}_0}{6(2\pi F_\pi)^2 m_\pi^2} \left[1 - \frac{5\pi}{4} \frac{m_\pi}{m_N} - \frac{\breve{\delta} m_\pi^2}{m_\pi^2} \right]. \tag{5.2.12}$$

The LO, isovector term is the result of Refs. [162, 91]. The NLO correction, which agrees with the $\bar{\theta}$ result of Ref. [99] when TC isospin violation is neglected, vanishes in the chiral limit but gives a relatively large correction to the isovector SM of about 60%, due to the numerical factor $5\pi/4$. Again, the isospin-breaking corrections are relatively small, and, as a consequence, at NLO the SM remains mostly isovector.

To this order, the SM is entirely given, apart for $\bar{g}_0$, by quantities that can be determined from other processes. In the case of $\bar{\theta}$, we can again use Eq. (4.1.5) to estimate

$$S_0' = -\frac{e g_A}{12(2\pi F_\pi)^2} \frac{\pi (\delta m_N)^2}{2\varepsilon m_\pi^3} \bar{\theta} \simeq -5.0 \cdot 10^{-6}\, \bar{\theta}\, e\,\mathrm{fm}^3, \tag{5.2.13}$$

$$S_1' = \frac{e g_A}{12(2\pi F_\pi)^2} \frac{\delta m_N}{\varepsilon m_\pi^2} \left[1 - \frac{5\pi}{4} \frac{m_\pi}{m_N} - \frac{\breve{\delta} m_\pi^2}{m_\pi^2} \right] \bar{\theta} \simeq 6.8 \cdot 10^{-5}\, \bar{\theta}\, e\,\mathrm{fm}^3, \tag{5.2.14}$$

where again we used the lattice-QCD value [133] for $\delta m_N/2\varepsilon$. From these results we can straightforwardly obtain the SM for the proton and the neutron. Although we could again use the isoscalar component as an estimate for a lower bound on the deuteron SM, there could be potentially significant contributions from the deuteron binding momentum.

The full momentum dependence of the EDFF is given in addition by the functions $H_i(Q^2)$ introduced in Eq. (5.1.3),

$$H_0(Q^2) = -\frac{4eg_A\bar{g}_0}{15(2\pi F_\pi)^2}\,\frac{3\pi}{4}\frac{\delta m_N}{m_\pi}\,h_0^{(1)}\left(\frac{Q^2}{4m_\pi^2}\right), \tag{5.2.15}$$

$$H_1(Q^2) = \frac{4eg_A\bar{g}_0}{15(2\pi F_\pi)^2}\left[h_1^{(0)}\left(\frac{Q^2}{4m_\pi^2}\right) - \frac{7\pi}{8}\frac{m_\pi}{m_N}\,h_1^{(1)}\left(\frac{Q^2}{4m_\pi^2}\right) - \frac{2\breve{\delta}m_\pi^2}{m_\pi^2}\,\breve{h}_1^{(1)}\left(\frac{Q^2}{4m_\pi^2}\right)\right]. \tag{5.2.16}$$

Here, the LO term,

$$h_1^{(0)}(x) = -\frac{15}{4}\left[\sqrt{1+\frac{1}{x}}\,\ln\left(\frac{\sqrt{1+1/x}+1}{\sqrt{1+1/x}-1}\right) - 2\left(1+\frac{x}{3}\right)\right], \tag{5.2.17}$$

is the one calculated in Refs. [91], while we now obtain the NLO isovector functions

$$h_1^{(1)}(x) = -\frac{1}{7}\left[3(1+2x)\,h_0^{(1)}(x) - 10x^2\right], \tag{5.2.18}$$

and

$$\breve{h}_1^{(1)}(x) = -\frac{1}{4(1+x)}\left(h_1^{(0)}(x) - 5x^2\right), \tag{5.2.19}$$

and the NLO isoscalar function

$$h_0^{(1)}(x) = 5\left(\frac{1}{\sqrt{x}}\arctan\sqrt{x} - 1 + \frac{x}{3}\right). \tag{5.2.20}$$

In compliance with the definition of H_i, the four functions behave as $h_i^{(n)}(x) = x^2 + \mathcal{O}(x^3)$ for $x \ll 1$.

As in lowest order, the momentum dependence is fixed by the pion cloud. Thus the scale for momentum variation is determined by $2m_\pi$. Both the SM and the functions $H_{0,1}(Q^2)$ are testable predictions of χPT. In Fig. 5.4 we plot the LO $h_1^{(0)}$,

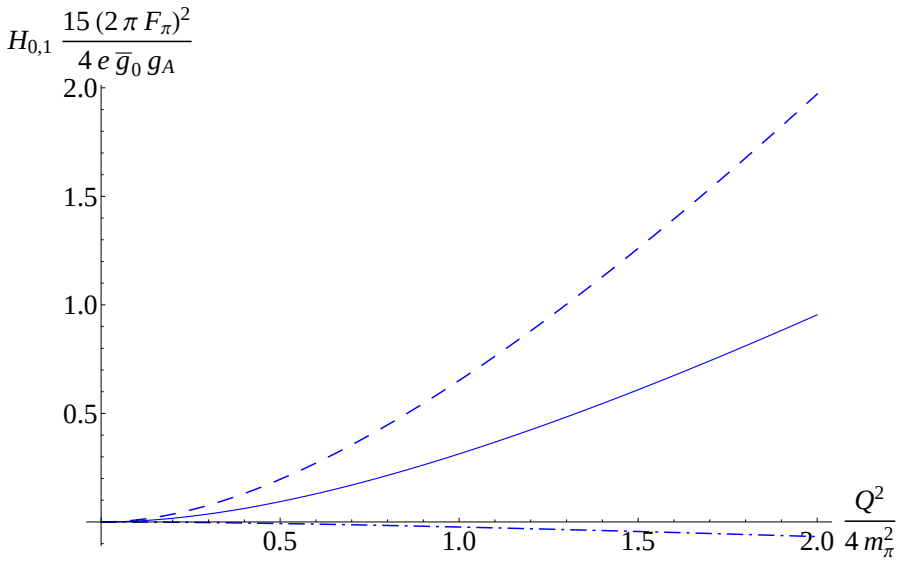

FIGURE 5.4. The isovector $H_1(Q^2)$ in LO (dashed line) and LO+NLO (solid line), and the isoscalar $H_0(Q^2)$ in LO+NLO (dash-dotted line), both in units of $4eg_A\bar{g}_0/15\,(2\pi F_\pi)^2$, as functions of Q^2 , in units of $4m_\pi^2$.

the LO+NLO combination $h_1^{(0)} - (7\pi m_\pi/8m_N)h_1^{(1)} - (2\breve{\delta}m_\pi^2/m_\pi^2)\breve{h}_1^{(1)}$, and the NLO $-(3\pi\delta m_N/4m_\pi)h_0^{(1)}$ as functions of Q^2. We use the same values of parameters as before. As for the SM, NLO corrections can be significant, but the isospin-breaking contributions are small.

5.3 The Nucleon EDFF. Dimension 6 sources

We discuss here the remaining dimension 6 sources of T violation, the qEDM, the gCEDM and the chiral-invariant, TV four-quark operators.

The tree level and one loop diagram contributing to the nucleon EDFF for T violation generated by a qEDM are shown in Fig. 5.5. At leading order, one finds only short-distance contributions, who have chiral index $\Delta = 1$ and are listed in Eq. (4.2.15). At this order, the EDFF is momentum-independent, and it coincides with the EDM. At N^{2}LO, there are other short-range contributions, from the $\Delta = 3$ Lagrangian, Eq. (4.2.17). To this order there are no contributions from pion-nucleon TV interactions, while the loop diagrams in Fig. 5.5, with TV interactions from Eq.

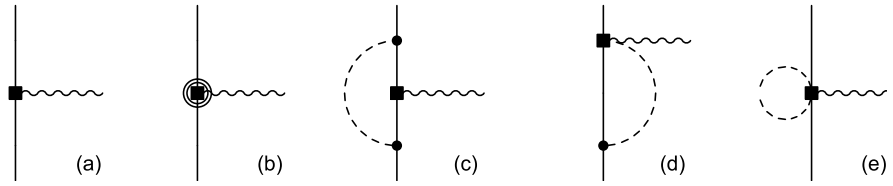

FIGURE 5.5. Diagrams contributing to the nucleon EDFF at N^{2}LO, for T violation from the qEDM. Squares represent the short-distance contributions to the nucleon EDM in $\mathcal{L}^{(1)}_{\text{qEDM},\,f=2,\,\text{em}}$ (4.2.15). Doubly circled squares represent short-distance operators in $\mathcal{L}^{(3)}_{\text{qEDM},\,f=2,\,\text{em}}$ (4.2.17) Other symbols are as in Fig. 5.1. For simplicity only one possible ordering is shown here.

(4.2.15), only renormalize the tree-level contributions without any energy dependence. To $\mathcal{O}(e\delta m_\pi^4/M_T^2 M_{\text{QCD}}^3)$, we find the EDMs

$$D_{0,\,\text{qEDM}} = \bar{D}^{(1)}_{q\,0} + \bar{D}^{(3)}_0 + \frac{3}{4}\bar{D}^{(1)}_{q\,0}\frac{m_\pi^2}{(2\pi F_\pi)^2}\left[(2+4g_A^2)\left(L - \ln\frac{m_\pi^2}{\mu^2}\right) + 2 + g_A^2\right], \tag{5.3.1}$$

$$D_{1,\,\text{qEDM}} = \bar{D}^{(1)}_{q\,1} + \bar{D}^{(3)}_{q\,1} + \frac{1}{4}\bar{D}^{(1)}_{q\,1}\frac{m_\pi^2}{(2\pi F_\pi)^2}\left[(2+8g_A^2)\left(L - \ln\frac{m_\pi^2}{\mu^2}\right) + 2 + 3g_A^2\right], \tag{5.3.2}$$

and the momentum dependence given entirely by the SMs,

$$S'_{i,\text{qEDM}} = \bar{S}'^{(3)}_i, \tag{5.3.3}$$

$$H_{i,\text{qEDM}}(Q^2) = 0. \tag{5.3.4}$$

In the case of the gCEDM, the relevant diagrams at N^{2}LO are shown in Fig. 5.6. Short-range contributions to the EDFF start at $\Delta = -1$, which dominate, and appear again at $\Delta = 1$, suppressed by m_π^2/M_{QCD}^2. At this order there are also contributions from the TV pion-nucleon interactions in Eq. (4.1.29) through diagrams 5.6(e)-(h), and from the photon-nucleon interactions in Eq. (4.2.7) through diagrams 5.6(c)-(d).

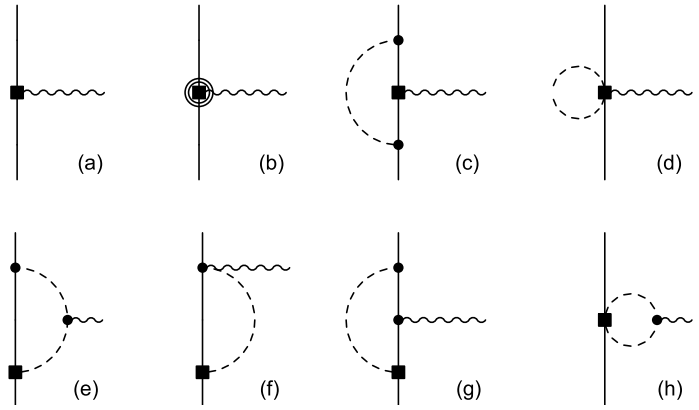

FIGURE 5.6. Diagrams contributing to the nucleon EDFF at N^{2}LO, for T violation from the chiral invariant, dimension 6 operators. Squares represent the short-distance contributions to the nucleon EDM in $\mathcal{L}^{(-1)}_{6,\,f=2,\,\mathrm{em}}$ (4.2.7) and TV pion-nucleon interactions from $\mathcal{L}^{(-1)}_{6,\,f=2}$ (4.1.29). Doubly circled squares represents short-distance operators in $\mathcal{L}^{(1)}_{w,\,f=2,\,\mathrm{em}}$ (4.2.9) Other symbols are as in Fig. 5.1. For simplicity only one possible ordering is shown here.

Thus, to $\mathcal{O}(ewm_\pi^2/M_I^2 M_{\mathrm{QCD}})$ we find the μ-independent EDMs

$$D_{0,\,w} = \bar{D}^{(-1)}_{w\,0} + \bar{D}^{(1)}_{w\,0} + 3g_A^2 \bar{D}^{(-1)}_{w\,0} \frac{m_\pi^2}{(2\pi F_\pi)^2}\left(L - \ln\frac{m_\pi^2}{\mu^2}\right)\,, \tag{5.3.5}$$

$$\begin{aligned} D_{1,\,w} &= \bar{D}^{(-1)}_{w\,1} + \bar{D}^{(1)}_{w\,1} + \bar{D}^{(1)\prime}_{w\,1} + \frac{m_\pi^2}{(2\pi F_\pi)^2}\left\{\left(1+g_A^2\right)\bar{D}^{(-1)}_{w\,1} + \frac{e\bar{\imath}_{0\,w}}{8}\right. \\ &\quad \left. + \left[\left(1+2g_A^2\right)\bar{D}^{(-1)}_{w\,1} + e\left(\frac{\bar{g}_{0\,w}g_A}{m_\pi^2} + \frac{\bar{\imath}_{0\,w}}{8}\right)\right]\left(L - \ln\frac{m_\pi^2}{\mu^2}\right)\right\}. \end{aligned} \tag{5.3.6}$$

The isoscalar momentum dependence is entirely due to short-range operators in Eq. (4.2.9),

$$S'_{0,\,w} = \bar{S}'^{(1)}_0. \tag{5.3.7}$$

$$H_{0,\,w}(Q^2) = 0. \tag{5.3.8}$$

The isovector part, on the other hand, receives also non-analytic contributions:

$$S'_{1,\,w} = \bar{S}_1'^{(1)} + \frac{e}{6(2\pi F_\pi)^2}\left[-\frac{\bar{\imath}_0}{8}\left(L - \ln\frac{m_\pi^2}{\mu^2}\right) + \frac{g_A\bar{g}_0}{m_\pi^2}\right], \tag{5.3.9}$$

$$\begin{aligned} H_{1,\,w}(Q^2) = {} & \frac{4em_\pi^2}{15(2\pi F_\pi)^2}\left\{\left(\frac{g_A\bar{g}_0}{m_\pi^2} + \frac{\bar{\imath}_0}{12}\right) h_1^{(0)}\left(\frac{Q^2}{4m_\pi^2}\right)\right. \\ & \left. + \frac{\bar{\imath}_0}{12}\frac{Q^2}{4m_\pi^2}\left[-\frac{5}{2}\frac{Q^2}{4m_\pi^2} + h_1^{(0)}\left(\frac{Q^2}{4m_\pi^2}\right)\right]\right\}, \end{aligned} \tag{5.3.10}$$

where the function $h_1^{(0)}(x)$ is defined in Eq. (5.2.17)

5.4 Discussion

First, we note that at NLO the nucleon EDFF stemming from the qCEDM has a form that is identical to that from the $\bar{\theta}$ term [91, 99]. In both cases the momentum dependence, and thus the SM, is predominantly isovector, has a scale (relative to the EDM) set by $2m_\pi$, and is determined by the lowest-order pion-nucleon coupling $\bar{g}_0$. The momentum dependence of the isoscalar EDFF is entirely due to the nucleon mass splitting, and the isoscalar SM is about the 10 % of the isovector. The EDFF depends on just three independent combinations of LECs, $\bar{g}_0$ and the short-range EDM contributions $\bar{D}_0^{(1)}$ and $\bar{D}_1^{(1)} + \bar{D}_1^{(1)'}$, which contain nucleon matrix elements of $\tilde{V}_4$ and $\tilde{W}_3$ for qCEDM and P_4 for the $\bar{\theta}$ term. The numerical factors relating these couplings to either $\tilde{\delta}_{0,3}$ or $\bar{\theta}$ will thus be different. In the case of $\bar{\theta}$, the matrix element in $\bar{g}_0$ can be determined from TC observables, because it is related to the matrix element of P_3 that generates the quark-mass contribution to the nucleon mass splitting: $\bar{g}_0/\bar{\theta} \simeq 3$ MeV. For the qCEDM, an argument identical to that in Ref. [93] serves to estimate D_1 in terms of $\bar{g}_0$, but no analogous constraint exists for $\bar{g}_0$ in this case and without a lattice calculation or a model we cannot do better than dimensional analysis. (For an estimate with QCD sum rules, see Ref. [176].) In any case, to the order we consider here, any EDFF measurement alone will be equally well reproduced by a certain value of $\bar{\theta}$ or a certain value of $\tilde{\delta}_{0,3}$. Note that the qCEDM

does give rise to an additional pion-nucleon coupling at LO, $\bar{g}_1$. $\bar{g}_1$ contributes additional momentum-independent pieces to the isovector and isoscalar nucleon EDFF at NLO, which, however, are unlikely to be phenomenologically relevant, since they cannot be distinguished from the LEC $\bar{D}_0$ and $\bar{D}_1 + \bar{D}_1'$. On the contrary, we will see that this coupling plays an extremely important role for other nuclear observables, for example the deuteron EDM. The NLO calculation shows good convergence of the chiral expansion, although NLO corrections are enhanced by extra factors of π. Under the assumption that higher-order results are not afflicted by anomalously-large dimensionless factors, the relative error of our results at momentum Q should be $\sim (Q/M_{QCD})^2$. The NLO isospin breaking contributions are relatively small, and could be overcome by isospin conserving contributions at N^{2}LO.

Second, the pion-nucleon sector of the qEDM is suppressed compared to that of the qCEDM because of the smallness of $\alpha_{\rm em}$ compared to $g_s^2/4\pi$ at low energies. The consequence is that, up to the lowest order where momentum dependence appears, both the EDM and the SM from the qEDM are determined by four combinations of six independent LECs, which at this point can only be estimated by dimensional analysis. The momentum dependence is expected to be governed by the QCD scale $M_{\rm QCD}$, small relative to the EDM, and nearly linear in Q^2.

Finally, in the case of the chiral-invariant gCEDM and TV four-quark operators pion loops are also suppressed, but do bring in non-analytic terms not only to isoscalar and isovector EDMs, but also to the isovector momentum dependence (and thus SM). Again the momentum dependence is governed by $M_{\rm QCD}$. In addition to seven short-range contributions to the EDMs and SMs, also two independent pion-nucleon LECs appear ($\bar{g}_{0\,w}$ and $\bar{\imath}_{0\,w}$) which endow the isovector EDFF with a richer momentum dependence than in other cases. The isoscalar momentum dependence is identical to qEDM. For the gCEDM, using the pion loop together with an estimate of $\bar{g}_0$ [177] is likely to be an underestimate of the EDM, because chiral symmetry allows a short-range contribution that is larger by a factor M_{QCD}^2/m_π^2.

Source	θ	qCEDM	qEDM	gCEDM 4-quark
$M_{\rm QCD}\, d_n/e$	$\mathcal{O}\left(\bar{\theta}\frac{m_\pi^2}{M_{\rm QCD}^2}\right)$	$\mathcal{O}\left(\tilde{\delta}\frac{m_\pi^2}{M_{\not T}^2}\right)$	$\mathcal{O}\left(\delta\frac{m_\pi^2}{M_{\not T}^2}\right)$	$\mathcal{O}\left(w\frac{M_{\rm QCD}^2}{M_{\not T}^2}\right)$
d_p/d_n	$\mathcal{O}(1)$	$\mathcal{O}(1)$	$\mathcal{O}(1)$	$\mathcal{O}(1)$
$m_\pi^2 S_p'/d_n$	$\mathcal{O}(1)$	$\mathcal{O}(1)$	$\mathcal{O}\left(\frac{m_\pi^2}{M_{\rm QCD}^2}\right)$	$\mathcal{O}\left(\frac{m_\pi^2}{M_{\rm QCD}^2}\right)$
$m_\pi^2 S_0'/d_n$	$\mathcal{O}\left(\frac{m_\pi}{M_{\rm QCD}}\right)$	$\mathcal{O}\left(\frac{m_\pi}{M_{\rm QCD}}\right)$	$\mathcal{O}\left(\frac{m_\pi^2}{M_{\rm QCD}^2}\right)$	$\mathcal{O}\left(\frac{m_\pi^2}{M_{\rm QCD}^2}\right)$

TABLE 5.1. Expected orders of magnitude for the neutron EDM (in units of $e/M_{\rm QCD}$), the ratio of proton-to-neutron EDMs, and the ratios of the proton and isoscalar SMs (in units of $1/m_\pi^2$) to the neutron EDM, for the $\bar{\theta}$ term and for the three dimension-6 sources of T violation discussed in the text.

As it is clear from Eqs. (5.2.15), (5.2.16), (5.3.4), (5.3.8) and (5.3.10) the full EDFF momentum dependences (for example, the second derivatives of F_i with respect to Q^2) are different for qCEDM (and $\bar{\theta}$), qEDM, and gCEDM (and TV four-quark operators). Although the isoscalar components all have linear dependences in Q^2 (with different slopes) to the order considered here, the isovector components show an increasingly complex structure as one goes from qEDM to $\bar{\theta}$ and qCEDM to gCEDM. Determination of nucleon EDMs and SMs alone would not be enough to separate the four sources, yet they would yield clues. Expectations about the orders of magnitude of various dimensionless quantities are summarized in Table 5.1.

In the first line of Table 5.1 one finds the expected NDA size of the neutron EDM. As it is well known [81], this is consistent with many other estimates, such as $d_n = \mathcal{O}(d_i)$ in the constituent quark model, and $d_n = \mathcal{O}(e\tilde{d}_i/4\pi, e d_W M_{\rm QCD}/4\pi)$ from QCD sum rules. If $\tilde{\delta}_{0,3} \sim \delta_{0,3} \sim w = \mathcal{O}(1)$ (as would be the case for $g_s \sim 4\pi$ and no small phases), then the gCEDM and the TV chiral-invariant four-quark operators give the biggest dimension-6 contribution to the EDFF because of the chiral-symmetry-breaking suppression $\mathcal{O}(m_\pi^2/M_{\rm QCD}^2)$ for the qCEDM and qEDM. However, models exist (for example, Refs. [178, 179]) where $\delta_{0,3}$ and $\tilde{\delta}_{0,3}$ are enhanced relative to w, and all the sources produce EDFF contributions of the same overall magnitude. Even so, there is no *a priori* reason to expect cancellations among the various sources. A

measurement of the neutron EDM d_n could be fitted by any one source. Conversely, barring unlikely cancellations, the current bound yields order-of-magnitude bounds on the various parameters at the scale where NDA applies: using $2\pi F_\pi \simeq 1.2$ GeV for $M_{\rm QCD}$,

$$\bar{\theta} \lesssim 10^{-10}, \tag{5.4.1}$$

$$\frac{\tilde{\delta}_{0,3}}{M_T^2}, \frac{\delta_{0,3}}{M_T^2} \lesssim \left(10^5 \text{ GeV}\right)^{-2}, \tag{5.4.2}$$

$$\frac{w}{M_T^2} \lesssim \left(10^6 \text{ GeV}\right)^{-2}. \tag{5.4.3}$$

(For comparison, Eq. (5.4.1) is consistent within a factor of a few with bounds obtained by taking representative values of μ in the non-analytic terms to estimate [93] the size of the renormalized LECs for the EDM, and using either $SU(2)$ [39] or $SU(3)$ [99] symmetry to constrain $\bar{g}_0$.) In all four cases we expect the proton and neutron EDMs to be comparable, $|d_p| \sim |d_n|$, but the presence of undetermined LECs does not allow further model-independent statements.

It is in the pattern of the S_i' that we see some texture. (This pattern is not evident in Ref. [175], possibly because of the way chiral symmetry is broken explicitly in the model used, both in the form of the T-conserving pion-nucleon Lagrangian and in the gCEDM magnitude of the T-violating pion-nucleon coupling.) While in all cases one expects $|S_p'| \sim |S_n'|$, the relative size to the EDMs, in particular of the isovector component, allows one in principle to separate qEDM and gCEDM from $\bar{\theta}$ and qCEDM. Since all these sources generate different pion-nucleon interactions thanks to their different chiral-symmetry-breaking properties, nuclear EDMs might provide further probes of the hadronic source of T violation.

More could be said with input from lattice QCD. For each source the pion-mass dependence is different. A fit to lattice data on the Q^2 *and* m_π^2 dependences of the nucleon EDFF with the expressions of this paper would allow in principle the separate determination of LECs. In this case a measurement of the neutron and proton alone would suffice to pinpoint a dominant source if it exists, but in the more general case

of two or more comparable sources further observables are needed.

One should keep in mind that our approach is limited to low energies. The contributions associated with quarks heavier than up and down are buried in the LECs, as done, for example, in other calculations of nucleon form factors: electric and magnetic [180, 181, 131, 182], anapole [183, 184], and electric dipole from $\bar{\theta}$ [91]. Heavy-quark EDMs and CEDMs are also singlets under $SU(2)_L \times SU(2)_R$, so they generate in two-flavor χPT interactions with the same structure as those from the gCEDM, and cannot be separated explicitly from the latter. (This is clear already in the one-loop running of d_W, which gets a contribution of the heavy-quark CEDMs [108].) The parameter w here should be interpreted as subsuming heavier-quark EDMs and CEDMs. With the additional assumption that m_s makes a good expansion parameter, effects of the s quark could be included explicitly. The larger $SU(3)_L \times SU(3)_R$ symmetry would yield further relations among observables (for example, between the EDFFs of the nucleon and of the Λ), and we could, in principle, isolate the contributions of the strange quark. Since our nucleon results, which can be used as input in nuclear calculations in two-flavor nuclear EFT, would be recovered in the low-energy limit anyway —as was explicitly verified in Ref. [99] for the $\bar{\theta}$ results of Ref. [91]— we leave a study of the identification of explicit s-quark effects to future work.

In summary, we have investigated the low-energy electric dipole form factor that emerges as a consequence of effectively dimension-6 sources of T violation at the quark-gluon level: the quark electric and color-electric dipole moments, and the gluon color-electric dipole moment. Only the full momentum dependence could in principle separate these sources, although the Schiff moments, if they were isolated, would partially exhibit a texture of T violation.

Chapter 6

The Deuteron Electric Dipole Moment

6.1 Introduction

The observation of the neutron and proton EDM in the next generation of experiments would be a clear signal of new physics. However, we argued in Chapter 5 that it would not be sufficient to unequivocally pinpoint the dominant mechanism of T violation at high energy. A signal for the neutron and proton EDM can be reproduced as well by a non zero value of the angle $\bar{\theta}$, or by any of the dimension 6 sources of T violation we considered. More clues could be extracted from the momentum dependence of the EDFF, which, unfortunately, is not going to be measured any time soon. In this light, experiments that probe EDMs (and, possibly, higher TV moments) of light nuclei can provide important additional insight.

In recent years the proposal and development of novel experimental techniques to measure the EDMs of charged particles in storage rings [87] have generated great excitement. These techniques have the potential to achieve a sensitivity comparable to that of classical neutron EDM experiments, if not greater. A proton EDM experiment at BNL, with the goal to see a signal of the order $d_p \sim 10^{-16} e$ fm, has already been approved, is in the Research and Development phase and it is projected to start taking data by 2016. In parallel, the possibility to study the deuteron EDM with the same accuracy at the COSY accelerator at the Jülich Forschungszentrum is under investigation. After the completion of these two experiments, one can envision the application of the same experimental methods to ^{3}He.

From the theoretical point of view, the challenge is to treat the one- and few-nucleon problems in a consistent framework, based upon QCD. This task is complicated by the non-perturbative nature of QCD at the scales relevant to nuclear physics. In recent years, remarkable progress has been achieved in tackling nuclear

physics problems directly from lattice QCD, and lattice simulations that are closer and closer to the physical light quark mass, $m_\pi \sim 140$ MeV, in large volumes and small lattice spacing are rapidly becoming available (for a review, see Ref. [185]). In the two-nucleon system, the unnatural values of the nucleon-nucleon scattering lengths and of the deuteron binding momentum point to a precise cancellation between different contributions, which only happens when the QCD parameters are fine-tuned to their physical value, and disappears as soon as one moves away from it. This was nicely confirmed in [186], where the S-wave nucleon-nucleon scattering lengths were computed on the lattice, and, for a value of $m_\pi \sim 350$ MeV were found to be natural, of size m_π^{-1}. Consequently, the simulation of the two-nucleon system on the lattice is complicated by the fact that it needs to be carried out with light quark masses very close to their physical value. At present, no lattice calculation of the deuteron EDM is yet available.

The approach we follow is based on nuclear Effective Field Theories, which are built on the bedrock of the symmetries of QCD, chiral symmetry in particular. In Chapter 5, we discussed applications to problems with one nucleon. Applications to problems with more than one heavy particle are complicated by the appearance of a new low energy scale, the binding energy, much smaller than the particles' momentum, and, in the particular case of nuclear physics, by the fine-tuning that makes the scattering lengths unnatural. We briefly discuss how to extend chiral EFT to few nucleon systems in Sec. 6.2 (for more in-depth discussions of these issues, we refer to the reviews [37, 38]). In particular, we introduce the Kaplan, Savage and Wise power counting (KSW) and the perturbative pion approach [187, 188, 189], which we use to study the TV electromagnetic moments of the deuteron. In this approach, the deuteron wavefunction is determined in leading order by a contact interaction, whose strength is fixed by the deuteron binding energy, while contributions from TC pion exchanges are treated as a perturbation.

In Sec. 6.3 we compute the deuteron EDM and MQM at leading order, for the

different TV sources introduced in Chapter 3. The deuteron EDM and MQM have been previously computed by Khriplovich and Korkin [157], using a zero range approach for the deuteron wavefunction. They assumed the EDM and MQM to be dominated by TV one-pion-exchange, and made no discrimination between the possible non-derivative TV pion-nucleon couplings. Later, Timmermans and Liu [159] repetead the calculation, with a more realistic deuteron wavefunction. They also included the contribution to the deuteron EDM from the nucleon isoscalar EDM, and supplemented the TV potential with the contributions of TV heavy-meson exchanges. The main advantage of our EFT approach is the closer relation between the couplings in the low-energy Lagrangian and the fundamental TV sources, which allows to assess, for each TV source, the relative size of the different contributions considered in Ref. [159]. We will see that for sources like the qCEDM, for which *i)* pion-nucleon couplings are the TV interactions with lowest chiral index, *ii)* the isoscalar and isovector TV pion-nucleon couplings have comparable size, our analysis reproduces the results in [157, 159]. On the other hand, sources for which either i) or ii) are not valid lead to qualitatively different results. We will discuss our results more in depth in Sec. 6.4.

6.2 Formalism and Power Counting

In the mesonic and one-nucleon sectors, chiral symmetry and its spontaneous breaking, and the heavy baryon formalism, justify a perturbative expansion of any amplitude in powers of the typical external momentum Q of the particles in the problem over the typical QCD scale, $M_{QCD} = 2\pi F_\pi \sim 1$ GeV. Eq. (3.3.14) and (3.3.15) show explicitly that to calculate an amplitude at a given accuracy ν only a finite number of interactions, up a to maximum chiral index Δ, and a finite number of loops have to be considered.

The power counting formulas (3.3.14) and (3.3.15) cannot be directly used in problems with more than one nucleon. A first issue is that in problems with two

nucleons a second energy scale, the nucleon binding energy, becomes relevant. This scale is of order Q^2/m_N, much smaller than the momentum Q, and it enhances diagrams in which the contour of integration cannot be deformed to avoid poles in the nucleon propagator. In a failure of perturbation theory, these diagrams must be resummed at all orders, and lead to the appearance of bound states. Weinberg [35, 36] proposed to split the calculation of amplitudes in two steps. First one evaluates the potential (and electromagnetic and weak currents), for which an expansion in powers of Q/M_{QCD} should be suitable. Then, the full amplitude is obtained by iterating the potential with A free nucleon propagators, *i.e.* by solving the Lippmann-Schwinger equation with the EFT potential. We return to this approach in Chapter 7, where we compute the TV potential at N^{2}LO, in the Weinberg power counting.

A second issue, more specific of nuclear physics, is the unnatural size of the nucleon S-wave scattering lengths. The scattering lengths for two nucleons in the isospin triplet channel, $a_t = -23.7$ fm, and isospin singlet channel, $a_s = 5.4$ fm, are much larger than the range of the nucleon-nucleon potential, $1/m_\pi \sim 1$ fm, which suggests that the QCD parameters are "fine-tuned" to cause large cancellations between different contributions to the scattering lengths. In the Weinberg power counting, the fine tuning manifests *a posteriori* in values of the coefficients C_{0s} and C_{0t} that are somewhat larger than their naive power counting size.

Kaplan, Savage and Wise (KSW) proposed a modification of the power counting to explicitly accommodate for unnatural scattering lengths [187, 188]. In the KSW power counting, S-wave four-nucleon operators are enhanced. While in a theory with natural scattering lengths, by naive dimensional analysis one would expect C_{0t} and C_{0s} to scale as $4\pi/m_N M_{NN}$, where M_{NN} is the range of validity of the theory, KSW assign these coefficients the behavior $C_{0s,t} = 4\pi/m_N Q$, where Q is the typical momentum of external particles in the problem, $Q \ll M_{NN}$. The KSW power counting is manifestly realized in the Power Divergence Subtraction (PDS) renormalization scheme [187, 188]. In this scheme, loop diagrams are regulated in dimensional regularization,

and counterterms are introduced to eliminate not only poles in $d = 4$ (as done, for example, in Minimal Subtraction), but also poles in $d = 3$, which would correspond to linear divergences if the theory were regulated with a cut-off (for a more nuanced descriptions of the scheme, and for alternative renormalization schemes compatible with the KSW power counting, we refer to Refs. [190, 191]).

In the PDS scheme, $C_{0s,t}$ follow a renormalization group equation, which is solved by [187, 188]

$$C_{0s,t}(\mu) = \frac{4\pi}{m_N} \frac{1}{1/a_{s,t} - \mu}, \tag{6.2.1}$$

with boundary condition $C_{0s,t}(0) = 4\pi a_{s,t}/m_N$. If μ is chosen to be of the order of the typical momentum in the problem, $\mu \sim Q$, Eq. (6.2.1) explicitly realizes the KSW power counting.

In the KSW power counting, the enhancement of the leading S-wave operators and renormalization group invariance drive the scaling of other S-wave four-nucleon operators. In general, the coefficient of a TC four-nucleon operator that connects two angular momentum states L and L', and has $2d = L + L' + 2n$ spatial derivatives and m insertions of the quark mass scale [189]

$$C^{n+m}_{L,L'}(\mu) \sim \begin{cases} \mu^{-n-m-1} & \text{if} \quad L,\, L' \in \{{}^1S_0, {}^3S_1, {}^3D_1\} \\ \mu^0 & \text{otherwise.} \end{cases} \tag{6.2.2}$$

For example, of the four-nucleon operators with two derivatives, $C_{2t,s}$, which connect two ${}^1S_0$ or two ${}^3S_1$ states, scale as $4\pi/m_N M_{NN} Q^2$, the operator responsible for the mixing between the ${}^3S_1$ and ${}^3D_1$ state scales as $4\pi/m_N M_{NN}^2 Q$, while P-wave operators scale as $4\pi/m_N M_{NN}^3$. Four-nucleon currents that connect S-waves are similarly enhanced. In the KSW power counting, the leading terms in the $f = 4$ Lagrangian are

$$\begin{aligned} \mathcal{L}_{f=4} \;=\; & -\sum_{i=s,t} \left(C_{0i} + D_{2i} m_\pi^2\right) \left(N^t P_i N\right)^\dagger \; N^t P_i N + \\ & + \sum_{i=s,t} \frac{C_{2i}}{8} \left[\left(N^t P_i N\right)^\dagger \; N^t P_i \overleftrightarrow{\nabla}^2 N + \text{h.c.}\right] + \ldots \end{aligned} \tag{6.2.3}$$

where the isospin triplet and isospin singlet projectors are

$$P_t^a = -\frac{1}{\sqrt{8}}\tau_2\tau_a\sigma_2 \qquad P_s^j = -\frac{1}{\sqrt{8}}\sigma_2\sigma^j\tau_2, \tag{6.2.4}$$

and the spin/isospin indices in Eq. (6.2.3) are appropriately contracted. All the other operators with two derivative are suppressed by Q/M_{NN} or Q^2/M_{NN}^2 with respect to D_{2i} and C_{2i}.

For momenta Q of the order of the pion mass, one has to introduce the pion as a propagating degree of freedom in the theory. Then one needs to assess the importance of pion-exchange relative to short-range interactions, and of diagrams with exchanges of pions relative to one-pion exchange. With the KSW assignment to $C_{0s,t}$, it turns out that the ratio between one-pion exchange and short-range, and between diagrams with two iterations of one-pion exchange and one-pion exchange is $g_A^2 m_N Q/4\pi F_\pi^2 = Q/M_{NN}$, where KSW identify the range of validity of the theory, M_{NN}, with $M_{NN} = 4\pi F_\pi^2/m_N g_A^2$. Numerically, $M_{NN} \sim 300$ MeV. In the perturbative pion approach, Q/M_{NN} is assumed to be much smaller than one, and TC pion effects do not need to be iterated in the EFT.

To summarize, in the KSW power counting amplitudes have a scaling in Q/M_{NN} (and, when subleading interactions in the $f = 2$ pion-nucleon Lagrangian are included, Q/M_{QCD}). The scaling of a diagram is obtained by assigning a power of $Q^5/(4\pi m_N)$ to each loop, m_N/Q^2 to each nucleon propagator, $1/Q^2$ to each pion propagator, a power of Δ as in Eq. (3.3.9) to each pion-nucleon vertex, while four-nucleon operators are counted as in Eq. (6.2.2). With these rules, the insertion of an arbitrary number of $C_{0s,t}$ vertices does not cost any power of Q/M_{NN}, and $C_{0s,t}$ must be iterated at all orders. Instead, all the other interactions in the theory cost powers of Q/M_{NN}, and, to reach a wanted accuracy, only a finite number of them is needed.

The expansion parameter in the perturbative pion approach, Q/M_{NN}, is not extremely small, $Q/M_{NN} \sim 0.5$ if one takes $Q \sim m_\pi$. One might therefore expect the EFT to converge slowly, and might wonder if it converges at all. The KSW power counting has been successfully applied to the P- and T-conserving electromagnetic

form factors of the deuteron [189]. NLO corrections to the electric charge form factor are about 25 % of the leading order, and the NLO calculation of the deuteron square radius is within 10 % of the experimental value. The deuteron magnetic moment is well approximated by the LO result, the isoscalar nucleon magnetic moment. At NLO there is one free parameter, a short-range contribution to the deuteron magnetic dipole moment, whose value is somewhat smaller than expected in the KSW power counting. The KSW power counting has been applied also to the P-violating and T-conserving deuteron anapole form factor, computed at LO in Ref. [192]. In nucleon-nucleon scattering, the S, D and P phase shifts have been calculated at N^{2}LO in Ref. [193]. In the spin-singlet channels $^1S_0$, $^1P_1$ and $^1D_2$, the perturbative series converges well also for momenta of the order of the pion mass. However, the spin-triplet channels are poorly described in the perturbative pion approach, and for momenta of order $Q \sim 100$ MeV, pion exchanges have to be considered at all orders.

In the TV Lagrangian, the KSW power counting alters the scaling of the coefficients of TV four-nucleon operators in Sec. 4.1.4 and 4.2.3. In the $f = 4$ sector, the leading operators with only nucleons have the form (reverting from the partial waves notation of Eq. (6.2.3) to the notation used in Sec. 4.1.4)

$$\begin{aligned} \mathcal{L}_{\not{T},\, f=4} \;=\; & \bar{C}_1 \bar{N} N \partial_\mu (\bar{N} S^\mu N) + \bar{C}_2 \bar{N} \boldsymbol{\tau} N \cdot \partial_\mu (\bar{N} \boldsymbol{\tau} S^\mu N) \\ & + \bar{C}_3 \bar{N} \tau_3 N \, \partial_\mu \left(\bar{N} S^\mu N \right) + \bar{C}_4 \bar{N} N \, \partial_\mu \left(\bar{N} \tau_3 S^\mu N \right) \ldots \end{aligned} \tag{6.2.5}$$

where we neglect the detailed chiral structure, which is not relevant in the deuteron calculation. As we discussed in Sec. 4.1.4, the QCD $\bar{\theta}$ term and the chiral invariant TV sources only contribute to the isospin symmetric operators $\bar{C}_{1,2}$ in lowest order, while the qCEDM also generates a contribution to $\bar{C}_{3,4}$. The operators $\bar{C}_{1,2}$ cause the TV and isospin conserving transitions of two nucleons in the $^1S_0$ configuration into the $^3P_0$ configuration, or from $^3S_1$ into $^1P_1$. The isobreaking operators $\bar{C}_{3,4}$ instead, are responsible for the transition $^3S_1$ to $^3P_1$, which also breaks isospin. All the operators in Eq. (6.2.5) involve one S-wave, and we expect them to scale as $1/Q$. This prejudice has to be confirmed by an analysis of the renormalization group equations in the PDS

scheme.

While the renormalization group equations in the PDS scheme unambiguously determine the dependence of the coefficient of a four-nucleon operator on the low-energy scale Q, the presence of two high-energy scales, M_{NN} and M_{QCD}, leaves room for some ambiguity in power-counting assignments, that cannot be fixed by the dimension of the coefficient alone. Here, we estimate the size of four-nucleon operators and currents by "matching" the perturbative pion EFT onto the non-perturbative pion EFT at scales $\mu \sim M_{NN}$. A real matching calculation is non-perturbative, so in practice what we do is to estimate the coefficients by applying dimensional analysis to loop diagrams in the non-perturbative pion theory with a cut-off of order M_{NN}, in the same spirit as the naive dimensional analysis of Ref. [123].

In the case of the QCD $\bar{\theta}$ term, we obtain

$$\bar{C}_{\bar{\theta}\,1,2} = \mathcal{O}\left(\bar{\theta}\frac{4\pi}{m_N Q}\frac{m_\pi^2}{M_{NN}^2 M_{QCD}}\right), \tag{6.2.6}$$

For the qCEDM

$$\tilde{\bar{C}}_{q\,i} = \mathcal{O}\left(\tilde{\delta}\frac{4\pi}{m_N Q}\frac{m_\pi^2 M_{QCD}}{M_{NN}^2 M_{\not T}^2}\right), \tag{6.2.7}$$

with $i = 1, \ldots, 4$, and the detailed dependence on $\tilde{\delta}_0$ and $\tilde{\delta}_3$ is as in Eq. (4.1.49). Finally, the chiral invariant TV sources give

$$\bar{C}_{w\,1,2} = \mathcal{O}\left(w\frac{4\pi}{m_N Q}\frac{M_{QCD}}{M_{\not T}^2}\right). \tag{6.2.8}$$

The relevant four-nucleon-one-photon operators are

$$\mathcal{L}_{\not T,\, f=4\,\mathrm{em}} = \bar{D}_{NN}\bar{N}S^\mu v^\nu N\,\bar{N}NF_{\mu\nu} + \bar{M}\varepsilon^{\alpha\beta\mu\nu}v_\alpha\,\bar{N}S_\beta N\,\bar{N}S_\lambda N\,\partial^\lambda F_{\mu\nu}, \tag{6.2.9}$$

which represent short-distance contributions to the deuteron EDM and MQM. These operators connect two S-waves, and we expect them to scale as $1/Q^2$. In the case of the $\bar{\theta}$ term, short-range contributions to the deuteron EDM and MQM go as

$$\bar{D}_{NN} = \mathcal{O}\left(e\bar{\theta}\frac{4\pi}{m_N Q^2}\frac{m_\pi^2}{M_{NN}M_{QCD}^2}\right),\ \bar{M}_{\bar{\theta}} = \mathcal{O}\left(e\bar{\theta}\frac{4\pi}{m_N Q^2}\frac{m_\pi^2}{M_{NN}^3 M_{QCD}}\right). \tag{6.2.10}$$

For the qCEDM,

$$\tilde{\bar{D}}_{q\,NN} = \mathcal{O}\left(e\tilde{\delta}\frac{4\pi}{m_N Q^2}\frac{m_\pi^2 M_{QCD}^2}{M_{NN}^3 M_{\not T}^2}\right),\ \tilde{\bar{M}}_q = \mathcal{O}\left(e\tilde{\delta}\frac{4\pi}{m_N Q^2}\frac{m_\pi^2 M_{QCD}}{M_{NN}^3 M_{\not T}^2}\right). \tag{6.2.11}$$

Again, we use $\tilde{\delta}$ for both $\tilde{\delta}_0$ and $\tilde{\delta}_3$, the detailed dependence is given in Sec. 4.2.3. For the qEDM,

$$\bar{D}_{q\,NN} = \mathcal{O}\left(e\delta\frac{4\pi}{m_N Q^2}\frac{m_\pi^2}{M_{NN} M_{\not T}^2}\right),\ \bar{M}_q = \mathcal{O}\left(e\tilde{\delta}\frac{4\pi}{m_N Q^2}\frac{m_\pi^2}{M_{NN} M_{QCD} M_{\not T}^2}\right). \tag{6.2.12}$$

Finally, for the gCEDM and the TV four-quark operators

$$\bar{D}_{w\,NN} = \mathcal{O}\left(ew\frac{4\pi}{m_N Q^2}\frac{M_{QCD}^2}{M_{NN} M_{\not T}^2}\right),\ \bar{M}_w = \mathcal{O}\left(ew\frac{4\pi}{m_N Q^2}\frac{M_{QCD}}{M_{NN} M_{\not T}^2}\right). \tag{6.2.13}$$

In Sec. 6.6 we will see how, with the assignment (6.2.10), $\bar{D}_{NN}$ gives a contribution to the deuteron EDM of exactly the right size to absorb the logarithmic divergences of certain one-pion-exchange diagrams, justifying, *a posteriori*, our NDA estimate.

6.3 Deuteron TV currents

The time and space components of the TV electromagnetic current of a spin 1 particle are expressed in terms of the Electric Dipole and Magnetic Quadrupole Form Factors. In the case of the deuteron

$$\langle \vec{p}'\, j|J^0_{\mathrm{em},\not T}|\vec{p}\, i\rangle = -\varepsilon^{ijm} q^m\, F_D(\vec{q}^{\,2}) + \frac{1}{4}\varepsilon^{nml}\frac{K^n}{m_d} q^l(\delta^{mi}q^j + \delta^{mj}q^i) F_M(\vec{q}^{\,2}), \tag{6.3.1}$$

$$\langle \vec{p}'\, j|J^k_{\mathrm{em},\not T}|\vec{p}\, i\rangle = -\varepsilon^{ijm} q^m \frac{K^k}{m_d}\, F_D(\vec{q}^{\,2}) + \frac{1}{4}\varepsilon^{kml} q^l\left(\delta^{mi}q^j + \delta^{mj}q^i\right) F_M(\vec{q}^{\,2}). \tag{6.3.2}$$

Here $|\vec{p}\, i\rangle$ denotes a deuteron state of momentum $\vec{p}$ and polarization $\varepsilon_i^\mu = \delta_i^\mu$ in the rest frame, normalized so that $\langle \vec{p}' j|\vec{p}\, i\rangle = \sqrt{1+\vec{p}^{\,2}/m_d^2}\,(2\pi)^3\delta^{(3)}(\vec{p}-\vec{p}')\delta_{ij}$. $\vec{q} = \vec{p}-\vec{p}'$ is the photon momentum, $\vec{K} = (\vec{p}'+\vec{p})/2$, and m_d is the deuteron mass, $m_d = 2m_N - \gamma^2/m_N$. γ is the deuteron binding momentum, $\gamma = 45$ MeV. In Eqs. (6.3.1)

and (6.3.2), $F_D(\vec{q}^2)$ represents the deuteron EDFF, and its value at $\vec{q}^2 = 0$ is the deuteron EDM, $d_d = F_D(0)$. Analogously, $F_M(\vec{q}^2)$ denotes the Magnetic Quadrupole Form Factor (MQFF), and its value at zero transfer momentum is the deuteron MQM, $\mathcal{M}_d = F_M(0)$.

In the perturbative pion approach, the form factors $F_D(\vec{q}^2)$ and $F_M(\vec{q}^2)$ are expanded in powers of Q/M_{NN}, where Q denotes scales of the order of the pion mass, and of the deuteron binding energy, which are assumed to be comparable. Our goal is to calculate the EDFF and MQFF stemming from the QCD $\bar{\theta}$ term and from the dimension 6 TV sources at leading order in this expansion.

Following the approach of Kaplan, Savage and Wise [189], the form factors are obtained by computing in perturbation theory the irreducible two-point function Σ and three-point function Γ^μ_{ij} of the deuteron interpolating field $\mathcal{D}_i$, where "irreducible" here means the sum of graphs which do not fall apart when cut at any C_0 vertex. The interpolating field $\mathcal{D}_i$ is any field with the same quantum numbers as the deuteron. We choose $\mathcal{D}_i(x) = N(x)P^j_s N(x)$. P^j_s is the spin 1, isospin 0 projector, in Eq. (6.2.4). Physical observables are independent of the choice of field, so long as it is used consistently.

The LSZ reduction formula relates the matrix element of the electromagnetic current to the irreducible three-point function Γ^μ_{ij} and the derivative of the two-point function Σ [189],

$$\langle \vec{p}'\, j|J^\mu_{\mathrm{em},T}|\vec{p}i\rangle = i\left[\frac{\Gamma^\mu_{ij}(\bar{E},\bar{E}',\vec{q})}{d\Sigma(\bar{E})/dE}\right]_{\bar{E},\bar{E}'\to -B}. \tag{6.3.3}$$

where $\bar{E}$ is the deuteron energy in the center of mass frame $\bar{E} = E - \vec{p}^2/4m_N$ and the deuteron form factors are obtained by setting $\bar{E}$ to the deuteron binding energy $\bar{E} = -B = -\gamma^2/m_N$.

We show in Fig. 6.1 the diagrams contributing to the irreducible two-point function $\Sigma(\bar{E})$ at NLO. It turns out that diagrams which only contain one TV vertex do not contribute to the two-point function, which is therefore identical to the two-point function in absence of T violation, computed in [189] at NLO in Q/M_{NN}. In particu-

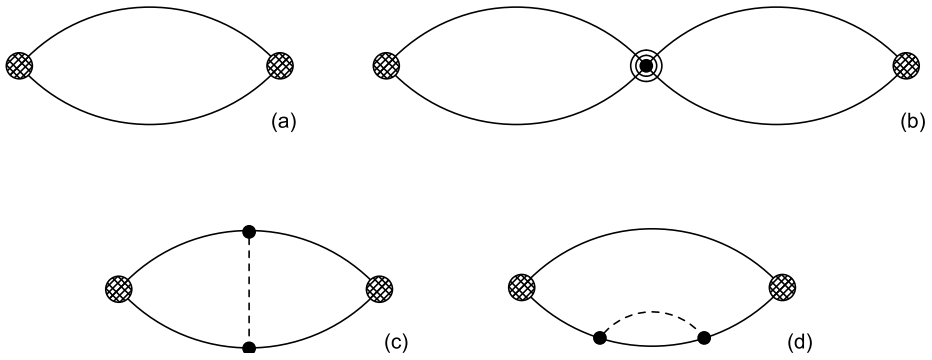

FIGURE 6.1. The irreducible two-point function $\Sigma(\bar{E})$ at NLO. Solid and dashed lines denote nucleons and pions. Filled circles mark the leading TC interactions, while the circled circle denotes the subleading four-nucleon operators C_{2s} or D_{2s}. The hatched circle denotes an insertion of the interpolating field $\mathcal{D}_i(x)$.

lar we are interested in the first derivative of Σ, which, at leading and next-to-leading order is

$$\left.\frac{d\Sigma_{(1)}}{d\bar{E}}\right|_{\bar{E}=-B} = -i\frac{m_N^2}{8\pi\gamma} \tag{6.3.4}$$

$$\begin{aligned}\left.\frac{d\Sigma_{(2)}}{d\bar{E}}\right|_{\bar{E}=-B} &= i\frac{m_N^2}{8\pi\gamma}\frac{m_N}{2\pi}\left[\frac{g_A^2}{F_\pi^2}\left(\mu-\gamma-\frac{m_\pi^2}{m_\pi+2\gamma}\right)+D_{2s}m_\pi^2(\mu-\gamma)\right.\\ &+ \left. C_{2s}\gamma(\mu-\gamma)(\mu-2\gamma)\right]\end{aligned} \tag{6.3.5}$$

where $\gamma=\sqrt{m_N B}\sim 45$ MeV.

In Ref. [189], the contribution to the two-point function from the correction to the nucleon mass coming from the diagram 6.1(d) and from the insertion of the sigma term Δm_N in the nucleon propagator was neglected. In the PDS scheme, the correction to the nucleon mass is μ-dependent, and the linear μ dependence is absorbed by the sigma term

$$\Delta_R m_N = \Delta m_N + \frac{3g_A^2}{2}\frac{m_\pi^2}{4\pi F_\pi^2}(\mu-m_\pi). \tag{6.3.6}$$

The net effect of this shift in the nucleon mass is to change the deuteron binding

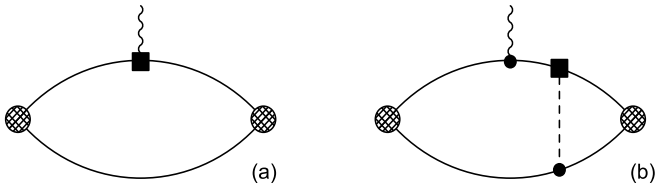

FIGURE 6.2. LO diagrams for the deuteron EDFF. Solid, dashed, and wavy lines represent nucleons, pions, and photons. A square marks TV interactions, filled circles the leading TC interactions. The hatched vertex represents the deuteron interpolating field $\mathcal{D}_i(x)$. Only one topology per diagram is shown.

momentum γ

$$\gamma' = \gamma + \delta\gamma \tag{6.3.7}$$

with

$$\delta\gamma = m_N \frac{\Delta_R m_N}{\gamma} = m_N \frac{\Delta m_N}{\gamma} + \frac{3g_A^2}{2} \frac{m_\pi^2 m_N}{4\pi F_\pi^2} \frac{(\mu - m_\pi)}{\gamma}. \tag{6.3.8}$$

Such a shift in γ is automatically taken care of when the physical value of the nucleon mass and γ are used in the evaluation of observables.

6.4 The Deuteron EDM and MQM at Leading Order

The calculation of the EDFF and MQFF involves at LO the diagrams of Figs. 6.2 and 6.3. The squares denote TV interactions constructed in Secs. 4.1 and 4.2. The circles denote the leading TC interactions in $\mathcal{L}^{(0)}_{\chi,\, f\leq 2}$, in Eq. (3.3.17). The pion-nucleon vertex is the standard axial-vector coupling, $g_A = 1.27$. The photon vertex denoted by a filled circle is the coupling to the charge e, and that denoted by a circled circle is the magnetic coupling parametrized by the anomalous magnetic moments, the isoscalar $\kappa_0 = -0.12$ and the isovector $\kappa_1 = 3.71$. The hatched circles denote insertions of the deuteron interpolating field $\mathcal{D}_i(x)$. We use dimensional regularization with power-divergence subtraction [187, 188, 189] at a renormalization scale μ. Our results depend on the ratio $\xi = \gamma/m_\pi$ and on three functions of the momentum in

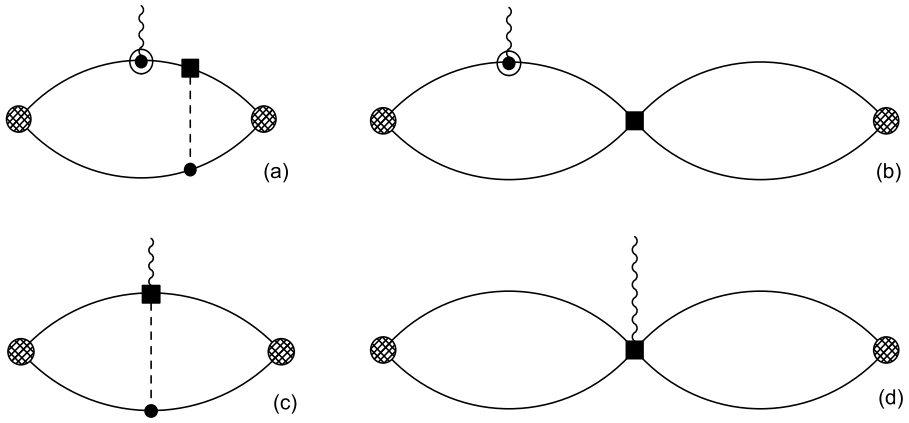

FIGURE 6.3. LO diagrams for the deuteron MQFF. Solid, dashed, and wavy lines represent nucleons, pions, and photons. A square marks TV interactions, circled circles subleading TC interactions. The hatched vertex represents the deuteron interpolating field $\mathcal{D}_i(x)$. Only one topology per diagram is shown.

the ratio $x = |\vec{q}|/4\gamma$:

$$F_1(x) = \arctan(x)/x, \tag{6.4.1}$$

which originates in a bubble with one photon coupling and appears also in the charge form factor [189], and two complicated functions that result from two-loop diagrams with a pion propagator, which can be expanded as

$$\begin{aligned} F_2(x) &= 1 - x^2 \frac{10 + 65\xi + 144\xi^2 + 72\xi^3}{30(1+\xi)(1+2\xi)^2} + \mathcal{O}(x^4), \\ F_3(x) &= 1 - x^2 \frac{\xi^2(12 + 8\xi)}{5(1-2\xi)(1+2\xi)^2} + \mathcal{O}(x^4); \end{aligned} \tag{6.4.2}$$

in all cases $F_i(0) = 1$. The scale of momentum variation, including that of the corresponding electromagnetic contribution to the Schiff moment, is set by 4γ.

The LO deuteron EDFF is due to diagrams Fig. 6.2(a,b). Diagram 6.2(a) represents the contribution to the deuteron EDFF from the neutron and proton EDMs, in particular their isoscalar combination, while in diagram 6.2(b) the deuteron EDM is caused by a TV correction to the deuteron wavefunction. We find

$$F_D(\vec{q}^2) = 2D_0 F_1(x) - \frac{e g_A \bar{g}_1 m_N}{6\pi F_\pi^2 m_\pi} \frac{1+\xi}{(1+2\xi)^2} F_2(x). \tag{6.4.3}$$

where D_0 is the isoscalar nucleon EDM, defined by Eq. (5.1.3), and $\bar{g}_1$ the isovector, TV non derivative pion-nucleon coupling. It is important to notice that the isoscalar pion-nucleon coupling $\bar{g}_0$ does not contribute to the deuteron EDM at LO. The reason is that TV one-pion exchange with $\bar{g}_0$ causes the deuteron wavefunction, whose quantum numbers are mainly ${}^3S_1$, to develop a ${}^1P_1$ component, which, however, has a vanishing dipole matrix element with the ${}^3S_1$ state. A non-vanishing dipole matrix element requires mixing with a spin 1 P-wave, the ${}^3P_1$ state, which also breaks isospin and it is realized by $\bar{g}_1$.

The relative importance of diagrams 6.2(a) and 6.2(b) is different for different sources of T violation.

We already remarked that long-distance physics is suppressed for the qEDM and the chiral-invariant sources of T violation, the gCEDM and the TV four-quark operators. As a consequence, it is not surprising that for both sources, the dominant contribution to the deuteron EDM comes from diagram 6.2(a). In the case of the qEDM, D_0 is given by a short-distance coefficient at LO, $D_0 = \bar{D}^{(1)}_{q\,0}$, Eq. (4.2.15). It follows that

$$d_{d,\,\mathrm{qEDM}} = 2\bar{D}^{(1)}_{q\,0} = \mathcal{O}\left(e\delta_0 \frac{m_\pi^2}{M_{\not T}^2}\frac{1}{M_{QCD}}\right). \tag{6.4.4}$$

For the qEDM, indirect electromagnetic pion-nucleon couplings only appear in the $\Delta_6 = 2$ Lagrangian, that is

$$\bar{g}_1 = \mathcal{O}\left((\delta_0+\delta_3)\frac{\alpha_{\mathrm{em}}}{4\pi}\frac{m_\pi^2}{M_{\not T}^2}M_{QCD}\right). \tag{6.4.5}$$

With the usual assumption $\alpha_{\mathrm{em}}/4\pi \sim \varepsilon m_\pi^3/M_{QCD}^3$, one can see that the TV pion-exchange contribution is suppressed by $m_\pi^2/M_{NN}M_{QCD}$ with respect to the contribution (6.4.4). Indeed, in the case of the qEDM, also the NLO is determined by short-range physics, by the four-nucleon current in Eqs. (4.2.23) (with scaling (6.2.11)), which is suppressed, in the PDS scheme, by Q/M_{NN} with respect to Eq. (6.4.4).

In the case of the gCEDM and the TV four-quark operators, D_0 is also purely

short-distance at leading order, $D_0 = \bar{D}^{(-1)}_{w\,0}$, Eq. (4.2.7), and

$$d_{d,\,w} = 2\bar{D}^{(-1)}_{w\,0} = \mathcal{O}\left(ew\frac{M_{QCD}}{M_T^2}\right). \tag{6.4.6}$$

In this case, the first contribution to $\bar{g}_1$ is given in Eq. (4.1.29) and from the scaling in Eq. (4.1.31) we see that the contribution of diagram 6.2(b) is only suppressed by Q/M_{NN}. Notice that if the pions are treated non-perturbatively, that is, if $Q/M_{NN} = \mathcal{O}(1)$, the two contributions in Eq. (6.4.3) arise at the same order. According to Eq. (6.2.13), four-nucleon currents also contribute an NLO.

We saw in Chapters 3 and 4 that for the chiral symmetry breaking $\bar{\theta}$ term and qCEDM, long-distance physics plays a more important role. However, the fact that the QCD $\bar{\theta}$ term does not break isospin causes the coupling $\bar{g}_1$ only to arise in the $\Delta = 3$ Lagrangian, two orders smaller than the leading TV coupling $\bar{g}_0$. As a consequence, the leading contribution to the deuteron EDM is still the isoscalar nucleon EDM D_0, given in Eq. (4.2.6), which, at leading order is once again given by a LEC constant only, $D_0 = \bar{D}^{(3)}_0$, so that

$$d_{d,\,\bar{\theta}} = 2\bar{D}^{(3)}_0 = \mathcal{O}\left(\bar{\theta}\frac{m_\pi^2}{M^3_{QCD}}\right). \tag{6.4.7}$$

The leading contribution to $\bar{g}_1$ is given in Eq. (4.1.27), and from the scaling (4.1.28), diagram 6.2(b) contributes at NLO. At this order one has to consider the NLO corrections to the isoscalar nucleon EDM, Eq. (5.2.6), which are also suppressed by Q/M_{NN} with respect to the LO, and also the contribution of the relativistic corrections to $\bar{g}_0$ and the other TV derivative couplings in Eq. (4.1.24). With the scaling (6.2.10), $\bar{D}_{NN}$ gives also a NLO contribution.

The qCEDM generates an isovector coupling $\bar{g}_1$ already in leading order, (4.1.29). In this case, the deuteron EDM is dominated by long distance physics,

$$d_{d,\,\mathrm{qCEDM}} = -\frac{eg_A\bar{g}_1 m_N}{6\pi F_\pi^2 m_\pi}\frac{1+\xi}{(1+2\xi)^2} = \mathcal{O}\left(e\tilde{\delta}_3\frac{M_{QCD}}{M_T^2}\frac{m_\pi}{M_{NN}}\right). \tag{6.4.8}$$

The isoscalar nucleon EDM is still given at leading order by a LEC, $D_0 = \tilde{\bar{D}}^{(1)}_{q\,0}$, in Eq. (4.2.11). From the scaling Eq. (4.2.13) we see that the one-body contribution,

diagram 6.2(a), is suppressed in this case by a factor of $m_\pi M_{NN}/M_{QCD}^2$. In the case of the qCEDM, the NLO is dominated by three-loop diagrams, with an extra TC pion-exchange or an insertion of the suppressed four-nucleon vertices C_{2s} and D_{2s}.

The LO MQFF comes from diagrams 6.3(a,b,c,d). Diagrams 6.3(a) and (b) are contributions to the MQM that come from TV corrections to the deuteron wavefunction, in the form of TV pion-exchange, or TV short-distance four-nucleon operators. Diagram 6.3(c) and (d) are a long- and short-distance contribution to the TV electromagnetic current. The resulting MQFF is

$$\begin{aligned} F_M(\vec{q}^2) &= \frac{eg_A}{2\pi F_\pi^2 m_\pi}\left[\bar{g}_0(1+\kappa_0)+\frac{\bar{g}_1}{3}(1+\kappa_1)\right]\frac{1+\xi}{(1+2\xi)^2}F_2(x) \\ &\quad +2\frac{g_A\bar{E}_1\gamma}{\pi F_\pi^2}\left(\frac{1-2\xi}{1+2\xi}F_3(x)+2\ln\frac{\mu/m_\pi}{1+2\xi}\right) \\ &\quad +\frac{e(1+\kappa_0)}{2\pi}(\mu-\gamma)\bar{C}_0F_1(x)+\frac{2\gamma}{\pi}(\mu-\gamma)^2\bar{M}, \end{aligned} \tag{6.4.9}$$

where $\bar{C}_0=(\bar{C}_1-3\bar{C}_2)/4$ and $\bar{E}_1$ is an isoscalar TV pion-nucleon-photon coupling, constructed in Eqs. (4.2.4), (4.2.11) and (4.2.15). Notice that in this case both the isoscalar $\bar{g}_0$ and the isovector $\bar{g}_1$ couplings contribute to the MQM. As a consequence, for both the $\bar{\theta}$ term and the qCEDM the MQFF is dominated by diagram 6.3(a). In the case of the $\bar{\theta}$ term, only $\bar{g}_0$ is relevant in leading order, and, with the scaling (4.1.20), we have

$$m_d\mathcal{M}_{d,\,\bar{\theta}}=\frac{eg_A\bar{g}_0m_N}{\pi F_\pi^2 m_\pi}(1+\kappa_0)\frac{1+\xi}{(1+2\xi)^2}=\mathcal{O}\left(\bar{\theta}\frac{1}{M_{QCD}}\frac{m_\pi}{M_{NN}}\right). \tag{6.4.10}$$

For the qCEDM, $\bar{g}_0$ and $\bar{g}_1$ are given in Eq. (4.1.29), and they lead to

$$\begin{aligned} m_d\mathcal{M}_{d,\,\mathrm{qCEDM}} &= \frac{eg_Am_N}{\pi F_\pi^2 m_\pi}\left[\bar{g}_0(1+\kappa_0)+\frac{\bar{g}_1}{3}(1+\kappa_1)\right]\frac{1+\xi}{(1+2\xi)^2} \\ &= \mathcal{O}\left(e\left(\tilde{\delta}_0+\varepsilon\tilde{\delta}_3+\tilde{\delta}_3\right)\frac{M_{QCD}}{M_T^2}\frac{m_\pi}{M_{NN}}\right). \end{aligned} \tag{6.4.11}$$

For TV from the $\bar{\theta}$ term and qCEDM, Diagrams 6.3(a,b,c) are at least NLO, at which level one has also to consider three-loop diagrams constructed by adding a TC one-pion exchange, or the operators C_{2s} and D_{2s}, to diagram 6.3(a).

In the case of the chiral-invariant sources of TV, even if the TV four-nucleon couplings $\bar{C}_{w\,1,2}$ appear with the same chiral index $\Delta_6 = -1$ as the leading pion-nucleon couplings in Eq. (4.1.29), the perturbative pion power counting enhances the former over the latter. The leading contribution to the MQM comes therefore from diagram 6.2(b), and, in the perturbative pion power counting, it goes as

$$m_d \mathcal{M}_{d,\,w} = \frac{e(1+\kappa_0)}{\pi}(\mu-\gamma) m_N \bar{C}_0 = \mathcal{O}\left(w \frac{M_{QCD}}{M_T^2}\right), \tag{6.4.12}$$

while the contribution of diagram 6.3(a) is suppressed by Q/M_{NN}.

Finally, TV currents dominate the MQM for TV from the qEDM. The coupling $\bar{E}_1 = \bar{E}_{q\,1}^{(1)}$ in defined in Eq. (4.2.15), and it generates a long-range contribution to the TV current. At the same level we find a short-range contribution to the current, defined in Eq. (6.2.9), with scaling (6.2.12), which is needed to absorb the logarithmic divergence of diagram 6.3(c). The MQM at LO is

$$\begin{aligned} m_d \mathcal{M}_{d,\,\mathrm{qEDM}} &= 4\frac{g_A \bar{E}_1 m_N \gamma}{\pi F_\pi^2}\left(\frac{1-2\xi}{1+2\xi} + 2\ln\frac{\mu/m_\pi}{1+2\xi}\right) + \frac{4\gamma}{\pi}(\mu-\gamma)^2 m_N \bar{M} \\ &= \mathcal{O}\left(e\delta_0 \frac{m_\pi^2}{M_T^2 M_{QCD}} \frac{\gamma}{M_{NN}}\right). \end{aligned} \tag{6.4.13}$$

6.5 Discussion

We can now discuss the implications of the various TV sources for the deuteron EDFF and MQFF. In Table 6.1 we list the orders of magnitude for the deuteron EDM, d_d, the ratio of deuteron-to-neutron EDMs, d_d/d_n, and the ratio of the deuteron MQM and EDM, $\mathcal{M}_d/d_d$, for the different TV sources: $\bar{\theta}$ [93, 91], and qCEDM, qEDM, and gCEDM [40]. Just as for d_n, a d_d signal by itself could be attributed to any source with a parameter of appropriate size. For $\bar{\theta}$, qEDM, and gCEDM the deuteron EDFF is determined by the LO isoscalar nucleon EDM, and thus, except for qCEDM, d_d is well approximated by the sum of neutron and proton EDM. For $\bar{\theta}$ in particular, using the most important long-range contributions, which appear at NLO, as a lower

Source	θ	qCEDM	qEDM	gCEDM
$m_d\, d_d/e$	$\mathcal{O}\left(\bar{\theta}\frac{m_\pi^2}{M_{\rm QCD}^2}\right)$	$\mathcal{O}\left(\tilde{\delta}\frac{m_\pi M_{\rm QCD}^2}{M_{NN} M_{\not T}^2}\right)$	$\mathcal{O}\left(\delta\frac{m_\pi^2}{M_{\not T}^2}\right)$	$\mathcal{O}\left(w\frac{M_{\rm QCD}^2}{M_{\not T}^2}\right)$
d_d/d_n	$\mathcal{O}(1)$	$\mathcal{O}\left(\frac{M_{\rm QCD}^2}{m_\pi M_{NN}}\right)$	$\mathcal{O}(1)$	$\mathcal{O}(1)$
$m_d\, \mathcal{M}_d/d_d$	$\mathcal{O}\left(\frac{M_{\rm QCD}^2}{m_\pi M_{NN}}\right)$	$\mathcal{O}(1)$	$\mathcal{O}\left(\frac{\gamma}{M_{NN}}\right)$	$\mathcal{O}(1)$

TABLE 6.1. Orders of magnitude for the deuteron EDM (in units of e/m_d), the ratio of deuteron-to-neutron EDMs, and the ratio of the deuteron MQM and EDM (in units of $1/m_d$), for TV sources of effective dimension up to six.

bound for $\bar{D}_0$ [41, 99], one finds $|d_d| \gtrsim 2.8 \cdot 10^{-4}\,\bar{\theta}\ e\,\text{fm}$. If, however, the dominant TV source is the qCEDM, d_d comes mainly from neutral-pion exchange. When we again take the long-range part of the nucleon EDM [40] as an estimate of its size, we find that $|d_d/d_n| \simeq 2$, which is smaller than expected from NDA. In any case, a measurement of $|d_d|$ significantly larger than $|d_n|$ would be indicative of a qCEDM.

Additional information comes from the ratio $\mathcal{M}_d/d_d$. For $\bar{\theta}$, $m_d|\mathcal{M}_d|$ is expected to be larger than $|d_d|$, whereas for the dimension-six sources we expect $m_d|\mathcal{M}_d|$ to be of similar size or somewhat smaller than $|d_d|$. For $\bar{\theta}$, $\mathcal{M}_d$ is determined by pion exchange, and we can again use the link with isospin violation [39] to find $\mathcal{M}_d \simeq 2.0 \cdot 10^{-3}\,\bar{\theta}\ e$ fm^2. An upper bound on $\mathcal{M}_d$ can therefore constrain $\bar{\theta}$ without relying on an estimate of short-range physics via the size of the chiral log, which is necessary when using d_n [93]. Moreover, if $m_d|\mathcal{M}_d|$ is found to be much smaller than $|d_d|$, the source would likely be qEDM. Clearly, a measurement of $\mathcal{M}_d$, in addition to d_n and d_d, would be very valuable.

The deuteron EDM and MQM were calculated previously in Refs. [157, 159]. In Ref. [157] the chiral limit $m_\pi \to 0$ and the zero-range approximation for the NN interaction were assumed, while Ref. [159] used a TV NN interaction with long-range one-pion exchange and a general short-range interaction parametrized by heavy-meson exchange, in addition to a realistic deuteron wavefunction. Since these calculations did not use the chiral properties of the fundamental TV sources, the TV pion-nucleon interactions were assumed to be all of the same size. When the dominant source is the

qCEDM, their results agree with ours. The advantage of our EFT framework is that it has a direct link to QCD by exploiting the chiral properties of the TV dimension 4 and 6 operators. This is demonstrated by the $\bar{g}_2 \bar{N} \pi_3 \tau_3 N$ interaction used in many previous calculations, which due to its chiral properties only comes in at higher order for all TV sources [39]. Consequently, for the qCEDM, the ratio of d_d to $\mathcal{M}_d$ depends at LO only on the ratio $\bar{g}_1/\bar{g}_0$,

$$\left| \frac{m_D \mathcal{M}_d}{2 d_d} \right| = \left(1 + \kappa_1 + \frac{3\bar{g}_0}{\bar{g}_1}(1+\kappa_0) \right). \tag{6.5.1}$$

If $\bar{g}_1$ is extracted from the deuteron EDM, and $\bar{g}_0$ from another observable, such as the proton Schiff moment [40] or the ^{3}He EDM [161], the ratio (6.5.1) becomes a testable, falsifiable prediction of our calculation. In addition, the power-counting scheme allows a perturbative framework with analytical results that can be improved systematically. Our estimates for d_d are consistent with those from QCD sum rules [194]. Our conclusions, of course, depend on how rapidly the chiral series converges.

In summary, we have investigated the leading-order, low-energy electric-dipole and magnetic-quadrupole form factors of the deuteron that result from the $\bar{\theta}$ angle, the quark electric and chromo-electric dipole moments, and the gluon chromo-electric dipole moment and the TV four-quark operators. While for qCEDM we expect $|d_d|$ to be larger than $|d_n|$ by a factor $\mathcal{O}(M_{\rm QCD}^2/m_\pi M_{NN})$, for the other TV sources we have shown that d_d is given by the sum of d_n and d_p. Furthermore, the Standard Model predicts $m_d|\mathcal{M}_d|$ to be larger than $|d_d|$, whereas beyond-the-SM physics prefers $m_d|\mathcal{M}_d|$ smaller than, or of similar size as $|d_d|$. EDM and MQM measurements are therefore complementary.

6.6 Some contribution to deuteron EDM at NLO

We discuss in this section some NLO corrections to the deuteron EDM from the QCD $\bar{\theta}$ term, in connection with our comment on the size of the counterterm $\bar{D}_{NN}$ in Sec. 6.2.

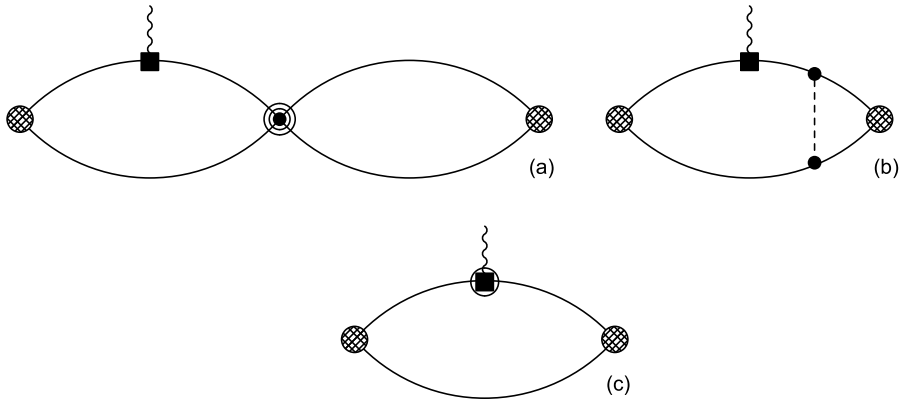

FIGURE 6.4. Corrections to the one-body contribution to the deuteron EDM. Solid, dashed and wavy lines represent nucleons, pions and photons. A square and a circled square denote the leading and next-to-leading isoscalar nucleon EDM. Circles represent interactions from the leading TC Lagrangian. The doubly circled circle denotes an insertion of the subleading four-nucleon operators C_{2s} and D_{2s}. The hatched vertex represents the deuteron interpolating field $\mathcal{D}_i(x)$. Only one topology per diagram is shown.

As remarked in Sec. 6.4, there are several NLO contributions. We first consider corrections to the one-body contribution, diagram 6.2(a). They are depicted in Fig. 6.4. Diagram 6.4(c) represents corrections to the isoscalar nucleon EDFF, which we computed in Sec. 5.2 and we give in Eqs. (5.2.6), (5.2.13) and (5.2.15). Diagrams 6.4(a) and 6.4(b) are corrections to the TC wavefunction, which go beyond the zero-range approximation. The doubly circled circle in diagram 6.4(a) denotes one insertion of the subleading S-wave four-nucleon operators C_{2s} and D_{2s}, while diagram 6.4(b) represents corrections to the wavefunction from one-pion exchange, which is a NLO effect in the perturbative pion approach.

We find that at NLO the one-body contribution is

$$\begin{aligned} F_D^{\text{one-body}}(\vec{q}^2) &= 2F_0(\vec{q}^2)\left\{F_1(x) - \frac{m_N\gamma}{2\pi}C_{2s}(\mu)(\mu-\gamma)^2\left(1-F_1(x)\right)\right. \\ &\left. + \frac{g_A^2 m_N\gamma}{2\pi F_\pi^2}\left[\frac{m_\pi^2}{m_\pi+2\gamma}\left(1-F_1(x)\right)+x^2H(x)\right]\right\}, \end{aligned} \tag{6.6.1}$$

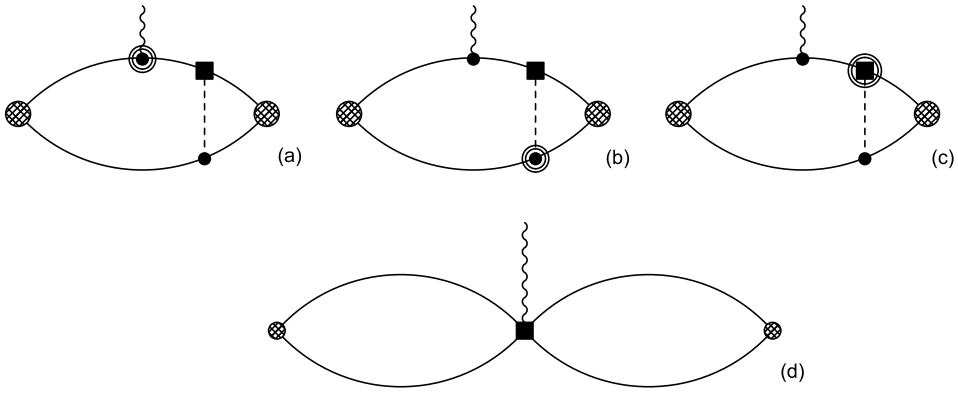

FIGURE 6.5. NLO diagrams for the deuteron EDM from TV corrections to the wavefunction. Solid, dashed and wavy lines represent nucleons, pions and photons. A square denote the leading TV pion-nucleon interaction, or the four-nucleon TV current. A doubly circled square denotes an interaction from the subleading, $\Delta = 3$ TV Lagrangians. Circles denote interactions from the leading TC Lagrangian, while doubly circled circles vertices from the $\Delta = 1$ TC Lagrangian.

where $F_0(\vec{q}^2)$ is the nucleon isoscalar EDFF, defined in Eqs. (5.1.2) and (5.1.3), and the function $H(x)$ is some complicated function of x and ξ, whose expansion starts at $\mathcal{O}(x^0)$. Notice that the contribution of D_{2s} cancels when taking the ratio of the two- and three-point Green's functions. Diagrams 6.4(a) and (b) do not contribute to the deuteron EDM, but only to the momentum dependence of the EDFF. This is analogous to what found for charge form factor in Ref. [189]. The only one-body NLO contribution to the deuteron EDM then comes from the NLO correction to the isoscalar nucleon EDM, Eq. (5.2.6). At NLO

$$d_d^{\text{one-body}} = 2\bar{D}_0 + \frac{e g_A \bar{g}_0}{4\pi F_\pi^2} \frac{3 m_\pi}{2 m_N} \left(1 - \frac{4}{3} \frac{m_N \delta m_N}{m_\pi^2} \right) . \tag{6.6.2}$$

Another class of contributions consists in diagrams of the same topology as diagrams 6.2(b), but with power-suppressed corrections to the TC and TV pion-nucleon couplings and to the photon-nucleon coupling. At this order, one has the contribution from diagram 6.5(c), with the TV isovector coupling $\bar{g}_1$, defined in Eqs. (4.1.27) and (4.4.4). At the same order, one has to consider diagram 6.5(b) with the leading

TV coupling $\bar{g}_0$, and the isospin breaking pion-nucleon coupling β_1, defined in Eq. (4.1.21), These two diagrams can be accounted for by replacing in Eq. (6.4.3) $\bar{g}_1$ with $\bar{g}_1 + \bar{g}_0\beta_1/2g_A$. There is a further isospin breaking contribution, coming from the nucleon mass difference. With the field redefinition of [138], which eliminates the nucleon mass difference from the nucleon propagator and the asymptotic states, this contribution manifests in a diagram with the same topology of diagram 6.5(b). The TC pion-nucleon coupling is a new isospin breaking coupling, induced by the field redefinition and proportional to δm_N, which is given in Eq. (G.3). The contribution to the deuteron EDFF from isospin-breaking effects is then

$$F_D^\varepsilon(\vec{q}^2) = -\frac{e g_A \bar{g}_0 m_N}{6\pi F_\pi^2 m_\pi}\left[\left(\frac{\bar{g}_1}{\bar{g}_0} + \frac{\beta_1}{2g_A}\right)\frac{1+\xi}{(1+2\xi)^2}F_2(x) + \frac{\delta m_N}{m_N}\frac{1}{1+2\xi}F_4(x)\right], \quad (6.6.3)$$

where the new two-loop function $F_4(x)$ is

$$F_4(x) = 1 - x^2\frac{20+166\xi+105\xi^2}{60(1+2\xi)^2} + \mathcal{O}(x^4). \quad (6.6.4)$$

It is interesting to compare the isospin-breaking contributions (6.6.3) to the non-analytic, NLO correction to the isoscalar nucleon EDM. At $x = 0$, the term proportional to δm_N in Eq. (6.6.3) is approximately 1/5 of the analogous δm_N term in Eq. (6.6.2), which, in its turn, is about 15 % of the largest non-analytic contribution to D_0. We can safely neglect it.

As discussed in Sec. 4.4, the ratios $\bar{g}_1/\bar{g}_0$ and $\beta_1/2g_A$ could both, in principle, be extracted by TC isospin breaking observables. In practice, this would require the evaluation of isospin violating observables at rather high order, and a precise extraction is, at present, not possible. Thus, we cannot, at the moment, do better than power counting. By replacing $\bar{g}_1/\bar{g}_0$ and $\beta_1/2g_A$ with their power counting estimate $\varepsilon m_\pi^2/M_{QCD}^2 \approx 10^{-2}$ (which is compatible with bounds on β_1 from phase shift analysis of nucleon-nucleon scattering), one finds that the contribution of Eq. (6.6.3) to the deuteron EDM is approximately 20 % of the non-analytic contribution to D_0 in (6.6.2). Isospin-breaking effects, then, do not modify the fact that, for TV

from the $\bar{\theta}$ term, the deuteron EDM is well approximated by the isoscalar nucleon EDM.

As we noted in Sec. 4.4, in the case of the QCD $\bar{\theta}$ term several derivative TV pion-nucleon couplings come into play at the same level as $\bar{g}_1$, in particular relativistic, $1/m_N^2$, corrections to $\bar{g}_0$. These interactions might contribute to the EDM at NLO, together with relativistic corrections to TC pion-nucleon vertex, to the nucleon-photon vertex (the spin-orbit interaction in Eq. (3.3.19)), and to the contact interaction C_{0s}.

The full calculation of the deuteron EDM from relativistic corrections is not complete yet. Here we simply quote a partial result to corroborate the discussion on the size of the counterterm $\bar{D}_{NN}$ of Sec. 6.2. We computed the correction due to the spin-orbit coupling of the nucleon to the photon, followed by a TV one-pion exchange, with the leading coupling $\bar{g}_0$, represented by diagram 6.5(a). While there are several other relativistic corrections, no other comes with the isoscalar anomalous magnetic moment κ_0, so, while large cancellations are in general possible, the part of the result proportional to κ_0 will not be affected. We find that the diagram has a logarithmic divergence. At $\vec{q}^{\,2} = 0$, the contribution to EDM is

$$\begin{aligned} d_d^{\text{spin-orbit}} &= \frac{e g_A \bar{g}_0 \gamma}{4\pi F_\pi^2 m_N} \left(1 + \kappa_0 - \frac{1}{2}\right) \left\{ -\frac{1-2\xi}{1+2\xi} \right. \\ &\quad \left. + \left[\frac{1}{d-4} + \gamma_E - \log\pi - \frac{4}{3} + \log\left(\frac{m_\pi + 2\gamma}{\mu}\right)^2 \right] \right\}. \end{aligned} \tag{6.6.5}$$

The divergence only affects the deuteron EDM, not the momentum dependence, and it can be absorbed by the short-range, four-nucleon current $\bar{D}_{NN}$, whose contributions, in the PDS scheme, is

$$F_D^{\text{short}}(\vec{q}^{\,2}) = \gamma\, \bar{D}_{NN}(\mu) \frac{(\mu - \gamma)^2}{2\pi}. \tag{6.6.6}$$

The evaluation of the remaining contributions to the deuteron EDM from relativistic corrections to g_A, $\bar{g}_0$ and C_{0s} is in progress.

Chapter 7

The Nuclear TV Potential

7.1 Introduction

We can summarize the results of Chapters 5 and 6 by saying that the observation of the neutron and proton EDM alone does not provide enough information to unequivocally determine the dominant source of TV at high energy. Experiments with nuclei have the potential to offer valuable complementary evidences, and to enable a more complete picture of T violation to emerge.

Nuclear EDMs and other moments receive various contributions. There are, of course, contributions from the individual nucleons' EDMs. In the deuteron, as detailed in Chapter 6, the isovector component cancels, while in ^{3}He one can expect a cancellation between the contributions of the two nearly anti-aligned protons. Thus, nuclear EDMs, in particular the deuteron's [194, 42], are sensitive to a different combination of hadronic TV parameters than the neutron EDM. However, these one-nucleon contributions are modified from their "in-vacuum" counterparts because the nucleons are not free but bound in the nucleus. There are many-nucleon effects that are TV. First, the TV component of the pion cloud can generate a TV pion-exchange interaction among nucleons, and no symmetry forbids interactions of shorter range, either. These TV nuclear forces will mix in components of the nuclear wave function that do not appear in the absence of TV. It is a source of polarization effects for the entire nucleus. Second, there maybe multi-nucleon contributions to the TV coupling of the photon; such TV currents can be generated by either pion exchange or shorter-range dynamics.

TV one-pion exchange (OPE) has long been recognized as an important component of the TV two-nucleon (NN) potential, and expressed [195, 196] in terms of three non-derivative pion-nucleon couplings [197], associated with isospin $I = 0, 1, 2$.

So far, the analysis of TV nuclear effects has been based on tree-level potentials where OPE is sometimes supplemented by the single exchange of heavier mesons, the eta [198], rho [199], and omega [199] being most popular. Allowing sufficiently many couplings of these mesons to nucleons one can produce [159] the most general short-range TV NN local interaction with one derivative [200]. This is the TV analog of the Desplanques-Donoghue-Holstein (DHH) approach [201] for nuclear TC P violation (PV).

The contributions from such potentials to the deuteron and ^{3}He EDMs have been calculated in the literature under various assumptions. OPE from the $I = 2$ TV pion-nucleon coupling does not contribute to the NN system at tree level. It was noticed early on [202] that OPE from the $I = 0$ TV pion-nucleon coupling does not contribute to the deuteron EDM, either, but it does for ^{3}He, where it was estimated with a phenomenological strong-interaction potential [203]. The deuteron EDM that arises from an $I = 1$ TV exchange of either pion- or shorter-range, together with a separable strong-interaction potential, was calculated in Ref. [202]. The effects of OPE on the deuteron EDM and MQM were calculated using both zero-range and phenomenological strong-interaction potentials in Ref. [157, 158]. More recent calculations of the deuteron EDM and MQM [159] and of the ^{3}He EDM [161] have considered other TV contributions besides those from the TV potential, and used more modern, "realistic" strong-interaction potentials. Meson-exchange currents were found small in the deuteron [159], and neglected in ^{3}He [161]. The TV-potential contributions are consistent with earlier results; they are dominated by OPE from the $I = 1$ pion-nucleon coupling in the case of the deuteron [159], and from all three pion-nucleon couplings in the case of ^{3}He [161].

TV moments of heavier nuclei are more difficult to calculate. It has been argued [195] that the TV potential can lead to an enhancement over the nucleon EDM thanks to the near-degeneracy of levels of opposite parity, while meson-exchange currents are comparatively small. The size of the effect can be estimated through the single-

particle potential obtained by averaging the NN potential over a closed nuclear core. The OPE from the $I = 0, 2$ pion-nucleon couplings are proportional to the nuclear I_3, $(N-Z)/A$ [195, 196, 204], while the OPE from the $I = 1$ coupling does not have such a suppressing factor [196, 204]. It has also been found that the matrix elements from the rho and omega are small compared to the $I = 1$ pion contribution [199]. EDMs and MQMs (for example from $I = 0$ OPE [195]) and SMs [205, 206, 207] of several interesting nuclei have been estimated. A sample of recent SM calculations can be found in Refs. [86, 208, 209]. There are, of course, other nuclear tests of TV, see for example Ref. [210]. The most promising for effects of the TV nuclear interaction seems to be neutron scattering [211]. On the proton, TV neutron scattering is again dominated by OPE, but sensitive mostly to the $I = 0, 2$ couplings [160]. For heavy nuclei, one can again obtain estimates using the single-particle potential [196, 210].

For consistency, we would like to describe nuclear TV observables in the same framework used for the calculation of the nucleon EDM. The non-analytic behavior of the nucleon EDM in m_π and the dominance of OPE in nuclear observables point to the need of a framework that can account for both effects simultaneously, with chiral symmetry playing a central role. In fact, the dimension 4 and dimension 6 sources of T violation that we consider have specific chiral properties, which imply that neither all pion-nucleon interactions are allowed, nor all allowed forms have the same strength. Here we use the chiral Lagrangian built in Chapter 4, where TV interactions stemming from the $\bar{\theta}$ term and the dimension 6 sources of T violation have been constructed and ordered according to the same power counting used to order TC interactions in χPT.

In addition to consistency between one- and few-nucleon TV interactions, nuclear TV also requires consistency between TV and TC forces, in order there to be no mismatch in the off-shell behaviors of the various ingredients. Of course, off-shell effects are dependent on the choice of fields, while physical quantities are not, provided the same choice of fields has been made throughout the calculation. As far as TV

nuclear interactions are concerned, phenomenological TC models bring additional uncertainties, such as the choice of zero-range or finite-range interactions and the role of heavy mesons. On the other hand, χPT has been extended to multi-nucleon systems [100, 37, 38], leading to the derivation of TC nuclear forces and currents. This opens the possibility of describing all necessary ingredients in a single framework.

The goal of this Chapter is to provide the first step in the extension of TV interactions in the EFT to the multi-nucleon sector. The TV nuclear potential is the most important ingredient in this extension. Most of the Chapter is dedicated to the TV potential from the QCD $\bar{\theta}$ term at N^{2}LO. For this source, it is necessary to work at high order because the $I = 1$ pion-nucleon TV coupling, which is the only non-derivative coupling that in nuclei is not suppressed by the factor $(N-Z)/A$, does not appear in the leading order Lagrangian. As we are going to see, new elements appear with respect to phenomenological treatments, such as two-pion exchange (TPE) at the same level as short-range interactions representing heavier-meson exchange. In the case of the qCEDM, the gCEDM and the TV four-quark operators it is enough to consider the LO TV potential. These TV potentials have to be used, for example, with the TC, parity-conserving (PC) potentials from Refs. [212, 213, 214, 215, 216, 217, 218, 219, 220, 145, 148, 149, 221, 222, 223, 138, 153, 154]. The construction here is similar to that of the TC PV potential [90, 224, 225, 226, 227], which extends the EFT from the TC, PV one-nucleon sector [89, 183, 184, 228, 229, 229] to multi-nucleon systems. Such a framework provides an alternative to the DDH approach [201], allowing for a model-independent analysis of nuclear TC PV phenomena [231, 232, 233, 234, 235, 236, 237, 238, 239, 240, 241]. Our present TV PV EFT framework stands in respect to previous approaches like this TC PV EFT framework with respect to the DDH approach.

The Chapter is organized as follows. In Sec. 7.2 we briefly consider processes involving momenta below $M_{nuc} \sim 100$ MeV, for which pion degrees of freedom can be integrated out, and we list the dominant TV contact interactions for various sources

of T violation. The nuclear potential from the QCD $\bar{\theta}$ term to subleading order in χPT is then presented in momentum (Sec. 7.3) and coordinate (Sec. 7.4) spaces. (We relegate details of the Fourier transformation to Appendix K.) In Sec. 7.3.1, we derive the LO potential from the qCEDM and the chiral invariant, dimension 6 sources of T violation. In Sec. 7.5 we discuss the size of different components of the potential, and we draw our conclusions in Sec. 7.6.

7.2 Pionless Theory

Before we discuss the TV potential in χPT, it is educative to consider a much simpler EFT. At momenta much smaller than the pion mass, pion degrees of freedom can be integrated out and one is left with a pionless EFT, in which the interactions are represented by operators involving only nucleon fields. If we denote by $M_{nuc} \sim 100$ MeV the scales associated with pion physics, this EFT applies to processes where all momenta $Q \ll M_{nuc}$. Power counting in this EFT is reviewed in Ref. [100, 37, 38].

The lowest-order TC two-nucleon interactions can be taken as [35, 36]

$$\mathcal{L}^{(0)}_{\not\pi,T} = -\frac{C_{11}}{2}\bar{N}N\bar{N}N - \frac{C_{\tau\tau}}{2}\bar{N}\boldsymbol{\tau}N\cdot\bar{N}\boldsymbol{\tau}N, \tag{7.2.1}$$

where $C_{11,\tau\tau} = \mathcal{O}(4\pi/m_N\aleph)$, with $\aleph < M_{nuc}$ a low-energy scale. The corresponding potential in momentum space is simply

$$V^{(0)}_{\not\pi,T} \;=\; \frac{1}{2}\left[C_{11} + C_{\tau\tau}\boldsymbol{\tau}^{(1)}\cdot\boldsymbol{\tau}^{(2)}\right], \tag{7.2.2}$$

where $\tau^{(i)}/2$ is the isospin of nucleon i. These interactions affect only the two S waves. Since the effect of free two-nucleon propagation is $\sim m_N Q/4\pi$, for momenta $Q \gtrsim \aleph$ these interactions have to be iterated to all orders [187, 242]. Using dimensional regularization with power divergence subtraction [187, 189] at a scale μ,

$$C_{0s} = C_{11} - 3C_{\tau\tau} = \frac{4\pi}{m_N}\left(\frac{1}{a_s} - \mu\right)^{-1}, \quad C_{0t} = C_{11} + C_{\tau\tau} = \frac{4\pi}{m_N}\left(\frac{1}{a_t} - \mu\right)^{-1}, \tag{7.2.3}$$

in terms of the isospin-singlet ($^3S_1$) and -triplet ($^1S_0$) scattering lengths, a_s and a_t. Because the coefficients $C_{11,\tau\tau}$ subsume physics at the scale of the pion mass, their scaling is different from the one in the pionful EFT.

In leading order, the $\bar{\theta}$ term, the qCEDM and the chiral-invariant TV sources induce TV four-nucleon operators similar to those in Eq. (6.2.5):

$$\begin{aligned}\mathcal{L}_{\not{\pi},\not{T}} &= \bar{C}_{11}\bar{N}N\,\partial_\mu(\bar{N}S^\mu N)+\bar{C}_{\tau\tau}\bar{N}\vec{\tau}N\cdot\partial_\mu(\bar{N}S^\mu\vec{\tau}N)\\ &\quad+\bar{C}_{\tau 1}\bar{N}\tau_3 N\,\partial_\mu(\bar{N}S^\mu N)+\bar{C}_{1\tau}\bar{N}N\partial_\mu(\bar{N}S^\mu\tau_3 N),\end{aligned}\tag{7.2.4}$$

where $\bar{C}_{11,\tau\tau}$ and $\bar{C}_{1\tau,\tau 1}$ are new short-range parameters. In momentum space the interaction Hamiltonian is given by

$$\begin{aligned}V_{\not{\pi},\not{T}}(\vec{q}) &= -\frac{i}{2}\left[\bar{C}_{11}+\bar{C}_{\tau\tau}\boldsymbol{\tau}^{(1)}\cdot\boldsymbol{\tau}^{(2)}\right]\left(\vec{\sigma}^{\,(1)}-\vec{\sigma}^{\,(2)}\right)\cdot\vec{q}\\ &\quad-\frac{i}{4}\left(\bar{C}_{1\tau}+\bar{C}_{\tau 1}\right)\left(\tau_3^{(1)}+\tau_3^{(2)}\right)\left(\vec{\sigma}^{\,(1)}-\vec{\sigma}^{\,(2)}\right)\cdot\vec{q}\\ &\quad-\frac{i}{4}\left(\bar{C}_{1\tau}-\bar{C}_{\tau 1}\right)\left(\tau_3^{(1)}-\tau_3^{(2)}\right)\left(\vec{\sigma}^{\,(1)}+\vec{\sigma}^{\,(2)}\right)\cdot\vec{q},\end{aligned}\tag{7.2.5}$$

where $\vec{\sigma}^{\,(i)}/2$ is the spin of nucleon i and $\vec{q}=\vec{p}_1-\vec{p}\,'_1=\vec{p}\,'_2-\vec{p}_2$ is the momentum transfer. In nucleon-nucleon scattering, operators that break P and T induce mixing between waves of different parity. At low energy, the most relevant effect is the mixing between S and P waves, and indeed the single momentum in Eq. (7.2.5) can only connect an S to a P wave. At leading order, the P wave is free. Since the short-range TV potential involves one S wave, we expect [100, 37, 38] in the pionless EFT that the coefficients $\bar{C}_{ij}$ scale as $1/\aleph$. Indeed, the amplitude for a nucleon-nucleon transition can be computed from Eq. (7.2.5) as done in the PV case in Refs. [90, 231, 232, 233, 234]. In leading order, it involves one insertion of the TV operators $\bar{C}_{ij}$, dressed by the all-order iteration of the appropriate S-wave operator, C_{0s} or C_{0t}. The renormalization-group invariance of the amplitude implies that the $\bar{C}_{ij}$ follow a renormalization-group equation of the form $d(\bar{C}_{ij}/C_0)/d\ln\mu=0$, which is satisfied if

the four independent parameters are taken to be

$$\bar{C}_{1s} = \bar{C}_{11} - 3\bar{C}_{\tau\tau} = \frac{4\pi\bar{c}_s}{m_N}\left(\frac{1}{a_s} - \mu\right)^{-1},\ \bar{C}_{1t} = \bar{C}_{11} + \bar{C}_{\tau\tau} = \frac{4\pi\bar{c}_t}{m_N}\left(\frac{1}{a_t} - \mu\right)^{-1},$$
$$\bar{C}_{3s} = \bar{C}_{1\tau} - \bar{C}_{\tau 1} = \frac{4\pi\bar{c}_{3s}}{m_N}\left(\frac{1}{a_s} - \mu\right)^{-1},\ \bar{C}_{3t} = \bar{C}_{1\tau} + \bar{C}_{\tau 1} = \frac{4\pi\bar{c}_{3t}}{m_N}\left(\frac{1}{a_t} - \mu\right)^{-1} \quad (7.2.6)$$

in terms of four μ-independent coefficients $\bar{c}_{s,t,3s,3t}$. As in the TC sector, the scaling of the short-range parameters is different in the pionless EFT than in ChPT. We can write

$$\bar{C}_{11,\tau\tau} = \mathcal{O}\left(\frac{4\pi}{m_N \aleph}\bar{c}_{s,t}\right), \qquad \bar{C}_{1\tau,\tau 1} = \mathcal{O}\left(\frac{4\pi}{m_N \aleph}\bar{c}_{3s,3t}\right). \quad (7.2.7)$$

In order to estimate the coefficients $\bar{c}_{s,t,3s,3t}$, we use naive dimensional analysis [123] with the pionful EFT as the underlying theory. We then find that at leading order the isoscalar $\bar{c}_{s,t}$ receive contributions from all the sources,

$$\bar{c}_{s,t} = \mathcal{O}\left(\frac{\bar{\theta}}{M_{QCD}}, (\tilde{\delta}_0 + \varepsilon\tilde{\delta}_3)\frac{M_{QCD}}{M_T^2}, w\frac{M_{QCD}}{M_T^2}\right), \quad (7.2.8)$$

while the isospin-breaking $\bar{c}_{3s,3t}$ only from the dimension-6 sources,

$$\bar{c}_{3s,3t} = \mathcal{O}\left(\tilde{\delta}_3\frac{M_{QCD}}{M_T^2}, \varepsilon w\frac{M_{QCD}}{M_T^2}\right). \quad (7.2.9)$$

In general, one would expect five possible amplitudes connecting S to P waves [159, 160]: three —one for each possible value of $I_3 = 1, 0, -1$— to describe the mixing of the isotriplet ${}^1S_0$ and ${}^3P_0$ waves, one for the mixing of the isosinglet ${}^3S_1$ and ${}^1P_1$ states, and one for the mixing of nucleons in the ${}^3S_1$ configuration with the isotriplet ${}^3P_1$ wave. The $\bar{\theta}$ term yields a short-range potential in the form of the isospin-conserving terms of Ref. [159]. Because the TV operator in Eq. (3.4.15) is isoscalar and isospin violation is a subleading effect in ChPT, for which the pionless EFT is the low-energy limit, the $\bar{\theta}$ term does not contribute at leading order to quantities that violate both T and isospin. The two terms contribute to ${}^3S_1$–${}^1P_1$ mixing and to ${}^1S_0$–${}^3P_0$ mixing, in equal way for the three I_3 configurations. The ${}^3S_1$–${}^3P_1$ mixing vanishes at leading order, a fact that has important consequences for the estimate

of the deuteron EDM [42]. If $\tilde{\delta}_3$ and ε are different from zero, the qCEDM and the chiral-invariant TV sources also contribute to isospin-breaking TV observables at leading order. The operator $\bar{C}_{3t}$ is proportional to the third component of the total isospin of the two-nucleon pair, and thus it does contribute to ${}^1S_0$–${}^3P_0$ mixing, but only for $I_3 = \pm 1$. $\bar{C}_{3s}$ is instead proportional to the total spin of the two nucleons, and it is relevant to ${}^3S_1$–${}^3P_1$ mixing, and, consequently, to the deuteron EDM.

7.3 The TV Potential in Momentum Space

In processes involving momenta $Q \sim M_{nuc}$, which presumably comprise the bound states of most nuclei, pion effects are important and pion degrees of freedom should be included explicitly in the theory. In this Section we use the interactions given in Chapters 3 and 4 to compute the TV nuclear potential from the QCD $\bar{\theta}$ term in momentum space up to $\nu = 3$, that is, including corrections of $\mathcal{O}(Q^2/M_{QCD}^2)$ with respect to the leading TV potential. For the $\bar{\theta}$ term, it is important to work at this accuracy, since the isovector coupling $\bar{g}_1$ only appears in the N^{2}LO Lagrangian. Therefore, for observables which are particularly sensitive to $\bar{g}_1$, as for example the deuteron EDM, a consistent calculation in the Weinberg power counting requires the knowledge of the full TV potential at N^{2}LO. We will return to the dimension 6 sources of T violation in Sec. 7.3.1. In this case, it is sufficient to work at LO, either because the interesting couplings $\bar{g}_0$ and $\bar{g}_1$ are both leading, as in the case of the qCEDM, or because, in the case of chiral invariant TV sources, short-distance effects overshadow the importance of corrections to the leading TV potential.

In the lowest orders, the TV nuclear potential involves only two nucleons. We write the two incoming momenta as $\vec{p}_1 = \vec{P}/2 + \vec{p}$ and $\vec{p}_2 = \vec{P}/2 - \vec{p}$, and the two outgoing momenta as $\vec{p}_1' = \vec{P}/2 + \vec{p}'$ and $\vec{p}_2' = \vec{P}/2 - \vec{p}'$. The potential in momentum space can be expressed as function not only of the momentum transfer $\vec{q} = \vec{p} - \vec{p}'$, but also of the center-of-mass momentum $\vec{P}$ and of the variable $\vec{K} = (\vec{p} + \vec{p}')/2$: $V_{\not T} = V_{\not T}(\vec{q}, \vec{K}, \vec{P})$. Expressions for the potential in the center-of-mass frame are obtained

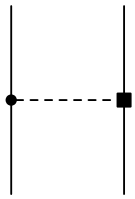

FIGURE 7.1. OPE diagrams contributing to the leading TV two-nucleon potential. The solid and dashed lines represent nucleon and pion, respectively; a square stands for the TV pion-nucleon coupling $\bar{g}_0$ in $\mathcal{L}^{(1)}_{\not T,\pi N}$ (4.4.7), while the filled circle represents an interaction from $\mathcal{L}^{(0)}_{\chi,f\leq 2}$ (3.3.17). Only one possible ordering is shown.

by setting $\vec{P}=0$. Notice that although some of the terms below vanish in the center-of-mass frame, they can be relevant to the calculation of the TV electromagnetic form factors of deuteron, or for calculations of T violation in nuclei with $A>2$, where the interaction with the photon or other nucleons changes the center-of-mass momentum of the nucleon pair.

In leading order, the TV nuclear potential comes from the OPE diagrams of Fig. 7.1, with TC and TV pion-nucleon interactions taken from $\mathcal{L}^{(0)}_{\chi,f\leq 2}$ and $\mathcal{L}^{(1)}_{\not\chi,f=2}$ in Eqs. (3.3.17) and (4.1.19), respectively. The strong-interaction vertex introduces a factor of $g_A Q/F_\pi$, while the TV vertex brings in a factor $\bar{g}_0 \propto m_\pi^2/M_{QCD}$. As a result this contribution goes as M_{QCD}^{-1} and it is of order $\nu=1$. In momentum space, the expression for the potential is simply

$$V_{\not T}^{(1)} = i\frac{g_A\bar{g}_0}{F_\pi^2}\boldsymbol{\tau}^{(1)}\cdot\boldsymbol{\tau}^{(2)}\left(\vec{\sigma}^{(1)}-\vec{\sigma}^{(2)}\right)\cdot\frac{\vec{q}}{\vec{q}^{\,2}+m_\pi^2}, \tag{7.3.1}$$

which agrees with Ref. [195]. Just like the potential (7.2.5) in the pionless theory, this OPE potential contributes to ${}^1S_0$–${}^3P_0$ and ${}^3S_1$–${}^1P_1$ mixing, but not to the isospin-violating ${}^3S_1$–${}^3P_1$ mixing. At this order, there is a single unknown TV parameter, $\bar{g}_0$. Contrary to the PC, TC case [100, 37, 38] and more like the PV, TC potential [90], pion physics is enhanced relative to short-range physics due to the absence of a derivative in the simplest pion-nucleon TV interaction and the presence of one in the simplest TV two-nucleon contact interaction.

The next contributions to the TV potential appear at orders $\nu = 2, 3$. According to Eq. (3.3.15), corrections at these orders come from one-loop diagrams involving $\mathcal{L}^{(0)}_{\chi,\leq 2}$ and $\mathcal{L}^{(1)}_{\chi,f=2}$ only, and tree diagrams with insertions of higher-order terms. The tree contributions come from the four-nucleon TV operators in $\mathcal{L}^{(3)}_{\chi,f=4}$, Eq. (4.1.44), and from OPE diagrams in which either the TC or the TV vertices originate in the power-suppressed $f \leq 2$ Lagrangians.

The most important loop diagrams are from TPE, depicted in Fig. 7.2. The T-odd pion-nucleon coupling $\bar{g}_0$ and one of the strong-interaction vertices bring in a factor of $\bar{g}_0 g_A/F_\pi^2$. The other two vertices of the box and crossed diagrams of Fig. 7.2 are strong-interaction pion-nucleon vertices from Eq. (3.3.17), and combined with the $(4\pi)^2$ from the loop integration, they yield the suppression factor $g_A^2/(4\pi F_\pi)^2 \sim 1/M_{QCD}^2$. For the triangle diagrams, the seagull vertex is the Weinberg-Tomozawa term, also from Eq. (3.3.17), which brings in a factor of $1/F_\pi^2$ that, combined with the $(4\pi)^2$ from the loop, also leads to a suppression of $1/(4\pi F_\pi)^2 \sim 1/M_{QCD}^2$. All these diagrams are thus of order M_{QCD}^{-3}. Care of course has to be taken with the subtraction from the box diagrams in Fig. 7.2 and the iterated static OPE, which is infrared enhanced and already included in the computation of wave functions. Following the procedure described for instance in Ref. [90], the subtraction is accomplished by exploiting the identity

$$\frac{i}{-v\cdot k + i\varepsilon} = -\frac{i}{v\cdot k + i\varepsilon} + 2\pi\delta(v\cdot k). \tag{7.3.2}$$

When Eq. (7.3.2) is used in place of one of the nucleon propagators in the box diagrams, the first term on the right hand side leads to a contour integral over the 0th component of the loop momentum, which can be performed without picking up the nucleon poles and is free of the infrared enhancement discussed in Sec. 3.3, while the delta function corresponds to the two-nucleon pole and must be discarded in the calculation of the potential. For the crossed-box and triangle diagrams, instead, it is always possible to avoid the nucleon poles, and these diagrams only contribute to the potential.

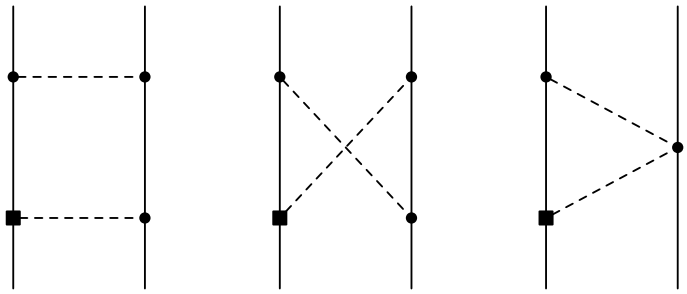

FIGURE 7.2. Box, crossed and triangle TPE diagrams contributing to the subleading TV two-nucleon potential. Notation as in Fig. 7.1. Only one possible ordering per topology is shown.

The TPE diagrams in Fig. 7.2 are ultraviolet divergent. We regulate them in dimensional regularization in d spacetime dimensions, where divergences get encoded in the factor

$$L = \frac{2}{4-d} - \gamma_E + \ln 4\pi, \tag{7.3.3}$$

where γ_E is the Euler constant. We denote by μ the renormalization scale. Proper renormalization requires that sufficiently many counterterms appear at the same order to compensate for the L and μ dependence of the loops. Indeed, here this dependence can be absorbed by the renormalization of the contact interaction $\bar{C}_2$ from $\mathcal{L}^{(3)}_{\chi,\, f=4}$, Eq. (4.1.44), which we do by redefining it through

$$\bar{C}_2 \to \bar{C}_2 + \frac{2 g_A \bar{g}_0}{F_\pi^2} \frac{1}{(2\pi F_\pi)^2} \left[\left(3 g_A^2 - 1\right) \left(L + \ln \frac{\mu^2}{m_\pi^2} \right) + 2 \left(g_A^2 - 1 \right) \right]. \tag{7.3.4}$$

Note that we chose to absorb in $\bar{C}_2$ some finite constant pieces. TPE graphs do not renormalize the coupling $\bar{C}_1$ at this order. With this redefinition, the contact interactions yield the short-range potential

$$V^{(3)}_{T,\mathrm{SR}}(\vec{q}) = -\frac{i}{2} \left[\bar{C}_1 + \bar{C}_2 \, \boldsymbol{\tau}^{(1)} \cdot \boldsymbol{\tau}^{(2)} \right] \left(\vec{\sigma}^{\,(1)} - \vec{\sigma}^{\,(2)} \right) \cdot \vec{q}, \tag{7.3.5}$$

which is formally identical to the leading potential in the pionless EFT, Eq. (7.2.5). The couplings, however, are different. We can see from Eq. (7.3.4) that the natural size of the coefficients $\bar{C}_i$ is, as advertised, $\bar{\theta} m_\pi^2 / F_\pi^2 M_{QCD}^3$, implying a suppression of Q^2/M_{QCD}^2 with respect to TV OPE.

Once the divergent, short-range part of TPE has been lumped with the contact terms, we are left with the non-analytic contributions of medium range,

$$V^{(3)}_{\not T,\mathrm{MR}} = -i\frac{2\bar{g}_0 g_A}{F_\pi^2}\frac{1}{(2\pi F_\pi)^2}\boldsymbol{\tau}^{(1)}\cdot\boldsymbol{\tau}^{(2)}\left(\vec{\sigma}^{(1)}-\vec{\sigma}^{(2)}\right)\cdot\vec{q}\left[2g_A^2\,B\left(\frac{\vec{q}^{\,2}}{4m_\pi^2}\right)-T\left(\frac{\vec{q}^{\,2}}{4m_\pi^2}\right)\right], \tag{7.3.6}$$

in terms of the functions

$$T(x)=\sqrt{\frac{1+x}{x}}\ln\left(\sqrt{x}+\sqrt{1+x}\right)=\frac{1+x}{1+\frac{3}{2}x}B(x), \tag{7.3.7}$$

As the leading OPE potential, Eq. (7.3.1), the TPE potential is a function only of the momentum transfer $\vec{q}$. The scale of momentum variation is, as one would expect, $2m_\pi$. TPE and leading OPE share the same spin-isospin structure, which means they can only be separated if we can probe their different momentum dependences.

A much richer structure arises from the remaining $\nu \leq 3$ contributions to the two-nucleon TV potential, which come from the OPE diagrams depicted in Fig. 7.3. Double-circled vertices in the first two diagrams denote $\mathcal{O}(Q^2/M_{QCD}^2)$ corrections to the TV and TC pion-nucleon couplings, given by the operators in the Lagrangians $\mathcal{L}^{(1,2)}_{\chi,\,f=2}$, $\mathcal{L}^{(1,2)}_{\not I,\,f\leq 2}$, $\mathcal{L}^{(3)}_{\chi^1,\,f=2}$ and $\mathcal{L}^{(3)}_{\chi^2,\,f=2}$ found in Eqs. (3.3.18), (3.3.19), (G.3), and Eqs. (4.1.24) and (4.1.27) (the effects of the elimination of the tadpoles on Eq. (4.1.27) are summarized in Eq. (4.3.17)). The last diagram is proportional to corrections to the pion mass in $\mathcal{L}^{(2)}_{\chi,\,f=0}$ and $\mathcal{L}^{(1,2)}_{\not I,\,f\leq 2}$, and to the nucleon mass difference in $\mathcal{L}^{(1,2)}_{\not I,\,f\leq 2}$. Note that there are no further loop diagrams to consider explicitly. The loop diagrams involving the leading S-wave TC four-nucleon operators and a TV pion exchange all vanish. The analysis of [124, 125, 126] showed that some P-wave four-nucleon operators are less suppressed than expected on the grounds of naive dimensional analysis, and they must be included in the leading order $f = 4$ Lagrangian. Loop diagrams with these P-wave operators and a TV pion exchange do not vanish. However, these diagrams do not depend on the momentum transfer $\vec{q}$ and they simply renormalize the couplings $\bar{C}_1$ and $\bar{C}_2$. We do not explicitly compute their contribution.

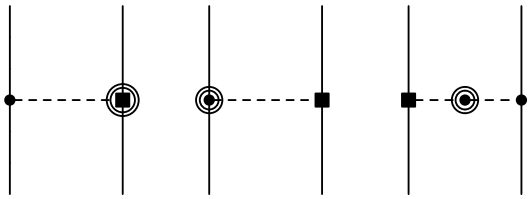

FIGURE 7.3. OPE corrections to the TV two-nucleon potential up to order $\mathcal{O}(Q^3/M_{QCD}^3)$. The double circles denote vertices in the $\Delta = 1, 2$ TC chiral Lagrangians, $\mathcal{L}^{(1)}_{\chi,\,f=2}$ (3.3.18), $\mathcal{L}^{(2)}_{\chi,\,f=2}$ (3.3.19), and $\mathcal{L}^{(1,2)}_{\not I,\,f\leq 2}$ (G.3). The double-circled square denote vertices from the $\Delta = 3$ TV Lagrangians, $\mathcal{L}^{(3)}_{\chi^1,\,f=2}$ (4.1.24) and $\mathcal{L}^{(3)}_{\chi^2,\,f=2}$ (4.1.27). Other notation as in Fig. 7.1.

Corrections that originate in the pion mass are closely connected to the leading OPE, Eq. (7.3.1). At the order we are considering, the pion mass receives corrections from one-loop diagrams, which we absorb [30, 31] in the renormalization of the coupling Δm_π^2 in Eq. (4.1.4). With the definitions of Eqs. (3.3.17), (3.3.21), (4.1.4), and (4.1.9), the physical masses of the neutral and charged pions are, respectively, $m_{\pi^0}^2 = m_\pi^2 + \Delta m_\pi^2 - \delta m_\pi^2 = (135\text{ MeV})^2$ and $m_{\pi^\pm}^2 = m_\pi^2 + \Delta m_\pi^2 + \breve{\delta} m_\pi^2 = (139.6\text{ MeV})^2$ [1]. The isospin-symmetric correction to the pion mass can be accounted at $\nu = 3$ by substituting $m_\pi^2 \to m_\pi^2 + \Delta m_\pi^2$ in the leading order TV potential. Isospin-breaking corrections come from the different masses of the neutral and charged pions. With the assumption $\alpha_{\rm em}/\pi \sim \varepsilon m_\pi^3/M_{QCD}^3$, which is numerically reasonable, the pion mass splitting is dominated by the electromagnetic contribution $\breve{\delta} m_\pi^2$, which gives rise to a potential of order $\nu = 2$. The quark mass difference δm_π^2 contributes at $\nu = 3$, when one should also consider diagrams with two insertions of $\breve{\delta} m_\pi^2$. The sum of these components generates two structures, an isoscalar

$$\begin{aligned} V_{\not I\not I,\mathrm{a}}^{(2+3)}(\vec{q}) &= -i\frac{\bar{g}_0 g_A}{3F_\pi^2}\boldsymbol{\tau}^{(1)}\cdot\boldsymbol{\tau}^{(2)}\left(\vec{\sigma}^{(1)}-\vec{\sigma}^{(2)}\right)\cdot\frac{\vec{q}}{(\vec{q}^{\,2}+m_\pi^2)^2} \\ &\quad\times\left(2\breve{\delta}m_\pi^2-\delta m_\pi^2-2\frac{(\breve{\delta}m_\pi^2)^2}{q^2+m_\pi^2}\right), \end{aligned} \tag{7.3.8}$$

and an isotensor

$$V^{(2+3)}_{\not{T}\not{P},\mathrm{b}}(\vec{q}) = i\frac{\bar{g}_0 g_A}{3F_\pi^2}\left(3\tau_3^{(1)}\tau_3^{(2)} - \boldsymbol{\tau}^{(1)}\cdot\boldsymbol{\tau}^{(2)}\right)\left(\vec{\sigma}^{(1)} - \vec{\sigma}^{(2)}\right)\cdot\frac{\vec{q}}{(\vec{q}^2 + m_\pi^2)^2} \times\left(\breve{\delta}m_\pi^2 + \delta m_\pi^2 - \frac{(\breve{\delta}m_\pi^2)^2}{q^2 + m_\pi^2}\right). \tag{7.3.9}$$

The isoscalar component, Eq. (7.3.8), can be expressed in a more convenient way by using the physical values of the neutral and charged pion mass in the leading potential, Eq. (7.3.1). We can write

$$V^{(1)}_{\not{T}}(\vec{q}) + V^{(2+3)}_{\not{T}\not{P},\mathrm{a}}(\vec{q}) = i\frac{\bar{g}_0 g_A}{3F_\pi^2}\boldsymbol{\tau}^{(1)}\cdot\boldsymbol{\tau}^{(2)}\left(\vec{\sigma}^{(1)} - \vec{\sigma}^{(2)}\right)\cdot\vec{q}\left(\frac{2}{\vec{q}^2 + m_{\pi^\pm}^2} + \frac{1}{\vec{q}^2 + m_{\pi^0}^2}\right), \tag{7.3.10}$$

which, expanding in $\breve{\delta}m_\pi^2$ and δm_π^2, reproduces Eq. (7.3.8). The combination of neutral and charged pion propagators in Eq. (7.3.10) represents an "average" pion static propagator, which naturally appears in the isoscalar contribution. Similarly, we can express the tensor component as

$$V^{(2+3)}_{\not{T}\not{P},\mathrm{b}}(\vec{q}) = -i\frac{\bar{g}_0 g_A}{3F_\pi^2}\left(3\tau_3^{(1)}\tau_3^{(2)} - \boldsymbol{\tau}^{(1)}\cdot\boldsymbol{\tau}^{(2)}\right)\left(\vec{\sigma}^{(1)} - \vec{\sigma}^{(2)}\right)\cdot\vec{q}\left(\frac{1}{\vec{q}^2 + m_{\pi^\pm}^2} - \frac{1}{\vec{q}^2 + m_{\pi^0}^2}\right). \tag{7.3.11}$$

In applications to nucleon-nucleon scattering, this tensor component would contribute at low energies to ${}^1S_0$–${}^3P_0$ mixing, affecting proton-proton and neutron-neutron ($I_3 = \pm 1$) and neutron-proton ($I_3 = 0$) scattering differently.

Corrections from the nucleon mass come in several guises. The use of a heavy-nucleon field ensures that the large scale m_N appears always in denominators. In the isospin-symmetric limit the first effects of m_N enter in the $\Delta = 1, 2$ TC Lagrangians, Eqs. (3.3.18) and (3.3.19), the two-derivative contribution to the $\Delta = 3$ TV Lagrangian, Eq. (4.1.24), and, via the on-shell condition for the nucleons, the energy of the potential pion propagator. They yield relativistic corrections to the leading OPE

with the same spin-isospin structure,

$$V^{(3)}_{\not\pi,\,\mathrm{a}}(\vec{q},\vec{K},\vec{P}) = -i\frac{g_A\bar{g}_0}{F_\pi^2 m_N^2}\boldsymbol{\tau}^{(1)}\cdot\boldsymbol{\tau}^{(2)}\left(\vec{\sigma}^{(1)}-\vec{\sigma}^{(2)}\right)\cdot\frac{\vec{q}}{\vec{q}^{\,2}+m_\pi^2} \times\left(\vec{K}^2+\frac{\vec{P}^2}{4}-\frac{1}{4}\frac{(\vec{P}\cdot\vec{q})^2}{\vec{q}^{\,2}+m_\pi^2}\right), \tag{7.3.12}$$

and with new structures,

$$\begin{aligned} V^{(3)}_{\not\pi,\mathrm{b}}(\vec{q},\vec{K},\vec{P}) &= -i\frac{g_A\bar{g}_0}{4F_\pi^2 m_N^2}\boldsymbol{\tau}^{(1)}\cdot\boldsymbol{\tau}^{(2)}\frac{1}{\vec{q}^{\,2}+m_\pi^2} \\ &\left\{\vec{P}\cdot\vec{q}\left[\left(\vec{\sigma}^{(1)}-\vec{\sigma}^{(2)}\right)\cdot\frac{\vec{P}}{2}+\left(\vec{\sigma}^{(1)}+\vec{\sigma}^{(2)}\right)\cdot\vec{K}\right]\right. \\ &\left.+i\vec{\sigma}^{(1)}\cdot\left[\vec{q}\times\left(\frac{\vec{P}}{2}+\vec{K}\right)\right]\vec{\sigma}^{(2)}\cdot\vec{q}+i\vec{\sigma}^{(1)}\cdot\vec{q}\,\vec{\sigma}^{(2)}\cdot\left[\vec{q}\times\left(\frac{\vec{P}}{2}-\vec{K}\right)\right]\right\}. \end{aligned} \tag{7.3.13}$$

This potential includes the contribution of the $1/m_N$ correction to g_A in Eq. (3.3.18). Naively, one would expect this correction to contribute at order $\nu = 2$; however the interaction brings in a factor of $v\cdot q$, which, for on-shell nucleons, becomes $v\cdot q = \vec{q}\cdot\vec{P}/2m_N$, suppressing the potential by a further factor of $1/m_N$. There is a subtlety in this argument. When one performs the integral involving both OPE with a pion energy in the numerator and another interaction in the potential, and picks the pion pole, one gets a one-loop contribution to the potential. However, by power counting, such diagrams are suppressed by a further Q/M_{QCD}. This of course does not preclude enhancements by factors of π that in principle might affect any χPT loop, but are hard to incorporate in power counting. The same on-shell condition was used to express $v\cdot q^2$ in the pion propagator in terms of the momentum of the nucleons.

Corrections to the nucleon mass can be removed from nucleon propagators by redefinitions of the nucleon field. The chiral-symmetry-breaking correction to the nucleon mass, Δm_N in Eq. (4.1.2), can be absorbed in m_N, $m_N \to m_N - \Delta m_N$, by a redefinition of the nucleon field of the same type of that which eliminates the mass from Eq. (3.3.17) in the first place. The isospin-violating nucleon mass splitting δm_N

can be dealt with the field redefinition of Ref. [138], which leads to Eq. (G.3). The corresponding potential linear in δm_N has a $1/m_N$ factor,

$$V^{(3)}_{\not T\not P,\mathrm{c}}(\vec{q},\vec{K},\vec{P}) = \frac{\bar{g}_0 g_A}{F_\pi^2}\frac{\delta m_N}{m_N}\frac{1}{\vec{q}^{\,2}+m_\pi^2}\left(\boldsymbol{\tau}^{(1)}\times\boldsymbol{\tau}^{(2)}\right)_3\left[\left(\vec{\sigma}^{(1)}+\vec{\sigma}^{(2)}\right)\cdot\vec{K} + \left(\vec{\sigma}^{(1)}-\vec{\sigma}^{(2)}\right)\cdot\left(\frac{\vec{P}}{2}+\frac{\vec{q}}{\vec{q}^{\,2}+m_\pi^2}\vec{P}\cdot\vec{q}\right)\right]. \tag{7.3.14}$$

This potential has the right quantum numbers to produce ${}^3S_1$–${}^3P_1$ mixing, and therefore must be included in a calculation of the deuteron EDM. Indeed, in the perturbative pion approach, one-pion exchange of the form (7.3.14) generates a NLO contribution to the deuteron EDM, as discussed in Sec. 6.6. In addition, there are terms quadratic in δm_N, which generates an additional contribution to the isoscalar and tensor potentials in Eqs. (7.3.8) and (7.3.9),

$$V^{(3)}_{\not T\not P,\mathrm{d}}(\vec{q}) = i\frac{\bar{g}_0 g_A}{3F_\pi^2}\delta m_N^2\left[2\boldsymbol{\tau}^{(1)}\cdot\boldsymbol{\tau}^{(2)}-\left(3\tau_3^{(1)}\tau_3^{(2)}-\boldsymbol{\tau}^{(1)}\cdot\boldsymbol{\tau}^{(2)}\right)\right] \times\left(\vec{\sigma}^{(1)}-\vec{\sigma}^{(2)}\right)\cdot\frac{\vec{q}}{(\vec{q}^{\,2}+m_\pi^2)^2}. \tag{7.3.15}$$

Finally we arrive at contributions from $\nu=3$ effects in the pion-nucleon vertices. At this order, several contributions can be absorbed into redefinitions of the couplings g_A, $\bar{g}_0$, and $\bar{C}_2$. One-loop corrections to g_A do not introduce any non-analytic contribution and, for an on-shell nucleon, they renormalize the coupling β_2 in Eq. (4.1.3) [243]. The operator with coefficient β_2 gives rise to a potential like Eq. (7.3.1), with g_A replaced by $-\beta_2/2$. For simplicity we absorb β_2 in g_A, $g_A\to g_A+\beta_2/2$. In Appendix J, we show that the one-loop corrections to $\bar{g}_0$ do not introduce any non-trivial momentum dependence, so they simply renormalize the coupling $\Delta\bar{g}_0=-2\delta_1^{(3)}m_N\rho$ in Eq. (4.1.27). These m_π^2 corrections to $\bar{g}_0$ can be absorbed in it, $\bar{g}_0\to\bar{g}_0-\Delta\bar{g}_0-\bar{g}_0\delta m_\pi^2/m_\pi^2$. As for the operators with coefficients c_1 in Eq. (3.3.19) and $\bar{\eta}_3=\rho\zeta_3$ in Eq. (4.1.24),

they give potentials of the form

$$\begin{aligned}&\boldsymbol{\tau}^{(1)}\cdot\boldsymbol{\tau}^{(2)}\left(\vec{\sigma}^{(1)}-\vec{\sigma}^{(2)}\right)\cdot\vec{q}\,\frac{\vec{q}^{\,2}}{\vec{q}^{\,2}+m_\pi^2}\\&=-\boldsymbol{\tau}^{(1)}\cdot\boldsymbol{\tau}^{(2)}\left(\vec{\sigma}^{(1)}-\vec{\sigma}^{(2)}\right)\cdot\vec{q}\frac{m_\pi^2}{\vec{q}^{\,2}+m_\pi^2}+\boldsymbol{\tau}^{(1)}\cdot\boldsymbol{\tau}^{(2)}\left(\vec{\sigma}^{(1)}-\vec{\sigma}^{(1)}\right)\cdot\vec{q},\end{aligned}\tag{7.3.16}$$

which cannot be distinguished from those of $g_A\bar{g}_0$ and $\bar{C}_2$, and can therefore be absorbed into further redefinitions of g_A, $\bar{g}_0$, and $\bar{C}_2$. Now the Goldberger-Treiman relation for the strong pion-nucleon constant, $g_{\pi NN}=2m_Ng_A/F_\pi$, applies without an explicit correction. If for the pion-nucleon coupling constant we use $g_{\pi NN}=13.07$ [244, 245], then in the leading-order TV potential we should use $g_A=1.29$.

The remaining contributions come from vertex corrections, both in the TV sector via the TV pion-nucleon coupling $\pi_3\bar{N}N$ in Eq. (4.1.27), and in the TC sector via the isospin-breaking pion-nucleon axial-vector coupling $\partial_\mu\pi_3\bar{N}S^\mu N$ in Eq. (G.3). We find

$$\begin{aligned}V_{T\!\!\!/,\mathrm{e}}^{(3)}(\vec{q}) &= i\frac{1}{2F_\pi^2}\frac{1}{\vec{q}^{\,2}+m_\pi^2}\left\{\left(g_A\bar{g}_1-\frac{\bar{g}_0\beta_1}{2}\right)\left(\tau_3^{(1)}+\tau_3^{(2)}\right)\left(\vec{\sigma}^{(1)}-\vec{\sigma}^{(2)}\right)\cdot\vec{q}\right.\\&\left.+\left(g_A\bar{g}_1+\frac{\bar{g}_0\beta_1}{2}\right)\left(\tau_3^{(1)}-\tau_3^{(2)}\right)\left(\vec{\sigma}^{(1)}+\vec{\sigma}^{(2)}\right)\cdot\vec{q}\right\},\end{aligned}\tag{7.3.17}$$

where defined $\bar{g}_1$ to absorb the tadpole contribution, like in Eq. (4.4.4)

$$\bar{g}_1=-4\rho\left(c_1^{(3)}-\Delta m_N\frac{\delta m_\pi^2}{2m_\pi^2}\right).\tag{7.3.18}$$

The first structure contributes to ${}^1S_0$–${}^3P_0$ mixing. Being proportional to I_3, the contribution vanishes in the case of neutron-proton scattering, and is only relevant for proton-proton or neutron-neutron scattering. Because of its isospin structure, it does not affect the ${}^3S_1$–${}^1P_1$ and ${}^3S_1$–${}^3P_1$ channels, and, in particular, it is not relevant for the calculation of the deuteron EDM. The second structure, in contrast, contributes to ${}^3S_1$–${}^3P_1$ mixing, and, consequently, to the deuteron EDM. Its contribution vanishes in the other low-energy channels.

One can proceed in the same manner to construct higher-order potentials. At next order there are further OPE and TPE contributions to the two-nucleon potential, and the appearance of the lowest-order three-nucleon TV potential. It arises from essentially three mechanisms: *(i)* a TPE component $\propto g_A \bar{g}_0 / m_N F_\pi^4$ involving a pion energy in a Weinberg-Tomozawa seagull vertex; *(ii)* a TPE component $\propto g_A^2 \bar{h}_0 / F_\pi^4$ involving the seagull vertex from $\mathcal{L}^{(2)}_{\not\chi,\, f=2}$, Eq. (4.1.21); and *(iii)* a one-pion/short-range component $\propto g_A \bar{\gamma}_i / F_\pi^2$ involving the short-range pion-two-nucleon interactions from $\mathcal{L}^{(2)}_{\not\chi,\, f=4}$, Eq. (4.1.42). The fact that, in the absence of an explicit delta isobar, the three-nucleon potential first shows up three orders beyond leading is completely analogous to the TC PC case [218, 219, 220]. An important difference is that, because of the relative enhancement of pion exchange compared to short-range physics, the leading TV PV three-nucleon force does not include a purely short-range component. Thus, this TV PV three-nucleon force is in principle determined by one- and two-nucleon physics.

7.3.1 The TV Potential from dimension 6 sources.

Our attention has been focused so far on the TV potential from the $\bar{\theta}$ term, in which case the vanishing of $\bar{g}_1$ at LO makes it important to consider N^{2}LO contributions. We now briefly turn our attention to the TV potential from the dimension 6 sources of T violation.

In the case of the qCEDM, the TV couplings $\bar{g}_0$ and $\bar{g}_1$ both appear at the same order, in the $\Delta_6 = -1$ Lagrangian in Eq. (4.1.29). As a consequence, the leading potential from the qCEDM has chiral index $\Delta_6 = -1$, and it has an isospin conserving part, identical to Eq. (7.3.1), and an isospin breaking one. The leading potential is

$$V^{(-1)}_{\rm qCEDM}(\vec{q}) = i \frac{g_A \bar{g}_{0\,q}}{F_\pi^2} \boldsymbol{\tau}^{(1)} \cdot \boldsymbol{\tau}^{(2)} \left(\vec{\sigma}^{\,(1)} - \vec{\sigma}^{\,(2)} \right) \cdot \frac{\vec{q}}{\vec{q}^{\,2} + m_\pi^2}$$
$$+ i \frac{g_A \bar{g}_{1\,q}}{2F_\pi^2} \frac{1}{\vec{q}^{\,2} + m_\pi^2} \left[\left(\tau_3^{(1)} + \tau_3^{(2)} \right) \left(\vec{\sigma}^{\,(1)} - \vec{\sigma}^{\,(2)} \right) \cdot \vec{q} + \left(\tau_3^{(1)} - \tau_3^{(2)} \right) \left(\vec{\sigma}^{(1)} + \vec{\sigma}^{(2)} \right) \cdot \vec{q} \right], \tag{7.3.19}$$

with $\bar{g}_{0\,q}$ and $\bar{g}_{1\,q}$ given in Eqs. (4.4.5) and (4.4.6).

At N^{2}LO, the potential receives corrections from one-loop diagrams, with the same topology as in Fig. 7.2, the square now denoting both $\bar{g}_{0\,q}$ and $\bar{g}_{1\,q}$, from tree-level OPE diagrams, with subleading TC and TV pion-nucleon vertices, and from short-range nucleon-nucleon interactions, the operators in Eq. (4.1.48). We refrain here from carrying out the complete calculation, which proceeds on lines that are very similar to Sec. 7.3, with the only difference of a richer isospin structure.

For the chiral invariant sources of T violation, the gCEDM and the TV four-quark operators, TV pion-nucleon couplings and four-nucleon interactions have the same importance, both of them appearing in the $\Delta_6 = -1$ Lagrangian, in Eqs. (4.1.29) and (4.1.50). As a consequence, the leading nucleon-nucleon potential consists of a pion-exchange contribution and a short-distance piece

$$
\begin{aligned}
V_w^{(-1)}(\vec{q}) &= i\frac{g_A \bar{g}_{0\,w}}{F_\pi^2}\boldsymbol{\tau}^{(1)}\cdot\boldsymbol{\tau}^{(2)}\,\left(\vec{\sigma}^{\,(1)}-\vec{\sigma}^{\,(2)}\right)\cdot\frac{\vec{q}}{\vec{q}^{\,2}+m_\pi^2}\\
&+i\frac{g_A \bar{g}_{1\,w}}{2F_\pi^2}\frac{1}{\vec{q}^{\,2}+m_\pi^2}\left[\left(\tau_3^{(1)}+\tau_3^{(2)}\right)\left(\vec{\sigma}^{\,(1)}-\vec{\sigma}^{\,(2)}\right)\cdot\vec{q}+\left(\tau_3^{(1)}-\tau_3^{(2)}\right)\left(\vec{\sigma}^{\,(1)}+\vec{\sigma}^{\,(2)}\right)\cdot\vec{q}\right]\\
&-\frac{i}{2}\left[\bar{C}_{w\,1}+\bar{C}_{w\,2}\,\boldsymbol{\tau}^{(1)}\cdot\boldsymbol{\tau}^{(2)}\right]\left(\vec{\sigma}^{\,(1)}-\vec{\sigma}^{\,(2)}\right)\cdot\vec{q}. \qquad (7.3.20)
\end{aligned}
$$

At N^{2}LO, along with contributions similar to those discussed in Sec. 7.3 (TPE diagrams, relativistic corrections to $\bar{g}_0$ and $\bar{g}_1$) one has to include all the possible TV four-nucleon operators with three derivatives.

In the case of the QCD $\bar{\theta}$ term, TV three-body forces only appear at N^{3}LO, one order higher than the accuracy of our analysis. One might wonder whether for chiral-invariant sources of T violation, which appear to be more sensitive to short-distance physics, TV three-body forces are more relevant. However, also in this case it turns out that the three-nucleon potential is a N^{3}LO effect. The lowest order three-nucleon potential receives various contributions: (*i*) a TPE component $\propto g_A\bar{g}_{0,1w}/m_N F_\pi^4$ involving a pion energy in the Weinberg-Tomozawa vertex, (*ii*) a TPE component $\propto g_A^2\bar{\imath}_{0\,w}/m_N F_\pi^4$ involving a pion energy in the leading TV seagull $\bar{\imath}_{0w}$ (*iii*) TPE components from TV seagulls in the $\Delta_6 = 0$ pion-nucleon Lagrangian, which we did

not explicitly construct, (iv) a one-pion/short-range component $\propto g_A\bar{\gamma}_i/F_\pi^2$, where in the case of TV from the gCEDM and TV four-quark operators, four-nucleon operators that contain at least one pion field first appear in the $\Delta_6 = 0$ Lagrangian, (v) short-range six-nucleon operators, which, according to Eq. (3.3.13) also appear in the $\Delta_6 = 0$ Lagrangian. From the power counting formula (3.3.15), all these three-body contributions are suppressed by three powers of m_π/M_{QCD} with respect to the effects of the two-body potential (7.3.20) in the three-body system.

Since in the Weinberg power-counting, three-nucleon electromagnetic currents are also small, even in the case of TV from dimension 6 chiral invariant sources the EDM of ^{3}He and ^{3}H does not involve, at least at leading order in the Weinberg power counting, any new three-body low-energy constant, and, if enough one- and two-nucleon observables are measured to fix the couplings $\bar{g}_{0,1\,w}$, $\bar{C}_{1,2\,w}$ and $\bar{D}^{(-1)}_{w\,0,1}$, it is a falsifiable prediction of the theory.

7.4 The TV Potential in Configuration Space

The evaluation of T-odd observables in nuclear and atomic systems is often more easily carried out in configuration space. In this section we give the TV nuclear potential derived in Sect. 7.3 in coordinate space.

In the two-body case, it is convenient to introduce the relative position of the two nucleons $\vec{r} = \vec{x}_1 - \vec{x}_2$, their center-of-mass coordinate $\vec{X} = (\vec{x}_1 + \vec{x}_2)/2$, and the conjugate variables $-i\vec{\nabla}_r \equiv -i\partial/\partial\vec{r}$ and $-i\vec{\nabla}_X \equiv -i\partial/\partial\vec{X}$. Translation invariance constrains the potential to commute with $\vec{\nabla}_X$ and, therefore, not to depend on $\vec{X}$, so that in general the potential is a function of $\vec{r}$ and of the nucleons' relative and center-of-mass momenta, $V_{\not T} = V_{\not T}(\vec{r}, \vec{\nabla}_r, \vec{\nabla}_X)$. The relations between the potential in momentum space and in coordinate space are defined in the Appendix K. Some care must be taken, and a regularization scheme has to be defined, when computing the Fourier transform of functions that blow up as $|\vec{q}|$ goes to infinity, as is the case of the subleading TV potential. As described in the Appendix K, we follow Ref. [246] and

define the Fourier transform in d dimensions. We apply the d-dimensional Fourier integration of the momentum-space potential before setting $d = 4$. This method eliminates naturally the divergent factor $\Gamma(2 - d/2)$ arising from loops and yields a finite result. As we will see, the divergent behavior at large momentum translates in a singular $\sim 1/r^4$ potential at short distances. Expressions in configuration space obtained with this method are equivalent to the procedure based on old-fashioned perturbation theory [246].

In order to write the results of the Fourier transform we introduce a few functions of the magnitude $r = |\vec{r}|$ of the radial coordinate:

$$U(r) = \frac{1}{12\pi r}\left[2\exp\left(-m_{\pi^\pm} r\right) + \exp\left(-m_{\pi^0} r\right)\right], \tag{7.4.1}$$

which reduces to the usual Yukawa function $U(r) = \exp(-m_\pi r)/4\pi r$ when we ignore the pion mass difference;

$$W(r) = \frac{1}{4\pi r}\left[\exp\left(-m_{\pi^\pm} r\right) - \exp\left(-m_{\pi^0} r\right)\right], \tag{7.4.2}$$

which is entirely a consequence of isospin breaking; and the TPE functions

$$X(r) = \frac{1}{4\pi(2\pi F_\pi)^2 r^3}\int_0^1 dx\left(3 + 3\beta r + \beta^2 r^2\right)\exp(-\beta r), \tag{7.4.3}$$

$$Y(r) = \frac{1}{2\pi(2\pi F_\pi)^2 r^3}\int_0^1 dx\,(1 + \beta r)\exp(-\beta r), \tag{7.4.4}$$

with $\beta^2 = m_\pi^2/x(1-x)$.

The Fourier transform of the leading OPE potential including the corrections to the pion mass (7.3.10) and those coming from the nucleon kinetic energy (7.3.12) is

$$\begin{aligned} &V_T^{(1)}(\vec{r}) + V_{TT,\mathrm{a}}^{(2+3)}(\vec{r}) + V_{T,\mathrm{a}}^{(3)}(\vec{r}, \vec{\nabla}_r, \vec{\nabla}_X) = -\frac{\bar{g}_0 g_A}{F_\pi^2}\boldsymbol{\tau}^{(1)}\cdot\boldsymbol{\tau}^{(2)}\left(\vec{\sigma}^{(1)} - \vec{\sigma}^{(2)}\right)\cdot \\ &\left[\left(\vec{\nabla}_r U(r)\right)\left(1 + \frac{\vec{\nabla}_X^2}{4m_N^2}\right) + \left\{\frac{\nabla_r^i}{2m_N}, \left\{\frac{\nabla_r^i}{2m_N}, \left(\vec{\nabla}_r U(r)\right)\right\}\right\}\right. \\ &\left. + \frac{(\vec{\nabla}_r\cdot\vec{\nabla}_X)^2}{8m_\pi m_N^2}\left(\vec{\nabla}_r r U(r)\right)\right], \end{aligned} \tag{7.4.5}$$

where $\{\cdots,\cdots\}$ denotes the anticommutator. The remaining pion-mass correction, Eq. (7.3.11), is

$$V_{\not T\not T,\mathrm{b}}^{(2+3)}(\vec{r}) = \frac{\bar{g}_0 g_A}{3F_\pi^2}\left(3\tau_3^{(1)}\tau_3^{(2)} - \boldsymbol{\tau}^{(1)}\cdot\boldsymbol{\tau}^{(2)}\right)\left(\vec{\sigma}^{(1)}-\vec{\sigma}^{(2)}\right)\cdot\left(\vec{\nabla}_r W(r)\right), \tag{7.4.6}$$

while the Fourier transform of the other relativistic corrections to the leading OPE, Eq. (7.3.13), is

$$\begin{aligned} V_{\not T,\mathrm{b}}^{(3)}(\vec{r},\vec{\nabla}_r,\vec{\nabla}_X) &= -\frac{\bar{g}_0 g_A}{8F_\pi^2 m_N^2}\boldsymbol{\tau}^{(1)}\cdot\boldsymbol{\tau}^{(2)}\Big[\left(\vec{\sigma}^{(1)}-\vec{\sigma}^{(2)}\right)\cdot\vec{\nabla}_X\left(\vec{\nabla}_r U(r)\right)\cdot\vec{\nabla}_X \\ &\quad + \left(\vec{\sigma}^{(1)}+\vec{\sigma}^{(2)}\right)\cdot\left\{\vec{\nabla}_r,\left(\vec{\nabla}_r U(r)\right)\cdot\vec{\nabla}_X\right\} \\ &\quad + 2i\varepsilon^{ijk}\left(\sigma^{(1)\,i}\sigma^{(2)\,l}-\sigma^{(1)\,l}\sigma^{(2)\,i}\right)\left(\nabla_r^l\nabla_r^k U(r)\right)\nabla_r^j \\ &\quad + i\varepsilon^{ijk}\left(\sigma^{(1)\,i}\sigma^{(2)\,l}+\sigma^{(1)\,l}\sigma^{(2)\,i}\right)\left(\nabla_r^l\nabla_r^k U(r)\right)\nabla_X^j\Big]. \end{aligned} \tag{7.4.7}$$

The nucleon mass-splitting corrections in Eq. (7.3.14) become

$$\begin{aligned} V_{\not T\not T,\mathrm{c}}^{(3)}(\vec{r},\vec{\nabla}_r,\vec{\nabla}_X) &= -i\frac{\bar{g}_0 g_A}{2F_\pi^2}\frac{\delta m_N}{m_N}\left(\boldsymbol{\tau}^{(1)}\times\boldsymbol{\tau}^{(2)}\right)_3\Big[\left(\vec{\sigma}^{(1)}+\vec{\sigma}^{(2)}\right)\cdot\left\{\vec{\nabla}_r,U(r)\right\} \\ &\quad + \left(\vec{\sigma}^{(1)}-\vec{\sigma}^{(2)}\right)\cdot\left(U(r)\vec{\nabla}_X - \frac{1}{m_\pi}\left(\vec{\nabla}_r\,\nabla_r^i\,rU(r)\right)\nabla_X^i\right)\Big], \end{aligned} \tag{7.4.8}$$

while those in Eq. (7.3.15) read

$$\begin{aligned} V_{\not T\not T,\mathrm{d}}^{(3)}(\vec{r}) &= -\frac{\bar{g}_0 g_A}{3F_\pi^2}\frac{\delta m_N^2}{m_\pi}\left[\vec{\tau}^{(1)}\cdot\vec{\tau}^{(2)} - \frac{1}{2}\left(3\tau_3^{(1)}\tau_3^{(2)}-\boldsymbol{\tau}^{(1)}\cdot\boldsymbol{\tau}^{(2)}\right)\right] \\ &\quad \times\left(\vec{\sigma}^{(1)}-\vec{\sigma}^{(2)}\right)\cdot\left(\vec{\nabla}_r\,rU(r)\right). \end{aligned} \tag{7.4.9}$$

The last OPE terms, Eq. (7.3.17), are

$$\begin{aligned} V_{\not T\not T,\mathrm{e}}^{(3)}(\vec{r}) &= -\frac{\bar{g}_0 g_A}{2F_\pi^2}\left[\left(\frac{\bar{g}_1}{\bar{g}_0}-\frac{\beta_1}{2g_A}\right)\left(\tau_3^{(1)}+\tau_3^{(2)}\right)\left(\vec{\sigma}^{(1)}-\vec{\sigma}^{(2)}\right)\right. \\ &\quad + \left.\left(\frac{\bar{g}_1}{\bar{g}_0}+\frac{\beta_1}{2g_A}\right)\left(\tau_3^{(1)}-\tau_3^{(2)}\right)\left(\vec{\sigma}^{(1)}+\vec{\sigma}^{(2)}\right)\right]\cdot\left(\vec{\nabla}_r U(r)\right). \end{aligned} \tag{7.4.10}$$

Finally, the Fourier transform of the TPE potential in Eq. (7.3.6) reads

$$V_{\not T,\,\mathrm{MR}}^{(3)}(\vec{r}) = -\frac{\bar{g}_0 g_A}{F_\pi^2}\boldsymbol{\tau}^{(1)}\cdot\boldsymbol{\tau}^{(2)}\left(\vec{\sigma}^{(1)}-\vec{\sigma}^{(2)}\right)\cdot\left[\vec{\nabla}_r\left(2g_A^2X(r)-Y(r)\right)\right]. \tag{7.4.11}$$

The potential in Eq. (7.4.11) is singular, and the cutoff dependence it introduces in the evaluation of matrix elements and observables is absorbed by the renormalization of $\bar{C}_2$ in the short-distance potential (7.3.5),

$$V^{(3)}_{\not T,\mathrm{SR}}(\vec{r}) = \frac{1}{2}\left[\bar{C}_1 + \bar{C}_2 \boldsymbol{\tau}^{(1)}\cdot\boldsymbol{\tau}^{(2)}\right]\left(\vec{\sigma}^{(1)} - \vec{\sigma}^{(2)}\right)\cdot\left(\vec{\nabla}_r\,\delta^{(3)}(\vec{r})\right). \tag{7.4.12}$$

The Fourier transform of the leading TV potential from dimension 6 sources can be immediately read from the results in Eqs. (7.4.5), (7.4.10) and (7.4.12).

We compare these various potentials with the literature in the next section.

7.5 Discussion

Traditionally the study on T violation in nuclear physics has been carried out by including the most general pion-nucleon *non*-derivative couplings in a phenomenological TV Lagrangian [197], which we write in our notation as

$$\mathcal{L}_{\not T,\mathrm{non}} = -\frac{\bar{g}_0}{F_\pi}\bar{N}\boldsymbol{\tau}\cdot\boldsymbol{\pi}N - \frac{\bar{g}_1}{F_\pi}\pi_3\bar{N}N - \frac{\bar{g}_2}{F_\pi}\bar{N}\left(3\tau_3\pi_3 - \boldsymbol{\tau}\cdot\boldsymbol{\pi}\right)N, \tag{7.5.1}$$

and by inferring from it the TV two-nucleon potential [196],

$$\begin{aligned} V_{\not T,\mathrm{non}}(\vec{r}) \;=\; & -\frac{g_A}{F_\pi^2}\left\{\left[\bar{g}_0\,\boldsymbol{\tau}^{(1)}\cdot\boldsymbol{\tau}^{(2)} + \frac{\bar{g}_1}{2}\left(\tau_3^{(1)}+\tau_3^{(2)}\right)\right.\right. \\ & \left. +\bar{g}_2\left(3\tau_3^{(1)}\tau_3^{(2)} - \boldsymbol{\tau}^{(1)}\cdot\boldsymbol{\tau}^{(2)}\right)\right]\left(\vec{\sigma}^{(1)} - \vec{\sigma}^{(2)}\right) \\ & \left. +\frac{\bar{g}_1}{2}\left(\tau_3^{(1)} - \tau_3^{(2)}\right)\left(\vec{\sigma}^{(1)} + \vec{\sigma}^{(2)}\right)\right\}\cdot\left(\vec{\nabla}U(r)\right), \end{aligned} \tag{7.5.2}$$

with $U(r)$ defined in Eq. (7.4.1). When short-distance contributions are included in the model, the most general TV two-nucleon local potential with the *minimum* number of derivative assumes the form [200]

$$\begin{aligned} V_{\not T,\mathrm{min}}(\vec{r}) \;=\; & \left(\vec{\sigma}^{(1)} - \vec{\sigma}^{(2)}\right)\cdot\vec{\nabla}\left[\mathcal{U}_0(r) + \boldsymbol{\tau}^{(1)}\cdot\boldsymbol{\tau}^{(2)}\mathcal{V}_0(r) + \frac{1}{2}\left(\tau_3^{(1)}+\tau_3^{(2)}\right)\mathcal{U}_1(r)\right. \\ + \;& \left.\left(3\tau_3^{(1)}\tau_3^{(2)} - \boldsymbol{\tau}^{(1)}\cdot\boldsymbol{\tau}^{(2)}\right)\mathcal{V}_2(r)\right] + \frac{1}{2}\left(\tau_3^{(1)} - \tau_3^{(2)}\right)\left(\vec{\sigma}^{(1)} + \vec{\sigma}^{(2)}\right)\cdot\vec{\nabla}\mathcal{V}_1(r) \end{aligned} \tag{7.5.3}$$

in terms of five radial functions $\mathcal{U}_{0,1}(r)$ and $\mathcal{V}_{0,1,2}(r)$. These functions are assumed to originate in one-boson exchange [198, 199, 159]: pion exchange is taken to give long-range contributions to $\mathcal{V}_0$, $(\mathcal{V}_1+\mathcal{U}_1)/2$ and $\mathcal{V}_2$, while eta, rho and omega mesons give shorter-range contributions to the same quantities, and to $\mathcal{U}_0$ and $\mathcal{V}_1-\mathcal{U}_1$. The five momentum-independent potentials in Eq. (7.5.3) are treated on the same footing, and they provide enough information to describe the five S–P mixing amplitudes discussed in Sec. 7.2.

For TV stemming from the QCD $\bar{\theta}$ term, the proper account of chiral symmetry radically changes the picture. As noticed in Ref. [93], at leading order the $\bar{\theta}$ term generates only the isoscalar pion-nucleon T-odd coupling $\bar{g}_0$, and thus contributes at tree level only to the $I=0$ potential [195]. A coupling of $\bar{g}_1$ form appears two orders down in the χPT expansion, and the one of $\bar{g}_2$ form is even more suppressed [39]. To evaluate the effects of the $\bar{\theta}$ term on observables which, like the deuteron EDM, are mostly sensitive to the $I=1$ components, it is necessary to consider the TV two-nucleon potential to next-to-next-to-leading order in χPT. As described in Sec. 7.3, this implies the consideration not only of the non-derivative pion-nucleon TV couplings, but also of subleading TV derivative couplings, of power-suppressed TC interactions (with particular care for isospin-breaking operators, which contribute to the $I=1$ and $I=2$ potentials), and of one-loop and short-range contributions to the two-nucleon potential. When all these elements are considered, the potential has a much richer structure than Eq. (7.5.3): *(i)* a hierarchy emerges between the five spin-isospin structures already present in Eq. (7.5.3), and *(ii)* momentum-dependent potentials appear, with the same importance as most of the momentum-independent ones.

We first analyze the implications of our results to $V_{\mathcal{T},\min}(\vec{r})$. Using the chiral index ν, as defined in Eq. (3.3.15), to keep track of the size of different pieces, the $\bar{\theta}$ term

contributions to Eq. (7.5.3) are

$$\mathcal{V}_0^{(1)}(r) = -\frac{g_A\bar{g}_0}{F_\pi^2}\,U(r), \tag{7.5.4}$$

$$\mathcal{V}_0^{(3)}(r) = -\frac{g_A\bar{g}_0}{F_\pi^2}\left[2g_A^2X(r) - Y(r) + \frac{(m_n-m_p)^2}{3m_\pi}r\,U(r)\right] + \bar{C}_2\frac{\delta(r)}{8\pi r^2}, \tag{7.5.5}$$

$$\mathcal{U}_0^{(3)}(r) = +\bar{C}_1\frac{\delta(r)}{8\pi r^2}, \tag{7.5.6}$$

$$\mathcal{V}_1^{(3)}(r) = -\frac{g_A\bar{g}_0}{F_\pi^2}\left(\frac{\bar{g}_1}{\bar{g}_0} + \frac{\beta_1}{2g_A}\right)U(r), \tag{7.5.7}$$

$$\mathcal{U}_1^{(3)}(r) = -\frac{g_A\bar{g}_0}{F_\pi^2}\left(\frac{\bar{g}_1}{\bar{g}_0} - \frac{\beta_1}{2g_A}\right)U(r), \tag{7.5.8}$$

$$\mathcal{V}_2^{(2+3)}(r) = +\frac{g_A\bar{g}_0}{3F_\pi^2}\left[\frac{(m_n-m_p)^2}{2m_\pi}rU(r) + W(r)\right], \tag{7.5.9}$$

where $U(r)$, $W(r)$, $X(r)$, and $Y(r)$ are defined in Eqs. (7.4.1), (7.4.2), (7.4.3), and (7.4.4), respectively. In Eq. (7.5.4) the use of the definition (7.4.1) to express $\mathcal{V}_0^{(1)}$ in terms of the physical pion masses introduces subleading corrections in the $\nu = 1$ term, which strictly speaking would use a function $U(r)$ that only depends on a common pion mass, say the neutral one, $U_0(r) = \exp(-m_{\pi^0}r)/4\pi r$. In Eqs. (7.5.5)–(7.5.9) we can neglect the pion mass difference in $U(r)$, and use $U_0(r)$, the error thus introduced being at higher orders in the χPT power counting. Similarly, in Eq. (7.5.4) the use of g_A and $\bar{g}_0$ with their m_π^2 corrections included accounts for some $\nu = 3$ corrections, while whether or not such m_π^2 corrections are included in Eqs. (7.5.5)–(7.5.9) is beyond the order we consider. In Eqs. (7.5.5) and (7.5.9) we replaced δm_N, the quark-mass-difference contribution to the nucleon mass splitting, with the physical value of the nucleon mass splitting itself, $m_n - m_p$, the difference being a higher order contribution in χPT.

As one can see, at order $\nu = 3$ in χPT all the possible spin-isospin structures considered in Refs. [200, 198, 199, 159] appear. The dominant component is the isoscalar $\mathcal{V}_0$ [195]. In Figs. 7.4 and 7.5 we plot, respectively, the momentum-space and configuration-space expressions for $\nabla\mathcal{V}_0$. The dashed line represents the leading-order $\nabla\mathcal{V}_0^{(1)}$, Eqs. (7.3.10) and (7.4.5) with the use of the definition (7.4.1) for $U(r)$

to express $\mathcal{V}_0^{(1)}$ in terms of the physical pion masses. The dashed-double-dotted line illustrates the effect of the difference between the leading OPE potential computed with the function $U(r)$ and with $U_0(r)$. Other isospin-breaking corrections, which come from the nucleon mass splitting in $\mathcal{V}_0^{(3)}$, Eqs. (7.3.15) and (7.4.9), are also very small, as indicated by the long-dashed-dotted line barely distinguishable from the x-axis. At next-to-next-to-leading order, $\mathcal{V}_0$ also exhibits a medium-range component originating in TPE diagrams and a short-range component. The dashed-dotted line depicts the non-analytic piece of the TPE diagrams, Eqs. (7.3.6) and (7.4.11). We estimate the short-range potential by assuming the coefficient $\bar{C}_2$ in Eq. (7.3.4) to be dominated by the $\ln \mu^2/m_\pi^2$ term with $\mu = m_N$. The rationale is that there is no obvious reason to expect that such a contribution, non-analytic in m_π, should get exactly canceled by m_π-independent short-distance contributions. However, the sign cannot be guessed reliably and our choice is purely arbitrary, for illustration only. Equation (7.3.5) gives rise to the straight dotted line in Fig. 7.4 but Eq. (7.4.12) does not appear in Fig. 7.5 since it is concentrated at $r = 0$. The solid line in both figures is the sum of the long, estimated medium, and short-range contributions to $\nabla\mathcal{V}_0$.

From Fig. 7.4, we can appreciate that, as expected from the χPT power counting, the medium and short-range corrections to the TV potential have comparable size in the momentum range we are considering, and for momenta $q \gtrsim m_\pi$ they noticeably affect the leading order. At momenta of order 300–400 MeV the medium and short-range contributions have roughly the same size as the leading potential. In this region, degrees of freedom which we have not explicitly included in the EFT, like the Δ isobar, become relevant, and the convergence of the perturbative expansion can be improved by extending the EFT to incorporate them. Isospin-breaking, long-range corrections, although of formally the same order as TPE and contact terms, are much smaller, at least in part because of factors of ε, except at very small momenta where their longer range compensates. In Fig. 7.5 we focus our attention on the long-distance region,

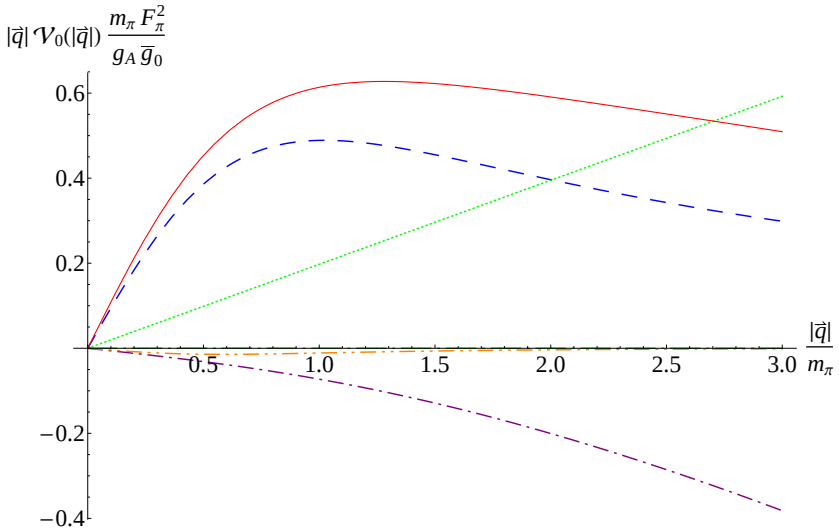

FIGURE 7.4. Components of the TV two-nucleon potential $|\vec{q}|\mathcal{V}_0$, in units of $g_A\bar{g}_0/m_\pi F_\pi^2$, as a function of the transferred momentum $|\vec{q}|$, in units of m_π. The (blue) dashed line denotes the leading-order OPE contribution with physical pion masses; the (orange) dashed-double-dotted line shows the effect of the pion mass difference on the leading OPE contribution; the (dark green) long-dashed-dotted line accounts for the even smaller effect of the nucleon mass splitting; the (purple) dashed-dotted line is the non-analytic TPE contribution; and the (green) dotted line presents an estimate of the short-range component of the potential. The (red) solid line is the sum of all the contributions up to next-to-next-to-leading order.

$r \geq 1/m_\pi$. At distances of up to $r \lesssim 2/m_\pi$ TPE is still the dominant correction to the potential, but it is overcome at longer distances, $r \gtrsim 2/m_\pi$, by the long-range effects of pion mass splitting in OPE.

It is instructive to compare our results for $\mathcal{V}_0$ to the corresponding TV potential obtained in a one-boson-exchange model. In such a model, T violation in the coupling of a rho-meson to the nucleon generates corrections to $\mathcal{V}_0$ of the form [199, 159]

$$\mathcal{V}_0^{(\rho)}(r) = -\frac{g_A\bar{g}_0}{F_\pi^2}\frac{g_{\rho NN}}{g_{\pi NN}}\frac{\bar{g}_{0\rho}F_\pi}{\bar{g}_0}\frac{e^{-m_\rho r}}{4\pi r}, \tag{7.5.10}$$

where $g_{\rho NN}$ is the TC rho-nucleon vector coupling and $\bar{g}_{0\rho}$ is an isoscalar, TV, one-derivative rho-nucleon coupling, defined, for example, in Ref. [159]. In the limit where the rho mass is large, $m_\rho \to \infty$, $\mathcal{V}_0^{(\rho)}(r)$ approximates a delta function and the

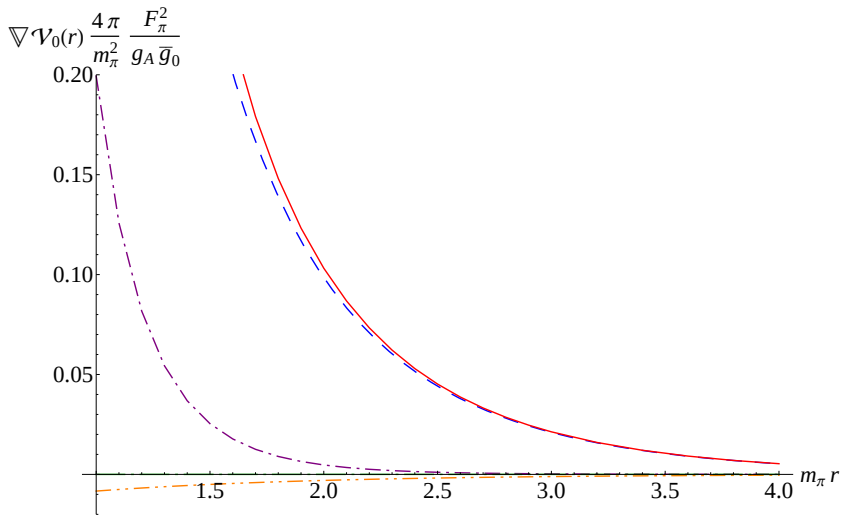

FIGURE 7.5. Components of the TV two-nucleon potential $\nabla\mathcal{V}_0$ in units of $g_A\bar{g}_0 m_\pi^2/4\pi F_\pi^2$, as functions of the distance between the two nucleons $r = |\vec{r}|$, in units of $1/m_\pi$. Curves as in Fig. 7.4, except that the short-range component of the potential is not shown.

effect of TV rho-exchange amounts to a contribution to $\bar{C}_2$ of the form

$$\bar{C}_2^{(\rho)} = -2\frac{g_A\bar{g}_0}{F_\pi^2}\frac{g_{\rho NN}}{g_{\pi NN}}\frac{\bar{g}_{0\rho}F_\pi}{\bar{g}_0}\frac{1}{m_\rho^2}. \tag{7.5.11}$$

Since $m_\rho \sim M_{QCD}$ and there is no reason for $\bar{g}_{0\rho}F_\pi/\bar{g}_0$ to be particularly big or small, the size of rho-meson contribution is comparable to the power-counting expectation, $\bar{C}_2 = \mathcal{O}(m_\pi^2/M_{QCD}^3)$, with some suppression coming from the numerical smallness of the TC rho-nucleon vector coupling compared to the pion-nucleon coupling. Assuming the TV pion-nucleon and rho-nucleon couplings to have the same strength, $\bar{g}_{0\rho}F_\pi/\bar{g}_0 = 1$, and using for the rho-nucleon vector coupling the value determined in modern high-precision two-nucleon potentials, $g_{\rho NN} = 3.2$ [247, 248], in Fig. 7.6 we compare the rho-meson contribution to $\nabla\mathcal{V}_0$ to the pion-mass-splitting and TPE medium-range corrections discussed above. For $r \gtrsim 1/m_\pi$, the contribution of the ρ meson is numerically small compared to both pion-mass-splitting and TPE corrections. At shorter ranges, $r \lesssim 1/m_\pi$, rho exchange overcomes the effect of pion mass splitting, but it always remains smaller than TPE. Of course we can make one-rho

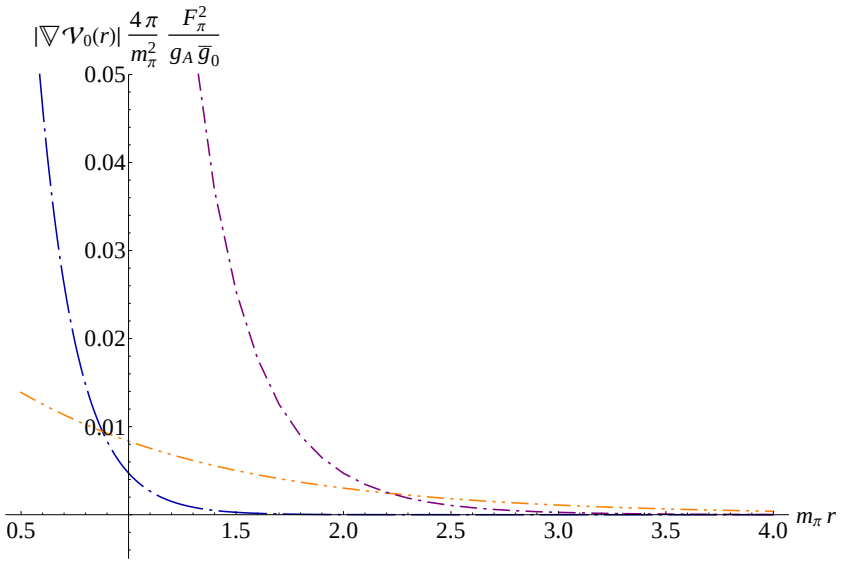

FIGURE 7.6. Comparison between one-rho-exchange and EFT contributions to the magnitude of the TV two-nucleon potential $|\nabla \mathcal{V}_0|$ in units of $g_A \bar{g}_0 m_\pi^2/4\pi F_\pi^2$, as functions of the distance r, in units of $1/m_\pi$. The rho-exchange contribution is depicted as a (blue) long-dashed-dotted line, while TPE and pion mass splitting in OPE are as in Fig. 7.4.

exchange more important by jacking up $\bar{g}_{0\rho} F_\pi/\bar{g}_0$, but we cannot compensate for the different ranges of the two contributions, m_ρ *versus* $2m_\pi$. We see little justification for neglecting TPE in the TV potential.

We now turn to the other spin-isospin structures in Eq. (7.5.3), which in EFT are all suppressed by one power of Q^2/M_{QCD}^2 with respect to the leading OPE TV potential. The function $\mathcal{U}_0^{(3)}$ only receives contributions from short-range physics. Again, in a one-boson-exchange scenario, contributions of exactly the size of $\bar{C}_1$ come from eta and omega exchanges [198, 199, 159],

$$\bar{C}_1^{(\eta,\omega)} = 2\frac{g_A \bar{g}_0}{F_\pi^2}\left(\frac{g_{\eta NN}}{g_{\pi NN}}\frac{\bar{g}_{0\eta} F_\pi}{\bar{g}_0}\frac{1}{m_\eta^2} - \frac{g_{\omega NN}}{g_{\pi NN}}\frac{\bar{g}_{0\omega} F_\pi}{\bar{g}_0}\frac{1}{m_\omega^2}\right), \tag{7.5.12}$$

where m_η (m_ω) is the eta (omega) mass, $g_{\eta NN}$ ($g_{\omega NN}$) is the TC eta-nucleon axial (omega-nucleon vector) coupling, and $\bar{g}_{0\eta}$ ($\bar{g}_{0\omega}$) is an isoscalar, TV no-derivative eta-nucleon (one-derivative omega-nucleon) coupling.

In contrast, $\mathcal{V}_1^{(3)}$, $\mathcal{U}_1^{(3)}$, and $\mathcal{V}_2^{(2+3)}$ sprout entirely from OPE. The TV, isospin-

breaking coupling $\bar{g}_1$ contributes equally to $\mathcal{V}_1$ and $\mathcal{U}_1$, as expected [196] from the identification at the Lagrangian level, *cf.* Eqs. (4.1.27) and (7.5.1). However, at this level, we cannot neglect the long-range piece of $\mathcal{U}_1 - \mathcal{V}_1$, which stems from the combination of the isospin-violating vertex β_1 and the TV vertex $\bar{g}_0$. As discussed in Sec. 4.4, strong-dynamics contributions to the coefficients of these $I = 1$ potentials are in principle determined by measurement of TC, isospin-breaking observables. For example $\bar{g}_1/\bar{g}_0$ could be extracted from a detailed analysis of isospin-breaking effects in pion-nucleon scattering. At present, however, even the very sophisticated, state-of-the art analysis of Ref. [168] stops one order shy of the accuracy required for such extraction. Similarly, the ratio β_1/g_A affects isospin violation in nucleon-nucleon scattering, but at present phase-shift analysis of two-nucleon data can only provide a bound on β_1, which is in accordance with the power-counting expectation [145, 148, 149]. In the absence of better constraints on the parameters in Eqs. (7.5.7) and (7.5.8), the ratios $\mathcal{V}_1^{(3)}/\mathcal{V}_0^{(1)}$ and $\mathcal{U}_1^{(3)}/\mathcal{V}_0^{(1)}$ can only be estimated by power counting, as $\mathcal{O}(\varepsilon m_\pi^2/M_{QCD}^2) \sim 5\%$. As for the last component of the phenomenological potential, $\mathcal{V}_2^{(2+3)}$, it originates entirely from the isospin-violating corrections to the pion and nucleon masses, and it is also relatively small.

In one-boson-exchange models the $I = 1, 2$ potentials are assumed to arise from pion, eta, rho, and omega isovector and tensor TV couplings to the nucleon [198, 199, 159]. In the χPT power counting, short-range contributions to these potentials are suppressed with respect to the long-range pieces, because of the isoscalar character of the $\bar{\theta}$ term, Eq. (3.4.15). (Of course, because of the factors ε in the long-range contributions of this order, short-range terms might not be entirely negligible.) This is consistent with the argument that the dominant meson-exchange contributions are from the pion and the eta [198].

There are, therefore, a few points of contact between the local part of our $\nu \leq 3$ potential and the phenomenological potential $V_{T,\min}(\vec{r})$ (7.5.3). However, as we have seen in Sects. 7.3 and 7.4, at this order EFT yields also momentum-dependent

interactions, which in coordinate space appear as non-local potentials and corrections that account for center-of-mass motion of the nucleon pair. They can be found in the relativistic and isospin-breaking corrections to OPE in Eqs. (7.4.5), (7.4.7), and (7.4.8).

At $\nu = 3$, the TV two-nucleon potential contains in the center-of-mass frame, $\vec{P} = 0$, four spin-isospin structures that are momentum-dependent,

$$\begin{aligned} V(\vec{r},\vec{p}_r) &= \frac{g_A\bar{g}_0}{4m_N^2F_\pi^2}\boldsymbol{\tau}^{(1)}\cdot\boldsymbol{\tau}^{(2)}\left[\left(\vec{\sigma}^{(1)}-\vec{\sigma}^{(2)}\right)\cdot\left\{p_r^i,\left\{p_r^i,\vec{\nabla}_r U(r)\right\}\right\}\right. \\ &\quad -\frac{2}{3}\left(\vec{\nabla}_r^2 U(r)\right)\left(\vec{\sigma}^{(1)}\times\vec{\sigma}^{(2)}\right)\cdot\vec{p}_r \\ &\quad \left.+\left(\vec{\sigma}^{(1)}\times\vec{\sigma}^{(2)}\right)^m\left(\nabla_r^m\nabla_r^l U(r)-\frac{1}{3}\delta^{lm}\vec{\nabla}_r^2 U(r)\right)p_r^l\right] \\ &\quad +\frac{g_A\bar{g}_0\,\delta m_N}{2m_N F_\pi^2}\left(\boldsymbol{\tau}^{(1)}\times\boldsymbol{\tau}^{(2)}\right)_3\left(\vec{\sigma}^{(1)}+\vec{\sigma}^{(2)}\right)\cdot\left\{\vec{p}_r,U(r)\right\}, \end{aligned} \tag{7.5.13}$$

where $\vec{p}_r = -i\vec{\nabla}_r$ denotes the quantum-mechanical relative momentum operator.

The general structure of the momentum-dependent TV potentials was considered previously in Ref. [200], where all possible Hermitian operators were constructed, which violate time-reversal and parity, and contain up to one power of momentum $\vec{p}_r$. The momentum-dependent TV potential was parameterized with eleven unknown functions $d_i(r)$, $i = 1, 2\ldots, 11$. The first term in Eq. (7.5.13) is quadratic in the momentum operator and was not considered in Ref. [200]. The second and third spin-isospin structures correspond, respectively, to the isoscalar functions $d_2(r)$ and $d_6(r)$. For TV from the QCD $\bar{\theta}$ term, these two functions are therefore dominated by pion-exchange, and their coefficients are fixed by Lorentz invariance and do not contain any new TV parameter. Isospin-breaking effects in the strong interaction give rise to the last term in Eq. (7.5.13), which is proportional to the nucleon mass difference, and it is the first contribution of the $\bar{\theta}$ term to $d_{10}(r)$. Once again, d_{10} is dominated by OPE diagrams, and the only TV parameter intervening is $\bar{g}_0$. We find that, at order $\nu = 3$ in χPT, the other isospin-conserving (the isoscalar d_1 and d_5) and isospin-breaking (d_3, d_4, d_7, d_8, d_9 and d_{11}) functions do not receive contributions

from $\bar{\theta}$.

In order to get a sense of the importance of the momentum-dependent contributions, we consider the effect of the relativistic correction in Eq. (7.5.13) that is quadratic in $\vec{p}_r$. In Fig. 7.7 we compare it (long-dashed-dotted line) to leading OPE (dashed line), medium-range TPE (dashed-dotted line), and pion mass-splitting corrections (double-dotted-dashed line), all applied to a simple bound-state wave function with the scale present in the ${}^1S_0$ channel, $a_s = -23.714$ fm:

$$\psi(r) = \frac{\exp(-r/a_s)}{r}. \tag{7.5.14}$$

pion mass splitting (orange double dotted dashed line), all applied to the same function. In this qualitative example the relativistic correction cannot be neglected with respect to the other $\nu = 3$ corrections, and we take Fig. 7.7 as an indication that also in actual calculations of TV observables it would not be justified to neglect Eq. (7.5.13), when the TV potential is needed to next-to-next-to-leading-order accuracy.

Finally, to the same order we find six contributions proportional to the center-of-mass momentum of the nucleon pair,

$$\begin{aligned} V(\vec{r},\vec{p}_r,\vec{P}) \;=\; & \frac{g_A\bar{g}_0}{8m_N^2F_\pi^2}\boldsymbol{\tau}^{(1)}\cdot\boldsymbol{\tau}^{(2)}\Big[\left(\vec{\sigma}^{\,(1)}+\vec{\sigma}^{\,(2)}\right)\cdot\Big\{\vec{p}_r,\,\Big(\vec{\nabla}_r U(r)\Big)\cdot\vec{P}\Big\} \\ & +\left(\vec{\sigma}^{(1)}-\vec{\sigma}^{(2)}\right)\cdot\Big(2\Big(\vec{\nabla}_r U(r)\Big)\,\vec{P}^2+\vec{P}\,\Big(\vec{\nabla}_r U(r)\Big)\cdot\vec{P}\Big) \\ & +\left(\vec{\sigma}^{(1)}-\vec{\sigma}^{(2)}\right)\cdot\left(\frac{1}{m_\pi}(\vec{P}\cdot\vec{\nabla}_r)^2\Big(\vec{\nabla}_r r U(r)\Big)\right) \\ & +\varepsilon^{ijk}\left(\sigma^{(1)\,i}\,\sigma^{(2)\,l}+\sigma^{(1)\,l}\,\sigma^{(2)\,i}\right)\,\left(\nabla_r^l\nabla_r^k U(r)\right)\,P^j\Big] \\ & +\frac{g_A\bar{g}_0\,\delta m_N}{2m_N F_\pi^2}\left(\boldsymbol{\tau}^{(1)}\times\boldsymbol{\tau}^{(2)}\right)_3\left(\vec{\sigma}^{(1)}-\vec{\sigma}^{(2)}\right) \\ & \cdot\left[U(r)\vec{P}-\frac{1}{m_\pi}\Big(\vec{\nabla}_r\,\nabla_r^i\,rU(r)\Big)\,P^i\right], \end{aligned} \tag{7.5.15}$$

where $\vec{P} = -i\vec{\nabla}_X$. Although the operators in Eq. (7.5.15) vanish in the two-nucleon center-of-mass frame and are not important for the study of T violation in nucleon-nucleon scattering, they impact observables like TV electromagnetic form factors of the deuteron, where the recoil against the photon changes the center-of-mass momentum of the nucleon pair, and they have to be considered in nuclear systems with

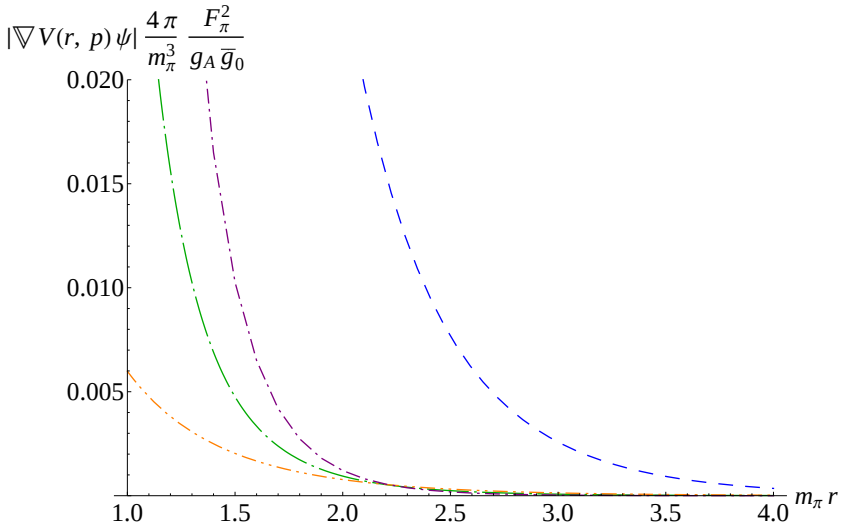

FIGURE 7.7. Comparison between a relativistic correction to OPE and local components of the TV two-nucleon potential $\nabla\mathcal{V}_0$ applied to an illustrative bound-state wave function ψ, in units of $g_A\bar{g}_0 m_\pi^3/4\pi F_\pi^2$, as functions of the distance r, in units of $1/m_\pi$. The (dark green) long-dashed-dotted line represents the term in the potential that is quadratic in momentum. Other curves are as in Fig. 7.4.

$A > 2$. An example of the effects of recoil on TC deuteron processes can be found in Compton scattering [249].

At leading order, the dimension 6 sources of TV only contribute to $V_{\not T,\min}(\vec{r})$, the two-nucleon potential with minimal number of derivatives, in Eq. (7.5.3). We find

$$\mathcal{V}_0^{(-1)}(r) = -\frac{g_A(\bar{g}_{0\,q}+\bar{g}_{0\,w})}{F_\pi^2}\,U(r) + \bar{C}_{w\,2}\frac{\delta(r)}{8\pi r^2}, \tag{7.5.16}$$

$$\mathcal{U}_0^{(-1)}(r) = +\bar{C}_{w\,1}\frac{\delta(r)}{8\pi r^2}, \tag{7.5.17}$$

$$\mathcal{V}_1^{(-1)}(r) = -\frac{g_A(\bar{g}_{1\,q}+\bar{g}_{1\,w})}{F_\pi^2}U(r), \tag{7.5.18}$$

$$\mathcal{U}_1^{(-1)}(r) = -\frac{g_A(\bar{g}_{1\,q}+\bar{g}_{1\,w})}{F_\pi^2}U(r). \tag{7.5.19}$$

In the case of the qCEDM, at leading order the potential is dominated by OPE, while in the case of the gCEDM and the TV four-quark operators, short-range effects are also leading.

7.6 Conclusions

The power-counting scheme of EFTs allowed us to organize the contributions to the potential in powers of M_{QCD}^{-1}. The TV PV potential from the QCD $\bar{\theta}$ term has a similar ordering as the TC PV potential [90]. At leading order, $\mathcal{O}(Q/M_{QCD})$, we find only the well-known OPE from the $I = 0$ pion-nucleon TV coupling [195]. The OPE from the $I = 1$ pion-nucleon TV coupling is suppressed by two orders in the expansion parameter and is of $\mathcal{O}(Q^3/M_{QCD}^3)$. Since the $I = 0$ OPE is suppressed in nuclei, higher orders in the potential could be important.

We have thus also examined the corrections in the next two orders, which are up to $\mathcal{O}(Q^2/M_{QCD}^2)$ relative to leading. We have found that the potential is purely two-body, and:

- At the longest, one-pion range, there are more general vertex corrections than usually assumed. We employed the results of Ref. [39] where the TV pion-nucleon vertex was examined to this order. In addition to the qualitatively different $I = 1$ pion-nucleon TV coupling, there are corrections to the local potential stemming from isospin breaking in the pion and nucleon masses, and in the TC pion-nucleon coupling. There are also recoil ($\propto 1/m_N$) and relativistic ($\propto 1/m_N^2$) corrections to leading OPE, which make the potential non-local and dependent on the total momentum of the nucleon pair.

- At this order, we find, additionally, two-pion exchange from the $I = 0$ TV coupling. The non-analytic, medium-range part of the TPE potential is independent of the choice of fields and regulators. Like the leading OPE potential, this part of the TPE potential has as only (so-far) unknown quantity the $I = 0$ TV pion-nucleon coupling. Under reasonable assumptions about the strengths of TV couplings, this potential is stronger, and has a different radial dependence, than phenomenological one-meson-exchange potentials. The main effect of TPE is to modify the potential in the same channels as the leading OPE

potential.

- The short-range part of the TPE potential, on the other hand, cannot be separated from contact interactions, the most general form of which we also write at this order. They are two of the terms given in the literature [159]. In the context of a theory without pions, this implies a contribution to only two of five possible S–P transitions. When pions are included explicitly, the short-range terms are expected to be of the same size as TPE, and thus their strengths depend on the renormalization scale. They subsume short-range dynamics that includes the effects of heavier mesons, but whether such effects are sufficient to saturate them is unknown.

The structure of the resulting potential is therefore significantly different than the phenomenological potential used in the literature, due to the specific way in which the $\bar{\theta}$ term breaks chiral symmetry. If consideration of short-range dynamics or $I = 1$ OPE is necessary, one should also include the TPE potential and OPE corrections calculated here. EFT offers a framework where the calculation of nuclear TV observables can be carried out in a model independent way.

Chapter 8
Conclusion

In this dissertation I have studied applications of Effective Field Theory techniques to problems in hadronic and nuclear physics.

Our first example, the exclusive decays of the χ_b and η_b into two D mesons, to which we devoted Chapter 2, is the perfect boot camp for effective-field-theorists to-be. The problem contains a non-relativistic bound state, the bottomonium states χ_b or η_b, that decays in a pair of fast-moving, but massive, final states. Its discussion in an EFT framework calls for a combination of non relativistic EFTs (NRQCD, pNRQCD) for the description of the initial state, and effective theories for fast-moving, almost light-like, but massive, particles for the final state (SCET with masses, bHQET). The EFT approach allows to achieve a factorization theorem for the decay rate, that can be written in terms of two matching coefficients and three non-perturbative matrix elements, one for each hadron. By solving the renormalization group equations in the EFTs we evolve the matching coefficients from their natural scales at high energy ($2m_b$ and m_c) to the low energy scale, where the non-perturbative matrix elements sit. In this way, we improve perturbation theory by resumming possibly large logarithms of the ratio of scales in the problem. The study of this process, thus, gave us the possibility to face various technical aspects of the three most important EFTs developed for QCD in a perturbative regime, HQET, NRQCD and SCET.

Unfortunately, our analysis shows that the branching ratios for these decay channels are rather small (see Fig. 2.12). As we argued in Sec. 2.5, even their interesting qualitative features, like the strong dependence on the light-cone structure of the D meson, require, before any quantitative information can be extracted from these channels, a refinement of our theoretical treatment (the inclusion of perturbative and non-perturbative corrections), which, in the absence of a measurement of the branch-

ing ratios, is not worthy to pursue. To reiterate, the most important lesson from our study is the familiarization with EFT techniques that are applicable to several other interesting processes involving highly energetic and massive particles. A two-step approach similar to that delineated in Chapter 2 can, for example, be applied to the study of the fragmentation of a highly energetic heavy quark into a heavy meson, in the process $e^+e^- \to D(B) + X$. Once again, we believe that an EFT approach can clarify the interplay between the different mass scales relevant to the process, and define in a systematic and model-independent way non-perturbative effects. We are currently working on this problem.

The second application I discussed carried us in the realm of nuclear physics. The main result of the work of my collaborators and I is the establishment of a coherent framework to study T violation in one- and few-nucleon systems, based on nuclear EFTs.

In Chapter 3 we identify the TV sources we are taking into account. We include all the TV operators with dimension up to 6 that can be written in terms of light degrees of freedom, light quarks, photons and gluons, and we catalog them according to their chiral properties. The second step, described in Chapter 4, is the construction of the low-energy Lagrangian. The interesting observation here is that different properties of the fundamental sources of T violation under chiral symmetry imply different relations between short- and long-distance contributions to nuclear TV observables. For example, for sources that violate chiral symmetry the interaction with lowest chiral index are pion-nucleon non derivative TV couplings. As a consequence, long-distance effects, mediated by pions, are likely to dominate TV observables. On the other hand, for chiral invariant sources, TV pion-nucleon couplings, short-distance nucleon EDM operators and short-distance TV four-nucleon couplings all appear at the same order, so that long- and short-distance physics contribute to many observables at the same level. Finally for the qEDM, indirect electromagnetic operators are suppressed by the electromagnetic coupling constant $\alpha_{\rm em}/\pi$, and TV observables like the nucleon and

deuteron EDMs are dominated by TV currents.

Not only it is important whether a TV source breaks chiral symmetry or not, it is also important how it breaks it. For example, the QCD $\bar{\theta}$ term breaks chiral symmetry, but not isospin, while the qCEDM is expected to break chiral symmetry and isospin at the same level. The consequence at low energy is that these two sources generate very different hierarchies between TV non derivative pion-nucleon couplings: $\bar{\theta}$ only contributes to the isoscalar coupling $\bar{g}_0$ in LO, while for the qCEDM $\bar{g}_1$ and $\bar{g}_0$ arise at the same level.

In the third step, we examine the implications of these different relations for TV observables in the one- and two-nucleon sectors. We dedicate Chapter 5 to the nucleon EDFF. The measurement of the neutron and proton EDMs alone, though would be an incredibly exciting finale to a hunt lasted for more than 50 years, would not provide enough information to differentiate between T violation from the $\bar{\theta}$ term or from the dimension 6 sources of T violation. In Chapter 6 we study the deuteron EDM and MQM. A measurement of the nucleon and deuteron EDM would give interesting clues. A deuteron EDM substantially bigger than the nucleon EDM (in particular, than the isoscalar nucleon EDM) would indicate the qCEDM as likely culprit. $\bar{\theta}$, the qEDM and the chiral invariant TV sources all predict that the deuteron EDM is well approximated by the isoscalar nucleon EDM, so a measurement of a deuteron EDM of the same size as the nucleon EDM would not be conclusive. If also the deuteron MQM were to be observed, and observed to be substantially bigger than the deuteron EDM, one would have good reasons to believe to be in the presence of TV from the $\bar{\theta}$ term.

Unfortunately, the indications we can receive from nucleon and deuteron experiments are qualitative. In the case of qCEDM, the isovector and isoscalar nucleon EDM, and the deuteron EDM and MQM depend on four LECs. An observation of these four quantities will then be sufficient to fix the LECs, but not enough to verify any prediction. In the case of the $\bar{\theta}$ term, the nucleon EDM and the deuteron MQM

depend on three TV LECs. Once the isoscalar nucleon EDM is observed, then the deuteron EDM is a prediction, but not sufficient to pinpoint $\bar{\theta}$ as dominant TV source. The deuteron MQM and the isovector nucleon EDM can fix the other two LECs, in particular $\bar{g}_0$, but once again there is no room for a model-independent predictions.

Even a measurement of the TV moments of the deuteron, then, will not be conclusive. However, and here we see the power of the EFT approach, the framework we set up can be extended to other observables. The most promising is the EDM of ^{3}He and ^{3}H, which is sensitive to both $\bar{g}_0$ and $\bar{g}_1$ [161], and thus, both for TV from the $\bar{\theta}$ term and the qCEDM, would be dominated by TV OPE correction to the three-nucleon wavefunction. Consequently, if nucleon and deuteron TV moments are observed, the EDM of ^{3}He and ^{3}H is a testable and falsifiable prediction of the theory, opening up the possibility to quantitatively discriminate between different TV sources.

The natural conclusion of our work on T violation in nuclear physics is the calculation of the EDM of ^{3}He and ^{3}H from the QCD $\bar{\theta}$ term and the dimension 6 sources, in the perturbative pion approach.

While we work to this goal, we also have to settle some interesting technical questions we have sidestepped. First of all, we have to check the convergence of the perturbative pion approach, by completing the NLO corrections to our results in Chapter 6. The indication that the range of validity of the perturbative pion approach is not significantly larger than that of the pionless theory [193] suggests that the pions should be treated non-perturbatively; we plan to repeat the calculation of the deuteron and ^{3}He EDMs with non-perturbative pions. To this goal, the derivation of the TV potential in Chapter 7 is a necessary prerequisite. Finally, in our work we have always neglected the strange quark, it is interesting to extend our analysis of T violation to $SU_L(3) \otimes SU_R(3)$ chiral symmetry, in particular to see whether more information can be extracted from the link between TV and isospin symmetry breaking.

Appendix A

Solution of the running equation in pNRQCD and bHQET

The RGE in Eq. (2.4.28) can be solved by applying the methods discussed in Ref. [60] to find the evolution of the B-meson distribution amplitude. We generalize this approach to the specific case discussed here, where two distribution amplitudes are present. Following Ref. [60], we define

$$\omega\Gamma(\omega,\omega',\alpha_s) = -\frac{\alpha_s C_F}{\pi}\left[\theta\left(\omega-\omega'\right)\left(\frac{1}{\omega-\omega'}\right)_+ + \theta\left(\omega'-\omega\right)\theta\left(\omega\right)\frac{\omega}{\omega'}\left(\frac{1}{\omega'-\omega}\right)_+\right] .$$

Lange and Neubert [60] prove that

$$\int d\omega'\omega\Gamma(\omega,\omega',\alpha_s)(\omega')^a = \omega^a\mathcal{F}(a,\alpha_s) , \tag{A.1}$$

with

$$\mathcal{F}(a,\alpha_s) = \frac{\alpha_s C_F}{\pi}\left[\psi(1+a)+\psi(1-a)+2\gamma_E\right] .$$

ψ is the digamma function and γ_E the Euler constant. Eq. (A.1) is valid if $-1 < \mathrm{Re}\, a < 1$. Exploiting (A.1), a solution of the running equation Eq. (2.4.28) with initial condition $T(\omega,\bar\omega,\mu_0') = (\omega/\mu_0')^\eta\,(\bar\omega/\mu_0')^\xi$ at a certain scale μ_0' is

$$F^2(\mu')T(\omega,\bar\omega,\mu') = F^2(\mu_0')f(\omega,\mu',\mu_0',\eta)f(\bar\omega,\mu',\mu_0',\xi) , \tag{A.2}$$

with

$$\begin{aligned}
&f(\omega,\mu',\mu_0',\eta) = \left(\frac{\omega}{\mu_0'}\right)^{\eta-g}(\bar n\cdot v)^g \exp U(\mu_0',\mu',\eta) ,\\
&g \equiv g(\mu_0',\mu') = \int_{\alpha_s(\mu_0')}^{\alpha_s(\mu')}\frac{d\alpha}{\beta(\alpha)}\Gamma_{\rm cusp}(\alpha) ,\\
&U(\mu_0',\mu',\eta) = \int_{\alpha_s(\mu_0')}^{\alpha_s(\mu')}\frac{d\alpha}{\beta(\alpha)}\left[\Gamma_{\rm cusp}(\alpha)\int_{\alpha_s(\mu_0')}^{\alpha}\frac{d\alpha'}{\beta(\alpha')}+\gamma_1(\alpha)+\mathcal{F}(\eta-g,\alpha)\right] ,\\
&\gamma_1(\alpha_s) = -2\frac{\alpha_s C_F}{4\pi} .
\end{aligned} \tag{A.3}$$

The function $f(\bar{\omega}, \mu', \mu_0', \xi)$ has the same form as $f(\omega, \mu', \mu_0', \eta)$ and is obtained by replacing $\omega \to \bar{\omega}$, $\eta \to \xi$, and $\bar{n} \cdot v \to n \cdot v'$ in Eq. (A.3). The integrals over α can be performed explicitly using the beta function in Eq. (2.3.24). The result is

$$\begin{aligned} f(\omega, \mu', \mu_0', \eta) f(\bar{\omega}, \mu', \mu_0', \xi) = & \left(\frac{\omega}{\mu_0'}\right)^{\eta - g} \left(\frac{\bar{\omega}}{\mu_0'}\right)^{\xi - g} (\bar{n} \cdot v \, n \cdot v')^g \exp\left[V(\mu_0', \mu')\right] \\ & \frac{\Gamma(1 - \eta + g)\Gamma(1 + \eta)}{\Gamma(1 + \eta - g)\Gamma(1 - \eta)} \frac{\Gamma(1 - \xi + g)\Gamma(1 + \xi)}{\Gamma(1 + \xi - g)\Gamma(1 - \xi)} , \end{aligned} \tag{A.4}$$

Where, at NLL,

$$g(\mu_0', \mu') = -\frac{\Gamma_{\text{cusp}}^{(0)}}{2\beta_0} \left\{ \ln r + \left(\frac{\Gamma_{\text{cusp}}^{(1)}}{\Gamma_{\text{cusp}}^{(0)}} - \frac{\beta_1}{\beta_0} \right) \frac{\alpha_{\text{s}}(\mu_0')}{4\pi} (r - 1) \right\} , \tag{A.5}$$

and

$$\begin{aligned} V(\mu_0', \mu') = & - \Gamma_{\text{cusp}}^{(0)} \frac{2\pi}{\beta_0^2} \left\{ \frac{r - 1 - r \ln r}{\alpha_s(\mu')} + \left(\frac{\Gamma_{\text{cusp}}^{(1)}}{\Gamma_{\text{cusp}}^{(0)}} - \frac{\beta_1}{\beta_0} \right) \frac{1 - r + \ln r}{4\pi} + \frac{\beta_1}{8\pi\beta_0} \ln^2 r \right\} \\ & + \frac{C_F}{\beta_0} (2 - 8\gamma_E) \ln r , \end{aligned} \tag{A.6}$$

with $r = \alpha_s(\mu')/\alpha_s(\mu_0')$. Notice that in the running from $\mu_0' = m_c$ to $\mu' = 1$ GeV only three flavors are active, so in the expressions for β_0, β_1, and $\Gamma_{\text{cusp}}^{(1)}$ we use $n_f = 3$.

Eq. (A.4) is the solution for the initial condition $T(\omega, \bar{\omega}, \mu_0') = (\omega/\mu_0')^\eta \, (\bar{\omega}/\mu_0')^\xi$. To solve the RGE for a generic initial condition, we express T as the Fourier transform with respect to $\ln \omega/\mu_0'$,

$$\begin{aligned} T(\omega, \bar{\omega}, \mu_0') &= \frac{1}{(2\pi)^2} \int_{-\infty}^{+\infty} dr ds \exp\left(-ir \ln \frac{\omega}{\mu_0'}\right) \exp\left(-is \ln \frac{\bar{\omega}}{\mu_0'}\right) F[T](r, s, \mu_0') \\ &= \frac{1}{(2\pi)^2} \int_{-\infty}^{+\infty} dr ds \left(\frac{\omega}{\mu_0'}\right)^{-ir} \left(\frac{\bar{\omega}}{\mu_0'}\right)^{-is} F[T](r, s, \mu_0') , \end{aligned}$$

where $F[T]$ denotes the Fourier transform of T. From the solution (A.2)-(A.4) it follows that

$$\begin{aligned} F^2(\mu') T(\omega, \bar{\omega}, \mu') = & \frac{F^2(\mu_0')}{(2\pi)^2} \int_{-\infty}^{+\infty} dr ds \left(\frac{\omega}{\mu_0'}\right)^{-ir-g} \left(\frac{\bar{\omega}}{\mu_0'}\right)^{-is-g} (\bar{n} \cdot v \, n \cdot v')^g \\ & F[T](r, s, \mu_0') \exp\left[V(\mu_0', \mu')\right] \frac{\Gamma(1 + ir + g)\Gamma(1 - ir)}{\Gamma(1 - ir - g)\Gamma(1 + ir)} \frac{\Gamma(1 + is + g)\Gamma(1 - is)}{\Gamma(1 - is - g)\Gamma(1 + is)} . \end{aligned} \tag{A.7}$$

The Fourier transform of the matching coefficient in Eq. (A.7) has to be understood in the sense of distributions [250]. That is, we define the Fourier transform of T as the function of r and s that satisfies

$$\frac{1}{(2\pi)^2}\int dr ds\, F[T](r,s,\mu')\varphi_A(r,\mu')\varphi_B(s,\mu') = \int_0^{+\infty}\frac{d\omega}{\omega}\frac{d\bar{\omega}}{\bar{\omega}}T(\omega,\bar{\omega},\mu')\phi_A(\omega,\mu')\phi_B(\bar{\omega},\mu')\ , \tag{A.8}$$

or, more precisely, $F[T](r,s,\mu')$ is the linear functional that acts on the test functions $\varphi_A(r)$ and $\varphi_B(s)$ according to

$$\frac{1}{(2\pi)^2}(F[T](r,s,\mu'),\ \varphi_A(r,\mu')\varphi_B(s,\mu')) = \int_0^{+\infty}\frac{d\omega}{\omega}\frac{d\bar{\omega}}{\bar{\omega}}T(\omega,\bar{\omega},\mu')\phi_A(\omega,\mu')\phi_B(\bar{\omega},\mu')\ . \tag{A.9}$$

The function φ_A is the Fourier transform of the D-meson distribution amplitude,

$$\varphi_A(r,\mu') = \int_0^{\infty}\frac{d\omega}{\omega}\left(\frac{\omega}{\mu'}\right)^{ir}\phi_A(\omega,\mu')\ , \tag{A.10}$$

where the integral on the r.h.s. should converge in the ordinary sense because of the regularity properties of the D-meson distribution amplitude. As in Sec. 2.4, the subscript A denotes the spin and polarization of the D meson.

In the distribution sense, the Fourier transform of the coefficient $1/(\omega+\bar{\omega})$ is

$$\begin{aligned} F\left[\frac{1}{\omega+\bar{\omega}}\right](r,s,\mu_0') &= (2\pi)^2\frac{1}{2\mu_0'}\delta(r+s+i)\,\mathrm{sech}\left[\frac{\pi}{2}(r-s)\right] \\ &= \frac{1}{2}(2\pi)^2\frac{1}{2\mu_0'}\delta(R+i)\,\mathrm{sech}\left[\frac{\pi}{2}S\right]\ , \end{aligned} \tag{A.11}$$

where $R=r+s$, $S=r-s$, and the factor $\frac{1}{2}$ comes from the Jacobian of the change of variables. The hyperbolic secant is defined as $\mathrm{sech}=1/\cosh$. Similarly, we find

$$F\left[\frac{\omega-\bar{\omega}}{\omega+\bar{\omega}}\right](R,S,\mu_0') = \frac{i}{2}(2\pi)^2\delta(R)\left(\mathrm{cosech}\left[\frac{\pi}{2}S+i\varepsilon\right]+\mathrm{cosech}\left[\frac{\pi}{2}S-i\varepsilon\right]\right)\ . \tag{A.12}$$

The δ function in Eq. (A.11) has complex argument. The definition is analogous to the one in real space [250],

$$(\delta(R+i),\varphi(R)) = \varphi(-i)\ . \tag{A.13}$$

Using Eqs. (A.11) and (A.12), we can perform the integral in Eq. (A.7), obtaining respectively $T(\omega,\bar{\omega},\mu,\mu';\,^3P_J)$ and $T(\omega,\bar{\omega},\mu,\mu';\,^1S_0)$. In order to give an explicit example, we proceed using Eq. (A.11). Integrating the δ function we are left with

$$\begin{aligned} F^2(\mu')T(\omega,\bar{\omega};\mu') = {} & F^2(\mu'_0)\exp\left[V(\mu'_0,\mu')\right]\frac{1}{\mu'_0}\left(\frac{\mu'^2_0}{\omega\bar{\omega}}\right)^{1/2+g}(\bar{n}\cdot v\, n\cdot v')^g \\ & \int_{-\infty}^{\infty} dS \exp\left[-i\frac{S}{2}\ln\frac{\omega}{\bar{\omega}}\right]\mathrm{sech}\left[\frac{\pi}{2}S\right]\frac{1}{1+S^2}\frac{\Gamma\left(\frac{3}{2}+g+\frac{i}{2}S\right)}{\Gamma\left(\frac{1}{2}-g-\frac{i}{2}S\right)}\frac{\Gamma\left(\frac{3}{2}+g-\frac{i}{2}S\right)}{\Gamma\left(\frac{1}{2}-g+\frac{i}{2}S\right)}\,. \end{aligned} \tag{A.14}$$

The integral (A.14) can be done by contour. The integrand has poles along the imaginary axis. In $S=\pm i$ there is a double pole, coming from the coincidence of one pole of the hyperbolic secant and the singularities in $1/(1+S^2)$. The Γ functions in the numerator have poles respectively in $S=\pm i\,(2n+3+2g)$ with $n>0$, while the other poles of sech are in $S=\pm i(2n+1)$, with $n\geq 1$. We close the contour in the upper half plane for $\bar{\omega}>\omega$ and in the lower half plan for $\omega>\bar{\omega}$, obtaining

$$\begin{aligned} F^2(\mu')T(\omega,\bar{\omega},\mu') = {} & F^2(\mu'_0)\exp\left[V(\mu'_0,\mu')\right]\,\theta(\bar{\omega}-\omega)\frac{1}{\bar{\omega}}\left(\frac{\mu'^2_0\bar{n}\cdot v\, n\cdot v'}{\omega\bar{\omega}}\right)^g \\ & \left\{\frac{\Gamma(1+g)\Gamma(2+g)}{\Gamma(1-g)\Gamma(-g)}\left[1-\ln\frac{\omega}{\bar{\omega}}+\psi(1-g)-\psi(-g)+\psi(1+g)-\psi(2+g)\right]\right. \\ & +\sum_{n=1}^{\infty}(-)^{n+1}\left(\frac{\omega}{\bar{\omega}}\right)^n\frac{1}{n(n+1)}\frac{\Gamma(1-n+g)\Gamma(2+n+g)}{\Gamma(-n-g)\Gamma(1-g+n)} \\ & \left.-\sum_{n=1}^{\infty}\left(\frac{\omega}{\bar{\omega}}\right)^{n+g}\frac{\pi}{(n-1)!}\csc(g\pi)\frac{1}{(n+g)(1+n+g)}\frac{\Gamma(2+n+2g)}{\Gamma(1+n)\Gamma(-n-2g)}\right\} \\ & +(\omega\to\bar{\omega})\ , \end{aligned} \tag{A.15}$$

with $\csc(g\pi)=1/\sin(g\pi)$ and ψ is the digamma function. More compactly, we can

express Eq. (A.15) using the hypergeometric functions ${}_4F_3$ and ${}_3F_2$,

$$
\begin{aligned}
&F^2(\mu')\,T(\omega,\bar\omega,\mu,\mu';\,{}^3P_J) = F^2(\mu'_c)\frac{C_F}{N_c^2}\frac{4\pi\alpha_s(\mu'_c)}{m_b}\exp\left[V(\mu'_c,\mu')\right]\,\left(\frac{{\mu'_c}^2\bar n\cdot vn\cdot v'}{\omega\,\bar\omega}\right)^g\\
&\frac{\theta(\bar\omega-\omega)}{\bar\omega}\left\{\frac{\Gamma(1+g)\Gamma(2+g)}{\Gamma(1-g)\Gamma(-g)}\left[1-\ln\frac{\omega}{\bar\omega}+\psi(1-g)-\psi(-g)+\psi(1+g)-\psi(2+g)\right]\right.\\
&+\frac{1}{2}\frac{\omega}{\bar\omega}\,\frac{\Gamma(g+2)\Gamma(g+3)}{\Gamma(1-g)\Gamma(2-g)}\,{}_4F_3\left(1,1,g+2,g+3;3,1-g,2-g;-\frac{\omega}{\bar\omega}\right)\\
&\left.-\left(\frac{\omega}{\bar\omega}\right)^{1+g}4\cos(g\pi)\frac{\Gamma(2+2g)^2}{g+2}\,{}_3F_2\left(g+1,2g+2,2g+3;2,g+3;-\frac{\omega}{\bar\omega}\right)\right\}\\
&+(\omega\to\bar\omega)\ ,
\end{aligned}
\tag{A.16}
$$

where we have introduced the constants that appear in the initial condition in Eq. (2.4.4). In the same way, we obtain

$$
\begin{aligned}
&F^2(\mu')\,T(\omega,\bar\omega,\mu,\mu';\,{}^1S_0) = F^2(\mu'_c)\frac{C_F}{2N_c^2}\frac{4\pi\alpha_s(\mu'_c)}{m_b}\exp\left[V(\mu'_c,\mu')\right]\,\theta(\bar\omega-\omega)\\
&\left(\frac{{\mu'_c}^2\bar n\cdot vn\cdot v'}{\omega\,\bar\omega}\right)^g\left\{2\frac{\Gamma(1+g)\Gamma(2+g)}{\Gamma(1-g)\Gamma(2-g)}\frac{\omega}{\bar\omega}\,{}_3F_2\left(1,g+1,g+2;1-g,2-g;-\frac{\omega}{\bar\omega}\right)\right.\\
&\left.+\frac{\Gamma^2(1+g)}{\Gamma^2(1-g)}-\left(\frac{\omega}{\bar\omega}\right)^{1+g}4\cos(g\pi)\Gamma(1+2g)\Gamma(2g+2)\,{}_2F_1\left(2g+2,2g+1;2;-\frac{\omega}{\bar\omega}\right)\right\}\\
&-(\omega\to\bar\omega)\ .
\end{aligned}
\tag{A.17}
$$

In Eqs. (A.16) and (A.17) we renamed the initial scale $\mu'_0=\mu'_c$ to denote its connection to the scale m_c. Setting $\mu'=\mu'_c$ or, equivalently, $g=0$, it can be explicitly verified that the solutions Eqs. (A.16) and (A.17) satisfy the initial conditions Eq. (2.4.4).

Appendix B

Boost transformation of the D-meson distribution amplitude

We derive in this Appendix the relation between the distribution amplitudes in the D-meson and in the bottomonium rest frames, as given in Eq. (2.5.3). In the D-meson rest frame, characterized by the velocity label $v_0 = (1, 0, 0, 0)$, the local heavy-light matrix element is defined as

$$\langle 0|\bar{\xi}^{\bar{l}}_n(0)\frac{\bar{n}\!\!\!/}{2}\gamma_5\, h^c_n(0)|D\rangle_{v_0} = -iF(\mu')\frac{\bar{n}\cdot v_0}{2}\ . \tag{B.1}$$

The matrix element of the heavy- and light-quark fields at a light-like separation $z^\mu_0 = n\cdot z_0\,\bar{n}^\mu/2$ defines the light-cone distribution $\tilde{\phi}_0(n\cdot z_0,\mu')$ in coordinate space:

$$\langle 0|\bar{\chi}^{\bar{l}}_n(n\cdot z_0)\,\frac{\bar{n}\!\!\!/}{2}\gamma_5\,\mathcal{H}^c_n(0)|D\rangle_{v_0} = -iF(\mu')\frac{\bar{n}\cdot v_0}{2}\,\tilde{\phi}_0(n\cdot z_0,\mu')\ . \tag{B.2}$$

Eqs. (B.1) and (B.2) imply $\tilde{\phi}_0(0,\mu') = 1$. In the definitions (B.1) and (B.2) the subscript 0 is used to denote quantities in the D-meson rest frame. This convention is used in the rest of this Appendix. In the bottomonium rest frame, where the velocity label in light-cone coordinates is $v = (n\cdot v, \bar{n}\cdot v, 0)$ and the light-like separation is $z^\mu = n\cdot z\,\bar{n}^\mu/2$, we define

$$\langle 0|\bar{\xi}^{\bar{l}}_n(0)\frac{\bar{n}\!\!\!/}{2}\gamma_5\, h^c_n(0)|D\rangle_{v} = -iF(\mu')\frac{\bar{n}\cdot v}{2} \tag{B.3}$$

and

$$\langle 0|\bar{\chi}^{\bar{l}}_n(n\cdot z)\,\frac{\bar{n}\!\!\!/}{2}\gamma_5\,\mathcal{H}^c_n(0)|D\rangle_{v} = -iF(\mu')\frac{\bar{n}\cdot v}{2}\,\tilde{\phi}(n\cdot z,\mu')\ . \tag{B.4}$$

Suppose that Λ is some standardized boost that takes the D meson from v, its velocity in the bottomonium rest frame, to rest. It is straightforward to find the relations between the D-meson momenta in the two frames:

$$n\cdot p_0 = \bar{n}\cdot v n\cdot p \quad \text{and} \quad \bar{n}\cdot p_0 = n\cdot v\bar{n}\cdot p\ .$$

There is a similar relation for the light-cone coordinates,

$$n \cdot z_0 = \bar{n} \cdot v \, n \cdot z \; .$$

With $U(\Lambda)$, the unitary operator that implements the boost Λ, one can write

$$U(\Lambda)|D\rangle_v = |D\rangle_{v_0} \; .$$

We choose Λ such that, for the Dirac fields,

$$U(\Lambda)\xi_n^{\bar{l}}(x)\, U^{-1}(\Lambda) = \Lambda_{1/2}^{-1}\, \xi^{\bar{l}}(\Lambda x) \quad \text{and} \quad U(\Lambda)h_n^c(x)\, U^{-1}(\Lambda) = \Lambda_{1/2}^{-1}\, h^c(\Lambda x) \; ,$$

where

$$\Lambda_{1/2} = \cosh\frac{\alpha}{2} + \frac{\not{\bar{n}}\not{n} - \not{n}\not{\bar{n}}}{4} \sinh\frac{\alpha}{2} \; ,$$

with α related to v by $e^{\alpha} = \bar{n} \cdot v$ and $e^{-\alpha} = n \cdot v$.

Now we can write the matrix element in Eq. (B.3) as

$$\begin{aligned}
&\langle 0|\, \bar{\xi}_n^{\bar{l}} \frac{\not{\bar{n}}}{2} \gamma_5 h_n^c(0)|D\rangle_v \\
&\quad = \langle 0|U^{-1}(\Lambda) \left(U(\Lambda)\bar{\xi}_n^{\bar{l}}(0)U^{-1}(\Lambda) \right) \frac{\not{\bar{n}}}{2}\gamma_5 \left(U(\Lambda)h_n^c(0)U^{-1}(\Lambda) \right) U(\Lambda)|D\rangle_v \\
&\quad = \langle 0|\bar{\xi}^{\bar{l}}(0)\Lambda_{1/2}\frac{\not{\bar{n}}}{2}\gamma_5\Lambda_{1/2}^{-1}h^c(0)|D\rangle_{v_0} = \bar{n}\cdot v\, \langle 0|\bar{\xi}^{\bar{l}}(0)\frac{\not{\bar{n}}}{2}\gamma_5 h^c(0)|D\rangle_{v_0} \\
&\quad = -iF(\mu')\frac{\bar{n}\cdot v}{2}\bar{n}\cdot v_0 = -iF(\mu')\frac{\bar{n}\cdot v}{2} \; .
\end{aligned} \tag{B.5}$$

where, in the last step, we have used $\bar{n} \cdot v_0 = 1$. Eq. (B.5) is thus in agreement with the definition in Eq. (B.3). Applying the same reasoning to Eq. (B.4), one finds

$$\begin{aligned}
\langle 0|\bar{\chi}_n^{\bar{l}}(n\cdot z)\, \frac{\not{\bar{n}}}{2}\gamma_5\, \mathcal{H}_n^c(0)|D\rangle_v &= \bar{n}\cdot v\, \langle 0|\bar{\chi}^{\bar{l}}(\bar{n}\cdot v\, n\cdot z)\, \frac{\not{\bar{n}}}{2}\gamma_5\, \mathcal{H}^c(0)|D\rangle_{v_0} \\
&= -iF(\mu')\frac{\bar{n}\cdot v}{2}\, \tilde{\phi}_0(n\cdot z_0, \mu') \; .
\end{aligned} \tag{B.6}$$

Comparing Eq. (B.6) with (B.4), we see that $\tilde{\phi}(n\cdot z, \mu') = \tilde{\phi}_0(\bar{n}\cdot v\, n\cdot z, \mu')$. Note that in the bottomonium rest frame the normalization condition for the distribution amplitude is also $\tilde{\phi}(0, \mu') = 1$.

In the main text of this paper we have used the D-meson distribution amplitudes in momentum space,

$$\phi_0(\omega_0,\mu') \equiv \frac{1}{2\pi}\int dn\cdot z_0\, e^{i\omega_0 n\cdot z_0}\tilde{\phi}_0(n\cdot z_0,\mu')\;,$$
$$\phi(\omega,\mu') \equiv \frac{1}{2\pi}\int dn\cdot z\, e^{i\omega n\cdot z}\tilde{\phi}(n\cdot z,\mu')\;.$$

Using Eq. (B.6), we can relate the two distributions:

$$\begin{aligned}\phi(\omega,\mu') &= \frac{1}{2\pi}\int dn\cdot z\, e^{i\omega n\cdot z}\tilde{\phi}(n\cdot z,\mu') = \frac{1}{2\pi}\int dn\cdot z\, e^{i\omega n\cdot z}\tilde{\phi}_0(\bar{n}\cdot v\, n\cdot z,\mu')\\ &= \frac{1}{2\pi}\frac{1}{\bar{n}\cdot v}\int dn\cdot z\, e^{i\frac{\omega}{\bar{n}\cdot v}n\cdot z}\tilde{\phi}_0(n\cdot z,\mu') = \frac{1}{\bar{n}\cdot v}\phi_0\left(\frac{\omega}{\bar{n}\cdot v},\mu'\right)\;,\end{aligned}$$

as stated in Eq. (2.5.3). The D-meson light-cone distribution is normalized to 1 in both frames,

$$\int d\omega_0\phi_0(\omega_0,\mu') = \int d\omega\phi(\omega,\mu') = 1,$$

as can be easily proved using $\tilde{\phi}_0(0,\mu') = \tilde{\phi}(0,\mu') = 1$.

Appendix C

Spontaneous Chiral Symmetry Breaking

Here we discuss spontaneous chiral symmetry breaking for two quark flavors combined in an isospin doublet, Eq. (3.2.2), following Refs. [32, 122]. The QCD Lagrangian (3.2.1) for massless and chargeless quarks is invariant under a chiral transformation (3.2.7). The $(G^A) = (\boldsymbol{t}, \boldsymbol{x})$ have the commutation relations

$$\begin{aligned} \left[t^i, t^j\right] &= i\varepsilon^{ijk}\, t^k, \\ \left[x^i, x^j\right] &= i\varepsilon^{ijk}\, t^k, \\ \left[t^i, x^j\right] &= i\varepsilon^{ijk}\, x^k, \end{aligned} \tag{C.1}$$

and generate the chiral group $SU_L(2) \times SU_R(2)$, which is isomorphic to the group $SO(4)$ of rotations in four-dimensional Euclidean space. Acting on four-dimensional vectors, the generators are written as

$$\begin{aligned} (\mathcal{T}^a)_{bc} &= -i\varepsilon^{abc}, & (\mathcal{T}^a)_{b4} &= (\mathcal{T}^a)_{4b} = (\mathcal{T}^a)_{44} = 0, \\ (\mathcal{X}^a)_{b4} &= -(\mathcal{X}^a)_{4b} = -i\delta_{ab}, & (\mathcal{X}^a)_{bc} &= (\mathcal{X}^a)_{44} = 0. \end{aligned} \tag{C.2}$$

The chiral symmetry of the QCD Lagrangian is spontaneously broken to its vector (isospin) subgroup $SU_V(2)$, isomorphic to $SO(3)$: $SU_L(2) \times SU_R(2) \to SU_V(2)$ or, equivalently, $SO(4) \to SO(3)$. Goldstone's theorem requires that for each broken symmetry a massless particle exists, with spin 0 and the same parity and internal quantum numbers as the current associated to the broken generators. Here there are three broken generators, $\boldsymbol{x}$, and thus three massless, spin-0 Goldstone bosons with negative parity, identified with the pions. The Goldstone bosons live in the coset space $SU_L(2) \times SU_R(2)/SU_V(2) \sim SO(4)/SO(3) \sim S^3$, the "chiral circle". We can parametrize this space with stereographic coordinates $\boldsymbol{\zeta}(x) = \boldsymbol{\pi}(x)/F_\pi$, where $\boldsymbol{\pi}(x)$ is the canonically normalized pion field and $F_\pi \simeq 186$ MeV (the "pion decay constant")

is the diameter of the chiral circle. The point on the chiral circle labeled by $\boldsymbol{\zeta}$ is obtained by a rotation $R_{\alpha\beta}[\boldsymbol{\zeta}]$,

$$\sum_{\gamma=1}^{4} R_{\alpha\gamma} R_{\beta\gamma} = \delta_{\alpha\beta}, \tag{C.3}$$

from the north pole $(\mathbf{0}\ 1)^T$, given by

$$R_{\alpha\beta}[\boldsymbol{\zeta}] = \begin{pmatrix} \delta_{ij} - \frac{2}{D}\zeta_i\zeta_j & \frac{2}{D}\zeta_i \\ -\frac{2}{D}\zeta_j & \frac{1}{D}(1-\boldsymbol{\zeta}^2) \end{pmatrix}, \tag{C.4}$$

where

$$D = 1 + \boldsymbol{\zeta}^2. \tag{C.5}$$

Under an infinitesimal isospin transformation, the Goldstone-boson field $\boldsymbol{\zeta}$ transforms like an isovector

$$\delta\boldsymbol{\zeta} = \boldsymbol{\theta}_V \times \boldsymbol{\zeta}, \tag{C.6}$$

while an infinitesimal axial transformation is non-linear in the field,

$$\delta\boldsymbol{\zeta} = (1-\boldsymbol{\zeta}^2)\boldsymbol{\theta}_A + 2\,(\boldsymbol{\theta}_A \cdot \boldsymbol{\zeta})\,\boldsymbol{\zeta}. \tag{C.7}$$

It is convenient to introduce the covariant derivative of the pion field,

$$D_\mu\boldsymbol{\zeta} = \frac{\partial_\mu\boldsymbol{\zeta}}{D}, \tag{C.8}$$

which has simpler transformation properties: it is an isovector,

$$\delta D_\mu\boldsymbol{\zeta} = \boldsymbol{\theta}_V \times D_\mu\boldsymbol{\zeta}, \tag{C.9}$$

that under an axial transformation transforms in the same way, but with a field-dependent angle $\boldsymbol{\zeta} \times \boldsymbol{\theta}_A$,

$$\delta D_\mu\boldsymbol{\zeta} = 2(\boldsymbol{\zeta} \times \boldsymbol{\theta}_A) \times D_\mu\boldsymbol{\zeta}. \tag{C.10}$$

One can also construct the covariant derivative of this covariant derivative,

$$\mathcal{D}_\nu D_\mu\boldsymbol{\zeta} = \partial_\nu D_\mu\boldsymbol{\zeta} - 2\,(\boldsymbol{\zeta} \cdot D_\mu\boldsymbol{\zeta})\,D_\nu\boldsymbol{\zeta} + 2\,(D_\nu\boldsymbol{\zeta} \cdot D_\mu\boldsymbol{\zeta})\,\boldsymbol{\zeta}, \tag{C.11}$$

and so on. These covariant objects make it simpler to construct interactions with the desired transformation properties.

Being light, pions are important degrees of freedom at low energies. In addition, the lightest baryons, the proton (p) and the neutron (n), are present in the ground state of strong-interacting systems. We then have to include a field $N(x) = (p\ n)^T$ and its interactions with pions. We choose N to transform non-linearly in the same way as $D_\mu \boldsymbol{\zeta}$. Being an isospin doublet, under an $SU(2)_V$ transformation,

$$\delta N = i\boldsymbol{t} \cdot \boldsymbol{\theta}_V N, \tag{C.12}$$

and under an infinitesimal axial transformation,

$$\delta N = 2i\boldsymbol{t} \cdot (\boldsymbol{\zeta} \times \boldsymbol{\theta}_A)\, N. \tag{C.13}$$

It is straightforward to show that the chiral-covariant derivative of this nucleon field is

$$\mathcal{D}_\mu N = (\partial_\mu + 2i\boldsymbol{t} \cdot \boldsymbol{\zeta} \times D_\mu \boldsymbol{\zeta})\, N. \tag{C.14}$$

As before, we can also define higher covariant derivatives. Notice that the covariant derivative of $D_\mu \boldsymbol{\zeta}$ in Eq. (C.11) is nothing but Eq. (C.14) in the adjoint representation, $(t^j)_{ik} = i\varepsilon^{ijk}$.

At the energies we are working at, a nucleon is non-relativistic since its typical momentum is much smaller than its mass, $Q \sim m_\pi \ll m_N$. The nucleon momentum can be written as

$$p^\mu = m_N v^\mu + k^\mu, \tag{C.15}$$

where the nucleon velocity satisfies $v^2 = 1$ and in the nucleon rest frame $v^\mu = (1, \vec{0})$, and the residual momentum $k \sim Q$. Pion-nucleon interactions do not modify the nucleon velocity but only the residual momentum. In this regime, the nucleon mass is not a dynamical scale and it can be eliminated from the theory by defining a velocity-dependent nucleon field [34]

$$N_v = \exp\left(im_N \not{v} \cdot x\right) N. \tag{C.16}$$

Derivatives of N_v are proportional to the residual momentum. The field N_v satisfies

$$\frac{1+\not{v}}{2}N_v = N_v, \tag{C.17}$$

which allows us to reduce the possible Dirac matrices to be used in the construction of operators bilinear in the heavy nucleon field to $\Gamma = \{1, S^\mu\}$. Here S^μ is the spin operator, satisfying

$$\begin{aligned} v\cdot S &= 0, \qquad S^2 N_v = -\frac{3}{4}N_v, \quad [S^\lambda, S^\sigma] = i\varepsilon^{\lambda\sigma\alpha\beta}v_\alpha S_\beta, \\ \{S^\lambda, S^\sigma\} &= \frac{1}{2}\left(v^\lambda v^\sigma - g^{\lambda\sigma}\right). \end{aligned} \tag{C.18}$$

In the nucleon rest frame, $S^\mu = (0, \vec{\sigma}/2)$. In the rest of this paper we drop the label v from the nucleon field.

The same procedure can be followed for other baryons. Since its mass difference to the nucleon is only a factor 2 larger than the pion mass, $m_\Delta - m_N \simeq 300$ MeV, the delta isobar is the most important of these resonances. For simplicity we neglect the delta in this paper. The method can be easily generalized for any baryon.

Chiral symmetry strongly constrains the form of the interactions among Goldstone bosons and other particles in the theory. The most general Lagrangian containing nucleons and pions, invariant under chiral symmetry, can be constructed by including all the operators that are invariant under isospin and contains the covariant derivative of the pion field $D_\mu \boldsymbol{\pi}$, the nucleon field N, and their covariant derivatives. Equations (3.3.10) and (3.3.11) are the most important examples.

Appendix D

Explicit Chiral Symmetry Breaking

Explicit symmetry breaking terms can be included in the effective Lagrangian by mimicking the breaking in the QCD Lagrangian [32, 122]. Consider the generic case in which the symmetry is explicitly broken by a linear combination of the components $\mathcal{O}_A$ of some representation D of the group:

$$\Delta\mathcal{L} = \sum_A c_A \mathcal{O}_A \tag{D.1}$$

with

$$\mathcal{O}_A \to \sum_B D_{AB}[g]\mathcal{O}_B \tag{D.2}$$

under a transformation g belonging to the symmetry group.

In a non-linear realization of the symmetry, two statements can be proved. First, there exists an element of the group $\gamma(\zeta)$ such that

$$\mathcal{O}_A[\boldsymbol{\zeta}, \psi] = \sum_B D[\gamma(\boldsymbol{\zeta})]_{AB}\mathcal{O}_B[0, \psi], \tag{D.3}$$

where ψ is a shorthand notation for the possible chiral-covariant fields in the theory, including nucleons, nucleon covariant derivatives, pion covariant derivatives, *etc.* Thus, operators with explicit Goldstone bosons, $\mathcal{O}[\boldsymbol{\zeta}, \psi]$, can be found if their representations and the form of the operators without Goldstone bosons, $\mathcal{O}[0, \psi]$, are known. Second,

$$\mathcal{O}_A[0, h\psi] = \sum_B D[h]_{AB}\mathcal{O}_B[0, \psi], \tag{D.4}$$

where h belongs to the unbroken subgroup $SO(3)$. That is, the operators without Goldstone bosons $\mathcal{O}[0, \psi]$ transform linearly under the unbroken subgroup, according to one of the representations of the subgroup that can be found in D_{AB}.

In the simplest example, the $SO(4)$ representation is the defining (vector) representation, so $D[\gamma(\zeta)] = \gamma(\zeta)$ and $\gamma(\zeta)$ has the form of Eq. (C.4). Thus, for $V = S, P$,

$$\begin{aligned} V_4[\boldsymbol{\pi}, N] &= \sum_{\alpha=1}^{4} R_{4\alpha}[\boldsymbol{\pi}] V_\alpha[0, N] = \frac{1}{D}\left(1 - \frac{\boldsymbol{\pi}^2}{F_\pi^2}\right) V_4[0, N] - \frac{2\boldsymbol{\pi}}{DF_\pi} \cdot \boldsymbol{V}[0, N], \\ V_i[\boldsymbol{\pi}, N] &= \sum_{\alpha=1}^{4} R_{i\alpha}[\boldsymbol{\pi}] V_\alpha[0, N] = \frac{2\pi_i}{DF_\pi} V_4[0, N] + \sum_{j=1}^{3}\left(\delta_{ij} - \frac{2\pi_i\pi_j}{DF_\pi^2}\right) V_j[0, N]. \end{aligned} \tag{D.5}$$

Moreover, $S_4[0, N]$ ($P_4[0, N]$) is isoscalar, parity-even (parity-odd) and time-reversal-even (time-reversal-odd), while $\boldsymbol{S}[0, N]$ ($\boldsymbol{P}[0, N]$) is isovector, parity-odd (parity-even) and time-reversal-odd (time-reversal-even).

The simplest vector, containing no nucleon fields nor pion covariant derivatives, is

$$S[0, 0] = \begin{pmatrix} \mathbf{0} \\ v_0 \end{pmatrix}, \tag{D.6}$$

with v_0 a real number determined by the details of the dynamics of spontaneous chiral symmetry breaking. From Eq. (D.5),

$$S[\boldsymbol{\zeta}, 0] = \frac{v_0}{D}\begin{pmatrix} 2\boldsymbol{\zeta} \\ 1 - \boldsymbol{\zeta}^2 \end{pmatrix}. \tag{D.7}$$

As a second example,

$$S[0, N] = \begin{pmatrix} \mathbf{0} \\ v_1 \bar{N} N \end{pmatrix}, \tag{D.8}$$

with v_1 another real number, yields

$$S[\boldsymbol{\zeta}, 0] = \frac{v_1}{D}\begin{pmatrix} 2\boldsymbol{\zeta}\bar{N}N \\ \left(1 - \boldsymbol{\zeta}^2\right)\bar{N}N \end{pmatrix}. \tag{D.9}$$

This method can be used to construct the chiral-variant terms in the effective Lagrangian. Consider $\mathcal{L}_m$ from Eq. (3.4.15) when $\varepsilon = 0$ and $\bar{\theta} = 0$. In this case, the fourth component of Eq. (D.7) generates, apart from a constant, a pion mass term in the Lagrangian, Eq. (4.1.1), where we introduce the pion mass $m_\pi^2 = 4v_0\bar{m}/F_\pi^2 = \mathcal{O}(\bar{m}M_{QCD})$. Similarly, Eq. (D.9) gives rise to the so-called sigma term, Eq. (4.1.2), where we introduce the nucleon mass correction $\Delta m_N = v_1\bar{m} = \mathcal{O}(m_\pi^2/M_{QCD})$.

Chiral symmetry relates this mass correction to a pion-nucleon seagull interaction. This procedure can be repeated *ad infinitum*.

In analogous fashion, one can construct the operators originating from the other mass terms of the QCD Lagrangian, Eq. (3.4.15), as we explicitly do in Sec. 4.1

Finally, we realize the chiral-symmetry-breaking operators due to the electromagnetic interaction of the quarks [122]. An obvious class of electromagnetic operators consists of operators that contain soft photons. These are obtained by minimally coupling the charged pions and the proton to the photon, using the covariant derivatives defined in Eq. (3.3.12), and by constructing the most general gauge-invariant operators involving $F_{\mu\nu}$. From Eq. (3.2.11), these operators are either chiral invariant or transform as the 3-4 component of an antisymmetric chiral tensor. For such a tensor,

$$T_{i4}[\boldsymbol{\pi}, N] = -\frac{1}{D}\left[\delta_{ik}\left(1-\frac{\boldsymbol{\pi}^2}{F_\pi^2}\right)+\frac{2\pi_i\pi_k}{F_\pi^2}\right]T_{4k}[0,N]+\frac{2}{DF_\pi}\left(\pi_j\delta_{ik}-\delta_{ij}\pi_k\right)T_{jk}[0,N], \tag{D.10}$$

where $T_{4i}[0,N]$ is an isovector and $T_{ij}[0,N]$, an antisymmetric tensor.

In the nucleon sector, the simplest objects with two Lorentz-tensor indices are

$$I^{\mu\nu}[0,N] = c_s^{(1)}\bar{N}i\left[S^\mu,S^\nu\right]N, \tag{D.11}$$

and

$$T^{\mu\nu}[0,N] = c_v^{(1)}\begin{pmatrix}\mathbf{0} & \bar{N}i\left[S^\mu,S^\nu\right]\tau_i N\\ -\bar{N}i\left[S^\mu,S^\nu\right]\tau^i N & 0\end{pmatrix}, \tag{D.12}$$

which lead to the lowest-order contribution of this type:

$$\begin{aligned}\mathcal{L}^{(1)}_{f=2,\mathrm{em}} &= c_s^{(1)}\bar{N}i\left[S^\mu,S^\nu\right]NeF_{\mu\nu}\\ &\quad +c_v^{(1)}\bar{N}\left[\tau_3-\frac{2}{F_\pi^2 D}\left(\boldsymbol{\pi}^2\tau_3-\pi_3\boldsymbol{\pi}\cdot\boldsymbol{\tau}\right)\right]i\left[S^\mu,S^\nu\right]NeF_{\mu\nu},\end{aligned} \tag{D.13}$$

where the coefficients scale as $c_{s,v}^{(1)} = \mathcal{O}(1/M_{QCD})$. The two operators in Eq. (D.13) are leading contributions to the isosinglet and isovector magnetic dipole moments of the nucleon, which, with the identification $c_{s,v}^{(1)} = (1+\kappa_{0,1})/4m_N$, we gave in Eq. (3.3.18). Other such "direct" electromagnetic interactions can be derived similarly.

There is, however, another type of electromagnetic contribution. As discussed at the beginning of Sec. 4.2, exchanges of hard photons between quarks cannot be resolved in the effective theory and generate purely hadronic operators. At lowest order in $\alpha_{\rm em}$ these operators involve the exchange of one hard photon and, as consequence of Eq. (3.2.11), they have the $SO(4)$ transformation properties of the tensor product $(I^\mu/6 + T_{34}^\mu) \otimes (I_\mu/6 + T_{34\,\mu})$. The resulting chiral-invariant operators simply represent $\mathcal{O}(\alpha_{\rm em})$ corrections to their strong-interaction counterparts. The mixed terms transform as antisymmetric tensors, Eq. (D.10). For the tensor product of two antisymmetric tensors,

$$\begin{aligned} T_{i4j4}[\boldsymbol{\pi}, N] =& \frac{1}{D^2}\left[\delta_{ik}\left(1-\frac{\boldsymbol{\pi}^2}{F_\pi^2}\right)+\frac{2\pi_i\pi_k}{F_\pi^2}\right]\left[\delta_{jl}\left(1-\frac{\boldsymbol{\pi}^2}{F_\pi^2}\right)+\frac{2\pi_j\pi_l}{F_\pi^2}\right] T_{4k4l}[0,N] \\ &- \frac{2}{F_\pi D^2}\left[\delta_{ik}\left(1-\frac{\boldsymbol{\pi}^2}{F_\pi^2}\right)+\frac{2\pi_i\pi_k}{F_\pi^2}\right](\pi_l\delta_{jm}-\delta_{jl}\pi_m)\, T_{4klm}[0,N] \\ &- \frac{2}{F_\pi D^2}(\pi_l\delta_{im}-\delta_{il}\pi_m)\left[\delta_{jk}\left(1-\frac{\boldsymbol{\pi}^2}{F_\pi^2}\right)+\frac{2\pi_j\pi_k}{F_\pi^2}\right] T_{lm4k}[0,N] \\ &+ \frac{4}{D^2F_\pi^2}(\pi_l\delta_{ik}-\delta_{il}\pi_k)(\pi_m\delta_{jn}-\delta_{jm}\pi_n)\, T_{klmn}[0,N]. \end{aligned} \tag{D.14}$$

In the mesonic sector, the first chiral-breaking operator induced by the electromagnetic interaction has the transformation properties of $T_{34} \otimes T_{34}$. The choices

$$T_{4k4l}[0,0] = v_{0,\rm em}\delta_{kl}, \qquad T_{klmn}[0,0] = \frac{v'_{0,\rm em}}{4}\left(\delta_{km}\delta_{ln}-\delta_{kn}\delta_{lm}\right), \tag{D.15}$$

with real numbers $v_{0,\rm em}$ and $v'_{0,\rm em}$, produce an isospin-breaking correction to the pion mass,

$$\mathcal{L}^{(1)}_{\chi,\,f=0,\,\rm em} = -\frac{\delta m^2_{\pi,\rm em}}{2D^2}\left(\boldsymbol{\pi}^2-\pi_3^2\right), \tag{D.16}$$

where $\delta m^2_{\pi,\rm em} = 8(v_{0,\rm em}-v'_{0,\rm em})/F_\pi^2 = \mathcal{O}(\alpha_{\rm em}M^2_{QCD}/\pi)$ is the dominant contribution to the pion mass splitting. Using m_ρ for M_{QCD}, this estimate is very close to the observed value, which corroborates our assignment of a factor $\alpha_{\rm em}/\pi$ for the contribution of hard photons.

In the pion-nucleon sector, the operators with the properties of $T_{34} \otimes T_{34}$ have a structure very similar to Eq. (D.16),

$$\mathcal{L}^{(2)}_{\not\chi,\, f=2,\,\mathrm{em}} = \frac{\beta_{1,\mathrm{em}}}{F_\pi^2 D^2} \left(\boldsymbol{\pi}^2 - \pi_3^2\right) \bar{N} N, \tag{D.17}$$

where $\beta_{1,\mathrm{em}} = \mathcal{O}(\alpha_{\mathrm{em}} M_{QCD}/\pi)$. More interesting operators come from the realization of the tensor product $T^\mu_{34} \otimes I_\mu/6$. The simplest tensor has the structure of Eq. (D.12), just without the commutator $i[S^\mu, S^\nu]$, which induces the operator

$$\mathcal{L}^{(2)}_{\not I,\, f=2,\,\mathrm{em}} = \frac{\breve{\delta} m_N}{2} \left[\bar{N}\tau_3 N + \frac{2}{F_\pi^2 D} \bar{N} \left(\pi_3 \boldsymbol{\pi}\cdot\boldsymbol{\tau} - \boldsymbol{\pi}^2 \tau_3\right) N\right], \tag{D.18}$$

where $\breve{\delta} m_N = \mathcal{O}(\alpha_{\mathrm{em}} M_{QCD}/\pi)$ is the leading electromagnetic contribution to the nucleon mass splitting. Again, this estimate is within a factor of two of the observed value, although in this case a quark-mass contribution of similar magnitude has to be accounted for.

These and other "indirect" electromagnetic operators have been discussed in more detail in Refs. [122, 145, 148, 149, 221, 222, 223, 153, 154, 134, 135, 136, 164, 165].

Appendix E
Linear Realization

Let us consider a linear realization Φ of the full group, here $SO(4)$. Suppose the effective potential is

$$V(\Phi) = V_0(\Phi) + V_1(\Phi), \tag{E.1}$$

where V_0 is the effective potential generated by the symmetric part of the Lagrangian, while V_1 is the small correction due to explicit symmetry breaking. If the explicit breaking is small, the vacuum $\bar{\Phi}$ of the full theory will not be far from the vacuum $\bar{\Phi}_0$ calculated in the absence of explicit breaking: $\bar{\Phi} = \bar{\Phi}_0 + \bar{\Phi}_1$, with $\bar{\Phi}_1$ small. From the equilibrium condition for the vacuum,

$$\left.\frac{\partial V(\Phi)}{\partial \Phi_\alpha}\right|_{\Phi=\bar{\Phi}_0+\bar{\Phi}_1} = 0, \tag{E.2}$$

using the invariance of the effective potential $V_0(\Phi)$, it can be shown [32] that, if V_1 and $\bar{\Phi}_1$ are small, the following condition holds:

$$\sum_\alpha \left(G^A \bar{\Phi}_0\right)_\alpha \left.\frac{\partial V_1(\Phi)}{\partial \Phi_\alpha}\right|_{\Phi=\bar{\Phi}_0} = 0, \tag{E.3}$$

where G^A are the generators of the group, in our case $SO(4)$. Equation (E.3) is called the "vacuum alignment" condition. If Eq. (E.3) does not hold, it means that the real vacuum is far from the unperturbed one, and the expansion around the vacuum $\bar{\Phi}_0$ is not perturbative. Let us assume, for example, that the perturbation to the effective potential has the form

$$V_1(\Phi) = \sum_\alpha u_\alpha \Phi_\alpha, \tag{E.4}$$

with u_α given parameters. The vacuum alignment condition becomes

$$\sum_\alpha u_\alpha (G^A \bar{\Phi}_0)_\alpha = 0, \tag{E.5}$$

and, being the generators of $SO(4)$ antisymmetric, this condition is satisfied if the vectors $\bar{\Phi}_0$ and u are parallel. This explains the name "vacuum alignment".

As a concrete example of chiral symmetry breaking we can consider a toy model —the linear sigma model— where the Lagrangian is

$$\mathcal{L}_\sigma = \frac{1}{2}\partial_\mu\Phi\partial^\mu\Phi - V_0(\Phi) = \frac{1}{2}\partial_\mu\Phi\partial^\mu\Phi - \frac{m^2}{2}\Phi^2 - \frac{\lambda}{4}\left(\Phi^2\right)^2, \tag{E.6}$$

with two real parameters m^2 and λ. When $m^2 < 0$, the minimum of the potential $V_0(\Phi)$ is given by the condition

$$\bar{\Phi}_0^2 = -\frac{m^2}{\lambda} = v^2. \tag{E.7}$$

We pick a vacuum in the fourth direction,

$$\bar{\Phi}_0 = v \begin{pmatrix} 0 \\ 0 \\ 0 \\ 1 \end{pmatrix}, \tag{E.8}$$

a spontaneous breaking of $SO(4)$ symmetry.

Let us add a small explicit breaking potential, in the form

$$V_1(\Phi) = g(\Phi_3 + \Phi_4), \tag{E.9}$$

with $g \ll m^2 v$. The vacuum we chose is not aligned with the symmetry-breaking potential and the situation is analogous to the case we discussed in Sec. 3.4 —there are two explicit symmetry-breaking terms of the same order, one aligned with the vacuum (Φ_4), the other not (Φ_3). If we calculate the minimum of the potential $V_0 + V_1$, we find that it is no longer degenerate and it is

$$\bar{\Phi} = v \begin{pmatrix} 0 \\ 0 \\ \frac{1}{\sqrt{2}} + \frac{g}{2m^2 v} \\ \frac{1}{\sqrt{2}} + \frac{g}{2m^2 v} \end{pmatrix} + \mathcal{O}(g^2). \tag{E.10}$$

We see that even a small perturbation rotates the vacuum dramatically, the angle between the true and the old vacuum being approximately $\pi/4$.

Consider now instead the explicit breaking

$$V_1(\Phi) = g\Phi_4 + \frac{g^2}{m^2 v}\Phi_3, \tag{E.11}$$

still with $g \ll m^2 v$. This situation resembles the second case we discussed in the text, with a non-aligned perturbation much smaller than the aligned one —see Secs. 4.1 and 4.3. We again can find a minimum,

$$\bar{\Phi} = v \begin{pmatrix} 0 \\ 0 \\ \frac{g}{m^2 v} \\ 1 + \frac{g}{2m^2 v} \end{pmatrix} + \mathcal{O}(g^2). \tag{E.12}$$

This time, the true vacuum is very close to the one we chose to expand the Lagrangian around.

Once the vacuum is aligned with the dominant perturbation, let us say, along the fourth direction, we can perform an explicit field redefinition to exhibit the Goldstone modes [32]:

$$\Phi_n = R_{n4}(x)\sigma(x), \tag{E.13}$$

where R is a rotation matrix that belongs to $SO(4)$, that is, satisfies Eq. (C.3). In the stereographic representation, we parameterize the rotation as in Eq. (C.4) and define the fields

$$\zeta_i = \frac{\Phi_i}{\Phi_4 + \sigma}, \qquad i = 1, 2, 3. \tag{E.14}$$

Under an infinitesimal isospin transformation with parameter $\boldsymbol{\theta}_V$,

$$\delta\Phi_i = \sum_{jk} \varepsilon_{ijk}\theta_{Vj}\Phi_k, \tag{E.15}$$

$$\delta\sigma = 0, \tag{E.16}$$

it is easy to see that $\boldsymbol{\zeta}$ is an isovector, Eq. (C.6). Likewise, under an infinitesimal axial transformation $\boldsymbol{\theta}_A$,

$$\delta\Phi_i = 2\theta_{Ai}\Phi_4, \tag{E.17}$$

$$\delta\Phi_4 = -2\sum_i \theta_{Ai}\Phi_i, \tag{E.18}$$

the transformation of the Goldstone boson field is non-linear, Eq. (C.7).

Defining the covariant derivative (C.8), the Lagrangian (E.6) can be recast in the form

$$\mathcal{L} = \frac{1}{2}\partial_\mu\sigma\partial^\mu\sigma - \frac{1}{2}m^2\sigma^2 - \frac{\lambda}{4}\sigma^4 + \frac{1}{2}\sigma^2 D_\mu\boldsymbol{\zeta}\cdot D^\mu\boldsymbol{\zeta}. \tag{E.19}$$

It is easy to see that the Lagrangian is still invariant under $SO(4)$. The aligned potential (E.11), on the other hand, when expressed in terms of the Goldstone boson fields, will depend on $\boldsymbol{\zeta}$ explicitly:

$$V_1(\Phi) = g\sigma\frac{1-\boldsymbol{\zeta}^2}{D} + \frac{g^2}{m^2 v}\sigma\frac{2\boldsymbol{\zeta}_3}{D}. \tag{E.20}$$

In the vacuum, $\bar{\sigma} = v + g/2m^2 + \mathcal{O}(g^2)$ and $\bar{\zeta_i} = \delta_{i3}g/2m^2 v + \mathcal{O}(g^2)$. For processes at momenta $Q \ll m$, we can integrate out the fluctuations of the field σ, obtaining a Lagrangian that for $g = 0$ is a function of $D^\mu\boldsymbol{\zeta}$ only. For $g \neq 0$, one can recognize in Eq. (E.20) the fourth and third components of the vector $S[\boldsymbol{\zeta}, 0]$ given by Eq. (D.7), with coefficients in the ratio $g : g^2/m^2 v$, just as in the original perturbation (E.11).

Appendix F

Resummation of pion tadpoles

In this Appendix we show how to resum the tadpole diagrams generated by the Lagrangian (3.4.3). The method is general and can in principle be applied to other quantities, but we illustrate it for the pion two-point Green's function at tree level. Some of the contributions from tadpoles in this case were displayed in Fig. 3.1.

We start by defining the full one-pion Green's function

$$iT_a = \frac{i}{2} g\tilde{m}_\pi^2 F_\pi \tilde{T}\delta_{a3}, \tag{F.1}$$

where a is the isospin index of the pion. In lowest order in the chiral expansion we need to worry only about tree-level diagrams. In Fig. F.1 we display the corresponding diagrams contributing to iT to order g^5 and, for convenience, we explicitly show the symmetry factor due to exchange of equivalent tadpoles. In the diagrams in Fig. F.1, the external neutral pion is connected to one of the basic vertices of the Lagrangian (3.4.3), with three, four, ..., n-branches. Each branch then develops into a tadpole tree and ends up with the disappearance of an arbitrary number of π_3s into the vacuum. The diagrams in Fig. F.1 can be rearranged as in Fig. F.2, and we can write the diagrammatic equation

$$\frac{i}{2}\tilde{m}_\pi^2 g F_\pi \tilde{T} = \frac{i}{2}\tilde{m}_\pi^2 g F_\pi + \sum_{n=2}^{\infty} \frac{1}{n!}\left(-\frac{i}{\tilde{m}_\pi^2}\right)^n \left(\frac{i}{2}\tilde{m}_\pi^2 F_\pi g\tilde{T}\right)^n V_n'(\tilde{m}_\pi^2), \tag{F.2}$$

where the factor $V_n'(\tilde{m}_\pi^2)$ can be obtained from the Lagrangian (3.4.3) and it is

$$\begin{aligned} V_{2m}'(\tilde{m}_\pi^2) &= \frac{i}{2}(-1)^m (2m+1)!\,\frac{g\tilde{m}_\pi^2}{F_\pi^{2m-1}}, \\ V_{2m+1}'(\tilde{m}_\pi^2) &= \frac{i}{2}(-1)^{m+1}(2m+2)!\,\frac{\tilde{m}_\pi^2}{F_\pi^{2m}}. \end{aligned} \tag{F.3}$$

Equation (F.2) can be rewritten as

$$\sum_{m=0}^{\infty}(-1)^m(2m+1)\left(\frac{g^2}{4}\right)^m \tilde{T}^{2m} - \sum_{m=0}^{\infty}(-1)^m(m+1)\left(\frac{g^2}{4}\right)^m \tilde{T}^{2m+1} = 0. \tag{F.4}$$

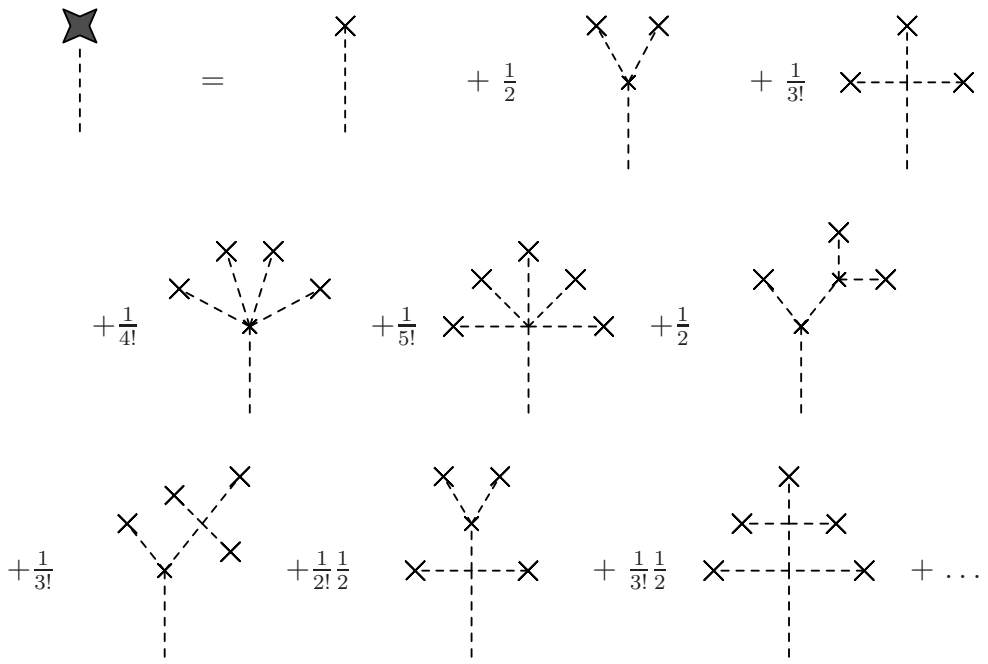

FIGURE F.1. Contributions to the pion one-point function iT at tree level up to order g^5. Vertices are from the Lagrangian (3.4.3). For each diagram, the symmetry factor is explicitly indicated.

The two series can be summed and we obtain

$$\frac{1}{\left(1+\frac{g^2}{4}\tilde{T}^2\right)^2}\left[1-\tilde{T}-\frac{g^2}{4}\tilde{T}^2\right]=0, \tag{F.5}$$

which admits two solutions,

$$\tilde{T}=-\frac{2}{g^2}\left(1\pm\sqrt{1+g^2}\right). \tag{F.6}$$

The non-analytic dependence on g is a direct consequence of the non-perturbative character of the problem.

With the one-pion Green's function, Eqs. (F.1) and (F.6), we can calculate the effect of pion tadpoles on quantities more directly related to experiment. Let us consider the two-point Green's function for a pion of four-momentum p and isospin index a, $G_a(p^2,\tilde{m}_\pi^2)$. The diagrams that contribute to the two-point function up to order g^4 are shown in Fig. 3.1. Let us call, with abuse of language, "one-particle

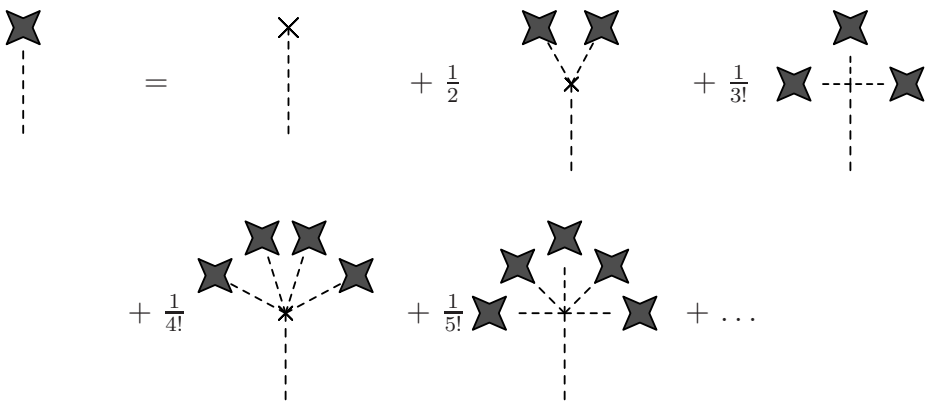

FIGURE F.2. Diagrammatic equation for the one-pion Green's function iT, Eq. (F.2).

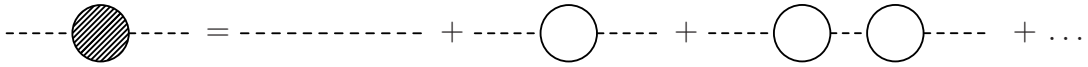

FIGURE F.3. The full pion propagator G, denoted by a shaded blob, as an iteration of the sum of 1PI diagrams $-i\Sigma$, denoted by an empty circle.

irreducible" (1PI), those diagrams that cannot be disconnected by cutting an internal line in which non-vanishing p flows, and denote the sum of all the 1PI diagrams by $-i\Sigma_a(p^2, \tilde{m}_\pi^2)$. The full propagator can be expressed as the geometric sum of 1PI diagrams —see Fig.F.3— and

$$\begin{aligned} G_a(p^2, \tilde{m}_\pi^2)\delta_{ab} &= \frac{i\delta_{ab}}{p^2 - \tilde{m}_\pi^2 + i\varepsilon}\left(1 + \frac{\Sigma_a(p^2, \tilde{m}_\pi^2)}{p^2 - \tilde{m}_\pi^2 + i\varepsilon} + \frac{\Sigma_a^2(p^2, \tilde{m}_\pi^2)}{\left(p^2 - \tilde{m}_\pi^2 + i\varepsilon\right)^2} + \dots\right) \\ &= \frac{i\delta_{ab}}{p^2 - \tilde{m}_\pi^2 - \Sigma_a(p^2, \tilde{m}_\pi^2) + i\varepsilon}. \end{aligned} \tag{F.7}$$

At tree level, contributions to the sum of 1PI diagrams $-i\Sigma_a(p^2, \tilde{m}_\pi^2)$ have the following structure: the vertex connected to the two lines in which p flows has a certain number of branches; from each branch a tadpole tree sprouts, which ends with the disappearance of an arbitrary number of π_3s into the vacuum. Diagrammatically, the sum of 1PI diagrams can be expressed in terms of the pion one-point Green's

function iT, as shown in Fig. F.4:

$$-i\Sigma_a(p^2,\tilde{m}_\pi^2) = \sum_{n=1}^{\infty} \frac{1}{n!}\left(\frac{-i}{\tilde{m}_\pi^2}\right)^n \left(\frac{i}{2}\tilde{m}_\pi^2 F_\pi g\tilde{T}\right)^n V_{a;n}(p^2,\tilde{m}_\pi^2), \tag{F.8}$$

where V_n is a factor coming from the Feynman rules for the $(n+2)$-pion vertex. It can be derived from the Lagrangians (3.3.17) and (3.4.3), and it is

$$\begin{aligned} V_{a;2m+1}(p^2,\tilde{m}_\pi^2) &= i(-1)^{m+1}\frac{g\tilde{m}_\pi^2}{F_\pi^{2m+1}}(m+1)(2m+1)!\left\{1+2(m+1)\delta_{a3}\right\}, \\ V_{a;2m+2}(p^2,\tilde{m}_\pi^2) &= i(-1)^{m+1}\frac{g}{F_\pi^{2m+2}}(m+2)(2m+2)! \\ &\qquad \left\{p^2-\left[1+2(m+1)\delta_{a3}\right]\tilde{m}_\pi^2\right\}. \end{aligned} \tag{F.9}$$

We can write

$$\begin{aligned} \Sigma_a(p^2,\tilde{m}_\pi^2) &= \frac{g^2}{2}\sum_{m=0}^{\infty}\left(-\frac{g^2}{4}\right)^m\left[(p^2-\tilde{m}_\pi^2)\frac{m+2}{2}\tilde{T}^{2m+2}+\tilde{m}_\pi^2(m+1)\tilde{T}^{2m+1}\right] \\ &\quad +\delta\Sigma_a(p^2,\tilde{m}_\pi^2), \end{aligned} \tag{F.10}$$

where

$$\delta\Sigma_a(p^2,\tilde{m}_\pi^2) = \tilde{m}_\pi^2 g^2\sum_{m=0}^{\infty}\left(-\frac{g^2}{4}\right)^m(m+1)\left[(m+1)\tilde{T}^{2m+1}-\frac{m+2}{2}\tilde{T}^{2m+2}\right]\delta_{a3}. \tag{F.11}$$

Summing the series and using Eq. (F.5), $\delta\Sigma_a(p^2,\tilde{m}_\pi^2)$ vanishes and the sum of 1PI diagrams becomes the same for charged and neutral pions:

$$\Sigma_a(p^2,\tilde{m}_\pi^2) = \frac{g^2}{2\left(1+\frac{g^2}{4}\tilde{T}^2\right)^2}\left[\left(p^2-\tilde{m}_\pi^2\right)\tilde{T}^2\left(1+\frac{g^2}{8}\tilde{T}^2\right)+\tilde{m}_\pi^2\tilde{T}\right]. \tag{F.12}$$

The inverse of the propagator (F.7) is now

$$G_a^{-1}(p^2,\tilde{m}_\pi^2) = \left(1+\frac{g^2}{4}\tilde{T}^2\right)^{-2}\left[p^2-\tilde{m}_\pi^2\left(1+\frac{g^2}{2}\tilde{T}\right)\right], \tag{F.13}$$

and it vanishes at the physical pion mass

$$m_\pi^2 = \tilde{m}_\pi^2\left(1+\frac{g^2}{2}\tilde{T}\right) = \pm\,\tilde{m}_\pi^2\sqrt{1+g^2}, \tag{F.14}$$

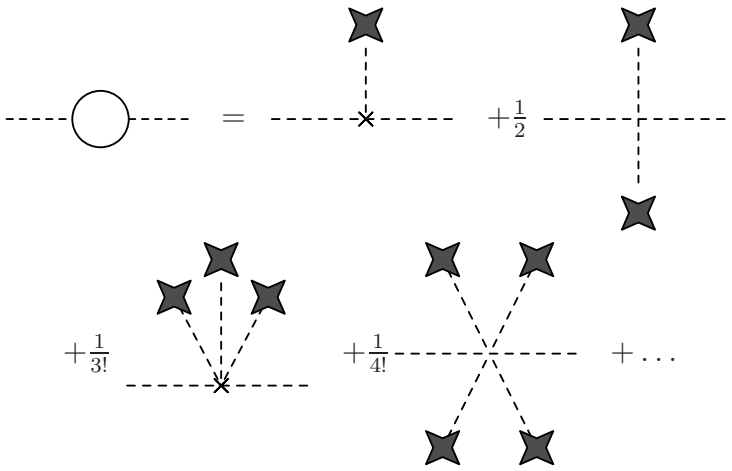

FIGURE F.4. Diagrammatic equation for $-i\Sigma$ in terms of the one-point Green's function iT, Eq. (F.8).

where we used the solutions (F.6). Inserting the values of $\tilde{m}_\pi^2$ and g, Eqs. (3.4.4) and (3.4.5),

$$m_\pi^2 = \pm \frac{4v_0}{F_\pi^2}\, \bar{m}\, r(\bar{\theta}). \tag{F.15}$$

Equation (F.15) shows that, as it should be, the physical pion mass is independent of the arbitrary angle α, and its value is equal to the one we would get by working directly with the aligned Lagrangian (4.1.1). Presumably the same can be shown for other observable quantities using this method.

Appendix G
Isospin violating Lagrangian

We summarize here the isospin violating terms given in Secs. 3.3 and 4.2, and we show the new isospin-breaking interactions induced in the $\Delta = 1$ and $\Delta = 2$ Lagrangian from the field redefinitions that eliminate the nucleon mass difference from the χPT Lagrangian.

Isospin-violating terms first contribute to the $\Delta = 1$ Lagrangian,

$$\mathcal{L}^{(1)}_{\not I,\, f\leq 2} = -\frac{\breve{\delta} m_\pi^2}{2D^2}\left(\boldsymbol{\pi}^2 - \pi_3^2\right) + \frac{\delta m_N}{2}\bar{N}\left(\tau_3 - \frac{2\pi_3}{F_\pi^2 D}\boldsymbol{\pi}\cdot\boldsymbol{\tau}\right)N, \tag{G.1}$$

while at order $\Delta = 2$,

$$\begin{aligned}\mathcal{L}^{(2)}_{\not I,\, f\leq 2} = &+\frac{\delta m_\pi^2}{2D^2}\pi_3^2 + \frac{\breve{\delta} m_N}{2}\bar{N}\left[\tau_3 + \frac{2}{F_\pi^2 D}\left(\pi_3\boldsymbol{\pi}\cdot\boldsymbol{\tau} - \boldsymbol{\pi}^{\,2}\tau_3\right)\right]N \\ &+ \frac{\beta_1}{F_\pi}\left(D_\mu\pi_3 - \frac{2\pi_3}{F_\pi^2 D}\boldsymbol{\pi}\cdot D_\mu\boldsymbol{\pi}\right)\bar{N}S^\mu N.\end{aligned} \tag{G.2}$$

Here $\breve{\delta} m_\pi^2 = \mathcal{O}\left(\alpha_{\rm em} M_{QCD}^2/4\pi\right)$ is the leading electromagnetic contribution to the pion mass splitting, while the quark-mass-difference contribution, $\delta m_\pi^2 = \mathcal{O}\left(\varepsilon^2 m_\pi^4/M_{QCD}^2\right)$, is smaller by a power of $\varepsilon m_\pi/M_{QCD}$. The leading contribution to the nucleon mass splitting is generated by the quark mass difference, $\delta m_N = \mathcal{O}(\varepsilon m_\pi^2/M_{QCD})$, while the electromagnetic contribution is $\breve{\delta} m_N = \mathcal{O}\left(\alpha_{\rm em} M_{QCD}/4\pi\right)$, that is, $\mathcal{O}\left(\varepsilon m_\pi^3/M_{QCD}^2\right)$ and about the 20% of δm_N. The operator with coefficient $\beta_1 = \mathcal{O}\left(\varepsilon m_\pi^2/M_{QCD}^2\right)$ is an isospin-violating pion-nucleon coupling.

For the solution of the Lippman-Schwinger equation, it is convenient to eliminate the nucleon mass difference $m_n - m_p$ from the nucleon propagator and from asymptotic states. This result can be accomplished through a field redefinition, defined in Ref.

[138]. After the field redefinition, Eqs. (G.1) and (G.2) become

$$\begin{aligned}\mathcal{L}^{(1,2)}_{\not I,\, f\leq 2} &= -\frac{1}{2D^2}\left(\breve{\delta}m_\pi^2-\delta m_N^2\right)\left(\boldsymbol{\pi}^2-\pi_3^2\right)-\frac{\delta m_\pi^2}{2D^2}\pi_3^2 \\ &\quad -(\delta m_N+\breve{\delta}m_N)\left(\boldsymbol{\pi}\times v\cdot D\boldsymbol{\pi}\right)_3+\frac{g_A\delta m_N}{F_\pi m_N}i\varepsilon_{3ab}\pi_a\bar{N}\tau_b S\cdot\mathcal{D}_- N \\ &\quad +\frac{\beta_1}{F_\pi}\left(D_\mu\pi_3-\frac{2\pi_3}{F_\pi^2 D}\boldsymbol{\pi}\cdot D_\mu\boldsymbol{\pi}\right)\bar{N}S^\mu N. \end{aligned} \tag{G.3}$$

We use Eq. (G.3) to check the isospin breaking contributions to the nucleon EDFF at NLO, in Sec. 5.2, to discuss isospin breaking corrections to the deuteron EDM in Sec. 6.6 and to incorporate isospin-breaking effects in the TV potential from the QCD $\bar{\theta}$ term at N^{2}LO in Chapter 7.

Appendix H

Higher-order interactions

We construct in this appendix operators that contribute to the chiral breaking pion-nucleon Lagrangian $\mathcal{L}^{(5)}_{\chi,f=2}$ and that do not contain covariant derivatives of the pion or of the nucleon field. Because they are strongly suppressed by $(m_\pi/M_{QCD})^4$ with respect to the leading pion-nucleon chiral-breaking vertices, these operators are not relevant for any phenomenological application. Nonetheless they are of some formal interest because, as we shall see, this is the first order in the purely hadronic sector of the chiral Lagrangian where the relation (4.1.5) between TV and isospin-breaking operators breaks down. This is also the lowest order where a purely hadronic TV vertex $\pi_3\bar{N}\tau_3 N$ appears.

The operators we consider here are obtained from the tensor products $P_a\otimes P_b\otimes S_4$, $P_a\otimes P_b\otimes P_c$, and $P_a\otimes S_4\otimes S_4$, and we write the non-derivative part of the Lagrangian as

$$\mathcal{L}^{(5)}_{\chi^3,f=2} = \mathcal{L}^{(5)}_{\chi^3,f=2,PPS} + \mathcal{L}^{(5)}_{\chi^3,f=2,PPP} + \mathcal{L}^{(5)}_{\chi^3,f=2,PSS}. \tag{H.1}$$

The tensor product $P_a \otimes P_b \otimes S_4$ can be decomposed into two $SO(4)$ vectors and a three-index tensor, symmetric in the first two indices: $P_a \otimes P_b \otimes S_4 = \delta_{ab}V_4 + (\delta_{a4}\delta_{bd} + \delta_{b4}\delta_{ad})\,W_d + S_{ab,4}$. The vectors V and W have the same properties under P and T as the vector S introduced in Eq. (3.2.13). In the realization of the third and fourth components of the tensor product, the third and fourth components of W appear, but only the fourth component of V does. In the $f = 2$ sector, $P_a \otimes P_b \otimes S_4$ generates the operators

$$\begin{aligned}\mathcal{L}^{(5)}_{\chi^3,f=2,PPS} = &\left[\rho^2 c_1^{(5)} + \left(1+\rho^2\right) c_2^{(5)}\right]\left(1 - \frac{2\boldsymbol{\pi}^2}{F_\pi^2 D}\right)\bar{N}N + \frac{2\rho c_1^{(5)}}{F_\pi D}\pi_3\bar{N}N \\ &+c_3^{(5)}\left(1 - \frac{2\boldsymbol{\pi}^2}{F_\pi^2 D}\right)\left[\frac{4\pi_3^2}{F_\pi^2 D^2} + \rho^2\left(1 - \frac{4\boldsymbol{\pi}^2}{F_\pi^2 D^2}\right) + \frac{4\rho\pi_3}{F_\pi D^2}\left(1 - \frac{\boldsymbol{\pi}^2}{F_\pi^2}\right)\right]\bar{N}N. \end{aligned}\tag{H.2}$$

Here the $c_3^{(5)}$ term has a similar structure to the $c_1^{(3)}$ term in Eq. (4.1.27). The $c_2^{(5)}$ term is nothing but a correction to the nucleon sigma term, Eq. (4.1.2). More interestingly, Eq. (H.2) shows that even at the hadronic level the relation (4.1.5) ceases to be valid at higher orders in the expansion in m_π/M_{QCD}. Indeed, it is not possible to disentangle the individual coefficients $c_1^{(5)}$ and $c_2^{(5)}$ by measuring a TC observable, and, therefore, it is not possible to constrain the coefficient of the TV operator in Eq. (H.2) with the properties of an S_3.

The tensor product $P_a \otimes P_b \otimes P_c$ yields symmetry-breaking terms that transform as components either of a four-vector with the same properties as the vector P defined in Eq. (3.2.14), or of a completely symmetric tensor. In the $f = 2$ sector, the corresponding operators are

$$\begin{aligned}
\mathcal{L}^{(5)}_{\chi^3,f=2,PPP} &= c_4^{(5)}\bar{N}\left[\tau_3 - \frac{2\pi_3}{F_\pi^2 D}\boldsymbol{\pi}\cdot\boldsymbol{\tau} - \frac{2\rho}{F_\pi D}\boldsymbol{\pi}\cdot\boldsymbol{\tau}\right]N \\
&\quad + c_5^{(5)}\left(\frac{2\pi_3}{F_\pi D}\right)^2\bar{N}\left(\tau_3 - \frac{2\pi_3}{F_\pi D}\boldsymbol{\pi}\cdot\boldsymbol{\tau}\right)N \\
&\quad + c_5^{(5)}\rho\frac{4\pi_3}{F_\pi D}\bar{N}\left[\tau_3 - \frac{2}{F_\pi^2 D}\left(2\pi_3\left(1 - \frac{3\boldsymbol{\pi}^2}{2F_\pi^2}\right)\boldsymbol{\pi}\cdot\boldsymbol{\tau} + \boldsymbol{\pi}^2\tau_3\right)\right]N \\
&\quad + c_5^{(5)}\rho^2\left(1 - \frac{2\boldsymbol{\pi}^2}{F_\pi^2 D}\right)\bar{N}\left[\tau_3 - \frac{10\pi_3}{F_\pi^2 D^2}\left(1 + \frac{\boldsymbol{\pi}^2}{5F_\pi^2}\right)\boldsymbol{\pi}\cdot\boldsymbol{\tau}\right]N \\
&\quad - \frac{2c_5^{(5)}}{F_\pi}\rho^3\left(1 - \frac{4\boldsymbol{\pi}^2}{F_\pi^2 D^2}\right)\bar{N}\boldsymbol{\pi}\cdot\boldsymbol{\tau}N. \qquad \text{(H.3)}
\end{aligned}$$

The $c_4^{(5)}$ term realizes the $SO(4)$ vector in the tensor product, and thus has a form identical to Eq. (4.1.19); it is simply a correction to δm_N. The other four operators correspond to the 3-3-3, 3-3-4, 3-4-4 and 4-4-4 components of the symmetric tensor. In them, a link between T violation and isospin breaking survives. The operator with coefficient $c_5^{(5)}\rho$ is the first purely hadronic contribution to the T-violating vertex $\pi_3\bar{N}\tau_3 N$.

The representation of tensor products $P_a \otimes S_4 \otimes S_4$ contains two $SO(4)$ vectors with the same properties as P and a three-index tensor. When we select the fourth component of the tensor product, the fourth component of both vectors appears,

while, if $a = 3$, we find only the third component of one of the two vectors. This implies that, in the $f = 2$ sector, the Lagrangian is

$$\begin{aligned}\mathcal{L}^{(5)}_{\chi^3,f=2,PSS} &= c_7^{(5)}\bar{N}\left(\tau_3 - \frac{2\pi_3}{F_\pi^2 D}\boldsymbol{\pi}\cdot\boldsymbol{\tau}\right)N - \frac{2\rho}{F_\pi D}\left(c_6^{(5)} + c_7^{(5)}\right)\bar{N}\boldsymbol{\pi}\cdot\boldsymbol{\tau}N \\ &+c_8^{(5)}\left(1 - \frac{4\boldsymbol{\pi}^2}{F_\pi^2 D^2}\right)\bar{N}\left[\tau_3 - \frac{2\pi_3}{F_\pi^2 D}\boldsymbol{\pi}\cdot\boldsymbol{\tau} - \frac{2\rho}{F_\pi D}\boldsymbol{\pi}\cdot\boldsymbol{\tau}\right]N \\ &+\frac{2c_9^{(5)}}{F_\pi D^2}\left(1 - \frac{2\boldsymbol{\pi}^2}{F_\pi^2 D}\right)\left[\frac{2\pi_3}{F_\pi} - \rho\left(1 - \frac{\boldsymbol{\pi}^2}{F_\pi^2}\right)\right]\bar{N}\boldsymbol{\pi}\cdot\boldsymbol{\tau}N. \qquad \text{(H.4)}\end{aligned}$$

Here some links between TV interactions and isospin breaking survive. The $c_7^{(5)}$ term is identical in form to the $c_4^{(5)}$ term in Eq. (H.3), so it also provides a correction to δm_N in Eq. (4.1.19). The $c_8^{(5)}$ term has a similar form. The $c_9^{(5)}$ term links a TV interaction to an isospin-breaking seagull. However, we see that the term with coefficient $c_6^{(5)}\rho$ does not have any TC partner, and cannot be determined from a measurement of a TC observable.

The coefficients in Eqs. (H.2), (H.3), and (H.4) scale as

$$\begin{aligned}c_{1-3}^{(5)} &= \mathcal{O}\left(\frac{\varepsilon^2 m_\pi^6}{r^4(\bar{\theta})M_{QCD}^5}\right), \quad c_{4,5}^{(5)} = \mathcal{O}\left(\frac{\varepsilon^3 m_\pi^6}{r^6(\bar{\theta})M_{QCD}^5}\right), \\ c_{6-9}^{(5)} &= \mathcal{O}\left(\frac{\varepsilon m_\pi^6}{r^2(\theta)M_{QCD}^5}\right). \qquad \text{(H.5)}\end{aligned}$$

Appendix I

Lorentz-Invariance Constraints

In this Appendix we derive the relations (4.1.26), which stem from Lorentz invariance. In the heavy-baryon formalism, Lorentz invariance is implemented order by order in a Q/m_N expansion that goes hand-in-hand with the Q/M_{QCD} expansion of χPT. It relates the coefficients of operators at different orders. There are many ways to derive such relations. One method, intrinsic to the formalism and dubbed reparametrization invariance, is to demand invariance under small changes of the velocity v^μ in Eq. (C.15) [251]. Going beyond $1/m_N$ corrections is complicated but can be done [252, 151]. Another method is to implement a Foldy-Wouthuysen transformation [253]. A third, more popular method [131, 150] is to start from a relativistic Lagrangian and perform an integration over antinucleon fields in the path integral. Here we follow a variant of the latter, where we match the non-relativistic Green's functions to their relativistic counterparts [1].

The TC dynamics of a relativistic nucleon is described by the Lagrangian

$$\mathcal{L} = \bar{N}\left(i\not{\mathcal{D}} - m_N + \frac{g_A}{F_\pi}\gamma^5 \boldsymbol{\tau}\cdot\not{\mathcal{D}}\boldsymbol{\pi}\right)N + \ldots, \tag{I.1}$$

where "..." denotes higher-dimension operators, with more nucleon or pion covariant derivatives and more powers of chiral-symmetry breaking parameters. The TV relativistic Lagrangian in the strong-interaction sector with operators containing up to

[1] Most of the results in this appendix were obtained independently by J. de Vries using the method of Ref. [151], which is a generalization of Ref. [252] to the χPT Lagrangian

two derivatives with respect to the leading TV coupling $\bar{g}_0$ is

$$\begin{aligned}
\mathcal{L}_T &= -\frac{\bar{g}_0}{F_\pi D}\bar{N}\boldsymbol{\pi}\cdot\boldsymbol{\tau}N - \frac{\bar{h}_0}{F_\pi^2 D}\boldsymbol{\pi}\cdot D_\mu\boldsymbol{\pi}\bar{N}\gamma^\mu\gamma_5 N \\
&\quad + \frac{\bar{\eta}_3}{2F_\pi}\frac{1}{D}\left(1-\frac{\boldsymbol{\pi}^2}{F_\pi^2}\right)\mathcal{D}_\mu D^\mu\boldsymbol{\pi}\cdot\bar{N}\boldsymbol{\tau}N \\
&\quad + \frac{\bar{\eta}_4}{4F_\pi^2}\frac{1}{D}\left(1-\frac{\boldsymbol{\pi}^2}{F_\pi^2}\right)(D_\mu\boldsymbol{\pi}\times D_\nu\boldsymbol{\pi})\cdot\bar{N}\sigma^{\mu\nu}\gamma^5\boldsymbol{\tau}N \\
&\quad - \frac{\bar{\eta}_9}{F_\pi^3 D}\boldsymbol{\pi}\cdot(D_\mu\boldsymbol{\pi}\times D_\nu\boldsymbol{\pi})\;\bar{N}i\sigma^{\mu\nu}N \\
&\quad - \frac{\bar{\eta}_{10}}{F_\pi^3 D}\boldsymbol{\pi}\cdot D_\mu\boldsymbol{\pi}\,D^\mu\boldsymbol{\pi}\cdot\bar{N}\boldsymbol{\tau}N - \frac{\bar{\eta}_{12}}{F_\pi^3 D}D_\mu\boldsymbol{\pi}\cdot D^\mu\boldsymbol{\pi}\,\boldsymbol{\pi}\cdot\bar{N}\boldsymbol{\tau}N, \qquad \text{(I.2)}
\end{aligned}$$

where, with abuse of notation, we denote the relativistic coupling constants by the same symbols used in the text for the non-relativistic constants.

We find the $f = 2$ TV heavy-baryon Lagrangian by equating (matching) the relativistic two-nucleon n-pion Green's functions, computed with the Lagrangians in Eqs. (I.1) and (I.2), to the non-relativistic Green's functions, obtained with the TV Lagrangians (4.1.19), (4.1.21), and (4.1.24) and the TC chiral Lagrangians (3.3.17), (3.3.18) and (3.3.19) Chiral-symmetry breaking operators induced by the quark mass $\bar{m}$ and by the quark mass difference $\bar{m}\varepsilon$ should be included in the relativistic and in the heavy-baryon Lagrangian, Eqs. (I.1) and (3.3.18) and (3.3.19). However, it turns out that these terms do not affect the matching of the TV one-pion and two-pion Green's functions at the order we consider.

We set the external nucleon on shell, and expand the relativistic Green's function in powers of $1/m_N$, retaining terms up to order $1/m_N^2$. We do the matching in the nucleon rest frame, $v = (1,\vec{0})$, where the spin operator is $S^\mu = (0,\vec{\sigma}/2)$. In the relativistic part of the matching, the incoming and outgoing nucleons are represented by the Dirac spinors $u(\vec{p})$ and $\bar{u}(\vec{p}')$, whose explicit expressions are

$$u(\vec{p}) = \sqrt{\frac{E+m_N}{2E}}\begin{pmatrix}\xi \\ \frac{\vec{p}\cdot\vec{\sigma}}{E+m_N}\xi\end{pmatrix}, \qquad \bar{u}(\vec{p}') = \sqrt{\frac{E'+m_N}{2E'}}\left(\xi^\dagger, -\xi^\dagger\frac{\vec{p}'\cdot\vec{\sigma}}{E'+m_N}\right), \quad \text{(I.3)}$$

where ξ is a two-component spinor, normalized to one, and the nucleon energy is $E = \sqrt{m_N^2+\vec{p}^2}$. In the heavy-baryon part of the matching, the nucleons are represented

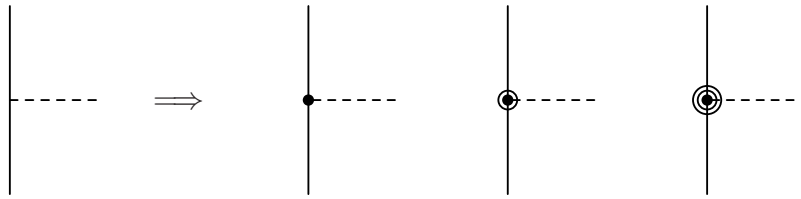

FIGURE I.1. Matching of the one-pion TC Green's function. The l.h.s. represents the relativistic Lagrangian (I.1). On the r.h.s., the circle denotes the interaction in the leading-order Lagrangian $\mathcal{L}^{(0)}_{\chi,f=2}$ (3.3.17), while the vertices with circled and doubly circled circles denote, respectively, once- and twice-suppressed interactions in the Lagrangian $\mathcal{L}^{(1,2)}_{\chi,f=2}$ (3.3.18) and (3.3.19).

by the spinor ξ.

The Feynman diagrams for the matching of the one-pion TC and TV Green's function are depicted in Figs. I.1 and I.2. On the relativistic side, the interactions are given by the Lagrangians (I.1) and (I.2). In Fig. I.1, on the heavy-baryon side the circle denotes the leading pion-nucleon interaction in Eq. (3.3.17), while diagrams with circled and doubly circled circles denote contributions suppressed by one or two powers of Q/M_{QCD} in Eqs. (3.3.18) and (3.3.19). Similarly, on the heavy-baryon side of Fig. I.2 the diagrams with zero and two circles denote contributions from, respectively, the leading TV Lagrangian $\mathcal{L}^{(1)}_{\chi,f=2}$ (4.1.19) and the subleading TV Lagrangian $\mathcal{L}^{(3)}_{\chi^1,\,f=2}$ (4.1.24). Equating the relativistic and non-relativistic TC Green's functions we reproduced the $1/m_N$ and $1/m_N^2$ terms in Eq. (3.3.18) and (3.3.19) and, for the TV Green's function, we find

$$\rho\,\delta m_N = \bar{g}_0, \qquad \rho\,\zeta_1 = \rho\,\zeta_6 = \frac{\bar{g}_0}{2m_N^2}. \tag{I.4}$$

The Feynman diagrams for the matching of the two-pion TV Green's function are shown in Fig. I.3. The first row shows the relativistic diagrams. As before, the TV vertices from Eq. (I.2) are denoted by squares: in the first diagram, the TV coupling is either $\bar{h}_0$ or $\bar{\eta}_4$, while the last four diagrams are proportional to $\bar{g}_0$ or $\bar{\eta}_3$. The TC vertices come from the Lagrangian (I.1) and are proportional to the axial coupling g_A. The second, third and fourth rows contain the diagrams evaluated in the heavy-

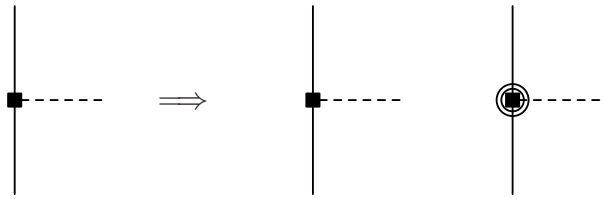

FIGURE I.2. Matching of the one-pion TV Green's function. The l.h.s represents the relativistic Lagrangian (I.2). On the r.h.s., the square denotes the TV vertex in the leading TV Lagrangian $\mathcal{L}^{(1)}_{\chi,f=2}$ (4.1.19), while the square with two circles the vertices in the power-suppressed Lagrangian $\mathcal{L}^{(3)}_{\chi^1,f=2}$ (4.1.24).

baryon theory. The double circle indicates that we consider vertices and corrections to the heavy-baryon propagator in the TC and TV chiral Lagrangians with up to two powers of Q/M_{QCD} with respect to $\mathcal{L}^{(0)}_{\chi,f=2}$ (3.3.17) and $\mathcal{L}^{(1)}_{\chi,f=2}$ (4.1.19). Equating the two-pion Green's functions we find

$$\rho\,\beta_1 = \bar{h}_0, \qquad \rho\,\zeta_8 = \frac{g_A \bar{g}_0}{m_N^2} - \frac{\bar{h}_0}{m_N}. \tag{I.5}$$

The relations for the subleading TC operators in Eq. (3.3.18) and (3.3.19) and for the isospin-breaking coefficients, summarized in Eqs. (I.4) and (I.5), reproduce those in Refs. [131, 150], obtained by integrating the antinucleon field out of a relativistic Lagrangian, once a field redefinition is used to eliminate the time derivatives acting on the nucleon field from the power-suppressed Lagrangians. We refer to [151] for more details. There the relations (I.4) and (I.5) are derived in a more sophisticated fashion, by adapting the method of [252] to the χPT Lagrangian and by using field redefinitions to eliminate time derivatives acting on the nucleon fields. The method there developed can be applied also to four-nucleon operators, and it is showed to reproduce the results of [254]

Equations (I.4) and (I.5) lead to Eq. (4.1.26). Equation (I.2) and the matching above imply that the coefficients ζ_3, ζ_4, ζ_9, ζ_{10}, and ζ_{12} are new arbitrary low-energy constants, not linked to the couplings appearing in the $\Delta = 1$ and $\Delta = 2$ TV Lagrangians. The operators proportional to ζ_{11} and ζ_{13} do not appear in the relativistic Lagrangian, so their coefficient could be linked to δm_N or β_1. In order to find

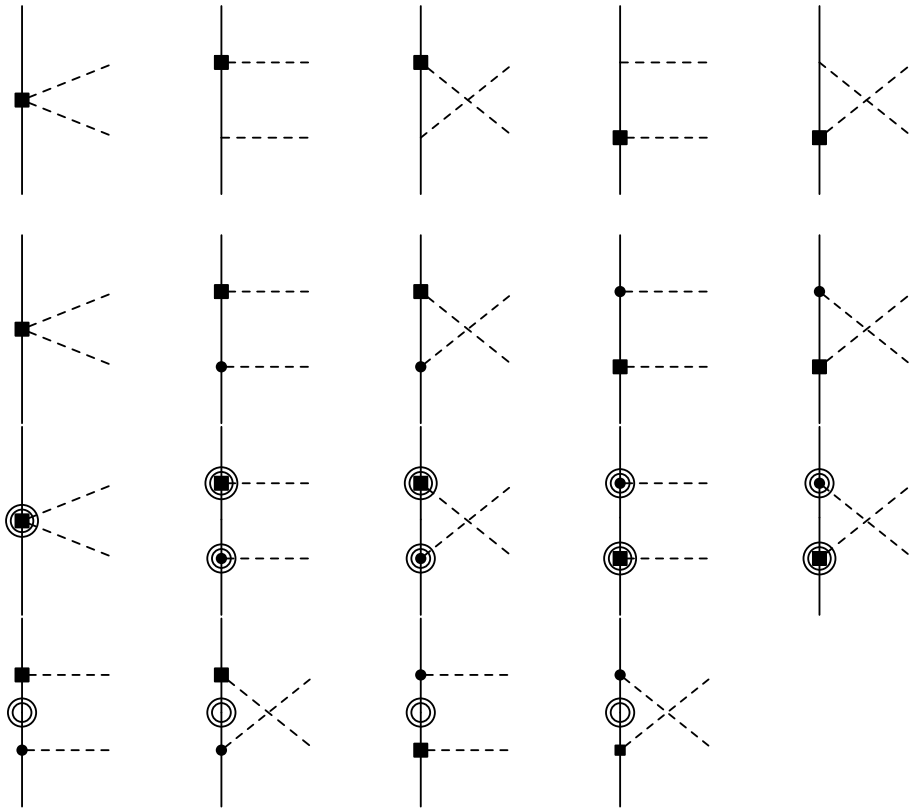

FIGURE I.3. Matching of the TV two-pion Green's function. In the top row, the nucleon is relativistic. In the bottom rows, the nucleon is described by the heavy-baryon Lagrangian. Circles and squares indicate vertices from the leading TC and TV Lagrangian, respectively. Doubly circled circles and squares vertices from the power suppressed TC and TV Lagrangian. The double circle in the propagator indicates that in each heavy-baryon diagram we consider corrections to the heavy-baryon propagator with up to two powers of Q/M_{QCD}.

the exact relation, we should match three-pion Green's functions. We refrain from doing this here because these three-pion operators play no role in any foreseeable phenomenological application.

The constraints on TV operators stemming from the qCEDM, Eq. (4.1.37), and on the TV electromagnetic operators generated by the QCD $\bar{\theta}$ term and the dimension 6 TV operators are obtained with the same method, by equating the relativistic and non-relativistic three-point Green's functions with two nucleon and one photon fields. Also in this case, our results have been checked with the alternative method described

in [151].

Appendix J

The Pion-Nucleon TV Form Factor

One ingredient in the calculation of the N^{2}LO potential from the QCD $\bar{\theta}$ term is the N^{2}LO pion-nucleon TV form factor. From Sec. 4.3, we see that the TV pion-nucleon interaction receives corrections two orders down. After the field redefinition of Sec. 4.3, and expanding in the number of pions,

$$\begin{aligned}\mathcal{L}^{(3)}_{T,\pi N} &= -\frac{1}{F_\pi}\left[\left(\Delta\bar{g}_0+\bar{g}_0\frac{\delta m_\pi^2}{m_\pi^2}\right)\boldsymbol{\pi}-\frac{\bar{\eta}_2}{2}(v\cdot\partial)^2\boldsymbol{\pi}-\frac{\bar{\eta}_3}{2}\partial^2\boldsymbol{\pi}\right]\cdot\bar{N}\boldsymbol{\tau}N\\ &\quad+\frac{1}{4F_\pi}\boldsymbol{\pi}\cdot\bar{N}\boldsymbol{\tau}\left[\bar{\eta}_5\left(v\cdot\partial_-\right)^2+\frac{\bar{g}_0}{2m_N^2}\partial_{\perp-}^2\right]N\\ &\quad+\frac{\bar{g}_0}{4m_N^2F_\pi}\left(\partial_\nu\boldsymbol{\pi}\right)\cdot\bar{N}\left[S^\mu,S^\nu\right]\boldsymbol{\tau}\partial_{\mu-}N\\ &\quad-\frac{\rho}{F_\pi}\left(-4c_1^{(3)}+2\Delta m_N\frac{\delta m_\pi^2}{m_\pi^2}\right)\pi_3\bar{N}N+\ldots,\end{aligned}\tag{J.1}$$

where the non-derivative couplings are given in Eqs. (4.1.27), they scale as

$$\Delta\bar{g}_0=-2\rho\delta_1m_N^{(3)}=\mathcal{O}\left(\frac{\rho\varepsilon m_\pi^4}{r^2(\bar{\theta})M_{QCD}^3}\right),\quad \rho c_1^{(3)}=\mathcal{O}\left(\frac{\rho\varepsilon^2 m_\pi^4}{r^2(\bar{\theta})M_{QCD}^3}\right),\tag{J.2}$$

and they receive a correction from the elimination of the tadpole, as detailed in Sec. 4.3. The derivative couplings are

$$\bar{\eta}_i=\rho\,\zeta_i=\mathcal{O}\left(\frac{\rho\varepsilon m_\pi^2}{r^2(\bar{\theta})M_{QCD}^3}\right).\tag{J.3}$$

In addition to a correction $\Delta\bar{g}_0$ to $\bar{g}_0$ and to the isospin-breaking non-derivative $\rho c_1^{(3)}$ coupling, plus the two terms from the field redefinition, the remaining terms all involve derivatives, either of the pion or the nucleon.

In fact, some of these other couplings are necessary to renormalize processes involving the coupling of pions and nucleons, while others lead to momentum dependence. To make this point evident, let us consider the three-point Green's function

for an incoming (outgoing) nucleon of momentum p^μ (p'^μ) and a pion of momentum $q^\mu = p^\mu - p'^\mu$ and isospin a. It can be written as

$$V_a(q,K) = -\frac{i}{F_\pi}\left[F_1(q,K)\tau_a + F_2(q,K)\delta_{a3} + F_3(q,K)\delta_{a3}\tau_3\right], \tag{J.4}$$

in terms of the functions $F_{1,2,3}$ of q^μ and $K^\mu = (p^\mu + p'^\mu)/2$. We will work up to relative $\mathcal{O}(Q^2/M_{QCD}^2)$, when the form factors $F_{1,2,3}(q,K)$ receive contributions from the TV pion-nucleon vertex (4.1.19) at tree and one-loop levels, and from the TV pion-nucleon vertices (J.1) at tree level.

The loops, shown in Fig. J.1, only contribute to $F_1(q,K)$. (Note that we do not include wavefunction renormalization here; this can be easily done if needed.) The leading TV interaction (4.1.19) is dressed by TC interactions from the $\Delta = 0$ Lagrangian (3.3.17). The one-loop diagrams are of course divergent; we use dimensional regularization in d spacetime dimensions, which introduces the renormalized scale μ and

$$L = \frac{2}{4-d} + \gamma_E + \ln 4\pi, \tag{J.5}$$

with $\gamma_E = 0.55721\ldots$. We define the renormalized parameters

$$\Delta\bar{\bar{g}}_0 = \Delta\bar{g}_0 + \frac{\bar{g}_0}{4}\frac{m_\pi^2}{(2\pi F_\pi)^2}\left[\left(1+3g_A^2\right)\left(L+1-\ln\frac{m_\pi^2}{\mu^2}\right) - 3g_A^2\right], \tag{J.6}$$

$$\bar{\bar{\eta}}_2 = \bar{\eta}_2 + \frac{\bar{g}_0}{(2\pi F_\pi)^2}\left(3-\frac{g_A^2}{4}\right)\left(L+2-\ln\frac{m_\pi^2}{\mu^2}\right), \tag{J.7}$$

$$\bar{\bar{\eta}}_5 = \bar{\eta}_5 + \frac{\bar{g}_0}{(2\pi F_\pi)^2}\left(\frac{3}{2}g_A^2-2\right)\left(L+2-\ln\frac{m_\pi^2}{\mu^2}\right). \tag{J.8}$$

At one loop, the form factors are found to be

$$\begin{aligned} F_1(q,K) &= \bar{g}_0\left[1+\frac{\delta m_\pi^2}{m_\pi^2} + \frac{m_\pi^2}{(2\pi F_\pi)^2} f\left(\frac{v\cdot q}{2m_\pi}, \frac{v\cdot K}{m_\pi}\right)\right] + \Delta\bar{\bar{g}}_0 + \frac{1}{2}\bar{\bar{\eta}}_2\,(v\cdot q)^2 \\ &\quad + \bar{\bar{\eta}}_5\,(v\cdot K)^2 - \frac{\bar{\eta}_3}{2}\vec{q}^{\,2} - \frac{\bar{g}_0}{2m_N^2}\vec{K}^2 - i\frac{\bar{g}_0}{2m_N^2}\vec{S}\cdot\left(\vec{K}\times\vec{q}\right), \end{aligned} \tag{J.9}$$

$$F_2(q,K) = -4\rho\left(c_1^{(3)} - \Delta m_N \frac{\delta^{(2)} m_\pi^2}{2m_\pi^2}\right), \tag{J.10}$$

$$F_3(q,K) = 0, \tag{J.11}$$

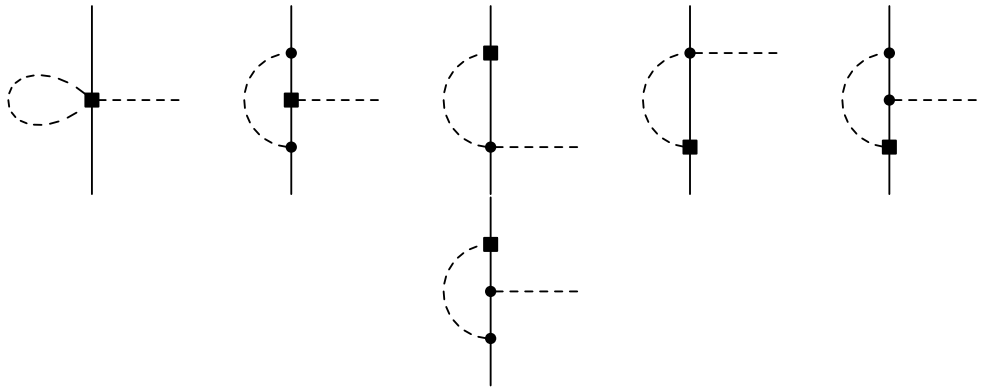

FIGURE J.1. One-loop contributions of $\mathcal{O}(\bar{g}_0 m_\pi^2/(2\pi F_\pi)^2)$ to the pion-nucleon form factor $F_1(q,K)$. A nucleon (pion) is represented by a solid (dashed) line; the TV vertex (4.1.19) is indicated by a square, while other vertices come from Eq. (3.3.17).

with

$$\begin{aligned} f(x,y) &= g_A^2 - \sqrt{1-(y+x)^2}\left\{2y+6x+\frac{g_A^2}{2x}\left[1-(y+x)^2\right]\right\}\arccos\left(-y-x\right) \\ &\quad -\sqrt{1-(y-x)^2}\left\{2y-6x-\frac{g_A^2}{2x}\left[1-(y-x)^2\right]\right\}\arccos\left(-y+x\right) \end{aligned} \tag{J.12}$$

The result greatly simplifies if we let the nucleons go on shell, which we write in a short-hand notation in terms of the nucleon isospin as

$$v\cdot q = \frac{\vec{K}\cdot\vec{q}}{m_N} + i\frac{\delta m_N}{2}\varepsilon^{3ab}\tau_b + \ldots, \tag{J.13}$$

$$v\cdot K = \frac{1}{2m_N}\left(\vec{K}^2+\frac{\vec{q}^{\,2}}{4}\right) - \Delta m_N - \frac{\delta m_N}{2}\delta_{a3}\tau_3 + \ldots \tag{J.14}$$

In this limit, $f(v\cdot q/2m_\pi, v\cdot K/m_\pi)$ is subleading,

$$f\left(\frac{v\cdot q}{2m_\pi},\frac{v\cdot K}{m_\pi}\right) = 0 + \mathcal{O}\left(\frac{m_\pi^3}{M_{QCD}^3}\right), \tag{J.15}$$

and, at the accuracy to which we are working, it can be neglected. The form factors for on-shell nucleons become

$$F_1(q,K) = \bar{g}_0\left(1+\frac{\delta m_\pi^2}{m_\pi^2}\right) + \Delta\bar{\bar{g}}_0 - \frac{\bar{\eta}_3}{2}\vec{q}^{\,2} - \frac{\bar{g}_0}{2m_N^2}\vec{K}^2 - i\frac{\bar{g}_0}{2m_N^2}\vec{S}\cdot\left(\vec{K}\times\vec{q}\right), \tag{J.16}$$

$$F_2(q,K) = -4\rho\left(c_1^{(3)} - \Delta m_N\frac{\delta m_\pi^2}{2m_\pi^2}\right), \tag{J.17}$$

$$F_3(q,K) = 0. \tag{J.18}$$

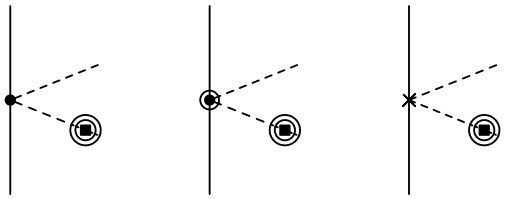

FIGURE J.2. Tadpole contributions to the pion-nucleon form factors $F_i(q,K)$, $i = 1,2,3$. The TV vertex from Eq. (4.1.9) is indicated by a twice-circled square. The circle is the Weinberg-Tomozawa term in Eq. (3.3.17). The circled circle denotes both the nucleon sigma term from Eq. (4.1.2) and a recoil correction to the Weinberg-Tomozawa term from Eq. (3.3.18), while the cross represents the isospin-breaking operator in Eq. (4.1.19).

They are in the form of a local expansion in momenta. The coupling $\Delta\bar{\bar{g}}_0$ and the tadpole factor $\bar{g}_0\delta m_\pi^2/m_\pi^2$ are chiral corrections of $\mathcal{O}(m_\pi^2/M_{QCD}^2)$ to the leading coupling $\bar{g}_0$. The vertex $-4c_1^{(3)}$ and the tadpole correction $-\rho\Delta m_N\delta m_\pi^2/m_\pi^2$ are the leading contributions to F_2. As far as the pion-nucleon form factor goes, one could as well absorb the tadpole terms in $\Delta\bar{\bar{g}}_0$ and $c_1^{(3)}$, as we do in Chapter 7. Note, however, that the tadpole contributions and the vertices have different tensorial properties and could, in principle, be separated in other reactions. The $\bar{\eta}_3$ term gives the F_1 form-factor radius, while the remaining two terms in Eq. (J.16) are relativistic corrections. Note that F_3 does not receive any contribution up to this order.

The results (J.16)-(J.18) can be obtained using the TV Lagrangian before the rotation of the tadpoles. We use the same Lagrangian (J.1), but with $\delta m_\pi^2 \to 0$. Instead, we have to include explicitly the tadpole in Eq. (4.1.9). It generates tadpole trees, shown in Fig. J.2, which contribute to all three form factors. The TV tadpole (4.1.9) connects to the outgoing pion via seagulls from the nucleon covariant derivative in Eq. (3.3.17) (the so-called Weinberg-Tomozawa term), from a recoil correction to it found in Eq. (3.3.18), from the nucleon sigma term (4.1.2), and from the isospin-breaking operator in Eq. (4.1.19).

In this case we get also an additional term in the form factor,

$$V_a(q,K) = -\frac{i}{F_\pi}\left[F_1(q,K)\tau_a + F_2(q,K)\delta_{a3} + F_3(q,K)\delta_{a3}\tau_3\right] + V_{a,\mathrm{tad}}, \qquad \text{(J.19)}$$

where

$$F_1(q,K) = \bar{g}_0\left[1+\frac{\delta m_\pi^2}{2m_\pi^2}+\frac{m_\pi^2}{(2\pi F_\pi)^2}f\left(\frac{v\cdot q}{2m_\pi},\frac{v\cdot K}{m_\pi}\right)\right]+\Delta\bar{\bar{g}}_0+\frac{1}{2}\bar{\bar{\eta}}_2\left(v\cdot q\right)^2$$
$$+\bar{\bar{\eta}}_5\left(v\cdot K\right)^2-\frac{\bar{\eta}_3}{2}\vec{q}^{\,2}-\frac{\bar{g}_0}{2m_N^2}\vec{K}^2-i\frac{\bar{g}_0}{2m_N^2}\vec{S}\cdot\left(\vec{K}\times\vec{q}\right), \qquad \text{(J.20)}$$

$$F_2(q,K) = -4\rho\left(c_1^{(3)}-\Delta m_N\frac{\delta m_\pi^2}{2m_\pi^2}\right), \qquad \text{(J.21)}$$

$$F_3(q,K) = -\bar{g}_0\frac{\delta m_\pi^2}{2m_\pi^2}, \qquad \text{(J.22)}$$

and

$$V_{a,\mathrm{tad}}(q,K)=\varepsilon^{3ab}\tau_b\frac{\rho}{F_\pi}\frac{\delta m_\pi^2}{2m_\pi^2}\left[v\cdot q-\frac{\vec{K}\cdot\vec{q}}{m_N}\right]. \qquad \text{(J.23)}$$

These relations are slightly different than in the case of the field redefinitions, Eqs. (J.9), (J.10), and (J.11). This is not surprising because in general a field redefinition changes quantities off-shell. When the nucleons are on-shell, Eqs. (J.13) and (J.14) hold. The function $f(v\cdot q/2m_\pi, v\cdot K/m_\pi)$ is still higher order. More care has to be taken, however, with Eq. (J.23), which gives

$$V_{a,\mathrm{tad}}(q,K)=-\frac{i\bar{g}_0}{F_\pi}\frac{\delta m_\pi}{2m_\pi^2}(\tau_a-\delta_{a3}\tau_3), \qquad \text{(J.24)}$$

so that the on-shell form factors become exactly Eqs. (J.16), (J.17), and (J.18).

The TV pion-nucleon form factor has recently been studied in Ref. [255] using a model relativistic Lagrangian for the interactions of nucleons, pions, ρ, ω and η mesons. The TV sector of the Lagrangian in Ref. [255] contains all the possible non-derivative one-pion/two-nucleon interactions —in particular an isoscalar coupling with coupling constant c_π— and interactions of the ρ, ω and η mesons with the nucleon. Similarly, the TC sector includes a pseudo-vector pion-nucleon coupling with coupling constant g_π, the coupling of the ρ meson to the nucleon and to two pions with constants g_ρ and $g_{\rho\pi}$ respectively, and the couplings of the η and ω mesons to the nucleon. The model Lagrangian in Ref. [255] does not include multi-pion terms and, therefore, it is not fully consistent with the chiral symmetry of the QCD Lagrangian.

On the other hand, our framework is limited to momentum transfer $Q \sim m_\pi \ll m_\rho$. It is instructive to make contact between Ref. [255] and the formalism presented here. For that, we have first of all to integrate out the contributions of the ρ, ω and η mesons. At energies much smaller than the η and ω masses, loops containing the ω and η mesons appear as short-distance contributions, absorbed in the coupling $\bar{g}_0$. At energies much smaller than m_ρ, the TC processes in which the nucleon emits a ρ meson that subsequently decays into two pions appear like a local seagull vertex, the Weinberg-Tomozawa term. We can thus establish the relation $g_\rho g_{\rho\pi}/m_\rho^2 = -1/F_\pi^2$. Analogously, the emission of a ρ meson via a TV interaction, followed by its decay into two pions, matches onto a TV seagull interaction with the form of the operator ζ_4 in Eq. (4.1.24). Loops containing such a vertex are subleading in the power counting. Terms cubic in the TV couplings are similarly of higher orders. Expanding the result of Ref. [255] in powers of m_π^2/m_N^2 and m_π^2/m_ρ^2, we find that the sum of the last five diagrams in Fig. J.1 reproduces the infrared behavior of the fully relativistic calculation, that is, the factors of $\ln m_\pi/\mu$ exactly match in the two calculations, provided that we use $c_\pi = -\bar{g}_0/F_\pi$ and the Goldberger-Treiman relation $g_\pi = 2m_N/F_\pi g_A$. However, the first diagram of Fig. J.1 does not have a counterpart in the calculation of Ref. [255], whose model Lagrangian does not include multi-pion terms. These multi-pion terms follow from the chiral properties of the TV operators, which are tied to their roots in the $\bar{\theta}$ term in the QCD Lagrangian.

The framework presented here thus affords a method to carry out hadronic calculations where the QCD symmetries are included properly. It also allows a systematic ordering of the infinite number of contributions allowed by the symmetries. The results (J.16), (J.17), and (J.18) can be used as input, for example, in nuclear calculations. If more accuracy is needed, one can compute the form factor in higher orders. For example, as we saw in Table 4.2, F_3 first appears at relative $\mathcal{O}(\alpha_{\rm em}/\pi)$, which, in the way we count powers of $\alpha_{\rm em}/\pi$, is the next order in the Q/M_{QCD} expansion. At this order one would have to include photon loops as well.

Appendix K
Fourier Transform

In general a potential obtained in EFT depends not only on the transferred momentum $\vec{q}$ but also on $\vec{K}$, and the center-of-mass momentum $\vec{P}$, $V(\vec{q},\vec{K},\vec{P})$. The Fourier transform of such a potential is defined as

$$V(\vec{r},\vec{r}\,',\vec{X},\vec{X}\,') = \int \frac{d^3K}{(2\pi)^3}\int \frac{d^3P}{(2\pi)^3}\int \frac{d^3q}{(2\pi)^3} e^{-i\vec{P}\cdot(\vec{X}-\vec{X}\,')} e^{-i\vec{K}\cdot(\vec{r}-\vec{r}\,')} e^{-\frac{i}{2}\vec{q}\cdot(\vec{r}+\vec{r}\,')} V(\vec{q},\vec{K},\vec{P}), \tag{K.1}$$

where, if $\vec{x}_1$ and $\vec{x}_2$ are the positions of the incoming nucleons and $\vec{x}_1'$ and $\vec{x}_2'$ the positions of the outgoing nucleons, the relative coordinates are $\vec{r} = \vec{x}_1 - \vec{x}_2$ and $\vec{r}\,' = \vec{x}_1' - \vec{x}_2'$, while the center-of-mass position of the incoming and outgoing pairs are $2\vec{X} = \vec{x}_1 + \vec{x}_2$ and $2\vec{X}' = \vec{x}_1' + \vec{x}_2'$. The potential in Eq. (K.1) has to be used in a two-nucleon Schrödinger equation of the form

$$i\frac{\partial}{\partial t}\psi(\vec{r}\,',\vec{X}\,') = -\left(\frac{\vec{\nabla}^2_{X'}}{4m_N} + \frac{\vec{\nabla}^2_{r'}}{m_N}\right)\psi(\vec{r}\,',\vec{X}\,') + \int d^3\vec{r}\int d^3\vec{X}\, V(\vec{r},\vec{r}\,',\vec{X},\vec{X}\,')\,\psi(\vec{r},\vec{X}). \tag{K.2}$$

For potentials that, like the ones in Sec. 7.3, are polynomials in $\vec{K}$ and $\vec{P}$,

$$V(\vec{q},\vec{K},\vec{P}) \propto \vec{K}^m\vec{P}^n f(\vec{q}), \tag{K.3}$$

$V(\vec{r},\vec{r}\,',\vec{X},\vec{X}\,')$ assumes the form

$$V(\vec{r},\vec{r}\,',\vec{X},\vec{X}\,') \propto \left(\vec{\nabla}^n_X\delta^{(3)}(\vec{X}-\vec{X}')\right)\left(\vec{\nabla}^m_r\delta^{(3)}(\vec{r}-\vec{r}')\right) f\left(\frac{\vec{r}+\vec{r}\,'}{2}\right), \tag{K.4}$$

where

$$f(\vec{r}) = \int \frac{d^3q}{(2\pi)^3} e^{-i\vec{q}\cdot\vec{r}}\, f(\vec{q}). \tag{K.5}$$

Plugging Eq. (K.4) in Eq. (K.2), and integrating by parts, the derivatives acting on the delta functions can be turned into derivatives acting on f and on the wave

function $\psi(\vec{r},\vec{X})$. The integrals in Eq. (K.2) then become trivial, and the Schrödinger equation assumes the form

$$i\frac{\partial}{\partial t}\psi(\vec{r}\,',\vec{X}\,') = -\left(\frac{\vec{\nabla}^{\,2}_{X'}}{4m_N}+\frac{\vec{\nabla}^{\,2}_{r'}}{m_N}\right)\psi(\vec{r}\,',\vec{X}\,') + V(\vec{r}\,',\vec{\nabla}_{r'},\vec{\nabla}_{X'})\,\psi(\vec{r}\,',\vec{X}\,'), \qquad \text{(K.6)}$$

where the two potentials in Eqs. (K.2) and (K.6) are related by integrations by parts. For a potential of the form (K.3), schematically we would have

$$V(\vec{r}\,',\vec{\nabla}_{r'},\vec{\nabla}_{X'}) \propto (-)^n(-)^m\left\{\frac{\nabla_{r'\,i_1}}{2},\ldots\left\{\frac{\nabla_{r'\,i_m}}{2},f(\vec{r}\,')\right\}\right\}\,\nabla^n_{X'}, \qquad \text{(K.7)}$$

where the indices $i_i,\ldots,i_m$ are appropriately contracted.

In order to obtain the potential in configuration space for functions that diverge as the momentum transfer $|\vec{q}|$ goes to infinity, one has to define a regularization scheme. Here, following Ref. [246], we find it convenient to extend the definition of the Fourier transform (K.5) to a space-time of $d = n+1$ dimensions:

$$V_n(\vec{r}\,) = \int\frac{d^nq}{(2\pi)^n}e^{-i\vec{q}\cdot\vec{r}}\,V(\vec{q}\,). \qquad \text{(K.8)}$$

The amplitude $V(\vec{q}\,)$ is the expression in momentum space of corresponding loop contributions right after the d-dimensional integration over loop momenta is performed, but before setting $d = 4$ or performing the integration over Feynman parameters. Writing

$$d^nq = q^{n-1}dq\,(1-\cos^2\theta)^{\frac{n-3}{2}}\,d\cos\theta\,d\Omega_{n-1}, \qquad \text{(K.9)}$$

the angular integrations are evaluated with the aid of the formulas

$$\int d\Omega_{n-1} = \frac{2\pi^{\frac{n-1}{2}}}{\Gamma\left(\frac{n-1}{2}\right)}, \qquad \text{(K.10)}$$

and

$$\frac{2\pi^{\frac{n-1}{2}}}{\Gamma\left(\frac{n-1}{2}\right)}\int_{-1}^{1}d\cos\theta\,(1-\cos^2\theta)^{\frac{n-3}{2}}e^{-iqr\cos\theta} = (2\pi)^{\frac{n}{2}}(qr)^{1-\frac{n}{2}}J_{\frac{n}{2}-1}(qr), \qquad \text{(K.11)}$$

where $q=|\vec{q}|$, $r=|\vec{r}|$, and $J_n(x)$ denotes a Bessel Function of the first kind. For momentum integrals, a useful relation is [256]

$$\int_0^\infty dq\,q^{\frac{n}{2}}\frac{J_{\frac{n}{2}-1}(qr)}{(q^2+\beta^2)^{\frac{m-n}{2}}} = \left(\frac{r}{2}\right)^{\frac{m-n}{2}-1}\frac{\beta^{n-\frac{m}{2}}}{\Gamma\left(\frac{m-n}{2}\right)}K_{\frac{m}{2}-n}\left(\beta r\right), \qquad \text{(K.12)}$$

where β is a constant and $K_n(x)$ is the modified Bessel function of the second kind.

For example, in the case of the triangle diagrams discussed in Sec. 7.3,

$$V_{\triangle}(\vec{q}) = -i\frac{g_A\bar{g}_0}{F_\pi^2}\frac{(4\pi\mu^2)^{\frac{3-n}{2}}}{(2\pi F_\pi)^2}\boldsymbol{\tau}^{(1)}\cdot\boldsymbol{\tau}^{(2)}\,(\vec{\sigma}^{(1)}-\vec{\sigma}^{(2)})\cdot\vec{q}\,\Gamma\left(\frac{3-n}{2}\right) \int_0^1 dx\left[m_\pi^2+q^2x(1-x)\right]^{\frac{n-3}{2}}. \tag{K.13}$$

For $m=3$ and $\beta^2=m_\pi^2/x(1-x)$, the result in Eq. (K.12) allows one to cancel the divergent factor of $\Gamma((3-n)/2)$ in Eq. (K.13) and get an expression that is finite for $r\neq 0$. Now we can set $d=4$ and with the aid of the properties of modified Bessel functions [256] we can write the potential in configuration space as

$$V_{\triangle}(\vec{r}) = \frac{g_A\bar{g}_0}{F_\pi^2}\frac{1}{(2\pi F_\pi)^2}\boldsymbol{\tau}^{(1)}\cdot\boldsymbol{\tau}^{(2)}\,(\vec{\sigma}^{(1)}-\vec{\sigma}^{(2)})\cdot\vec{\nabla}\left[\frac{1}{2\pi r^3}\int_0^1 dx(1+\beta r)\,e^{-\beta r}\right]. \tag{K.14}$$

The contributions from box and crossed diagrams can be obtained in a similar fashion, leading to the result in Eq. (7.4.11).

Alternatively, we can isolate the short-range, divergent part of the interaction with integration by parts. In Eq. (K.13), for instance, we then obtain

$$\begin{aligned} V_{\triangle}(\vec{q}) &= -i\frac{g_A\bar{g}_0}{F_\pi^2}\frac{(4\pi\mu^2)^{\frac{3-n}{2}}}{(2\pi F_\pi)^2}\boldsymbol{\tau}^{(1)}\cdot\boldsymbol{\tau}^{(2)}\,(\vec{\sigma}^{(1)}-\vec{\sigma}^{(2)})\cdot\vec{q} \\ &\quad\left[\Gamma\left(\frac{3-n}{2}\right)m_\pi^{n-3}+\Gamma\left(\frac{5-n}{2}\right)\int_0^1 dx\frac{q^2x(1-2x)}{\left[m_\pi^2+q^2x(1-x)\right]^{\frac{5-n}{2}}}\right] \end{aligned} \tag{K.15}$$

The first, divergent piece in Eq. (K.15) is a contribution to a delta-function potential. Applying the d-dimensional Fourier transform to Eq. (K.15) and taking the $d\to 4$ limit we find

$$\begin{aligned} V_{\triangle}(\vec{r}) &= \frac{g_A\bar{g}_0}{F_\pi^2}\frac{1}{(2\pi F_\pi)^2}\boldsymbol{\tau}^{(1)}\cdot\boldsymbol{\tau}^{(2)}\,(\vec{\sigma}^{(1)}-\vec{\sigma}^{(2)})\cdot\vec{\nabla} \\ &\quad\left[\delta^{(3)}(\vec{r})\left(L+\ln\frac{\mu^2}{m_\pi^2}\right)-\frac{1}{4\pi r}\int_0^1 dx\frac{1-2x}{1-x}\beta^2\,e^{-\beta r}\right], \end{aligned} \tag{K.16}$$

where L is given in Eq. (7.3.3). Proceeding in this way also for box and crossed

terms, we find that Fourier transform of the TPE potential can be expressed as

$$\begin{aligned} V_{TPE}^{(3)}(\vec{r}) &= \frac{g_A \bar{g}_0}{F_\pi^2} \frac{1}{(2\pi F_\pi)^2} \boldsymbol{\tau}^{(1)} \cdot \boldsymbol{\tau}^{(2)} \left(\vec{\sigma}^{(1)} - \vec{\sigma}^{(2)}\right) \cdot \vec{\nabla} \\ &\quad \left\{ -\delta^{(3)}(\vec{r}) \left[(3g_A^2 - 1) \left(L + \ln \frac{\mu^2}{m_\pi^2} \right) + 2g_A^2 \right] \right. \\ &\quad \left. + \frac{1}{4\pi r} \int_0^1 dx \left[g_A^2 \left(4 - \frac{3}{2x(1-x)} \right) - \frac{1-2x}{1-x} \right] \beta^2 e^{-\beta r} \right\} . \quad \text{(K.17)} \end{aligned}$$

The piece proportional to the delta function can then be absorbed in a redefinition of $\bar{C}_2$ very similar to Eq. (7.3.4), the only difference residing in the finite pieces. Integrating by parts, it can be explicitly verified that the non-analytic piece of the expression (K.17) gives the medium-range potential in the form of Eq. (7.4.11).

As a further check of our results, we computed the Fourier transform of the triangle diagrams with a Gaussian regulator $\exp(-q^2/\Lambda^2)$, for different values of the cutoff Λ. The calculation was performed numerically with *Mathematica* [257] and we focused on the region $r > 1/m_\pi$. For $\Lambda \simeq m_\rho$, the result we get is still quite different from the Fourier transform obtained in dimensional regularization, but as we increase the cutoff to 1–2 GeV, it approximates Eq. (K.14) better and better.

As pointed out in Ref. [246], in the d-dimensional Fourier-transform procedure the infinities are "regularized" away because the nucleon distance is kept finite. The ultraviolet divergences and the regulator dependence are now hidden in the singular behavior ($\sim 1/r^4$) of the potential for small r, which forces the reintroduction of a regulator in the calculation of matrix elements of $V(r)$. If the chosen regulator were dimensional regularization, then the $d \to 4$ limit of Eq. (K.12), which lead to the $1/r^3$ singularity in Eq. (K.14), must be taken in the sense of generalized functions; the singularity is then encoded by a delta function, proportional to the divergent factor $2/(d-4)$, while the $1/r^3$ behaviour is replaced by a more regular plus distribution [250].

References

[1] K. Nakamura *et al.* [Particle Data Group Collaboration], J. Phys. G **G37**, 075021 (2010).

[2] B. Grinstein, Nucl. Phys. B **339**, 253 (1990).

[3] E. Eichten and B. R. Hill, Phys. Lett. B **234**, 511 (1990).

[4] H. Georgi, Phys. Lett. B **240**, 447 (1990).

[5] A. Manohar and M. Wise, *Heavy Quark Physics*, Cambridge University Press, Cambridge, 2000.

[6] G. T. Bodwin, E. Braaten, and G. P. Lepage, Phys. Rev. D **51**, 1125 (1995). [Erratum-ibid. D **55**, 5853 (1997)] [arXiv:hep-ph/9407339].

[7] A. Pineda and J. Soto, Nucl. Phys. Proc. Suppl. **64**, 428 (1998). [arXiv:hep-ph/9707481].

[8] N. Brambilla, A. Pineda, J. Soto, and A. Vairo, Nucl. Phys. B **566**, 275 (2000). [arXiv:hep-ph/9907240].

[9] N. Brambilla, A. Pineda, J. Soto, and A. Vairo, Rev. Mod. Phys. **77**, 1423 (2005). [arXiv:hep-ph/0410047].

[10] M. E. Luke and A. V. Manohar, Phys. Rev. D **55**, 4129 (1997). [arXiv:hep-ph/9610534].

[11] M. E. Luke, A. V. Manohar, and I. Z. Rothstein, Phys. Rev. D **61**, 074025 (2000). [arXiv:hep-ph/9910209].

[12] A. V. Manohar and I. W. Stewart, Phys. Rev. D **62**, 014033 (2000). [arXiv:hep-ph/9912226].

[13] A. H. Hoang and I. W. Stewart, Phys. Rev. D **67**, 114020 (2003). [arXiv:hep-ph/0209340].

[14] N. Brambilla *et al.* [Quarkonium Working Group], arXiv:hep-ph/0412158.

[15] N. Brambilla, S. Eidelman, B. K. Heltsley, R. Vogt, G. T. Bodwin, E. Eichten, A. D. Frawley, A. B. Meyer *et al.*, Eur. Phys. J. **C71**, 1534 (2011). [arXiv:1010.5827 [hep-ph]].

[16] C. W. Bauer, S. Fleming, and M. E. Luke, Phys. Rev. D **63**, 014006 (2000). [arXiv:hep-ph/0005275].

[17] C. W. Bauer, S. Fleming, D. Pirjol, and I. W. Stewart, Phys. Rev. D **63**, 114020 (2001). [arXiv:hep-ph/0011336].

[18] C. W. Bauer, D. Pirjol, and I. W. Stewart, Phys. Rev. D **65**, 054022 (2002). [arXiv:hep-ph/0109045].

[19] C. W. Bauer, S. Fleming, D. Pirjol, I. Z. Rothstein, and I. W. Stewart, Phys. Rev. D **66**, 014017 (2002). [arXiv:hep-ph/0202088].

[20] A. K. Leibovich, Z. Ligeti, and M. B. Wise, Phys. Lett. B **564**, 231 (2003). [arXiv:hep-ph/0303099].

[21] V. Ahrens, T. Becher, M. Neubert, L. L. Yang, Phys. Rev. **D79**, 033013 (2009). [arXiv:0808.3008 [hep-ph]].

[22] V. Ahrens, T. Becher, M. Neubert, L. L. Yang, Eur. Phys. J. **C62**, 333-353 (2009). [arXiv:0809.4283 [hep-ph]].

[23] C. F. Berger, C. Marcantonini, I. W. Stewart, F. J. Tackmann, W. J. Waalewijn, [arXiv:1012.4480 [hep-ph]].

[24] C. W. Bauer, F. J. Tackmann, J. Thaler, JHEP **0812**, 011 (2008). [arXiv:0801.4028 [hep-ph]].

[25] C. W. Bauer, F. J. Tackmann, J. Thaler, JHEP **0812**, 010 (2008). [arXiv:0801.4026 [hep-ph]].

[26] T. Becher, M. D. Schwartz, JHEP **0807**, 034 (2008). [arXiv:0803.0342 [hep-ph]].

[27] R. Abbate, M. Fickinger, A. H. Hoang, V. Mateu, I. W. Stewart, [arXiv:1006.3080 [hep-ph]].

[28] R. S. Azevedo, B. Long, E. Mereghetti, Phys. Rev. **D80**, 074026 (2009). [arXiv:0909.1995 [hep-ph]].

[29] S. Weinberg, Physica **A96**, 327 (1979).

[30] J. Gasser, H. Leutwyler, Annals Phys. **158**, 142 (1984).

[31] J. Gasser, H. Leutwyler, Nucl. Phys. **B250**, 465 (1985).

[32] S. Weinberg, "The quantum theory of fields. Vol. 2: Modern applications," Cambridge, UK: Univ. Pr. (1996) 489 p.

[33] V. Bernard, N. Kaiser, U. -G. Meissner, Int. J. Mod. Phys. **E4**, 193-346 (1995). [hep-ph/9501384].

[34] E. E. Jenkins, A. V. Manohar, Phys. Lett. **B255**, 558-562 (1991).

[35] S. Weinberg, Phys. Lett. B **251**, 288 (1990).

[36] S. Weinberg, Nucl. Phys. B **363**, 3 (1991).

[37] P. F. Bedaque and U. van Kolck, Ann. Rev. Nucl. Part. Sci. **52**, 339 (2002). [arXiv:nucl-th/0203055].

[38] E. Epelbaum, H. -W. Hammer, U. -G. Meissner, Rev. Mod. Phys. **81**, 1773-1825 (2009). [arXiv:0811.1338 [nucl-th]].

[39] E. Mereghetti, W. H. Hockings and U. van Kolck, Annals Phys. **325**, 2363 (2010). [arXiv:1002.2391 [hep-ph]].

[40] J. de Vries, R. G. E. Timmermans, E. Mereghetti, U. van Kolck, Phys. Lett. **B695**, 268-274 (2011). [arXiv:1006.2304 [hep-ph]].

[41] E. Mereghetti, J. de Vries, W. H. Hockings, C. M. Maekawa, U. van Kolck, Phys. Lett. **B696**, 97-102 (2011). [arXiv:1010.4078 [hep-ph]].

[42] J. de Vries, E. Mereghetti, R. G. E. Timmermans and U. van Kolck, arXiv:1102.4068 [hep-ph].

[43] V. L. Chernyak and A. R. Zhitnitsky, Phys. Rept. **112**, 173 (1984).

[44] S. J. Brodsky and G. P. Lepage, Adv. Ser. Direct. High Energy Phys. **5**, 93 (1989).

[45] M. Beneke, A. P. Chapovsky, A. Signer, and G. Zanderighi, Phys. Rev. Lett. **93**, 011602 (2004) [arXiv:hep-ph/0312331].

[46] M. Beneke, A. P. Chapovsky, A. Signer, and G. Zanderighi, Nucl. Phys. B **686**, 205 (2004). [arXiv:hep-ph/0401002].

[47] S. Fleming, A. H. Hoang, S. Mantry, and I. W. Stewart, Phys. Rev. D **77**, 074010 (2008). [arXiv:hep-ph/0703207].

[48] S. Fleming, A. H. Hoang, S. Mantry, and I. W. Stewart, Phys. Rev. D **77**, 114003 (2008). [arXiv:0711.2079 [hep-ph]].

[49] G. T. Bodwin, E. Braaten, D. Kang, and J. Lee, Phys. Rev. D **76**, 054001 (2007). [arXiv:0704.2599 [hep-ph]].

[50] D. Kang, T. Kim, J. Lee, and C. Yu, Phys. Rev. D **76**, 114018 (2007). [arXiv:0707.4056 [hep-ph]].

[51] V. V. Braguta, A. K. Likhoded, and A. V. Luchinsky, arXiv:0902.0459 [hep-ph].

[52] V. V. Braguta and V. G. Kartvelishvili, arXiv:0907.2772 [hep-ph].

[53] B. Aubert *et al.* [BABAR Collaboration], Phys. Rev. Lett. **101**, 071801 (2008). [Erratum-ibid. **102**, 029901 (2009)] [arXiv:0807.1086 [hep-ex]].

[54] D. M. Asner *et al.*, Phys. Rev. D **78**, 091103 (2008). [arXiv:0808.0933 [hep-ex]].

[55] R. A. Briere *et al.* [CLEO Collaboration], Phys. Rev. D **78**, 092007 (2008). [arXiv:0807.3757 [hep-ex]].

[56] R. J. Hill, Phys. Rev. D **73**, 014012 (2006). [arXiv:hep-ph/0505129].

[57] A. V. Manohar and I. W. Stewart, Phys. Rev. D **76**, 074002 (2007). [arXiv:hep-ph/0605001].

[58] G. P. Korchemsky and A. V. Radyushkin, Nucl. Phys. B **283**, 342 (1987).
I. A. Korchemskaya and G. P. Korchemsky, Phys. Lett. B **287**, 169 (1992).

[59] B. I. Eisenstein *et al.* [CLEO Collaboration], arXiv:0806.2112 [hep-ex].

[60] B. O. Lange and M. Neubert, Phys. Rev. Lett. **91**, 102001 (2003). [arXiv:hep-ph/0303082].

[61] C. Amsler *et al.* [Particle Data Group], Phys. Lett. B **667**, 1 (2008).

[62] R. Barbieri, R. Gatto, R. Kogerler, and Z. Kunszt, Phys. Lett. B **57**, 455 (1975).
W. Celmaster, Phys. Rev. D **19**, 1517 (1979).

[63] G. T. Bodwin, D. K. Sinclair, and S. Kim, Phys. Rev. D **65**, 054504 (2002). [arXiv:hep-lat/0107011].

[64] E. J. Eichten and C. Quigg, Phys. Rev. D **52**, 1726 (1995). [arXiv:hep-ph/9503356].

[65] W. Buchmuller and S. H. H. Tye, Phys. Rev. D **24**, 132 (1981).

[66] V. M. Braun, D. Y. Ivanov, and G. P. Korchemsky, Phys. Rev. D **69**, 034014 (2004). [arXiv:hep-ph/0309330].

[67] A. G. Grozin and M. Neubert, Phys. Rev. D **55**, 272 (1997). [arXiv:hep-ph/9607366].

[68] M. Beneke, G. Buchalla, M. Neubert, and C. T. Sachrajda, Phys. Rev. Lett. **83**, 1914 (1999). [arXiv:hep-ph/9905312].

[69] S. J. Lee and M. Neubert, Phys. Rev. D **72**, 094028 (2005). [arXiv:hep-ph/0509350].

[70] V. Pilipp, arXiv:hep-ph/0703180.

[71] A. H. Hoang, Z. Ligeti, and A. V. Manohar, Phys. Rev. Lett. **82**, 277 (1999). [arXiv:hep-ph/9809423].

[72] Z. Ligeti, I. W. Stewart, and F. J. Tackmann, Phys. Rev. D **78**, 114014 (2008). [arXiv:0807.1926 [hep-ph]].

[73] G. T. Bodwin, E. Braaten, and G. P. Lepage, Phys. Rev. D **46**, R1914 (1992). [arXiv:hep-lat/9205006].

[74] N. Brambilla, D. Eiras, A. Pineda, J. Soto, and A. Vairo, Phys. Rev. Lett. **88**, 012003 (2002). [arXiv:hep-ph/0109130].

[75] N. Brambilla, D. Eiras, A. Pineda, J. Soto, and A. Vairo, Phys. Rev. D **67**, 034018 (2003). [arXiv:hep-ph/0208019].

[76] A. Vairo, Mod. Phys. Lett. A **19**, 253 (2004). [arXiv:hep-ph/0311303].

[77] F. Maltoni and A. D. Polosa, Phys. Rev. D **70**, 054014 (2004). [arXiv:hep-ph/0405082].

[78] S. Stracka, private communication.

[79] C. Jarlskog, Phys. Rev. Lett. **55**, 1039 (1985).

[80] A. G. Cohen, D. B. Kaplan, A. E. Nelson, Ann. Rev. Nucl. Part. Sci. **43**, 27-70 (1993). [hep-ph/9302210].

[81] M. Pospelov and A. Ritz, Annals Phys. **318**, 119 (2005) [arXiv:hep-ph/0504231].

[82] C. A. Baker, D. D. Doyle, P. Geltenbort, K. Green, M. G. D. van der Grinten, P. G. Harris, P. Iaydjiev, S. N. Ivanov *et al.*, Phys. Rev. Lett. **97**, 131801 (2006). [hep-ex/0602020].

[83] T. M. Ito, J. Phys. Conf. Ser. **69**, 012037 (2007). [nucl-ex/0702024 [NUCL-EX]].

[84] K. Bodek, S. .Kistryn, M. Kuzniak, J. Zejma, M. Burghoff, S. Knappe-Gruneberg, T. Sander-Thoemmes, A. Schnabel *et al.*, [arXiv:0806.4837 [nucl-ex]].

[85] W. C. Griffith, M. D. Swallows, T. H. Loftus, M. V. Romalis, B. R. Heckel, E. N. Fortson, Phys. Rev. Lett. **102**, 101601 (2009).

[86] V. F. Dmitriev, R. A. Sen'kov, Phys. Rev. Lett. **91**, 212303 (2003). [nucl-th/0306050].

[87] F. J. M. Farley, K. Jungmann, J. P. Miller, W. M. Morse, Y. F. Orlov, B. L. Roberts, Y. K. Semertzidis, A. Silenko *et al.*, Phys. Rev. Lett. **93**, 052001 (2004). [hep-ex/0307006].

[88] I. B. Khriplovich, S. K. Lamoreaux, Berlin, Germany: Springer (1997) 230 p.

[89] D. B. Kaplan, M. J. Savage, Nucl. Phys. **A556**, 653 (1993).

[90] S. -L. Zhu, C. M. Maekawa, B. R. Holstein, M. J. Ramsey-Musolf, U. van Kolck, Nucl. Phys. **A748**, 435 (2005). [nucl-th/0407087].

[91] W. H. Hockings and U. van Kolck, Phys. Lett. B **605**, 273 (2005). [arXiv:nucl-th/0508012].

[92] W.H. Hockings, Ph.D. dissertation, University of Arizona (2006).

[93] R. J. Crewther, P. Di Vecchia, G. Veneziano and E. Witten, Phys. Lett. B **88**, 123 (1979) [Erratum-ibid. B **91**, 487 (1980)].

[94] H. -Y. Cheng, Phys. Rev. **D44**, 166-174 (1991).

[95] A. Pich, E. de Rafael, Nucl. Phys. **B367**, 313-333 (1991).

[96] P. L. Cho, Phys. Rev. **D48**, 3304-3309 (1993). [hep-ph/9212274].

[97] B. Borasoy, Phys. Rev. **D61**, 114017 (2000). [hep-ph/0004011].

[98] S. Narison, Phys. Lett. **B666**, 455-461 (2008). [arXiv:0806.2618 [hep-ph]].

[99] K. Ottnad, B. Kubis, U. G. Meissner and F. K. Guo, Phys. Lett. B **687**, 42 (2010). [arXiv:0911.3981 [hep-ph]].

[100] U. van Kolck, Prog. Part. Nucl. Phys. **43**, 337-418 (1999). [nucl-th/9902015].

[101] C. G. Callan, Jr., R. F. Dashen, D. J. Gross, Phys. Lett. **B63**, 334-340 (1976).

[102] R. Jackiw, C. Rebbi, Phys. Rev. Lett. **37**, 172-175 (1976).

[103] G. 't Hooft, Phys. Rev. Lett. **37**, 8-11 (1976).

[104] G. 't Hooft, Phys. Rev. **D14**, 3432-3450 (1976).

[105] K. Fujikawa, Phys. Rev. Lett. **42**, 1195 (1979).

[106] W. Buchmuller and D. Wyler, Nucl. Phys. B **268**, 621 (1986).

[107] A. De Rujula, M. B. Gavela, O. Pene and F. J. Vegas, Nucl. Phys. B **357**, 311 (1991).

[108] S. Weinberg, Phys. Rev. Lett. **63**, 2333 (1989).

[109] E. Braaten, C. S. Li and T. C. Yuan, Phys. Rev. Lett. **64**, 1709 (1990).

[110] M. J. Ramsey-Musolf and S. Su, Phys. Rept. **456**, 1 (2008). [arXiv:hep-ph/0612057].

[111] B. Grzadkowski, M. Iskrzynski, M. Misiak and J. Rosiek, JHEP **1010**, 085 (2010). [arXiv:1008.4884 [hep-ph]].

[112] T. Ibrahim and P. Nath, Rev. Mod. Phys. **80**, 577 (2008). [arXiv:0705.2008 [hep-ph]].

[113] B. C. Regan, E. D. Commins, C. J. Schmidt and D. DeMille, Phys. Rev. Lett. **88**, 071805 (2002).

[114] G. W. Bennett *et al.* [Muon (g-2) Collaboration], Phys. Rev. D **80**, 052008 (2009). [arXiv:0811.1207 [hep-ex]].

[115] G. W. Bennett *et al.* [Muon G-2 Collaboration], Phys. Rev. D **73**, 072003 (2006). [arXiv:hep-ex/0602035].

[116] A. Adelmann, K. Kirch, C. J. G. Onderwater and T. Schietinger, J. Phys. G **37**, 085001 (2010).

[117] A. Czarnecki and B. Krause, Phys. Rev. Lett. **78**, 4339 (1997). [arXiv:hep-ph/9704355].

[118] M. E. Pospelov, Phys. Lett. B **328**, 441 (1994). [arXiv:hep-ph/9402317].

[119] W. Fischler, S. Paban, S. D. Thomas, Phys. Lett. **B289**, 373-380 (1992). [hep-ph/9205233].

[120] A. Pilaftsis, Nucl. Phys. **B644**, 263-289 (2002). [hep-ph/0207277].

[121] D. A. Demir, O. Lebedev, K. A. Olive, M. Pospelov, A. Ritz, Nucl. Phys. **B680**, 339-374 (2004). [hep-ph/0311314].

[122] U. van Kolck, Ph.D. dissertation, University of Texas (1993); Few-Body Syst. Suppl. **9** (1995) 444.

[123] A. Manohar, H. Georgi, Nucl. Phys. **B234**, 189 (1984).

[124] S. R. Beane, P. F. Bedaque, L. Childress, A. Kryjevski, J. McGuire and U. v. Kolck, Phys. Rev. A **64**, 042103 (2001). [arXiv:quant-ph/0010073].

[125] S. R. Beane, P. F. Bedaque, M. J. Savage, U. van Kolck, Nucl. Phys. **A700**, 377-402 (2002). [nucl-th/0104030].

[126] A. Nogga, R. G. E. Timmermans, U. van Kolck, Phys. Rev. **C72**, 054006 (2005). [nucl-th/0506005].

[127] M. C. Birse, Phys. Rev. **C74**, 014003 (2006). [nucl-th/0507077].

[128] E. Epelbaum, U. -G. Meissner, [nucl-th/0609037].

[129] B. Long and U. van Kolck, Annals Phys. **323**, 1304 (2008). [arXiv:0707.4325 [quant-ph]].

[130] M. P. Valderrama, Phys. Rev. C **83**, 024003 (2011). [arXiv:0912.0699 [nucl-th]].

[131] V. Bernard, N. Kaiser, J. Kambor, U. G. Meissner, Nucl. Phys. **B388**, 315-345 (1992).

[132] N. Fettes, U. -G. Meissner, S. Steininger, Nucl. Phys. **A640**, 199-234 (1998). [hep-ph/9803266].

[133] S. R. Beane, K. Orginos, M. J. Savage, Nucl. Phys. **B768**, 38-50 (2007). [hep-lat/0605014].

[134] U. van Kolck, J. A. Niskanen, G. A. Miller, Phys. Lett. **B493**, 65-72 (2000). [nucl-th/0006042].

[135] D. R. Bolton, G. A. Miller, Phys. Rev. **C81**, 014001 (2010). [arXiv:0907.0254 [nucl-th]].

[136] A. Filin, V. Baru, E. Epelbaum, J. Haidenbauer, C. Hanhart, A. E. Kudryavtsev, U. -G. Meissner, Phys. Lett. **B681**, 423-427 (2009). [arXiv:0907.4671 [nucl-th]].

[137] J. Gasser, H. Leutwyler, Phys. Rept. **87**, 77-169 (1982).

[138] J. L. Friar, U. van Kolck, M. C. M. Rentmeester and R. G. E. Timmermans, Phys. Rev. C **70**, 044001 (2004). [arXiv:nucl-th/0406026].

[139] R. F. Dashen, Phys. Rev. **D3**, 1879-1889 (1971).

[140] V. Baluni, Phys. Rev. **D19**, 2227-2230 (1979).

[141] C. Vafa and E. Witten, Phys. Rev. Lett. **53** (1984) 535;

[142] M.B. Einhorn and J. Wudka, Phys. Rev. D **67** (2003) 045004.

[143] C. Vafa and E. Witten, Nucl. Phys. B **234** (1984) 173.

[144] J. Nuyts, Phys. Rev. Lett. **26** (1971) 1604.

[145] U. van Kolck, J. L. Friar, J. T. Goldman, Phys. Lett. **B371**, 169-174 (1996). [nucl-th/9601009].

[146] G. A. Miller, B. M. K. Nefkens, I. Slaus, Phys. Rept. **194**, 1-116 (1990).

[147] G. A. Miller, A. K. Opper, E. J. Stephenson, Ann. Rev. Nucl. Part. Sci. **56**, 253-292 (2006). [nucl-ex/0602021].

[148] U. van Kolck, M. C. M. Rentmeester, J. L. Friar, J. T. Goldman, J. J. de Swart, Phys. Rev. Lett. **80**, 4386-4389 (1998). [nucl-th/9710067].

[149] N. Kaiser, Phys. Rev. **C73**, 044001 (2006). [nucl-th/0601099].

[150] N. Fettes, U.-G. Meißner, M. Mojžiš, and S. Steininger, Ann. Phys. **283** (2000) 273; **288** (2001) 249 (E).

[151] J. de Vries, R. Timmermans, and U. van Kolck, in preparation.

[152] S. A. Coon, B. H. J. McKellar, V. G. J. Stoks, Phys. Lett. **B385**, 25-32 (1996). [nucl-th/9606054].

[153] E. Epelbaum, U. -G. Meissner, J. E. Palomar, Phys. Rev. **C71**, 024001 (2005). [nucl-th/0407037].

[154] J. L. Friar, G. L. Payne, U. van Kolck, Phys. Rev. **C71**, 024003 (2005). [nucl-th/0408033].

[155] J. de Vries, E. Mereghetti, R.G.E. Timmermans, and U. van Kolck, in preparation;

[156] M. Gorchtein, Phys. Rev. **C77**, 065501 (2008). [arXiv:0803.0343 [hep-ph]].

[157] I. B. Khriplovich, R. A. Korkin, Nucl. Phys. **A665**, 365-373 (2000). [nucl-th/9904081].

[158] R. V. Korkin,

[nucl-th/0504078].

[159] C. -P. Liu, R. G. E. Timmermans, Phys. Rev. **C70**, 055501 (2004). [nucl-th/0408060].

[160] C. -P. Liu, R. G. E. Timmermans, Phys. Lett. **B634**, 488-492 (2006). [nucl-th/0602010].

[161] I. Stetcu, C. -P. Liu, J. L. Friar, A. C. Hayes, P. Navratil, Phys. Lett. **B665**, 168-172 (2008). [arXiv:0804.3815 [nucl-th]].

[162] S. D. Thomas, Phys. Rev. **D51**, 3955-3957 (1995). [hep-ph/9402237].

[163] D. O'Connell and M. J. Savage, Phys. Lett. B **633**, 319 (2006). [arXiv:hep-lat/0508009].

[164] A. Gardestig, C. J. Horowitz, A. Nogga, A. C. Fonseca, C. Hanhart, G. A. Miller, J. A. Niskanen, U. van Kolck, Phys. Rev. **C69**, 044606 (2004). [nucl-th/0402021].

[165] A. Nogga, A. C. Fonseca, A. Gardestig, C. Hanhart, C. J. Horowitz, G. A. Miller, J. A. Niskanen, U. van Kolck, Phys. Lett. **B639**, 465-470 (2006). [nucl-th/0602003].

[166] E. J. Stephenson, A. D. Bacher, C. E. Allgower, A. Gardestig, C. Lavelle, G. A. Miller, H. Nann, J. Olmsted *et al.*, Phys. Rev. Lett. **91**, 142302 (2003). [nucl-ex/0305032].

[167] A. K. Opper, E. J. Korkmaz, D. A. Hutcheon, R. Abegg, C. A. Davis, R. W. Finlay, P. W. Green, L. G. Greeniaus *et al.*, Phys. Rev. Lett. **91**, 212302 (2003). [nucl-ex/0306027].

[168] M. Hoferichter, B. Kubis and U.-G. Meißner, *Nucl. Phys. A* **833** (2010) 18.

[169] S. J. Brodsky, S. Gardner, D. S. Hwang, Phys. Rev. **D73**, 036007 (2006). [hep-ph/0601037].

[170] F. Berruto, T. Blum, K. Orginos, A. Soni, Phys. Rev. **D73**, 054509 (2006). [hep-lat/0512004].

[171] E. Shintani, S. Aoki, Y. Kuramashi, Phys. Rev. **D78**, 014503 (2008). [arXiv:0803.0797 [hep-lat]].

[172] S. Aoki, R. Horsley, T. Izubuchi, Y. Nakamura, D. Pleiter, P. E. L. Rakow, G. Schierholz, J. Zanotti, [arXiv:0808.1428 [hep-lat]].

[173] W. Wilcox, Phys. Rev. **D66**, 017502 (2002). [hep-lat/0204024].

[174] J. Kuckei, C. Dib, A. Faessler, T. Gutsche, S. Kovalenko, V. E. Lyubovitskij, K. Pumsa-ard, Phys. Atom. Nucl. **70**, 349-357 (2007). [hep-ph/0510116].

[175] C. Dib, A. Faessler, T. Gutsche, S. Kovalenko, J. Kuckei, V. E. Lyubovitskij, K. Pumsa-ard, J. Phys. G **G32**, 547-564 (2006). [hep-ph/0601144].

[176] V. M. Khatsymovsky and I. B. Khriplovich, Phys. Lett. B **296**, 219 (1992).

[177] V. P. Gudkov, Z. Phys. A **343**, 437 (1992).

[178] R. L. Arnowitt, J. L. Lopez and D. V. Nanopoulos, Phys. Rev. D **42**, 2423 (1990).

[179] R. L. Arnowitt, M. J. Duff and K. S. Stelle, Phys. Rev. D **43**, 3085 (1991).

[180] R. Lewis, N. Mobed, Phys. Rev. **D59**, 073002 (1999). [hep-ph/9810254].

[181] B. Kubis, R. Lewis, Phys. Rev. **C74**, 015204 (2006). [nucl-th/0605006].

[182] V. Bernard, H. W. Fearing, T. R. Hemmert, U. G. Meissner, Nucl. Phys. **A635**, 121-145 (1998). [hep-ph/9801297].

[183] C. M. Maekawa, U. van Kolck, Phys. Lett. **B478**, 73-78 (2000). [hep-ph/0006161].

[184] C. M. Maekawa, J. S. Veiga, U. van Kolck, Phys. Lett. **B488**, 167-174 (2000). [hep-ph/0006181].

[185] S. R. Beane, W. Detmold, K. Orginos, M. J. Savage, [arXiv:1004.2935 [hep-lat]].

[186] S. R. Beane, P. F. Bedaque, K. Orginos, M. J. Savage, Phys. Rev. Lett. **97**, 012001 (2006). [hep-lat/0602010].

[187] D. B. Kaplan, M. J. Savage, M. B. Wise, Nucl. Phys. **B534**, 329-355 (1998). [nucl-th/9802075].

[188] D. B. Kaplan, M. J. Savage, M. B. Wise, Phys. Lett. **B424**, 390-396 (1998). [nucl-th/9801034].

[189] D. B. Kaplan, M. J. Savage, M. B. Wise, Phys. Rev. **C59**, 617-629 (1999). [nucl-th/9804032].

[190] T. Mehen, I. W. Stewart, Phys. Rev. **C59**, 2365-2383 (1999). [nucl-th/9809095].

[191] D. R. Phillips, S. R. Beane, M. C. Birse, J. Phys. A **A32**, 3397-3407 (1999). [hep-th/9810049].

[192] M. J. Savage, R. P. Springer, Nucl. Phys. **A686**, 413-428 (2001). [nucl-th/9907069].

[193] S. Fleming, T. Mehen, I. W. Stewart, Nucl. Phys. **A677**, 313-366 (2000). [nucl-th/9911001].

[194] O. Lebedev, K. A. Olive, M. Pospelov, A. Ritz, Phys. Rev. **D70**, 016003 (2004). [hep-ph/0402023].

[195] W. C. Haxton, E. M. Henley, Phys. Rev. Lett. **51**, 1937 (1983).

[196] P. Herczeg, in *Tests of Time-Reversal Invariance in Neutron Physics*, N.R. Robertson, C.R. Gould, and J.D. Bowman (editors), World Scientific, Singapore (1987).

[197] G. Barton, Nuovo Cim. **19**, 512-527 (1961).

[198] V. P. Gudkov, X. -G. He, B. H. J. McKellar, Phys. Rev. **C47**, 2365-2368 (1993). [hep-ph/9212207].

[199] I. S. Towner, A. C. Hayes, Phys. Rev. **C49**, 2391-2397 (1994). [nucl-th/9402026].

[200] P. Herczeg, *Nucl. Phys.* **75** (1966) 665.

[201] B. Desplanques, J. F. Donoghue, B. R. Holstein, Annals Phys. **124**, 449 (1980).

[202] Y. Avishai, *Phys. Rev. D* **32** (1985) 314.

[203] Y. Avishai, M. Fabre De La Ripelle, Phys. Rev. Lett. **56**, 2121-2123 (1986).

[204] A. Griffiths, P. Vogel, Phys. Rev. **C43**, 2844-2848 (1991).

[205] V. V. Flambaum, I. B. Khriplovich, O. P. Sushkov, Sov. Phys. JETP **60**, 873 (1984).

[206] V. V. Flambaum, I. B. Khriplovich, O. P. Sushkov, Phys. Lett. **B162**, 213-216 (1985).

[207] V. V. Flambaum, I. B. Khriplovich, O. P. Sushkov, Nucl. Phys. **A449**, 750 (1986).

[208] J. Dobaczewski, J. Engel, Phys. Rev. Lett. **94**, 232502 (2005). [nucl-th/0503057].

[209] J. H. de Jesus, J. Engel, Phys. Rev. **C72**, 045503 (2005). [nucl-th/0507031].

[210] P. Herczeg, in *Symmetries and Fundamental Interactions in Nuclei*, W.C. Haxton and E.M. Henley (editors), World Scientific, Singapore (1995).

[211] V. P. Gudkov, Phys. Rept. **212**, 77-105 (1992).

[212] C. Ordonez, U. van Kolck, Phys. Lett. **B291**, 459-464 (1992).

[213] C. Ordonez, L. Ray, U. van Kolck, Phys. Rev. Lett. **72**, 1982-1985 (1994).

[214] C. Ordonez, L. Ray, U. van Kolck, Phys. Rev. **C53**, 2086-2105 (1996). [hep-ph/9511380].

[215] N. Kaiser, R. Brockmann, W. Weise, Nucl. Phys. **A625**, 758-788 (1997). [nucl-th/9706045].

[216] N. Kaiser, S. Gerstendorfer, W. Weise, Nucl. Phys. **A637**, 395-420 (1998). [nucl-th/9802071].

[217] J. L. Friar, Phys. Rev. **C60**, 034002 (1999). [nucl-th/9901082].

[218] U. van Kolck, Phys. Rev. **C49**, 2932-2941 (1994).

[219] J. L. Friar, D. Huber, U. van Kolck, Phys. Rev. **C59**, 53-58 (1999). [nucl-th/9809065].

[220] E. Epelbaum, A. Nogga, W. Gloeckle, H. Kamada, U. G. Meissner, H. Witala, Phys. Rev. **C66**, 064001 (2002). [nucl-th/0208023].

[221] J. L. Friar, U. van Kolck, Phys. Rev. **C60**, 034006 (1999). [nucl-th/9906048].

[222] J. A. Niskanen, Phys. Rev. **C65**, 037001 (2002). [nucl-th/0108015].

[223] J. L. Friar, U. van Kolck, G. L. Payne, S. A. Coon, Phys. Rev. **C68**, 024003 (2003). [nucl-th/0303058].

[224] N. Kaiser, Phys. Rev. **C76**, 068201 (2007). [arXiv:0711.2237 [nucl-th]].

[225] Y. -R. Liu, S. -L. Zhu, Chin. Phys. **32**, 700-704 (2008). [arXiv:0711.3838 [nucl-th]].

[226] L. Girlanda, Phys. Rev. **C77**, 067001 (2008). [arXiv:0804.0772 [nucl-th]].

[227] H. W. Griesshammer, M. R. Schindler, Eur. Phys. J. **A46**, 73-83 (2010). [arXiv:1007.0734 [nucl-th]].

[228] P. F. Bedaque, M. J. Savage, Phys. Rev. **C62**, 018501 (2000). [nucl-th/9909055].

[229] S. -L. Zhu, C. M. Maekawa, B. R. Holstein, M. J. Ramsey-Musolf, Phys. Rev. Lett. **87**, 201802 (2001). [hep-ph/0106216].

[230] S. -L. Zhu, C. M. Maekawa, G. Sacco, B. R. Holstein, M. J. Ramsey-Musolf, Phys. Rev. **D65**, 033001 (2002). [hep-ph/0107076].

[231] B. R. Holstein, Fizika **B14**, 165-216 (2005). [nucl-th/0607038].

[232] D. R. Phillips, M. R. Schindler, R. P. Springer, Nucl. Phys. **A822**, 1-19 (2009). [arXiv:0812.2073 [nucl-th]].

[233] J. W. Shin, S. Ando, C. H. Hyun, Phys. Rev. **C81**, 055501 (2010). [arXiv:0907.3995 [nucl-th]].

[234] M. R. Schindler, R. P. Springer, Nucl. Phys. **A846**, 51-62 (2010). [arXiv:0907.5358 [nucl-th]].

[235] C. -P. Liu, Phys. Rev. **C75**, 065501 (2007). [nucl-th/0609078].

[236] C. H. Hyun, S. Ando, B. Desplanques, Eur. Phys. J. **A32**, 513-515 (2007). [nucl-th/0609015].

[237] C. H. Hyun, S. Ando, B. Desplanques, Phys. Lett. **B651**, 257-262 (2007). [nucl-th/0611018].

[238] J. A. Niskanen, T. M. Partanen, M. J. Iqbal, Eur. Phys. J. **A36**, 295-301 (2008). [arXiv:0712.2399 [nucl-th]].

[239] B. Desplanques, C. H. Hyun, S. Ando, C. -P. Liu, Phys. Rev. **C77**, 064002 (2008). [arXiv:0803.2075 [nucl-th]].

[240] R. Schiavilla, M. Viviani, L. Girlanda, A. Kievsky, L. E. Marcucci, Phys. Rev. **C78**, 014002 (2008). [arXiv:0805.3599 [nucl-th]].

[241] M. Viviani, R. Schiavilla, L. Girlanda, A. Kievsky, L. E. Marcucci, Phys. Rev. **C82**, 044001 (2010). [arXiv:1007.2052 [nucl-th]].

[242] U. van Kolck, Nucl. Phys. **A645**, 273-302 (1999). [nucl-th/9808007].

[243] T.S. Park, D.P. Min, and M. Rho, *Phys. Rept.* **233** (1993) 341.

[244] V. G. J. Stoks, R. Timmermans, J. J. de Swart, Phys. Rev. **C47**, 512-520 (1993). [nucl-th/9211007].

[245] M. C. M. Rentmeester, R. G. E. Timmermans, J. L. Friar, J. J. de Swart, Phys. Rev. Lett. **82**, 4992-4995 (1999). [nucl-th/9901054].

[246] J. L. Friar, Mod. Phys. Lett. **A11**, 3043-3048 (1996). [nucl-th/9601013].

[247] V. G. J. Stoks, R. A. M. Klomp, C. P. F. Terheggen, J. J. de Swart, Phys. Rev. **C49**, 2950-2962 (1994). [nucl-th/9406039].

[248] R. Machleidt, Phys. Rev. **C63**, 024001 (2001). [nucl-th/0006014].

[249] S. R. Beane, M. Malheiro, J. A. McGovern, D. R. Phillips, U. van Kolck, Nucl. Phys. **A747**, 311-361 (2005). [nucl-th/0403088].

[250] I.M. Gelfand and G.E. Shilov, *Generalized Functions*, Vol. 1 (Academic Press, New York, 1964).

[251] M. E. Luke, A. V. Manohar, Phys. Lett. **B286**, 348-354 (1992). [hep-ph/9205228].

[252] R. Sundrum, Phys. Rev. **D57**, 331-336 (1998). [hep-ph/9704256].

[253] B. Long, V. Lensky, [arXiv:1010.2738 [hep-ph]].

[254] L. Girlanda, S. Pastore, R. Schiavilla, M. Viviani, Phys. Rev. **C81**, 034005 (2010). [arXiv:1001.3676 [nucl-th]].

[255] P. G. Blunden, S. Kondratyuk, J. Phys. G **G35**, 115001 (2008). [arXiv:0710.5913 [nucl-th]].

[256] M. Abramowitz and I. Stegun, *Handbook of Mathematical Functions* (Dover, New York, 1965); I.S. Gradshteyn and I.M. Ryzhik, *Table of Integrals, Series and Products*, Fifth Edition, Ed. A. Jeffrey (Academic Press, Boston, 1994).

[257] Wolfram Research, Inc., *Mathematica*, Version 7.0 (Champaign, 2008).